ANALYTICAL AND NUMERICAL MODELING OF PROGRESSIVE FAILURE OF ONSHORE AND OFFSHORE SLOPES WITH SENSITIVE CLAY LAYER

by

© Rajib Dey

A Thesis is submitted to the

School of Graduate Studies

in partial fulfillment of the requirements for the degree of

Doctor of Philosophy

Faculty of Engineering and Applied Science

Memorial University of Newfoundland

May, 2015

St. John's Newfoundland and Labrador Canada

ABSTRACT

Landslides in both onshore and offshore environments are always a potential hazard and a great threat to many communities and infrastructure. There are some similarities and differences between failure mechanisms and potential causes of failure of slopes in these two environments. Large landslides in both environments are generally progressive in nature. This becomes more pronounced when the slide occurs in sensitive clays, generally assumed under undrained condition. Post-peak softening of sensitive clays is considered as one of the main reasons for pronounced progressive failure. Sensitive clays found in both environments show nonlinear post-peak strain softening behavior at large strain/displacement during undrained loading. Post-slide investigations show that failure patterns of many large-scale submarine landslides through marine clays could be very similar to onshore landslides through sensitive clays as encountered in Eastern Canada and Scandinavia (e.g. translational progressive slide, and spreads). As onshore slope failures in sensitive clays are better documented than submarine landslides in marine clays, information on onshore sensitive clays available in the literature can be utilized as the basis to model both submarine and subaerial landslides in sensitive clays. The main focus of the present study is to model slope failure through weak sensitive clay layers under undrained conditions. A nonlinear mathematical model for post-peak degradation of undrained shear strength of sensitive clay, applicable to small to large-strains, is proposed in this study based on available experimental results. The slope failure mechanisms are examined using the concept of shear band propagation.

Various factors have been identified in the past that could trigger a large-scale slope failure in both environments. Among them, the effects of toe erosion, surcharge loading, and strength

reduction in a section of a weak layer are considered in this study. In a marine environment, strength reduction in a section of a weak layer in an offshore slope might result in initiation and propagation of a shear band in both upslope and downslope directions at the same time. By incorporating a nonlinear post-peak softening model, an analytical solution is developed to examine a possible mechanism of failure of mild submarine slopes containing a weak zone of low shear strength. In comparison, due to toe erosion, a shear band formation could be initiated and propagated upward (inward) from the river bank which could lead to a spread type failure forming horsts and grabens. Upslope surcharge loading (e.g. the placement of fill) could also generate shear bands that might propagate down towards the river bank. Numerical modeling of these types of slope failure is considered as a large deformation problem. Finite element (FE) models in Lagrangian framework cannot model the complete process of these slides, as significant mesh distortion occurs. Coupled Eulerian Lagrangian (CEL), a finite element approach in Abaqus FE software is used in this study to model these progressive failures of slopes. A nonlinear strain softening model for undrained shear strength of sensitive clays is incorporated in the FE simulation. Upward progressive failure leading to spread due to toe erosion, downward progressive failure due to a construction load in the upslope area, and combined effects of upward and downward propagation of shear bands on stability of a river bank slope have been simulated in this study. Simulations are also carried out to model submarine landslides due to the existence of a weak layer. The FE simulated results and failure patterns of ground surface or seabed are compared with the slide morphology presented in the literature. The main advantages of the present FE modeling are: (i) extremely large strains in the shear bands can be successfully simulated without numerical issues, (ii) a prior definition of shearing zones with special mesh and/or element type is not required to capture extreme strains

in the shear bands, and (iii) the FE program automatically identifies the location of critical shear band formation and direction of propagation.

ACKNOWLEDGEMENTS

First of all, I would like to praise and thank the Almighty to provide me an excellent opportunity to do research on this topic as well as give me enough courage and strength to complete the research successfully.

The research work was mainly carried out under the supervision of Dr. Bipul Hawlader, Associate professor, Memorial University, NL, Canada. I am extremely grateful to him for his overall guidance, help and affectionate encouragement throughout this study period. I am particularly obliged to him for his patience and the valuable time spent. Without his advice and constructive criticism, preparation of this dissertation might not be possible. Your advice on both research and my career has been priceless.

Deep and sincere gratitude to my co-supervisors Dr. Ryan Phillips, Principal Consultant, C-CORE, NL, Canada and Prof. Kenichi Soga, Professor, Cambridge University, UK for their invaluable suggestions, comments and guidance throughout the work. It was a great privilege and honor to work and study under their guidance.

Special thanks to RDC, NSERC, School of the Graduate Studies, Memorial University and C-CORE for their financial support which helped me to make my thesis possible. Also, my sincerest thanks go to Mr. John Barrett of C-CORE for his suggestions and Mr. Sujan Dutta & Mr. Biswajit Saha for their help on finite element modeling.

Thanks to all my friends for their assistances, friendship and great memories. Also thanks to all the faculties and staff in the Faculty of Engineering and Applied Science as well as the people around me in St John's who helped me directly or indirectly throughout this study period.

Furthermore, I wish to express my heartiest appreciation to my parents in Bangladesh for their endless love and support. Last but by no means least, I would also like to thank my wife Munmun, for her love, and support that she has shown during the past few years. The dissertation is dedicated to them.

Table of Contents

List of Figures

List of Tables

List of Symbols

As the thesis is written in manuscript format, symbols used in this study are listed at the end of each chapter (Chapter 3-6).

CHAPTER 1

Introduction

1.1 Background

Landslides occur in both onshore and offshore environments and can be a great threat to many communities and infrastructure. Submarine landslides generally happen unobserved as they occur below water level. Large-scale submarine landslides could displace several thousand cubic kilometers of sediments and could be order of magnitude larger than subaerial landslides. After a submarine slope failure, the failed soil mass could travel a large distance (in excess of 100 km) on very gentle slopes (Hampton et al. 1996, Masson et al. 2006). Although there are significant differences between onshore and offshore landslides, they have similarities in terms of slope failure mechanics (Hampton et al. 1996, Locat and Lee 2000). In both environments, landslides may be a result from a single triggering factor or the combined effects of a number of factors. The consequences of a catastrophic slope failure could be very devastating in both cases and might have significant impacts, raising economic, safety, regulatory and environmental issues. Figure 1.1 shows some examples of catastrophic landslides which occurred in offshore and onshore environments.

During the last few decades, the exploration for oil and gas in deep water has increased the demand for offshore research not only in Canada but also in other parts of the world. There are various issues in offshore development, and offshore geohazards is one of the critical ones (see Fig. 1.2). For example, the liquid hydrocarbon and natural gas products are usually transported through offshore pipelines which traverse large distances across a variety of soils. Failure of slopes might impact a pipeline and could pose a significant threat to pipeline integrity that may

result in pipeline damage and potential failure. Moreover, submarine landslides can cause a tsunami which is again a great threat to the coastal communities. Slides might also retrogress towards the shore and present potential hazards to mankind and infrastructure. Similarly, large-scale onshore landslides in sensitive clays which are progressive in nature have been also considered as major hazards because of their retrogressive potential and high mobility (Quinn 2009, Locat et al. 2011). Although numerous submarine slope failures have been reported in the literature, compared to onshore landslides, information on soil properties and landslide processes in marine environments is still very limited (Masson et al. 2006).

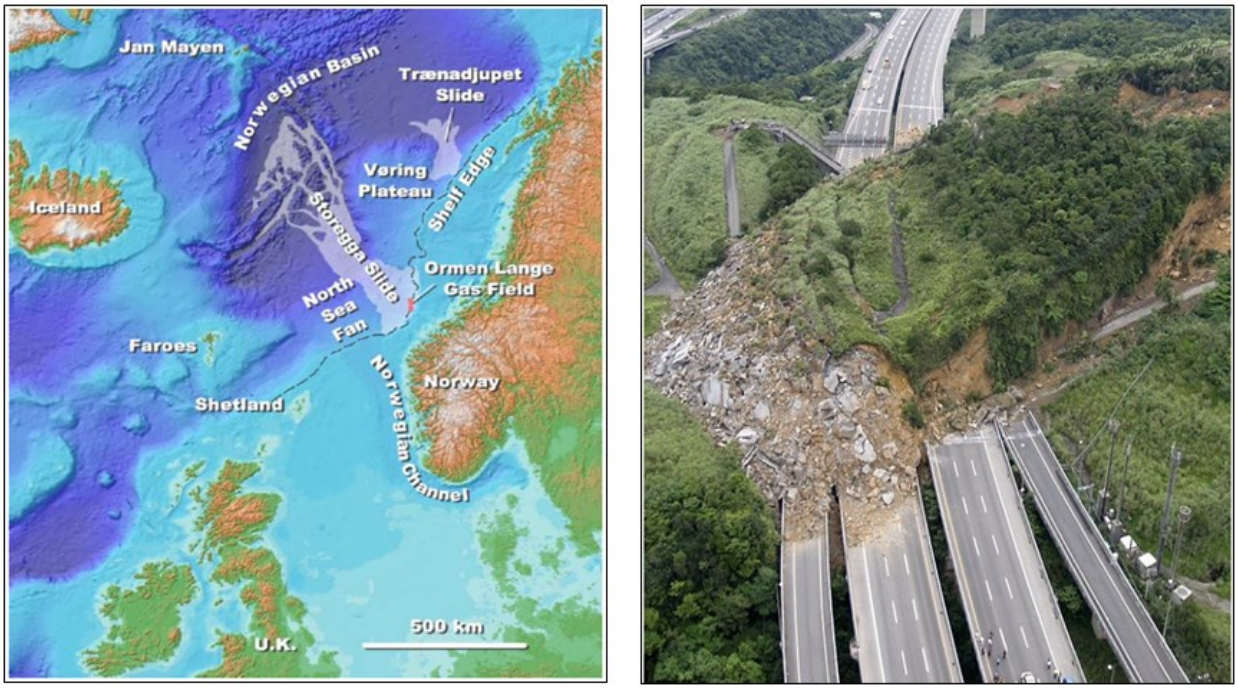

Figure 1.1: The Storegga slide Offshore Norway (after Bryn et al. 2005) and slide in Taiwan (after Dave 2010)

Investigating post-slide seabed morphology, scars and debris formation, recent studies showed that the existence of weak layers such as a marine sensitive clay layer could be one of the main

causal factors of many offshore landslides (e.g. Bryn et al. 2005, Kvalstad et al. 2005a, Dan et al. 2007). Moreover, the failure pattern of some of these slopes could be very similar to onshore large-scale landslides in soft sensitive clays as commonly encountered in Eastern Canada and Scandinavia (Kvalstad et al. 2005a). Therefore, the failure mechanisms inferred from onshore landslides could be used to examine offshore slope failure events and to identify potential mechanisms involved in slope failure.

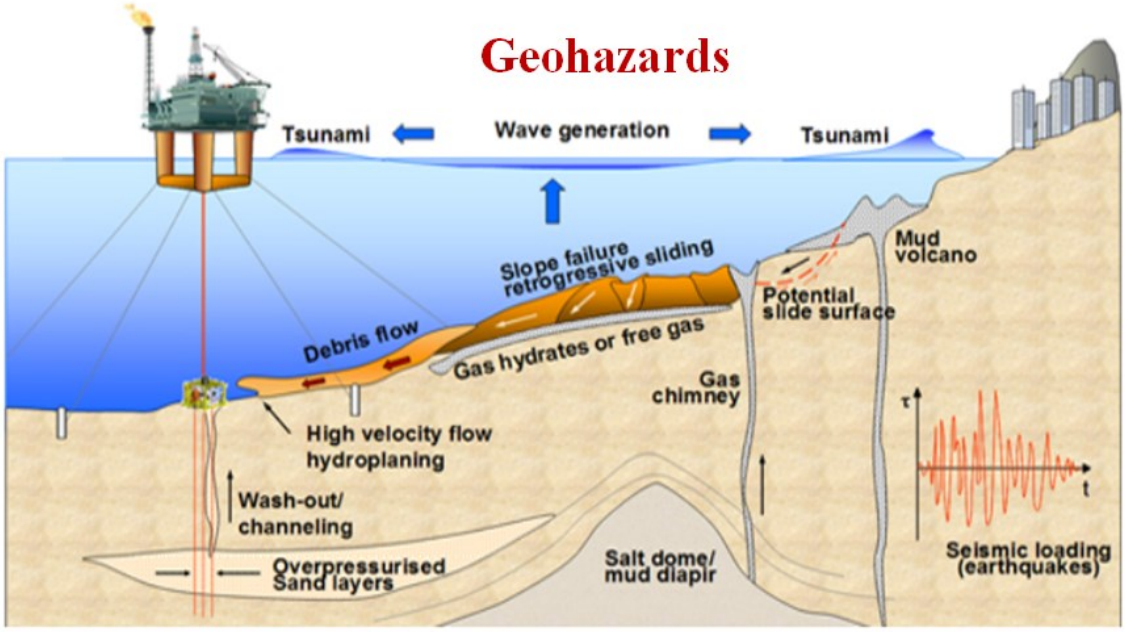

Figure 1.2: Various types of geohazards and associated ground movement (after ICG 2010)

1.2 Focus of the research

Limit equilibrium (LE) methods have been widely used in geotechnical engineering to calculate the stability of slopes. Computer programs such as SLOPE/W have been developed in the LE framework in order to accommodate complex geometries and varying soil properties in the analysis. However, the LE methods cannot model the progressive failure of slopes. As mentioned

before, many landslides occurred in the past in onshore and offshore environments involved with sensitive clay layers were progressive in nature. To calculate the stability of these types of slopes alternative numerical modeling techniques are required. Finite element (FE) methods have been also used in the past to model stability of the slopes. However, FE modeling of failure of sensitive clay slopes has some additional technical challenges. One of the challenges is that this is fundamentally a large deformation problem. Moreover, because of strain-softening behavior of sensitive clays, large plastic shear strains accumulate in narrow shear bands and the failure surfaces develop progressively.

There are a limited number of studies available in the literature that explains the mechanisms involved in progressive failure of slopes. Most of the available studies are for drained loading of overconsolidated clays and clay shales (Bjerrum 1967, Burland et al. 1977, Lo and Lee 1973, Potts et al. 1990). As recognized by some researchers, more specifically in recent studies, progressive failure of sensitive clay slopes in undrained condition is equally important which could explain possible mechanisms of many onshore and offshore landslides (Bernander 2000, Puzrin and Germanovich 2005, Quinn 2009, Locat 2012, Gylland 2012). While these studies explain many features of landslides and shear band formation in sensitive clay layers, they have some limitations and cannot simulate the complete failure processes. Most of these numerical models were developed for idealized conditions, such as infinite slopes, predefined shear zone, and idealized triggering effects and soil properties.

For sensitive clays, the post-peak reduction of undrained shear strength occurs with large plastic shear strains. An appropriate model for the post-peak shear strength degradation is required for successful simulation of progressive failure. In addition, this type of model is not available as a built-in model in the commercial FE software for geotechnical analysis.

Depending on the nature of the triggering factors, progressive failure might be initiated in a fully stable and/or marginally stable slope. Once the failure is initiated, it might propagate further in the form of a shear band through the weak sensitive clay layer. Depending upon the location of disturbing agents, the shear band can propagate towards upslope areas (*upward* progressive failure), downslope areas (*downward* progressive failure), or both upslope and downslope directions simultaneously (*lateral* progressive failure). In most cases, the locations of the shear band are not known beforehand, which makes FE modeling more challenging. Therefore, an advanced FE modeling technique is required to simulate this complex process.

1.3 Objectives

The main purpose of this study is to understand the mechanisms involved in large-scale slope failures in sensitive clays for three different triggering factors namely toe erosion, placement of fill in the upslope areas and existence of a discontinuity. The discontinuity could be developed in a weak sensitive clay layer due to various reasons such as geological activities, pore pressure generation, earthquake and another form of plastic shear deformation. In this study, both analytical and numerical models are developed to perform stability analyses of onshore and offshore slopes containing a strain softening clay layer. The Coupled Eulerian-Lagrangian (CEL) technique available in Abaqus FE software is used for numerical analysis. The following are the main objectives of this research:

- Develop a mathematical model for post-peak softening behavior of sensitive clay;
- Implement the model in Abaqus FE software for progressive failure analysis of slopes;

- Develop FE model to simulate upward progressive failure of sensitive clay slopes due to river bank erosion;
- Investigate the combined effects of toe erosion and placement of fill in the upslope areas that could cause large-scale landslides;
- Develop an analytical model that could calculate the length of the discontinuity required for propagation of shear band along a thin sensitive clay layer leading to large-scale submarine landslides in mild offshore slopes; and
- Develop FE models for lateral progressive failure of submarine slopes to explain failure patterns and seafloor morphology as observed in post-failure investigations.

1.4 Outline of Thesis

This thesis contains seven chapters. This first chapter demonstrates the background, scope and objectives of the research.

Chapter 2 contains the literature review. Landslides occur in different type of soils, loading conditions and due to various triggering factors. However, considering the focus of this study, the literature review is presented mainly for sensitive clay slopes in onshore and offshore environments.

In Chapter 3, the modeling of nonlinear post-peak stress-strain behavior of sensitive clay and its effects on submarine slope failure are discussed. This chapter has been submitted as a technical paper for publication in a journal (Dey et al. 2015a). A part of this study has been published earlier as a conference paper (Dey et al. 2012 in Appendix-II).

Chapter 4 presents the FE modeling of upward progressive failure of sensitive clay slopes due to toe erosion. This chapter has been published as a technical paper in Géotechnique (Dey et al. 2015b). A preliminary study on this topic has been published and presented earlier as a conference paper (Dey et al. 2013 in Appendix-III).

Chapter 5 discusses the combined effects of toe erosion and placement of fill in the upslope area on the stability of a river bank slope. This chapter has been submitted for publication as a technical paper in a journal (Dey et al. 2015c). A part of this study has been published earlier as a conference paper (Dey et al. 2014 in Appendix-IV).

Chapter 6 presents FE modeling of submarine landslides. This chapter has been submitted as a technical paper for publication in a journal (Dey et al. 2015d). A study on modeling of submarine landslides has been published earlier as two conference papers (Dey et al. 2011 in Appendix-I, and Dey et al. 2015e in Appendix-V).

Chapter 7 presents some conclusions and recommendations for future studies.

This thesis is prepared in manuscript format. Conclusions of Chapters 3–6 are provided at the end of each chapter after each technical paper. Overall conclusions are provided in Chapter 7. The references cited in Chapters 1 and 2 are listed in the Reference chapter at the end of the thesis.

CHAPTER 2

Literature Review

2.1 General

Many large-scale landslides have been reported in both onshore and offshore environments. There are however some similarities and differences between failure mechanisms and potential causes of failure of slopes in these two environments. In general, the landslides in onshore environments are well-documented as compared to submarine landslides. Post-slide investigation of many submarine landslides shows some similarities between onshore and offshore slope failure and therefore, the knowledge and experience from onshore landslides might be extrapolated to examine submarine slope failure mechanisms. The main focus of the present study is to model both onshore and offshore landslides involving sensitive clays. Therefore, the literature review presented in the following sections is focused primarily on slopes with sensitive clays. The author understands that landslides in other types of soil are equally important. As a part of this thesis, a brief study on the failure of slopes in sand has been also conducted (Dey et al. 2011), which is presented in Appendix-I. The thesis has been written in manuscript format; therefore, problem specific literature reviews are presented in the following chapters (3–6) and are not repeated in this chapter.

This chapter on literature review is organized as follows. First, a brief review of historic onshore and offshore landslides which occurred mainly in sensitive clays is presented in Section 2.2. Slide mechanisms and the effects of different factors such as soil properties, loading and strength reduction, slope geometry on stability of slopes are discussed in Section 2.3. Finally, analytical

and numerical modeling techniques used by previous researchers to analyze the stability of sensitive clay slopes are discussed in Section 2.4.

2.2 Brief Review of Historic Landslides in Sensitive Clays

Many landslides in sensitive clays have been reported in the past. Most of these slope failures have been characterized as progressive in nature. Progressive failure in strongly overconsolidated clays is time dependent and decades may be needed for the final failure to occur under drained conditions (Skempton 1964). However, undrained failure could be catastrophic especially if there is a presence of strain softening material such as sensitive clays. Terzaghi and Peck (1948) emphasized the potential risks associated with progressive failure in brittle clays. Bernander (2000) recognized that the progressive failure in normally consolidated sensitive clays is also a major concern which has not been properly studied so far. Several researchers (e.g. Bernander 2000, Quinn 2009, Locat 2012, Gylland 2012) showed that the soft sensitive clays found in Eastern Canada and Scandinavian countries are normally consolidated or lightly overconsolidated, and most of the large-scale landslides in these clays are mainly progressive in nature. Recent studies (e.g. Bryn et al. 2005, Kvalstad et al. 2005a, Andresen and Jostad 2007) also show that marine clays found in offshore environments could be normally consolidated soft sensitive clays, and progressive failure in these marine clays can trigger large-scale submarine landslides. Undrained strain softening behavior of these sensitive clays is the main reason causing such large-scale failures of slopes in sensitive clays. Figure 2.1 provides some examples of progressive landslides in sensitive clays in onshore and offshore environments.

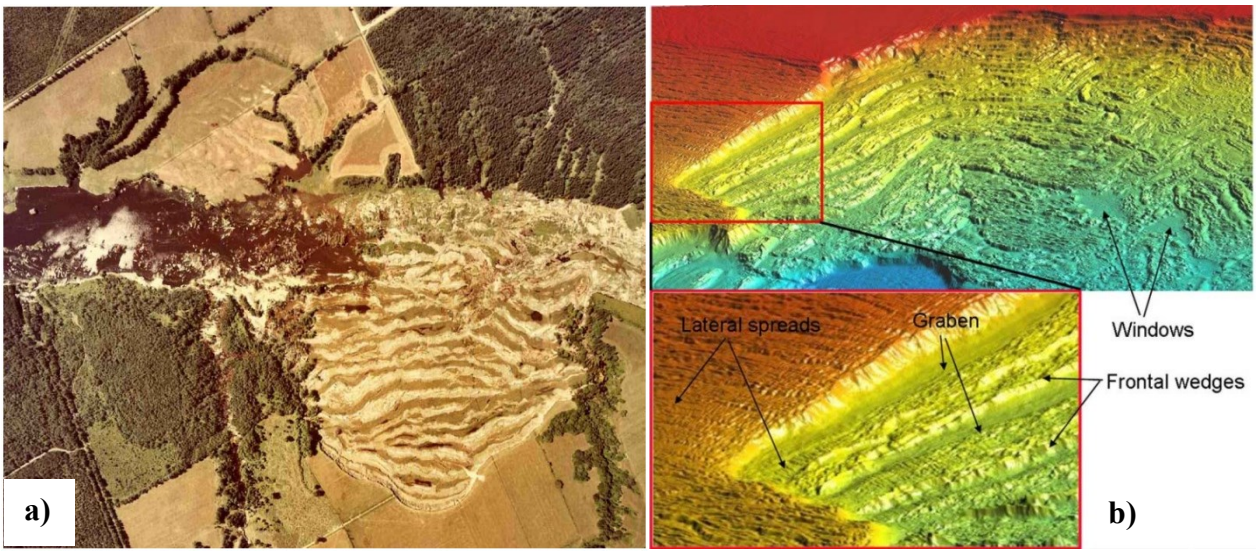

Figure 2.1: Progressive failure of slopes in sensitive clays: a) the 1971 South Nation River slide (Quinn 2009), b) bathymetric views of upper part of the Storegga slide (Kvalstad et al. 2005a)

2.2.1 *Onshore Landslides*

Large-scale landslides in sensitive clays are common in Eastern Canada and Scandinavia. According to Tavenas (1984) and Karlsrud et al. (1984), these slides could be in the form of single rotational slides, multiple retrogressive slides (earthflows), translational progressive or spreads (as classified by Cruden and Varnes 1996). Among them, the last three types of progressive slides in sensitive clays might initiate very suddenly and often cover an area greater than 1 ha (Locat et al. 2011). These three types of slides are schematically shown in Fig. 2.2.

Among these large landslides in sensitive clays, flows are well described in the literature (Bjerrum 1955, Tavenas 1984). It is believed that a multiple retrogressive slide occurs when successive numbers of slides are formed, and debris of the previously generated slide becomes

completely remoulded and flows out of the crater leaving an unstable scarp. The retrogression stops when a stable scarp is formed (Fig. 2.2a).

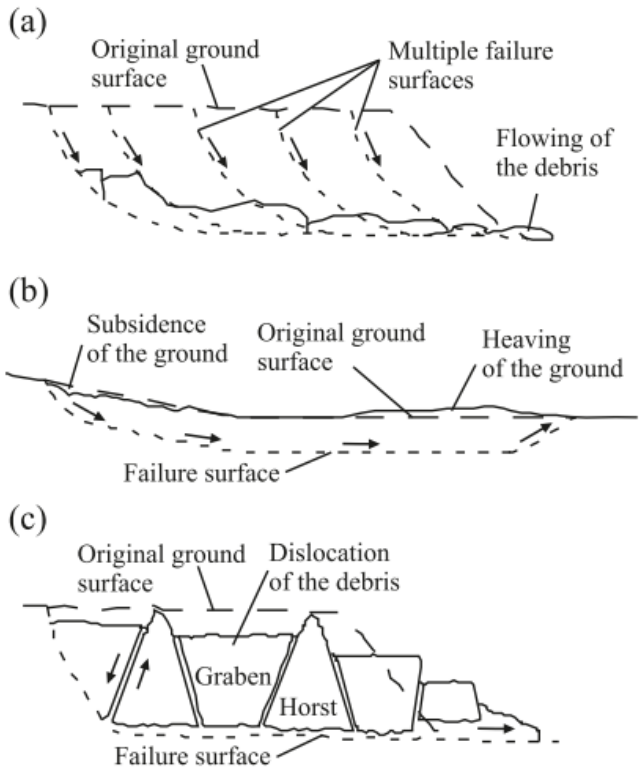

Figure 2.2: Progressive slides in sensitive clays; a) Flows, b) Translational progressive slide, c) Spreads (after Locat et al. 2011)

Translational progressive landslides result when a shear surface parallel to the ground surface is developed above which the soil mass displaces downhill (Cruden and Varnes 1996). Figure 2.2b shows that a zone of subsidence occurs at the head of the slope and an extensive heave zone forms beyond the toe of the slope. These slides are often observed in Scandinavian countries. A number of disastrous landslides in sensitive clays (for example, the Svärta river slide, the Surte landslide in Sweden, the Tre-styckevattnet slide, and the Småröd slide) are listed in the literature

where this type of progressive failure is believed to be the dominating mechanism (Bernander 2000, Gylland 2012). Once this type of slide is initiated near the river bank, the movement of the slide mass could constrict or completely block the river path, for example, as happened during the Surte landslide in Sweden.

According to Cruden and Varnes (1996), spreads result because of the extension and dislocation of the soil mass above the failure surface. Horsts and grabens are formed during the spread where horsts are blocks of more-or-less intact clay pointing upward, and grabens are blocks having typically a flat top surface (Fig. 2.2c). Spreads can be distinguished from other retrogressive landslides because of their unique geomorphologic shape. According to Fortin et al. (2008), 42% of large landslides which occurred in Eastern Canada can be categorized as spreads. Many spread failures such as Sköttorp landslide in Sweden (Odenstad 1951) and the landslides which occurred in Quebec including the 1989 Saint-Liguori landslide (Grondin and Demers 1996), Saint-Ambroise-de-Kildare landslide (Carson 1977), Saint-Barnabé-Nord slide (Locat et al. 2008) are reported in the literature.

In this study, initiatives are taken to model these types of slides. Further discussion on modeling of these types of slides is presented below and in Chapters 3–6.

2.2.2 *Submarine Landslides*

Submarine landslides are large underwater slides that typically occurred in gentle marine slopes. They are considered to be a major potential offshore geohazard and a serious threat to offshore industry all over the world. Numerous failures of submarine slopes have been reported in the literature; some of which are small while others are very large, such as Storegga slide in the

Norwegian Sea or Grand Banks slide in offshore Newfoundland. A large number of studies are available in the literature which describes various slides, their morphologies and potential causes (Coleman and Prior 1978, Hadj-Hamou and Kavazanjian 1985, Hampton et al. 1996, McAdoo 1999, McAdoo et al. 2000, Locat and Lee 2000, 2002, Canals et al. 2004, Sultan et al. 2004, Hühnerbach et al. 2004, Gee et al. 2005, Solheim et al. 2005, Krastel et al. 2006, Masson et al. 2006, Locat et al. 2009, Twichell et al. 2009, Harders et al. 2011, Conway et al. 2012, Li et al. 2014). From the available literature, 16 very large-scale submarine landslides are listed in Table 2.1. Various features of these slides such as slope angle, triggering factor(s), soil type, depth of the failure plane, volume of the slide mass, run out distance, etc. are summarized in Table 2.1 which provides a general picture of the nature of submarine landslides.

Table 2.1 shows that these large-scale submarine slope failures occurred in low gradient continental shelf slopes having typical slope angles between 1° and 5°. The failure occurred at depths of 20–100 m below seabed with volumes of sliding sediment from 0.1 to more than 1,000 km^3. The failed sediments could travel a distance of 0.5 to greater than 100 km. The slope failures occurred in a wide range of water depth varying between 50 m (shallow water) to more than 1000 m (deep water). It is also observed that slope failures could occur either in a clayey seabed with a presence of weak layer or in sand. In previous studies, a number of potential triggering factors have been identified which could weaken a layer of soil in the seabed from where failure might be initiated. The major factors could be:

- earthquake or seismic loading (e.g. Grand Banks failure) (Piper et al. 1999, Fine et al. 2005),
- ii) wave loading and hurricanes (e.g. Mississippi delta failures) (Prior & Coleman 1982),
- iii) gas hydrate dissociation (e.g. east coast US, Storegga slides) (Sultan et al. 2003),

- iv) under-consolidation or over pressure due to rapid sedimentation (e.g. Mississippi delta) (Prior & Coleman 1982),
- v) over steepening of slopes (e.g. Nice, Canary islands) (Assier-Rzadkiewicz et al. 2000),
- vi) presence of geological weak layers or weak layers parallel to the slope surface (e.g. east coast US, Storegga, west Africa) (O'Leary 1991, Haflidason et al. 2005, Bryn et al. 2005),
- vii) ground water seepage and high pore water pressure,
- viii) volcanic activities (Hawaii, Canaries) (Moore et al. 1989, Masson et al. 2002),
- ix) glacial loading,
- x) change in the sea level, (Maderia Abyssal Plain) (Weaver & Kuijpers, 1983),
- xi) gas charging, and
- xii) human activities (1979 Nice landslides) (Dan et al. 2007, Sultan et al. 2010).

The scars of the previous slides may often act as traps and thus increase the risk of further landslides. The Norwegian margin is an example where the weak layers developed within the slide scars that increase the landslide risks (Bryn et al. 2005, Solheim et al. 2005). It is found that landslides could be initiated in a mild slope due to one or more combined effects of multiple triggering factors. For example, in the case of the Storegga slide, which occurred on the continental slope west of Norway, it is believed that generation of excess pore pressure due to several triggering factors such as earthquake, rapid sedimentation, and also the presence of weak layers caused the initial triggering of the slide (Bryn et al. 2005, Kvalsted et al. 2005a).

Various stages are involved in the event of an offshore slope failure and corresponding mass movement. These are failure initiation, displacement as glide block, transition into debris flow, subsequent formation of a turbidity current and movement on the sea floor until final deposition

(Locat and Lee 2002). Figure 2.3 shows various stages of a submarine slope failure. Broadly, two groups of researchers have been working in this area (Locat and Lee 2000); Group I primarily deals with failure mechanisms using the concept of soil mechanics, and Group II considers the soil as fluidized materials and applies the concept of fluid mechanics to model turbidity current and debris flow. In the present study, the mechanisms involved in the initiation of submarine slope failure are investigated using the concept of soil mechanics.

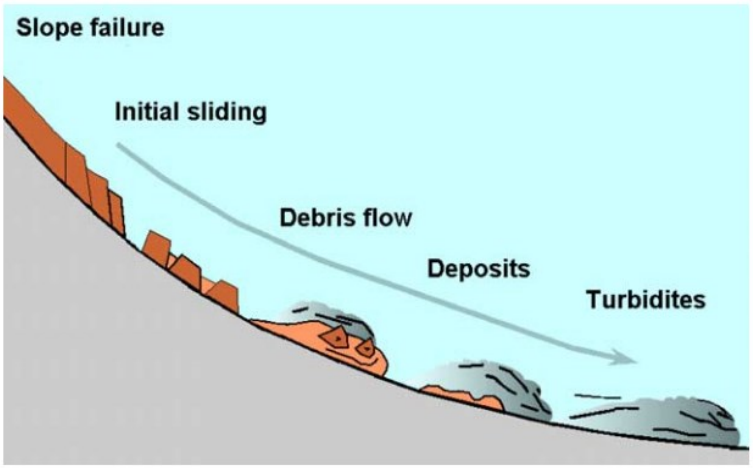

Figure 2.3: Schematic presentation of various components of a marine slide (Bryn et al. 2005)

Table 2.1: Summary of some large-scale submarine slides

No	Landslide	Triggering Mechanism(s)	Seismic activity	Slope angle (°)	Soil type	Vol. (km^3)	Water depth (m)	Slide depth or thickness (m)	Run out distance (km)	Reference(s)
1	The Storegga slide	Presence of weak layers / EPWP due to rapid sedimentation / possibly seismic activity	Yes	several failure planes (0.5 - 2°)	weak layer contains marine clay	2500-3500	1100	less than 100	160	Kvalstad et al. 2005a, b, Bryn et al. 2005.
2	Kitimat Arm failure	EPWP due to extremely low tide / liquefaction	No	delta front 4-7°; large area <1°	soft marine clay/silty sands	0.6	200	avg -7.5; max - 30	6	Murty & Brown 1979, Prior et. al. 1982.
3	Fraser River slide	Liquefaction due to high sedimentation / presence of gas / cyclic wave loading / strong tidal currents / seismic activity	Yes	delta fore-slope 0.5 to 23°; avg between 2-3°	silty sands and clayey silts	0.1	100-300	up to 100	denser soil deposit at 0.3 km	Christian et al. 1994, McKenna et al. 1992.
4	Gulf of Cadiz	Over steepened slope / presence of gas / seepage / seismic activity	Yes	uniform 1.5°	fine sand with overlaying clay	12	157-440	75-95	1km ; slumps in 12km long area	Lee & Baraza 1999
5	Eureka Retrogressive slump	Rapid sedimentation / seismic activity / presence of gas	Yes	4°	thin-bedded clayey silt	6	200-500	50-65	6-10	Gardner et al. 1999
6	Cape Kidnappers	Seismic loading / rapid sedimentation (might be)	Yes	4-5° (south); < 2° (north); 1° (center)	metastable sands & silty layers	33	200-900	15-140	-	Barnes and Lewis 1991

No	Landslide	Triggering Mechanism(s)	Seismic activity	Slope angle (°)	Soil type	Vol. (km^3)	Water depth (m)	Slide depth or thickness (m)	Run out distance (km)	Reference(s)
7	Ohau Slide, Hawaii	Hurricane Iwa	No	20° (1500m deep)	silt and clay	-	1500	10	2.4	Normark et al. 1993
8	Albatross debris flow	Unknown, earthquake or gas hydrates	Yes	6°	wide range of mud in debris	>600	500-700	~ 50	200	Mulder et al. 1997
9	Verrill Canyon rotational slumps	Earthquake with possible excess pore water pressure from gas hydrates or rapid sedimentation	Yes	varies from 5 to 2.5°	bioturbated sandy mud	5.75	>500-600	10-20	slump 30km long	Mosher et al. 1994, Piper et al. 1985a
10	Logan Canyon debris flow	Unknown, probably similar to Verrill Canyon	Yes	-	reddish brown and brown mud	-	400	DF-1 16 DF-2 08 *DF-3 07 *debris flow	at least 150	Piper et al. 2000
11	Grand bank failure, 1929	Earthquake with a magnitude of 7.2 with epicenter at 2000m water depth	Yes	200-500 mbsl 2°; >500 mbsl 5°; failure occurred 10°	strain softening sensitive clay (NC or lightly OC)	> 150	500-700	20-25	> 100	Piper et al. 1999
12	Canary islands landslides	Volcanic activity (not well understood); series of block failures, debris avalanche	No	upper slope 10°; lower slope 5°	coarse volcaniclas-tic mineral	50-200	3000-4000	-	50-100	Masson et al. 2006
13	Mississippi delta	Hurricane or cyclic-wave loading or over pressured or high PWP due to gas	No	0.2-1.5°	soft organic rich clay	0.04	5-100	not greater than 35	-	Coleman and Prior 1978

No	Landslide	Triggering Mechanism(s)	Seismic activity	Slope angle (°)	Soil type	Vol. (km^3)	Water depth (m)	Slide depth or thickness (m)	Run out distance (km)	Reference(s)
14	Chile, 1922	Earthquake with a magnitude of 8.3	Yes	6°	sand with silt	-	-	-	-	Morgenstern 1967
15	California, 1980	Earthquake with a magnitude of 6.5-7.2	Yes	0.25°	fine sand	-	-	apprx 35	-	Field et al. 1982
16	Valdez Alaska, 1964	Earthquake with a magnitude of 8.3	Yes	varied from 4-10°	silty sand	-	-	-	-	Morgenstern 1967; Seed 1968

2.3 Mechanics of Landslides in Sensitive Clays

Failure mechanics of slopes in sensitive clays are complex because of strain-softening behaviour of sensitive clays where large strain concentrations occur along the failure plane. In addition, loading, strength reduction and geometry of the slope also influence the formation of failure planes.

Post-slide field investigations show that the existence of a marine sensitive clay layer could be one of the main causal factors of many offshore landslides (Dan et al. 2007, Sultan et al. 2010). Dan et al. (2007) identified the existence of sensitive clay layers between 30 and 45 m below the seabed near the 1979 Nice harbour catastrophe area. Thin layers of interbedded marine/glaciomarine clay layer were also encountered in many other places (e.g. Laberg et al. 2003, Yang et al. 2006, Bryn et al. 2005, Solheim et al. 2005). As an example, during the development of the Ormen Lange gas field, deep water slide areas in offshore Norway such as; the Storegga slide and the Trænadjupet slide have been investigated intensively (Yang et al. 2006), based on seismic profiles, geoborings up to several hundred meters below the seabed and geotechnical laboratory testing (Bryn et al. 2005), which provides an idea of seabed layering and existence of fine grained marine clay layers (Bryn et al. 2002, Tjelta et al. 2002). It is stated that the failure of these slopes occurred through the marine/glaciomarine sensitive clay layers. Over the last decades the focus on mapping and characterization of weak layer(s) has increased significantly (Lastras et al. 2004, Kvalstad et al. 2005a, L'Heureux et al. 2010, L'Heureux et al. 2012, Locat et al. 2014). Locat et al. (2014) discussed the formation and role of a weak layer on submarine landslides and highlighted that the strain softening behaviour of a weak layer could be the cause of many large-scale progressive failures in mild submarine slopes.

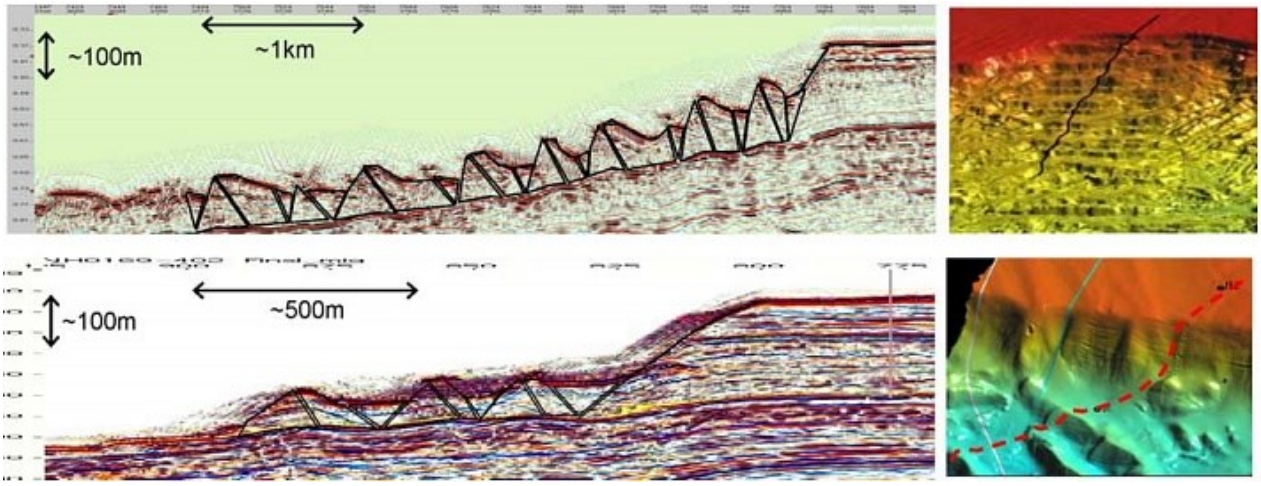

Figure 2.4: Interpretation of retrogressive slide through bathymetry and seismic profile (after Kvalstad et al. 2005a)

While a large volume of data on seafloor morphology is available in the literature, studies on slope failure mechanisms are limited. Based on high resolution seismic profiles and close examination of the Storegga Slide morphology, previous studies (e.g. Bryn et al. 2005, Gauer et al. 2005, Kvalstad et al. 2005a) described the failure pattern of this submarine slope as very similar to onshore large-scale landslides in sensitive clays commonly encountered in Eastern Canada and Scandinavia. It was interpreted that retrogressive failure occurred over a basal failure plane with formation of a series of graben and ridges as shown in Fig. 2.4, which is similar to onshore spread failure as typically occurred near a river bank slope (Fig. 2.2c). Geotechnical laboratory tests on onshore sensitive clays and offshore marine clays show strain softening behaviour under undrained loading (Tavenas et al. 1983, Lefebvre et al.1988, Ladanyi et al. 1994, Stark and Contreras 1996, Devin and Sandford 2000, Tjelta et al. 2002, Kvalstad et al. 2005a,b, Yang et al. 2006, Lunne and Andersen 2007, DeGroot et al. 2007, Schlue et al. 2011,

Quinn et al. 2011, Locat et al. 2015). The strain-softening behaviour is the main reason of progressive large-scale landslides in these sensitive clays.

2.3.1 *Behavior of sensitive clays*

During the Ormen Lange gas field development, an intensive geological and geotechnical investigation was carried out to evaluate potential risks associated with submarine slope failure in this area. The sediments in this area have been categorized in two groups: relatively strong glacial clays and weak marine and/or glaciomarine clays. It is reported that marine clays have a high clay content, plasticity index, high water content, and liquidity index as compared to glacial clays. The marine clays are sensitive, while the glacial clay may be insensitive or slightly sensitive (Kvalstad et al. 2005a, 2005b; Yang et al. 2006, 2007; Lunne and Andersen 2007). Marine clays show significant strain softening behavior during undrained loading as compared to glacial clays (Fig. 2.5a) (Kvalstad et al. 2005a). The behavior of marine clay is very similar to onshore sensitive clay as shown in Fig. 2.5(b) (Locat et al. 2015). Moreover, the marine clays are generally found in normally consolidated to lightly overconsolidated states (Stark and Contreras 1996, Kvalstad et al. 2002, Kvalstad et al. 2005a, Jostad et al. 2006, Lunne et al. 2006, Lunne and Andersen 2007, Andresen and Jostad 2007, Low et al. 2010, DeGroot et al. 2011). For marine clays, Kvalstad et al. (2005a, b) showed that peak shear strength (s_{up}) increases with vertical effective stress (σ'_v) as $s_{up} \approx 0.2\sigma'_v$ in direct simple shear (DSS) conditions that better represents the basal failure through the sensitive clay layer. As shown in Fig. 5(a), post-peak degradation of shear strength could occur at large strains in case of glacial clays (Kvalstad et al. 2005a).

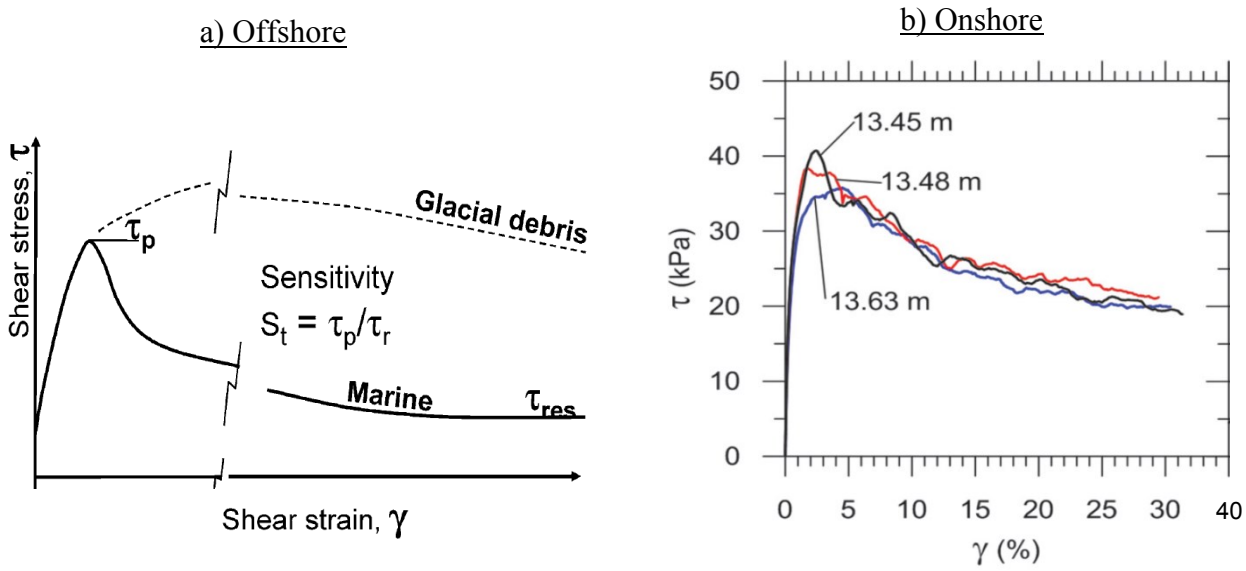

Figure 2.5: Typical stress-strain behaviour: (a) Offshore glacial and marine clays (Kvalstad et al. 2005a), (b) onshore sensitive clay (Locat et al. 2015)

Unlike quick clays which could be highly sensitive, offshore marine/glaciomarine clays are generally moderately sensitive (DeGroot et al. 2007). Post-peak degradation of undrained shear strength (s_u) of sensitive clay occurs with plastic shear strain/displacement. Generally a large displacement/strain is required to reach the remoulded condition; however, in most typical laboratory tests such large strains cannot be accurately achieved. For example, in the experimental study during the Ormen Lange development project (Kvalstad et al. 2005a) and also in other studies (e.g. Lunne et al. 2006), mostly direct simple shear (DSS) and triaxial tests were conducted where shear strains of the order of 20% could be applied. However, in submarine landslides, shear strains in the failure plane could be significantly higher than 20%, and s_u of marine/glaciomarine clays could decrease with strain even after 20%. In other words,

triaxial and DSS tests do not cover the whole range of strains for s_u degradation from the peak to residual.

The collection of high quality soil samples especially soft sensitive clays from deepwater sites involves huge challenges. Higher sample disturbance could significantly change the stress-strain behavior (Lunne et al. 2006, DeGroot et al. 2011). Also, it is very difficult to perform satisfactory field investigations in deepwater sites due to both technical and financial constraints. In most of the cases, sites were investigated after the failure, and laboratory tests were performed to figure out the characteristics of the soil in the failure zone. Since the information of stress-strain behavior of marine sensitive clays, especially at large strain, is very limited, data available on onshore sensitive clays could be utilized for the development of model for post-peak softening behavior of sensitive clays.

As mentioned earlier, standard shear tests (e.g. triaxial, direct shear, simple shear) cannot reach the required strain/displacement level to achieve fully remoulded strength without excessive sample distortion. Vane shear testing is a standard practice to obtain such shear strength at very large deformation. The ring shear test is another promising option for large strain behavior of soil. However, very limited ring shear tests on sensitive clays are available in the literature. For example, a ring shear test on sensitive Drammen clay was reported by Stark and Contreras (1996); however, the test was stopped at less than 60 mm displacement which is small compared to the shear displacement required to reach the residual or remoulded shear strength.

Tavenas et al. (1983) conducted four different tests on sensitive Champlain clays collecting samples from 7 sites in Quebec in eastern Canada. They estimated the strain energy (w_n) required to remould those sensitive clays with various levels of sensitivity. The results were reported in terms of strain energy and reduction in shear strength (remoulding index) as shown in Fig. 2.6a.

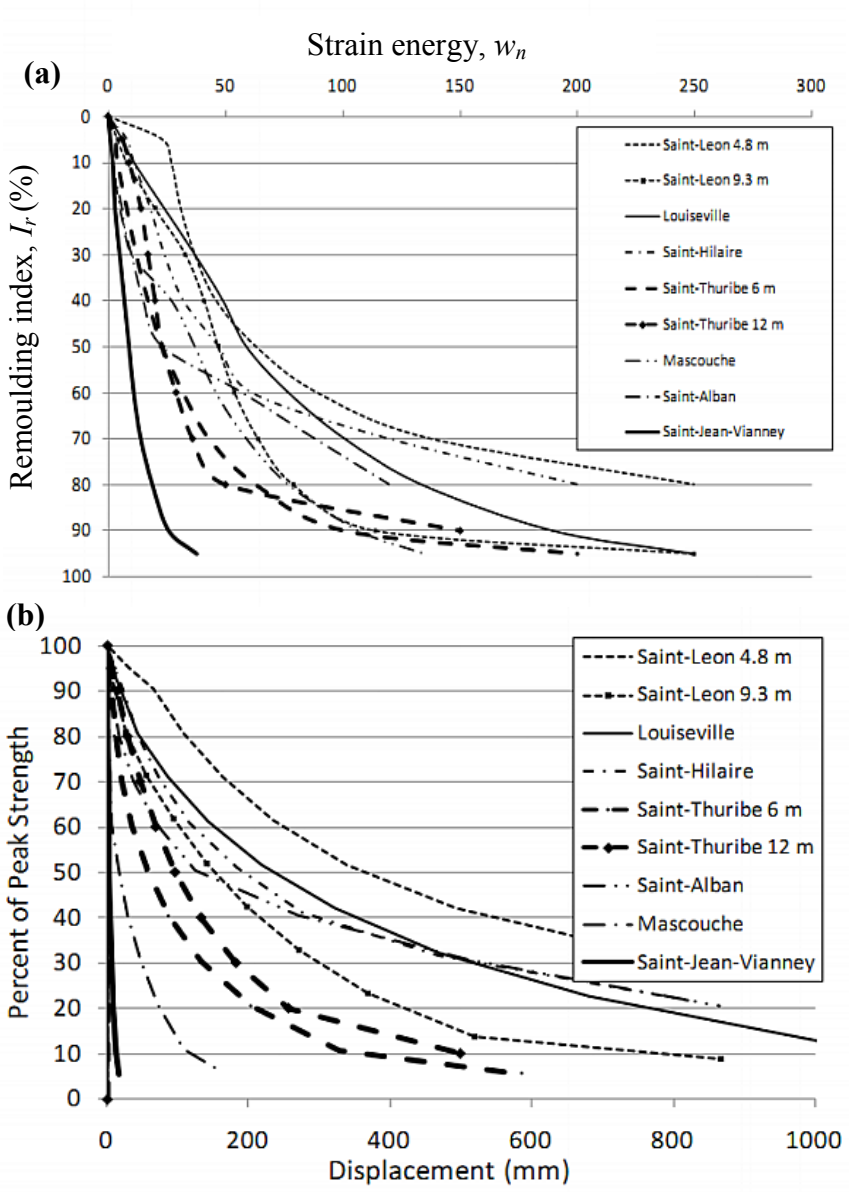

Figure 2.6: Undrained shear strength degradation of Champlain clay (after Tavenas et al. 1983 & Quinn 2009)

Quinn et al. (2011) showed that s_u degradation from small to large strains might be inferred from the test results reported by Tavenas et al. (1983). Based on some realistic assumptions, Quinn et al. (2011) reanalyzed these data and plotted the results in terms of relative displacement (δ) as

shown in Fig. 2.6b. They also argued that it is better to represent the post-peak softening behavior in terms of shear displacement, rather than shear strain, as the shear strains mainly localized in the shear band. Similarly, during the failure of a slope through sensitive clay layers the shear strains localized in narrow shear bands due to post-peak softening.

The following are the key features of s_u/s_{up} vs δ plots in Fig. 2.6(b): (i) s_u decreases nonlinearly with δ and the rate of decrease is high at the beginning and very low at large values of δ; (ii) the rate of decrease of s_u with δ is not the same for all clays tested; (iii) the percentage of reduction from s_{up} is not the same for all clays, and depends upon sensitivity (S_t). Quinn et al. (2011) also showed that the residual shear strength is mobilized at very large displacements (δ_r), as shown in Table 2.2. In most cases, this value cannot be estimated properly because the rate of decrease of s_u at large δ is very small (Fig. 2.6b). For example, they reported δ_r>3.0 m for Saint-Hilaire clay and >5.0 m for Saint-Léon clay from 4.8 m depth. At this stage one important question needs to be answered—does the value of δ_r need to be defined properly in progressive failure analysis and if not, what displacement and corresponding mobilized s_u could be used for an acceptable analysis. Bernander (2000) argued that post-slide investigations does not show relevance of completely remoulded shear strength (s_{ur}) and therefore, recommended an undrained shear strength s_{uR} (>s_{ur}) for progressive failure analysis that mobilizes in the shear band as a result of considerable shear displacement. Further discussion on this issue is provided in Chapters 3–6. In the present study, a non-linear post-peak degradation model is developed using these test data, which is discussed in detail in Chapter 3.

Table 2.2: Estimated shear displacement required to mobilize residual shear strength (after Quinn 2009)

Site	δ_r (mm)
Saint-Léon. 4.8 m	>5000
Saint-Léon. 9.3 m	~2000
Louiseville. 6 m	>3000
Saint-Hilaire	>3000
Saint-Thuribe. 6 m	~1000
Saint-Thuribe. 12 m	~1000
Mascouche. 9 m	~500
Saint-Alban. 6.6 m	>3000
Saint-Jean-Vianney. 30 m	~50

2.3.2 *Loading and Strength Reduction*

Failure might be initiated in a fully stable and/or marginally stable slope depending on the nature of the triggering factors. Loading from different sources such as earthquake, toe erosion, construction or filling, and strength reduction in a section of a weak layer, due to various reasons such as geological activities, pore pressure generation, earthquake and plastic shear deformation, all could trigger the failure of a slope. However, the following is the focus of this study.

Depending upon the location of disturbing agents, progressive failure can be mainly divided into two categories: *upward* and *downward*. Upward progressive failure might be initiated due to excavation, erosion or small slides in river bank slopes (Quinn et al. 2007, Locat et al. 2008, Demers et al. 2013). In the upward progressive failure the disturbing agents are located downslope and therefore, shear band formation or local failure initiates near the toe of the slope, and propagate towards upslope areas (Fig. 2.7a). Examining field evidence, in recent studies (e.g. Locat et al. 2008, 2011, 2013, 2015, Quinn et al. 2011) it is shown that an initial horizontal shear band could form due to erosion, excavation or small slides near the bank. Spreads could result

when the soil mass above this horizontal failure surface are dislocated forming horsts and grabens (Fig. 2.2c). Many spread failures in the literature are reported to be triggered by erosion at the toe of the slope (Bernander 2000, Locat et al. 2008, Quinn et al. 2007, Locat et al. 2011), even though it is very difficult to identify the true triggering mechanisms. The spread type of failures could also be explained by progressive failure mechanisms (Locat et al. 2013).

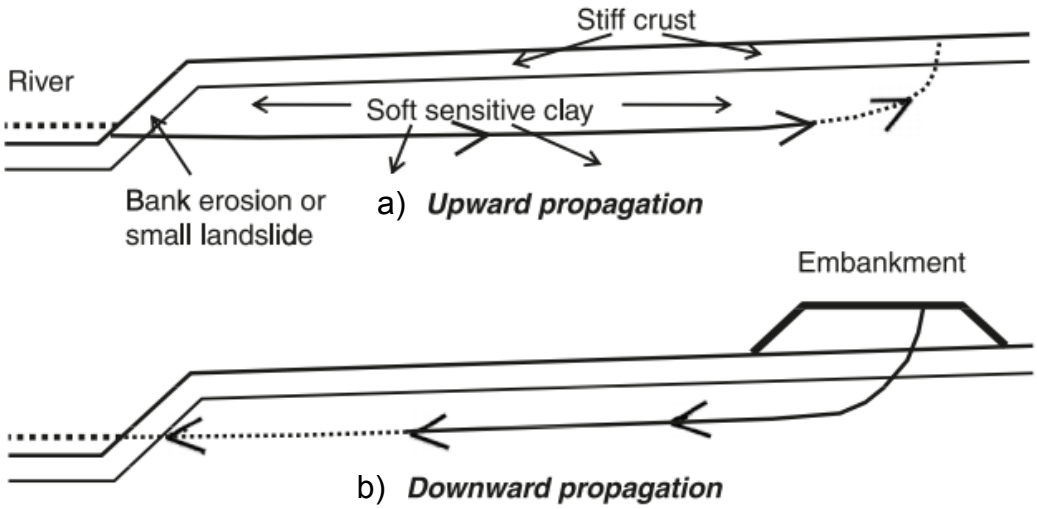

Figure 2.7: Development of upward and downward failure due to river bank erosion and embankment construction respectively (Quinn et al. 2011)

On the other hand, downward progressive failure could be triggered by human activities such as construction, earth filling or pile driving in the upslope areas (Bernander 2000, Gylland et al. 2010). These activities can increase shear stresses along the potential failure planes. When the disturbing agents are in upslope areas, shear bands start to develop near the loaded area and propagate further downslope leading to downward progressive failure (Fig. 2.7b). According to Bernander (2008), downward progressive failures generally occur in long, gently inclined slopes.

Figure 2.8 shows another type of failure, which mainly occurs in long offshore slopes, due to the reduction of shear strength of a section of the weak layer (named as *discontinuity*) that has strain softening behaviour (Lastras et al. 2004, Locat et al. 2014). If the shear stress along the discontinuity is greater than the shear strength, the stress will be transferred to the surrounding soil elements through which shear band propagation might occur if the soil has strain-softening behaviour. Thus the existence of a strain-softening layer and a "discontinuity" might result in propagation of a shear band in an offshore slope both in the upslope and downslope directions at the same time and could trigger large-scale offshore landslides (Fig. 2.8). This type of failure is termed as lateral progressive failure in the literature (Bernander 2000).

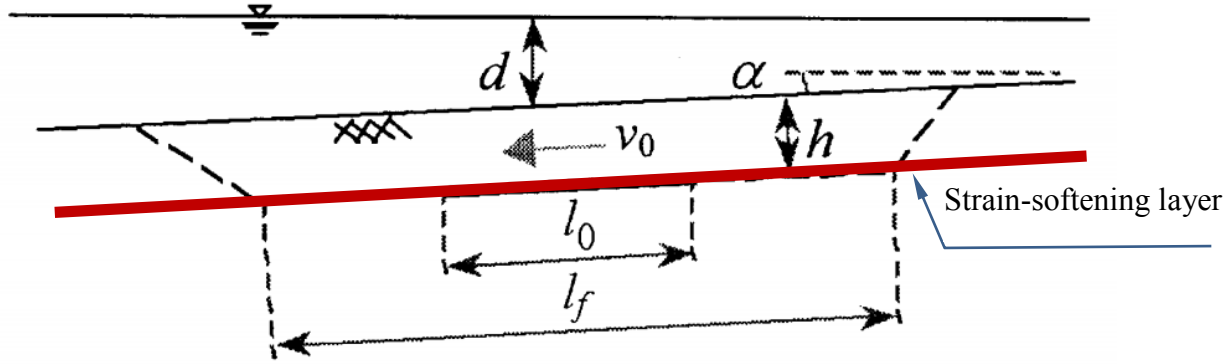

Figure 2.8: Shear band propagation mechanism in submarine landslides (modified after Puzrin and Germanovich 2003)

Both loading and strength reduction might be the causes of initiating large-scale landslides in sensitive clays. A combination of both natural factors (e.g. toe erosion) and human activities (e.g. placement of fill) might trigger an onshore landslide in sensitive clay (L'Heureux et al. 2014).

In summary, the mechanisms involved in slope failures could be different depending upon the triggering factors, soil types and slope geometry. The whole process of slope failure can be divided into four stages: pre-failure, failure, post-failure and re-activation stage. The present study mainly focuses on failure stage and corresponding failure mechanisms. In sensitive clay the failure planes develop progressively by formation of shear bands, which is one of the main focuses of this study. Upward progressive failure leading to spread, combined effects of upward and downward progressive failure on stability of river bank slopes, and lateral progressive failure of offshore slopes are studied.

2.4 Modeling of Progressive Failure of Slopes

The limit equilibrium (LE) method has been widely used to calculate the stability of both offshore and onshore slopes. For example, previous studies used the LE method to assess the stability of submarine slopes assuming an infinite slope (e.g. Karlsrud and Edgers 1982, Lee and Edwards 1986, Hampton et al. 1996, Locat and Lee 2000, Leynaud et al. 2004, Kvalstad et al. 2005a, Brink et al. 2009). Computer programs, such as Slope/W, have been also used in some studies in order to accommodate complex geometry and soil properties (Almagor and Wiseman 1991, Mello and Pratson 1999, Dimakis et al. 2000, Leynaud et al. 2004, Kvalstad et al. 2005b). Although these traditional methods of slope stability analysis might be useful for preliminary analysis, they cannot explain the mechanics of many large-scale landslides in sensitive clays because the failure planes develop progressively due to strain-softening behaviour of the soil.

In a state-of the-art report, Duncan (1996) showed the advantages of FE analysis over limit equilibrium methods for slope stability analysis. Griffiths and Lane (1999) also showed that FE

methods are a powerful alternative approach because, unlike limit equilibrium methods, fewer assumptions are required and the failure occurs through the zones where shear stress reaches the shear strength of the soil. Most of the FE models developed at that time for slope stability analysis were in the purely Lagrangian framework. One of the main disadvantages of these types of FE models is that significant mesh distortion occurs around the failure planes and the solutions generally suffer from mesh dependency, numerical instabilities and lack of convergence. The non-convergence to a solution due to significant mesh distortion has been considered as one of the conditions of failure in some studies (e.g. Griffiths and Lane 1999). The application of FE methods becomes further complex in stability analysis of slopes in soils with strain softening behaviour because this problem is associated with very large deformation, and large strain concentration occurs in narrow zones forming shear bands. Moreover, most of the failure of slopes in sensitive clays is progressive in nature. Approaches available in the literature to model progressive failure of slopes in sensitive clays are discussed in the following sections.

A number of attempts have been taken in the past to study the progressive failure mechanism involved in slope failure with a strain-softening clay layer. Using FE methods, Lo and Lee (1973) developed computer programs to determine the stresses and displacements in an onshore sensitive clay slope. Kovacevic et al. (2004, 2007) conducted FE modeling of progressive failure in excavated clay slopes of stiff OC clays. Moreover, FE methods have been used for progressive failure analyses of slopes and embankments in drained conditions (e.g. Potts et al. 1990, Conte et al. 2010). As the drained analysis is not the focus of the present study, the literature review presented in the following sections is on undrained analysis of clay slopes having strain softening behaviour.

Upward Progressive Failure

Several decades ago it was recognized that the existence of a horizontal weak layer could explain the upward progressive failure leading to spreads (Odenstad 1951, Carson 1977). In recent years, attempts have been taken to model upward progressive failure of slopes in sensitive clays in onshore environments (e.g. Bernander 2000, Locat et al. 2008, 2011, 2013, Quinn et al. 2011, 2012). By examining field evidence, it has been shown that an initial horizontal shear band might form due to erosion, excavation or small slides near the bank (e.g. Locat et al. 2008, 2011, 2013, 2015, Quinn et al. 2011). Locat et al. (2011) demonstrated the mechanisms of quasi-horizontal shear band formation in an infinite slope by applying an external force parallel to the ground surface near the toe above the predefined shear zone. The soil above the shear zone is assumed to be linear elastic. The variation of shear stress, in relation to the shear strength, with distance from the point of load is discussed. Locat et al. (2013) extended their work (Locat et al. 2011) through numerical modeling using PLAXIS 2D (PLAXIS, 2011) and BIFURC (Jostad and Andresen 2002) FE programs. In this decoupled modeling, the initial stresses of soil are calculated using the PLAXIS 2D with the Mohr-Coulomb model. The calculated stresses from PLAXIS are then used in BIFURC to simulate the initiation and progression of a quasi-horizontal shear band, simply by pulling the top of the predefined shear zone at the toe of slope (see Fig. 2.9). The strain softening behaviour of the predefined failure zone was modeled using a zero thickness interface element. A linear post-peak strength degradation model was considered where failure is assumed in simple shear condition (Fig. 2.10).

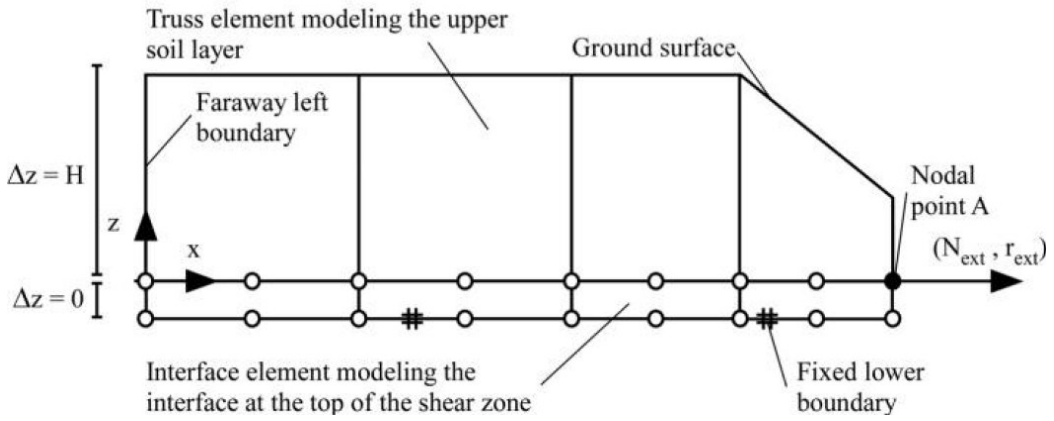

Figure 2.9: Schematic representation of the model used by Locat et al. (2013) to model upward progressive failure

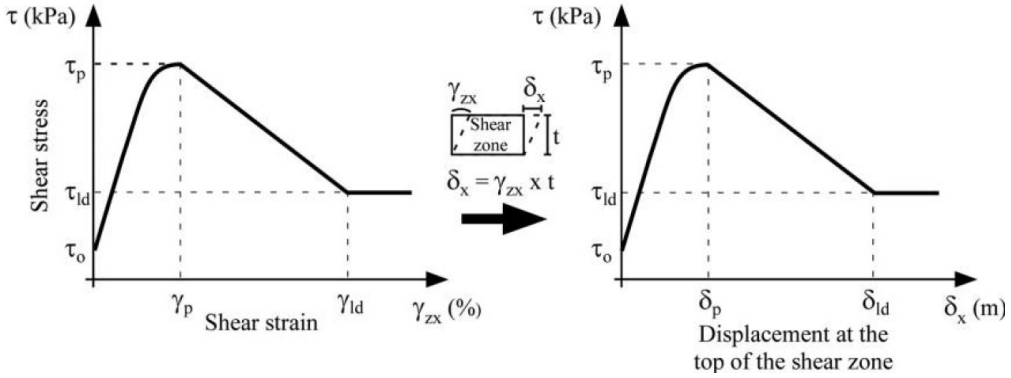

Figure 2. 10: Stress-displacement behavior considered in Locat et al. (2013) FE modeling

Using the concepts of linear elastic fracture mechanics (LEFM) (Palmer and Rice 1973), Quinn et al. (2011) proposed an analytical model for development of a shear band in an infinite slope with a vertical step cut (see Fig. 2.11). The critical length required to initiate the propagation of the shear band is calculated. They hypothesize that the failure of the slope would occur when the length of the shear band is sufficiently large such that the downward unbalanced force could cause active shear failure (Fig. 2.11). Linear strength degradation s_u from peak to residual was assumed along the end zone (ω). For any point outside the band, even after the end point of the

shear band, elastic stress-strain behavior was assumed. Note that similar problems were also examined by previous researchers (e.g. Christian & Whitman 1969, Palmer & Rice 1973, Chowdhury 1978) to determine the shear band propagation criteria. Using the *J*-integral (fracture mechanics) approach, Palmer and Rice (1973) presented a solution assuming that the band length (*l*) is large enough compared to the thickness of the layer (*h*) and end zone (ω). The analyses were performed for OC clay under drained conditions. On the other hand, Chowdhury (1978) assumed an arbitrary distribution of shear resistance along the shear band during the development of shear band propagation criteria.

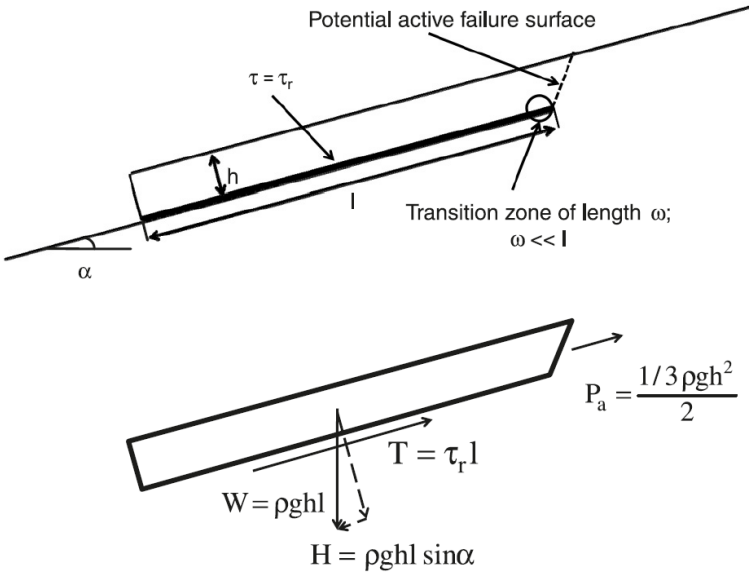

Figure 2. 11: Propagation of shear band in an infinite slope due to vertical cut (Quinn et al. 2011)

The main difference between Palmer and Rice (1973) and Quinn et al. (2011) is that Quinn et al. (2011) performed an undrained analysis in determining the shear band propagation criteria in sensitive clays instead of drained analysis of OC clays. Quinn et al. (2011) also showed that the end zone length (ω) decreases with an increase in sensitivity. Quinn et al. (2012) also conducted

some preliminary FE analysis to demonstrate the effects of erosion on the propagation of a shear band through a weak predefined shear zone utilizing fracture mechanics principles.

While these attempts partly explain the mechanics involved in shear band formation, the complete process of upward progressive failure leading to spread was not simulated. These studies have some limitations. They could simulate the formation of a quasi-horizontal shear band only, because the soil above the shear zone is assumed to be elastic. They also assumed that the global failure occurs when the active failure condition is reached. With their numerical modeling techniques, the formation of subsequent horsts and grabens (Fig. 2.2c) could not be simulated. The present study simulates the complete process using an advanced FE approach incorporating a nonlinear post-peak softening model of sensitive clays.

Downward Progressive Failure

Studies on modeling of downward progressive failure are very limited. As mentioned earlier (Fig. 2.7b), in case of downward progressive failure the disturbing agents (e.g. embankment construction) are in upslope areas and the shear band formation initiates upslope. Bernander (2000, 2008) presented a finite difference method to simulate the downward progressive failure of long infinite slopes. The effect of fill in the upslope area was idealized as a downward force (N_x) acting parallel to a predefined failure plane. The failure zone was defined as a sensitive clay layer with strain softening behaviour, while the soil above the failure plane was assumed to be elastic. The post-peak softening behaviour of the sensitive clay in the failure zone was modeled by decreasing linearly the mobilized undrained shear strength (s_u) with shear displacement. Increasing N_x with time, the propagation of shear band and the variation of shear stress along the

predefined failure planes were examined. This model was further used by Locat et al. (2011) to explain some features of downward progressive landslides. Andresen and Jostad (2007) modeled downward progressive failure using the BIFURC FE program where the strain softening behaviour of the predefined failure zone was modeled using a finite thickness interface element. They highlighted the importance of strain softening behavior of marine clays and FE modeling of progressive failure in the case of offshore slope stability analysis. Gylland (2012) extended this work further and showed the effects of some key input parameters such as in situ shear stress along the failure plane, brittleness, stiffness of soil mass, etc. on the stability of the slope.

Toe erosion may not always cause a global failure. Without causing any global failure, toe erosion or excavation could simply create a shear band which may not be visible or detected during geotechnical investigation even though it might be a segment of a critical failure plane. This is because the shear strength in the shear band might be significantly reduced due to strain softening behaviour of the soil. Depending upon soil properties and loading conditions in upslope areas, shear band propagation might continue towards the initially developed shear band due to toe erosion. The combined effects of these two triggering factors may or may not cause global failure of the slope. These issues are investigated in this study as presented in Chapter 5.

Analytical Modeling of Offshore Landslides

Based on the concept of shear band propagation, Puzrin and Germanovich (2005) developed analytical models to calculate the stability of an infinite slope using three different approaches: LEFM, energy balance and process zone. It is assumed that a “discontinuity” parallel to the seabed (solid thick line in Fig. 2.12a) has been formed in the strain softening layer. The

undrained shear strength in this discontinuity reduces to its residual value. However, shear resistance gradually increases from the residual to peak value within the end zones ω_1 and ω_2 (dashed lines in Fig. 2.12a) with distance from the discontinuity. Using a linearly decreasing post-peak stress-displacement relationship they showed that if the length of the discontinuity exceeds a critical length (l_{cr}) the propagation of the shear band will continue parallel to the slope, and at one stage a global failure will occur at $l=l_f$ by forming two inclined failure planes as shown in Fig. 2.12(b).

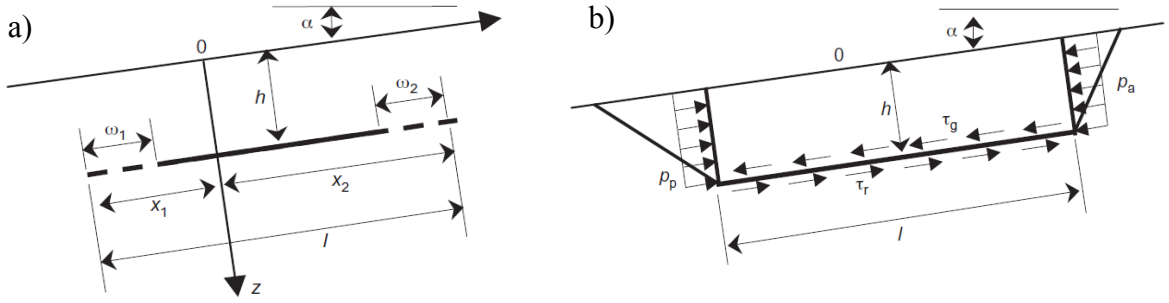

Figure 2.12: Shear band propagation caused by discontinuity parallel to the slope; a) geometry, b) equilibrium at failure (after Puzrin et al. 2004)

Although these analytical solutions can explain the failure mechanisms of an offshore slope up to the first global failure, they cannot model the subsequent, possibly retrogressive failure. They cannot be used for any geometry other than an infinite slope and therefore, numerical modeling is warranted. Moreover, the post-peak softening curves of sensitive clays are not linear as shown in Fig. 2.6. Therefore, the problem stated in Fig. 2.12(a) is further considered in this study, and a new method is presented in Chapter 3 to evaluate the potential failure mechanisms of submarine

slopes having a marine sensitive clay layer where nonlinear strain softening behavior of sensitive clays is incorporated.

Numerical Modeling of Submarine Landslides

During the development of the Ormen Lange gas field in offshore Norway, analytical/numerical methods were developed for analyzing the progressive failure of submarine slopes in sensitive clays in order to assess the risks associated with this geohazard. Researchers at the Norwegian Geotechnical Institute (NGI) (Jostad and Andresen 2002, 2004, Andresen and Jostad 2002, 2004, 2007, Kvalstad et al. 2005a, 2005b, Jostad et al. 2006, Thakur 2007, Gylland et al. 2010, Gylland 2012) put huge efforts into modeling of progressive failure of slopes and associated strain localization zones (shear band) developing the computer program BIFURC. Andresen (2001) conducted numerical simulations to evaluate the effects of undrained strain softening behavior of a sensitive clay layer on the development of progressive failures in the Storegga slopes using PLAXIS software (PLAXIS 2001) and BIFURC. Unloading of the headwall was considered as a triggering factor. Simulations were carried out considering a thick non-sensitive normally consolidated clay layer resting on a sensitive clay layer over a strong base. However, the FE analyses suffered from significant mesh distortion and the location of shear bands were inferred from the strain concentrated zones in FE model (Fig. 2.13a). FE results also show that softening of the base layer could have occurred during the unloading process (Kvalstad et al. 2005a). Jostad and Andresen (2002, 2004) introduced interface elements to model the strain softening behaviour of the predefined failure zone (shear band) and claimed that finite thickness interface elements could better model the behaviour than zero thickness interface elements.

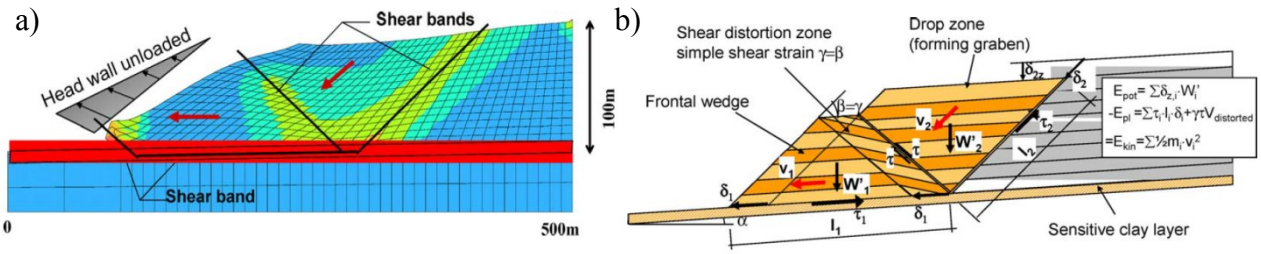

Figure 2.13: a) FE analysis of the Storegga slope with strain-softening layer and formation of shear bands, b) Wedge (tri-block) model (after Kvalstad et al. 2005a)

Based on observed shear bands shown by distorted mesh in FE model, Kvalstad et al. (2005a) proposed a simplified tri-block/wedge model (Fig. 2.13b) and solved for the displacement of the blocks using the energy principle (upper bound solution) to evaluate the dynamics in the initial run-out phase of a slide. As shown in Fig. 2.13(b), the model consists of an intact front wedge (triangle) moving down on the basal slip plane by the weight of a rhombus (shear distorted zone) and another triangle (drop zone) sliding down along a steep inclined slip surface. The motion of the blocks will continue until the released potential energy is dissipated by friction (i.e. kinetic energy is zero). Instead of doing any FE analysis, the modeling of retrogressive sliding was carried out simply extending this single wedge/tri-block model further to a large number of tri-blocks as shown in Fig. 2.14. The final shape of the failed soil mass depends on drop height (Δh) and inclination of the frontal wedge (β) (Fig. 2.14). Calculating released potential energy, and dissipated energy along slip surfaces and in internal shear of failed soil blocks, they determined the final number of tri-blocks. The run-out length of the slide was then calculated based on the number of tri-blocks and geometry.

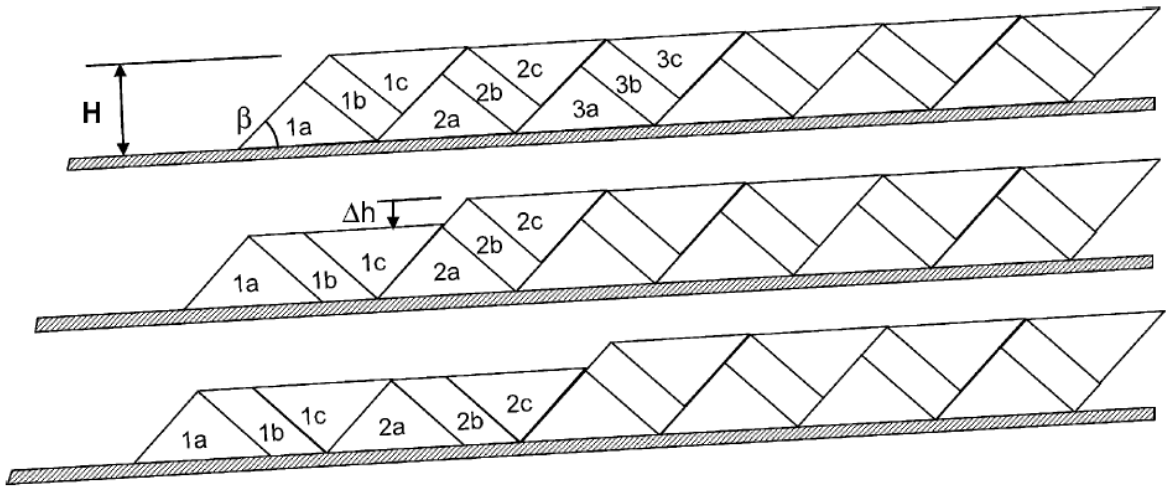

Figure 2.14: Retrogressive multi-wedge model (Kvalstad et al. 2005a)

Gauer et al. (2005) used the concept of computational fluid dynamics and simulated the retrogressive development of the last phase of the Storegga slide (Fig. 2.15). Shear strength of the marine clay was modelled as a Bingham fluid with strain softening yield strength and simulations were carried out for different rate of strain softening. It is shown that simulation results could reproduce a retrogressive sliding process with a final deposition pattern similar to the morphology observed in the upper part of the slide scar.

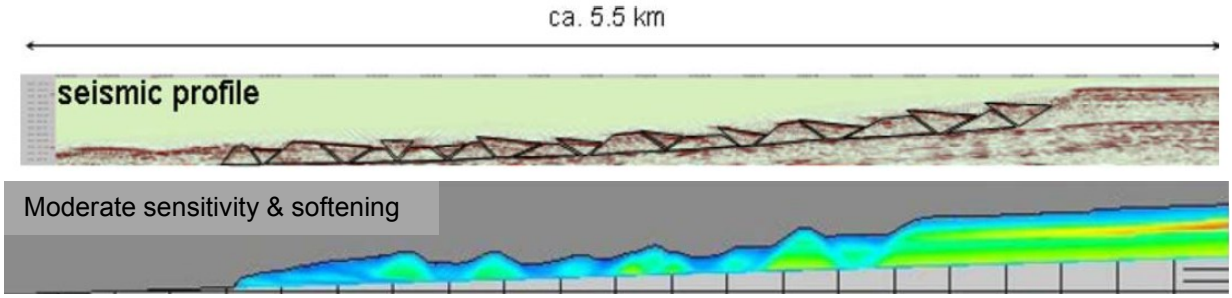

Figure 2.15: Comparison between seismic profile and final deposition pattern from numerical simulation (after Gauer et al. 2005)

2.5 Summary

Progressive failure could occur in both onshore and offshore environments, and failure could be catastrophic especially if there is the presence of a sensitive clay layer. Undrained post-peak softening behavior of sensitive clays is the main reason for progressive failure of slopes containing such clays. Test results indicate nonlinear post-peak softening behavior of sensitive clays.

Very limited numerical studies are available in the literature for modeling progressive failure. Most of them are limited to idealized conditions, such as infinite slopes, predefined shear zones, ideal triggering effects (such as concentrated force) and elastic behaviour outside the shear bands. One of the main challenges in FE modeling of sensitive clay slopes is that significant strains accumulate in the shear band and therefore, the typical FE approach in Lagrangian framework cannot model such behavior because excessive mesh distortion occurs in the shear band. In order to overcome these issues, large deformation FE analyses are performed in this study using an advanced FE modeling technique incorporating an appropriate soil constitutive model for undrained behaviour.

CHAPTER 3

Modeling of Large Deformation Behaviour of Marine Sensitive Clays and Its Application to Submarine Slope Stability Analysis

Co-Authorship: This chapter has been submitted as a technical paper for publication in a journal as: Dey, R., Hawlader, B., Phillips, R. and Soga, K. (2015) "Modeling of large deformation behaviour of marine sensitive clays and its application to submarine slope stability analysis."
Most of the research work presented in this chapter was conducted by the first author. He also prepared the draft manuscript. The other authors supervised the research and reviewed the manuscript.

3.1 Abstract

Post-slide investigations show that marine sensitive clay layers contribute to causing many large-scale submarine landslides. In this paper, a nonlinear mathematical model for post-peak degradation of undrained shear strength of sensitive clay, applicable to small- to large-strains, is proposed based on experimental results. A new method for the estimation of model parameters is also presented. Incorporating the new model, an analytical solution is developed to examine possible mechanisms of failure of mild submarine slopes. Analyses are performed for a new class of problem involving a weak zone of low shear strength (discontinuity). Post-peak progressive development of zones of large inelastic shear deformation (shear bands) due to strain-softening behaviour of sensitive clays occurs both in upslope and downslope directions. When the length of the discontinuity is greater than a critical length, shear band propagation

continues that could result in a large-scale offshore landslide. A simple design chart is provided to calculate the critical length. Traditional limit equilibrium analyses cannot explain such progressive development of a large failure plane.

Key words: sensitive clay; large deformation; submarine landslides; shear band; undrained shear strength

3.2 Introduction

Submarine landslides near the base of the continental slope are a major threat to many offshore facilities such as pipelines, foundation systems and wellheads. The occurrence of numerous submarine landslides has been reported in the literature—some of them are small while some are very large such as the Storegga slide in the Norwegian Sea or the Grand Banks slide in offshore Newfoundland. Using advanced technologies, some slide morphologies and potential causes have been explained (Hampton et al. 1996; McAdoo 1999; Locat and Lee 2000, 2002; Canals et al. 2004; Sultan et al. 2004; Gee et al. 2005; Solheim et al. 2005; Krastel et al. 2006; Masson et al. 2006; Locat et al. 2009; Twichell et al. 2009; Conway et al. 2012) and some risk frameworks have been proposed (Lee and Edwards 1986; Lee et al. 1991; Angell et al. 2003; Nadim et al. 2003, 2005; Nadim and Locat 2005; Niedoroda et al. 2003; Masson et al. 2006; Mosher 2009; Laccase & Nadim 2009). Offshore slopes are typically very mild (<10°, Hadj-Hamou and Kavazanjian 1985). Therefore, the question is why such large-scale landslides occur in mild slopes. Post-slide field investigations show that the existence of a marine sensitive clay layer could be one of the main causal factors of many offshore landslides (Dan et al. 2007; Sultan et al.

2010). Dan et al. (2007) identified the existence of sensitive clay layers between 30 and 45 m below the seabed near the 1979 Nice harbour catastrophe area. Their analysis shows that the failure of the slope was progressive in nature through the sensitive clay layers. Thin layers of interbedded marine/glacimarine clay layer were also encountered in many other places (e.g. Laberg et al. 2003; Yang et al. 2006; Bryn et al. 2005; Solheim et al. 2005). As an example, Fig. 3.1 shows the stratigraphic sub-division of the layers involved in Storegga slide inferred from a field investigation, including seismic profiles, geoborings up to several hundred meters below the seabed and geotechnical laboratory testing (Bryn et al. 2005). The failure occurred through the marine/glacimarine sensitive clay layers. Over the last decades the focus on mapping and characterization of weak layer has increased significantly (Lastras et al. 2004; Kvalstad et al. 2005a; L'Heureux et al. 2010; L'Heureux et al. 2012; Locat et al. 2014). Locat et al. (2014) discussed the formation and role of weak layers on submarine landslides and highlighted that the strain softening behaviour of a weak layer could be the cause of many large-scale progressive failures in mild submarine slopes. Many studies also reported that the failure initiates locally in a section of the weak zone and then propagates. Therefore, the role of a weak layer in triggering a landslide is twofold. The shear strength of a section of the weak layer might be decreased due to various reasons such as geological activities, pore pressure generation, earthquakes and plastic shear deformation (Lastras et al. 2004; Locat et al. 2014), which could create a "discontinuity." If the shear stress along the discontinuity is greater than the reduced shear strength, the stress will be transferred to the surrounding soil elements through which shear band propagation might occur if the soil has strain-softening behaviour.

Limit equilibrium analyses has been used for stability assessment of submarine slopes (e.g. Karlsrud and Edgers 1982; Lee and Edwards 1986; Hampton et al. 1996; Lee and Baraza 1999;

Brink et al. 2009; Leynaud et al. 2004; Kvalstad et al. 2005a). While some of the researchers used computer programs, such as Slope/W, in order to accommodate complex geometry and soil profiles, a large number of studies simply assume infinite slope conditions (Almagor and Wiseman 1991; Mello and Pratson 1999; Dimakis et al. 2000; Leynaud et al. 2004; Kvalstad et al. 2005b; Nixon and Grozic 2007). One of the major limitations of the limit equilibrium method is that it cannot explain the progressive development of a failure surface due to post-peak softening of sensitive clays. The formation of large inelastic shear deformation zones (shear bands) in the sensitive clay layer and its propagation could explain the development of a failure surface and many other mechanisms involved in these large landslides, as discussed in this paper. In the past, progressive failure of onshore slopes with sensitive clays has been analyzed for some idealized conditions (e.g. Locat et al. 2008, 2011, 2013; Quinn et al. 2011). Using the concepts of linear elastic fracture mechanics (LEFM) (Palmer and Rice 1973), Quinn et al. (2011) proposed an analytical model for development of a shear band in an infinite slope with a vertical step cut. Quinn et al. (2012) conducted FE analysis to demonstrate the effects of toe erosion on propagation of a shear band through a weak predefined shear zone. Locat et al. (2011) demonstrated the mechanisms of shear band formation for an idealized condition in an infinite slope by applying an external force parallel to the ground surface near the toe above a predefined shear zone. Locat et al. (2013) extended their work (Locat et al. 2011) through numerical modeling using PLAXIS 2D (PLAXIS 2011) and BIFURC (Jostad and Andresen 2002) FE programs. The role of a shear band in long-term progressive failure of overconsolidated clay slopes has also been investigated by a number of researchers (Skempton 1964; Bjerrum 1967; Bishop 1967; Lo 1972; Burland et al. 1977; Take and Bolton 2001). Moreover, FE methods have been used for progressive failure analyses of slopes and embankments in drained conditions (e.g.

Potts et al. 1990; Conte et al. 2010). The authors of the present study also conducted large-deformation FE analyses to model spread due to toe erosion as observed in onshore sensitive clay slopes (Dey et al. 2015a). However, the focus of the present study is to model submarine slope failure under undrained conditions involving a sensitive clay layer.

The failure of an onshore sensitive clay slope might occur due to toe erosion and upslope loading that result in upslope and downslope propagation of shear bands, respectively. However, in a long offshore slope, the existence of a weak layer and a discontinuity might result in propagation of a shear band both in the upslope and downslope directions at the same time (Puzrin and Germanovich 2005). Puzrin and Germanovich (2005) solved this problem for a long infinite slope using three different approaches: LEFM, energy balance and process zone. They showed that, if the length of the discontinuity exceeds a critical length, the shear band propagation will continue leading to large-scale catastrophic global failure. Their analyses also show that post-peak softening significantly influences the results.

The aim of this study is to present a mathematical model for post-peak nonlinear stress-strain behaviour of sensitive clays based on experimental results available in the literature. This model is then used to calculate shear band propagation that could cause large-scale submarine landslides. Detailed mathematical formulations and a parametric study are also presented.

3.3 Problem Definition and Assumptions

Figure 3.2 shows the geometry of a typical offshore slope inclined at an angle β. In most real cases, the soil is not homogeneous and may have different soil layers similar to the one shown in Fig. 3.1. The slope might contain strain softening clay layer(s) such as marine clay. In Fig. 3.2, the upper soil layer represents a relatively strong soil such as glacial clay. Below the upper soil

layer of thickness h, a strain-softening layer, such as a marine clay layer, is assumed. The thickness of the softening layer could be very thin to a couple of meters. In this study, a thin marine clay layer is considered. Multiple strain softening clay layers might be encountered in the field (e.g. Fig. 3.1); however, for simplicity, this study considers only one strain-softening clay layer. It is also assumed that the lower soil layer below the strain softening clay layer is stronger than the strain-softening layer. The geometry of the problem shown in Fig. 3.2 is similar to Puzrin et al. (2004) and Puzrin and Germanovich (2005). Similar to those studies, the following three assumptions are made: (i) a discontinuity parallel to the seabed (solid thick line *CD* in Fig. 3.2) has been formed in the strain softening clay layer (Puzrin and Germanovich 2005); (ii) the undrained shear strength in the discontinuity is reduced because of significant plastic deformation along this sliding plane; and (iii) the length of discontinuity is considerably larger than its depth. If limit equilibrium analysis is performed on this scenario, failure of the slope may not be predicted as discussed later. Moreover, submarine slope failures occur over a large distance and in some cases several kilometers length (Masson et al. 2006). Now the question is whether this large failure plane is formed by an extension of the discontinuity in the form of shear band propagation, and if so, what is the minimum length of discontinuity required to initiate continuous shear band propagation such that it extends over a sufficiently large distance to cause a global failure of the slope. In order to answer these questions, the strain-softening behaviour of the weak sensitive clay layer is investigated first.

3.4 Modeling of Post-Peak Shear Strength Degradation of Sensitive Clay

Based on high resolution seismic profiles and close examination of the Storegga Slide morphology, previous studies (e.g. Bryn et al. 2005; Gauer et al. 2005) showed that the failure pattern of this submarine slope is very similar to onshore large-scale landslides through sensitive clays commonly encountered in Eastern Canada and Scandinavia. However, unlike quick clay which could be highly sensitive, offshore marine/glacimarine clays are generally moderately sensitive (DeGroot et al. 2007). Post-peak degradation of undrained shear strength (s_u) of sensitive clay occurs with plastic shear strain/displacement. Generally a large displacement/strain is required to reach the remoulded condition; however, in most typical laboratory tests such large strains cannot be applied. For example, in the comprehensive experimental study during the Ormen Lange development project (Kvalstad et al. 2005a) and also in other studies (e.g. Lunne et al. 2006), mostly direct simple shear (DSS) and triaxial tests were conducted where shear strains of the order of 20% could be applied. However, in submarine landslides, shear strains in the failure plane could be significantly higher than 20%, and s_u of marine/glaciomarine clays generally decreases with strain even after 20%. In other words, triaxial and DSS tests do not cover the whole range of strains for s_u degradation from the peak to residual.

Quinn et al. (2011) showed that s_u degradation from small- to large- strain might be inferred from different types of tests as conducted by Tavenas et al. (1983). Conducting four different types of tests, Tavenas et al. (1983) reported the variation of s_u with strain energy for marine sensitive Champlain clays collected from 7 sites in Quebec in eastern Canada. Based on some realistic assumptions, Quinn et al. (2011) reanalyzed these data and plotted the results in terms of relative displacement (δ) as shown by the symbols in Fig. 3.3. These data are used for

development of a post-peak s_u degradation model although the authors understand that more experimental studies are required.

The following are the key features of s_u/s_{up} vs δ plots in Fig. 3.3: (i) s_u decreases nonlinearly with δ and the rate of decrease is high at the beginning and very low at large values of δ; (ii) the rate of decrease of s_u with δ is not the same for all clays tested, (iii) the percentage of reduction from s_{up} is not same for all clays, which depends upon sensitivity (S_t). In order to capture these features, the following exponential function is proposed for post-peak s_u variation, as shown in Fig. 3.4.

[1] $$s_u = (1+(S_t-1)e^{-3\delta/\delta_{95}})s_{uR}$$

where s_u is the mobilized undrained shear strength at δ; δ_{95} is the value of δ at which the undrained shear strength is reduced by 95% of (s_{up}-s_{uR}) and S_t=s_{up}/s_{uR}. Equation (1) is similar to the strength degradation equation proposed by Einav and Randolph (2005), but in terms of δ not in plastic shear strain.

Quinn et al. (2011) showed that the residual shear strength is mobilized at very large displacements (δ_r). In most cases, this value cannot be estimated properly because the rate of decrease of s_u at large δ is very small (Fig. 3.3). For example, they reported δ_r>3.0 m for Saint-Hilaire clay and >5.0 m for Saint-Léon clay from 4.8 m depth. At this stage one important question needs to be answered—does the value of δ_r need to be defined properly in progressive failure analysis and if not, what displacement and corresponding mobilized s_u could be used for an acceptable analysis. Bernander (2000) argued that post-slide investigations does not show relevance of completely remoulded shear strength (s_{ur}) and therefore recommended an undrained shear strength s_{uR} (>s_{ur}) for progressive failure analysis that mobilizes in the shear band as a

result of considerable shear displacement. The following method is proposed to estimate the two model parameters (δ_{95} and S_t) in Eq. (1).

To estimate S_t, find the value of s_u/s_{up} when the slope of s_u/s_{up} vs δ curve is very small, as shown by large open circles in Fig. 3.3. The vertical coordinates of these points represent s_{uR}/s_{up}. The inverse of s_{uR}/s_{up} gives an approximate value of S_t. Table 3.1 shows the values of estimated S_t for the marine sensitive clays presented in Fig. 3.3. The sensitivity of these clays would be higher if the completely remoulded shear strength (s_{ur}) is considered (Tavenas et al. 1983; Quinn et al. 2011); however, that may not have significant effects on the initiation of slope failure as discussed below (also see Bernendar 2000).

Although reasonable estimation of s_{uR}/s_{up} is possible, estimation of δ at this s_{uR}/s_{up} is not easy because a slight change in s_{uR}/s_{up} results in a large variation of δ as the curve is very flat in this range of δ. In the proposed model (Eq. 1), δ_{95} is required instead of δ at s_{uR}/s_{up}. To estimate δ_{95}, the following steps are followed:

(i) Calculate s_u/s_{up} for 50% reduction of (s_{up}-s_{uR}), denoted as s_{u50}/s_{up} (Fig. 3.4), as

[2] $$\frac{s_{u50}}{s_{up}} = \left(1 + 1/S_t\right)/2$$

which is shown by large open triangles in Fig. 3.3.

(ii) From test results find the value of δ required to mobilize s_{u50}/s_{up}, which is denoted as δ_{50} (Fig. 3.4). As an example, δ_{50} for Louiseville clay (183 mm) is shown in Fig. 3.3 by a vertical arrow.

(iii) Rearranging Eq. (1) and inserting s_u=s_{u50} and δ=δ_{50}, the value of δ_{95} can be calculated as

[3] $$\delta_{95} = -\frac{3\delta_{50}}{\ln\left(1 - S_t\left(s_{u50}/s_{up}\right)\right)/(S_t - 1)}$$

Table 3.1 shows calculated values of δ_{95} for these soils. Now, using the values of S_t and δ_{95}, the post-peak variation of s_u are calculated using Eq. (1), which are shown by the solid lines in Fig. 3.3. The calculated s_u/s_{up} matches reasonably well with the test results for a wide range of δ.

In above calculations, the point at 50% reduction of (s_{up}-s_{uR}) is considered because at lower displacements a slight change in δ results in a significant change in s_u while at large displacements a small change in s_u significantly changes the value of δ. Both δ and s_u are required in the calculation of δ_{95} as shown in the right side of Eq. (3). Eq. (1) fits better with test data for a wide range of δ if the point at 50% reduction of (s_{up}-s_{uR}) is considered as discussed above.

A question still remains—what is the effect of S_t as it has been estimated from the flat segment of the s_u/s_{up} vs δ curve. To show this effect, assume that there are ±10% error in estimation of S_t. Now using 110% and 90% sensitivity values of column 2 in Table 3.1 and following steps (i)–(iii) the values of δ_{50} and δ_{95} are recalculated and are shown in parentheses in columns 3 and 4 in Table 3.1. The dashed and dotted lines in Fig. 3.3 show the variation of s_u/s_{up} for 110% and 90% of S_t, respectively. Small difference between these curves suggests that ±10% error in estimation of S_t does not change the post-peak strength degradation curves significantly.

Eq. (1) is rearranged in a form similar to Skempton's "Residual Factor" (Skempton 1964) as

$$[4] \qquad (s_{up} - s_u)/(s_{up} - s_{uR}) = 1 - e^{-3\delta/\delta_{95}}$$

Figure 3.5 shows that Eq. (4) can model the trend of test data very well in this normalized form. The proposed post-peak softening model (Eq. 1 or 4) has the following advantages. It can model the nonlinear degradation of s_u with δ. The model parameter S_t is obtained from the lower part of the s_u/s_{up} vs δ curve where a small variation of s_u occurs with δ and therefore potential error in

estimation of s_{uR} is low. However, the other key model parameter δ_{95} is not estimated from the lower part, because potential error in estimation could be high. The linear models (L1–L3) shown in this figure is discussed later.

In the following section, this model (Eq. 1) is used to examine shear band propagation in a submarine slope having a layer of sensitive clay (Fig. 3.2).

3.5 Shear Band Propagation in Submarine Slopes

As Eq. (1) is an exponential curve, a very large δ is required to mobilize s_{uR}. Therefore, in this analytical formulation the strength degradation from s_{u95} to s_{uR} is defined by a step decrease at δ_{95}, which means that the curve *bcc′d* is used instead of *bcd* (Fig. 3.4). If the shear strength in the discontinuity is less than the shear stress in the *x* direction, the downward driving force will be transferred to the adjacent soil elements near both ends of discontinuity (Fig. 3.2), which creates two end zones in the softening layer (BD and CA) where s_u gradually increases from s_{u95} (at D and C) to s_{up} (at A and B) as a function of relative displacement between the upper soil and the strain-softening clay layers (δ). These transition zones BD and CA are referred to as "end zones" and are shown by thick dashed lines in Fig. 3.2. In other words, $s_u(x)=s_{uR}$ in the discontinuity and $s_{u95}\leq s_u(x)\leq s_{up}$ in the end zones. The effect of this assumption is also shown later in this paper by a step decrease of s_u at $2\delta_{95}$.

The sum of the lengths of the discontinuity and end zones (ω_1, ω_2) defines the total length of shear band, l (*AB* in Fig. 3.2). In other words, $s_u\leq s_{up}$ in the shear band. In the absence of any additional triggering effects, two possible scenarios might be encountered: (i) a short discontinuity could generate two end zones but the slope is globally stable; (ii) if the length of

discontinuity exceeds a certain length, shear band propagation continues over a large distance which might cause a catastrophic global failure.

Referring to Fig. 3.2, as the vertical stress increases with depth, the normal stress acting on a plane perpendicular to the slope (σ_x) also increases with depth. Assume that the average σ_x over depth h is $\overline{\sigma}_x$, and $\overline{\sigma}_x = p_0$ at the locations far from the discontinuous zone (large x) in intact slope or the location where δ=0. Above the shear band $\overline{\sigma}_x \neq p_0$ at all locations because the shear stress caused by gravitational force (τ_g) is greater than shear resistance in the shear band. Therefore, the redistribution of forces results in $\overline{\sigma}_x < p_0$ in the right (unloading) and $\overline{\sigma}_x > p_0$ in the left side (loading) of the shear band.

Somewhere along the shear band $\overline{\sigma}_x = p_0$ and that plane (point O in Fig. 3.2) is chosen as the origin (see also Puzrin and Germanovich 2005). With respect to the origin, the segment of the shear band and the end zones are defined by x_i and ω_i, respectively, where the subscript i=1 and 2 represent the values for the left (x<0) and right (x>0) sides of the origin, respectively. Also it is assumed that E_1 and E_2 are the undrained Young's modulus of the upper soil layer in plane strain condition for loading (x<0) and unloading (x>0), respectively.

3.6 Mathematical Formulations

For a mild submarine slope (β<10°), shear stress along the plane AB is

[5] $$\tau_g \approx \gamma' h \sin\beta$$

where γ' is the submerged unit weight. Using the equilibrium conditions of a small slice of depth h above the shear band, the variation of $\overline{\sigma}_x$ in the upper soil layer can be written as

[6] $$h\frac{\partial \bar{\sigma}_x}{\partial x} = s_u(x) - \tau_g$$

where the mobilized $s_u(x)$ in the end zones can be found from Eq. (1), and in the discontinuity $s_u(x)=s_{uR}$.

Considering only the right side of the origin and assuming uniform elastic deformation, the change in $\bar{\sigma}_x$ in the upper soil layer above the end zone CA (Fig. 3.2) can be expressed as:

[7] $$\frac{\partial \bar{\sigma}_x}{\partial x} = E_2 \frac{\partial \bar{\varepsilon}_x}{\partial x} = E_2 \frac{\partial^2 \delta}{\partial x^2}$$

where $\bar{\varepsilon}_x$ is the average normal strain in the upper soil layer in the x direction, which is related to δ as $\delta(x) = \int \bar{\varepsilon}_x dx$.

Substituting Eqs. (1) and (7) into Eq. (6), the following equation can be obtained for the end zone.

[8] $$hE_2 \frac{\partial^2 \delta}{\partial x^2} = (s_{up} - s_{uR}) e^{-3\delta/\delta_{95}} - (\tau_g - s_{uR})$$

Equation (8) can be written in terms of normalized displacement and coordinate as:

[9] $$\frac{\partial^2 \hat{\delta}}{\partial \hat{x}^2} = e^{-3\hat{\delta}} - r$$

where $\hat{\delta} = \delta / \delta_{95}$ and $\hat{x} = x / l'_u$. The characteristics length (l'_u) and stress ratio (r) are defined as

[10] $$l'_u = \sqrt{hE_2\delta_{95}/(s_{up} - s_{uR})}$$

[11] $$r = (\tau_g - s_{uR})/(s_{up} - s_{uR})$$

The displacement boundary conditions at the tips of the upper end zone CA (Fig. 3.2) are

[12a] $\hat{\delta}(\hat{x}_2) = 0$ at point A

[12b] $\hat{\delta}(\hat{x}_2 - \hat{\omega}_2) = 1$ at point C

where $\hat{x}_2 = x_2 / l'_u$ and $\hat{\omega}_2 = \omega_2 / l'_u$.

Now, consider a point on the discontinuity just left side of point *C*. The average normal stress in the upper soil layer above this point is

[13] $\bar{\sigma}_x(x_2 - \omega_2) = p_0 - (\tau_g - s_{uR})(x_2 - \omega_2)/h$

On the other hand, just on right side of point *C*, the average normal stress is

[14] $\bar{\sigma}_x(x_2 - \omega_2) = p_0 + E_2\bar{\varepsilon}_x = p_0 + E_2\dfrac{\partial\delta}{\partial x}$

Equating Eqs. (13) and (14) by satisfying the overall stress equilibrium at Point *C*, the following equation is obtained in normalized form,

[15] $\dfrac{\partial\hat{\delta}}{\partial\hat{x}} = -r(\hat{x}_2 - \hat{\omega}_2)$

which actually denotes the slope of the displacement curve at point C where x=x_2-ω_2. The negative sign indicates the reduction of displacement with distance from this point.

Assuming $\partial\hat{\delta}/\partial\hat{x} = \hat{Y}$, Eq. 9 can be written as a first order differential equation as

[16] $\dfrac{\partial\hat{Y}}{\partial\hat{x}} = e^{-3\hat{\delta}} - r$

which can be rearranged further as

[17] $\hat{Y}\cdot\partial\hat{Y} = (e^{-3\hat{\delta}} - r)\partial\hat{\delta}$

Now, integrating equation (17) with boundary conditions at point C and then equating it with the gradient of the displacement curve given by Eq. (15), the following expression can be found after some algebraic manipulation.

[18] $$\frac{\partial \hat{\delta}}{\partial \hat{x}} = \sqrt{\Omega}$$

where

[19] $$\Omega = -(2/3)\cdot e^{-3\hat{\delta}} - 2\cdot r\cdot \hat{\delta} + r^2\left(\hat{x}_2 - \hat{\omega}_2\right)^2 + (2/3)\cdot e^{-3} + 2\cdot r\,.$$

Equation (18) shows the gradient of $\hat{\delta}$ vs $\hat{x}$ curve in the end zone. A viable solution is possible only if $\Omega \geq 0$. Inserting $\hat{\delta}=0$ in Eq. (19), the gradient of this curve at the tip of the shear band (point A in Fig. 3.2) can be obtained.

[20] $$\left[\frac{\partial \hat{\delta}}{\partial \hat{x}}\right]_{\hat{\delta}=0} = \sqrt{2r - 0.634 + r^2\left(\hat{x}_2 - \hat{\omega}_2\right)^2}$$

Equation (20) shows that the gradient of $\hat{\delta}$ vs $\hat{x}$ curve at the tip of the end zone increases with r and normalized length of discontinuity $\left(\hat{x}_2 - \hat{\omega}_2\right)$. For a small seabed slope (i.e. low r), a large discontinuity is required for a viable solution (+ve value in the square root); however, for a steep seabed slope a solution is possible even with zero discontinuity, although solutions for $(\hat{x}_2 - \hat{\omega}_2) > 0$ are of the interest of this study.

Similarly, the gradient of $\hat{\delta}$ vs $\hat{x}$ at point C (Fig. 3.2) can be calculated as

[21] $$\left[\frac{\partial \hat{\delta}}{\partial \hat{x}}\right]_{\hat{\delta}=1} = -r\left(\hat{x}_2 - \hat{\omega}_2\right)$$

which shows that displacement gradient at this point also increases with r and the length of discontinuity $\left(\hat{x}_2 - \hat{\omega}_2\right)$. In summary, the shape of $\hat{\delta}$ vs $\hat{x}$ curve in the end zone depends on r and the length of the discontinuity, which also influences the length of the end zone because $\hat{\delta}$ varies between 0 and 1 in this zone.

Similar to shear crack propagation in fracture mechanics, continuous propagation of shear band under existing gravity load will occur only if

[22] $d\hat{\omega}_2 \le d\hat{x}_2$ for $d\hat{x}_2 \ge 0$,

In other words, the end zone length decreases with increase in shear band length, which can be shown by calculating $\hat{\omega}_2$ for incremental lengths of $\hat{x}_2$.

In order to find $\hat{\omega}_2$ for a given $\hat{x}_2$, Eq. (18) is integrated numerically, as it cannot be done analytically, using Newton-Raphson method, writing a code in MATLAB. Integration is performed for the end zone with limits of $\hat{\delta}$= 0 to 1 and $\hat{x} = \hat{x}_2$ to $(\hat{x}_2 - \hat{\omega}_2)$ from point A to C in Fig. 3.2. Once the values of $\hat{\omega}_2$ and $\hat{x}_2$ in Eq. (19) are known for a specific value of *r*, variation of $\hat{\delta}$ in the end zone (from point A to C) is calculated integrating Eq. (18) numerically, which is then used to calculate the values of δ $(= \hat{\delta} \times \delta_{95})$ along the end zone.

Rearranging Eqs. (6) and (7) for the discontinuity, where $s_{u(x)}=s_{uR}$, the following equation can be obtained.

[23] $$hE_2 \frac{\partial^2 \delta}{\partial x^2} = s_{uR} - \tau_g$$

Now integrating Eq. (23) twice and using the boundary conditions (at x=0, $\bar{\varepsilon}_x = \partial\delta / \partial x = 0$ and at $x=x_2-\omega_2$, $\delta=\delta_{95}$) the following equation can be obtained.

[24] $$\delta = \frac{s_{uR} - \tau_g}{hE_2} \frac{x^2 - (x_2 - \omega_2)^2}{2} + \delta_{95}$$

Once δ is known, s_u can be calculated using Eq. (1), which represents the shear stress along the shear band.

So far the calculation has been shown only for the right side of the origin. For the left side, similar equations can be obtained except for Eq. (10) where E_2 should be replaced by E_1. Therefore, in normalized term ($\hat{x}, \hat{\delta}$), a similar solution can be obtained, which means that $\hat{x}_1 = \hat{x}_2$, $\hat{\omega}_1 = \hat{\omega}_2$; however, $x_1/x_2 = \omega_1/\omega_2 = \sqrt{E_1/E_2}$. For further details of this derivation readers are referred to Puzrin et al. (2004).

Therefore, the total length of the shear band (l=x_1+ x_2) can be calculated as

[25] $$l = \hat{x}_2\left(1+\sqrt{E_1/E_2}\right)l'_u$$

At critical length, $l^{cr} = x_1^{cr} + x_2^{cr}$, where x_1^{cr} and x_2^{cr} are the minimum length of the shear band segments in the left and right side of the origin, respectively, for initiation of shear band propagation.

3.7 Geometry and Soil Parameters

Table 3.2 shows the geometry and soil parameters used in the "base case" analysis. The depth of the sliding plane is h=20 m and the slope angle is varied from 3 degrees to 10 degrees. An extensive site investigation program for the Ormen Lange gas field development project in the Norwegian Sea provided a wide range of geotechnical properties of offshore sediments. Kvalstad et al. (2005a,b) summarized the soil conditions and geotechnical properties obtained from different phases of site investigations, where geoborings were performed to a maximum depth of 230 m below the seabed. Based on cone penetration, unconsolidated undrained triaxial, direct simple shear, ring shear, Atterberg limits, and fall cone tests, they showed the variation of undrained shear strength and sensitivity in the different soil layers. They divided the soils mainly

into two categories: (i) marine and/or glaciomarine clay and (ii) glacial clay. Significant strain softening occurs in marine clay, while glacial clays show little or no strain softening. The sensitivity of the marine clays varied between 3 and 6.

Kvalstad et al. (2005a, b) also showed that s_{up} increases with vertical effective stress (σ'_v) and overconsolidation ratio (*OCR*) as

$$[26] \quad \left(\frac{s_{up}}{\sigma'_v}\right)_{oc} = \left(\frac{s_{up}}{\sigma'_v}\right)_{NC} (OCR)^m$$

Based on triaxial test results, they reported m=0.7, and $\left(s_{up}/\sigma'_v\right)_{NC}$=0.27 for these marine clays. Moreover, the ratio between s_{up} in DSS and triaxial compression tests is about 0.8 (Kvalstad et al., 2005b). Now, using γ' of the top soil layer, the value of σ'_v at the depth of sensitive clay layer (h=20 m) can be calculated. The DSS condition better represents the failure condition through the sensitive clay layer shown in Fig. 3.2. As the marine clays were found to be normally to lightly overconsolidated (Biscontin et al. 2003; Leynaud et al. 2004; Kvalstad et al. 2005b; Yang et al. 2006; Lunne and Andersen 2007), an *OCR* of 1 is used. Based on the above information, s_{up}=40 kPa is used for the marine clay layer. For the upper glacial clay, Gauer et al. (2005) assumed s_u=25 kPa at the seabed increasing linearly at 2.4 kPa per metre depth. An average $\bar{s}_u$ =50 kPa is therefore assumed for the upper clay layer. The undrained Young's modulus E_u=600s_u is used. As glacial clay is not very sensitive (Kvalsted et al. 2005a), S_t=1 is used for the upper glacial clay layer.

3.8 Results

In the discussion of results, the symbols $\hat{x}_i (= \hat{x}_1, \hat{x}_2)$, $\hat{\omega}_i (= \hat{\omega}_1, \hat{\omega}_2)$ are used for brevity. Moreover, to explain the mechanisms mainly the right side of the origin is considered (left side is similar); therefore, the symbols x_2, ω_2 and (x_2-ω_2) are used for the length of shear band, end zone and discontinuity, respectively.

Shear Band and End Zone

Figure 3.6 shows the relationship between the length of discontinuity (x_i-ω_i) where $s_{u(x)}$=s_{uR} and shear band x_i where $s_u \leq s_{up}$. The vertical distance of any point on these lines from the line AB (1:1 slope) represents the end zone (ω_i) where $s_{u95} \leq s_u \leq s_{up}$. As an example, for β=5°, when the discontinuity is 200 m (e.g. x_i-ω_i=100 m) the end zone length in each side (ω_i) is 50 m. Note that in this case x_1= x_2 and ω_1=ω_2 because E_1=E_2, as discussed above. In other words, 33% of the shear band length is the end zone. The ratio between the length of the end zone and discontinuity (ω_i/(x_i-ω_i)) decreases with an increase in shear band length. Figure 3.6 also shows that, for a given length of discontinuity, the end zone length is larger for a smaller slope angle. Therefore, for mild offshore slopes, the end zones cannot be neglected or assumed to be zero especially at low x_i where (ω_i/(x_i-ω_i)) is high.

The normalized length of the discontinuity and the shear band are also shown in the top horizontal and right vertical axes, respectively (Fig. 3.6).

The solid lines in Fig. 3.7 show the variation of normalized end zone length $\hat{\omega}_i$ with shear band length $\hat{x}_i$ for different values of slope angles. The following key features are noted from Figs. 3.6 and 3.7:

i) The very left point of each curve, shown by a solid circle, represents the minimum length of discontinuity required for the initiation of shear band propagation. As an example, for β=4°, a discontinuity of at least 200 m (i.e. x_i-ω_i=100 m) is required for continuous shear band propagation (Fig. 3.6). If it is less than 200 m, a shear band will not propagate continuously. The value of shear band length $\hat{x}_i$ at this point represents the minimum normalized length required for shear band propagation ($\hat{x}_i^{cr}$). At this point the length of the end zone ($\hat{\omega}_i^{cr}$) is the maximum.

ii) The length of the end zone decreases with an increase in the shear band length, which means that the relative size of the residual shear strength zone in the shear band increases with shear band length $\hat{x}_i$. Figure 3.7 also shows that the required condition, $d\hat{\omega}_i \le d\hat{x}_i$ (Eq. 22), for shear band propagation.

iii) Unlike J-integral based propagation criterion (Palmer and Rice 1973), a complete solution for a wide range of shear band length $\hat{x}_i$, including the solution for low values of x_i, is obtained in the present analysis. Palmer and Rice (1973) presented the solutions only for the cases in which shear band length is very large compared to the end zones. Figures 3.6 and 3.7 show that this condition is approximately valid only for large $\hat{x}_i$ when $\hat{\omega}_i / \hat{x}_i$ is small. However, the current analysis shows that propagation could initiate at lower values of shear band lengths when the end zone length is not negligible. As an example, for β=4° in Fig. 3.6, continuous shear band propagation could be initiated at a minimum length of shear band of 366 m (=2×183 m) when the end zone length is 166 m (=2×83 m) which is 45% of the shear band length. Therefore, J-integral based propagation criterion is not valid for this condition.

iv) $\hat{x}_i^{cr}$ increases with a decrease in β and therefore $\hat{x}_i$ vs $\hat{\omega}_i$ curves shift to the right for low β (Fig. 3.7). In other words, the minimum length required for shear band propagation is higher for lower β. Moreover, for a given shear band length $\hat{x}_i$ the end zone length $\hat{\omega}_i$ decreases with increasing β.

The inset of Fig. 3.7 shows the ratio $\hat{\omega}_i / \hat{x}_i$ for different values of stress ratio *r* at the initiation of shear band propagation, which is related to the slope angle β. As shown, $\hat{\omega}_i / \hat{x}_i$ increases almost linearly with *r* and at $r \approx 0.53$ (i.e. β=7.0°) $\hat{\omega}_i / \hat{x}_i \approx 1$. This implies that the end zone length is almost the same as the shear band length for $r \geq 0.53$; however, for $r < 0.53$ a finite length of discontinuity is required to initiate shear band propagation.

Displacement and Shear Stress along Shear Band

Figures 3.8(a) and 3.9(a) show the variation of δ along the shear band for β=4° and 7°, respectively, for different values of shear band length $\hat{x}_i$ shown by point P_1-P_{10} in Fig. 3.7. The solid red lines represent the end zone while the dashed blue lines represent the discontinuity where $s_u = s_{uR}$. For clarity, only the right side of x=0 (Fig. 3.2) is shown. The leftmost lines in Figs. 3.8 and 3.9 show the variation of δ for the minimum length of the shear band that could cause the propagation (Fig. 3.7). Again, as shown in Fig. 3.8(a), for β=4°, a 100 m discontinuity is required for initiation of shear band propagation. This will result in total 183 m long shear band in one side of origin with 83 m end zone.

For β=7°, almost the whole length of the shear band is the end zone (≈87m) (Fig. 3.9a). In other words, shear band propagation might be initiated in a steep slope just after formation of a

discontinuity of s_u=s_{uR}. The shape of δ–x curves is also different from the β=4° case. At the end of the shear band (point A in Fig. 3.2), the slope of δ–x curve is almost zero for β=4° while it is greater than zero for β=7°. This can be explained by putting $\hat{\delta}$=0 in Eq. (19). With an increase in shear band length, the end zone length decreases and the slope of δ–x curves increase for both β=4° and 7°. A shorter end zone means more stress concentration that makes propagation of the shear band easier.

Figures 3.8(b) and 3.9(b) show the variation of shear stress along the shear band. The shear stress in the discontinuity is $s_{u\mathrm{R}}$ (dashed blue line); however, in the end zone it increases gradually from s_{u95} to s_{up}. The pattern of shear stress variation is very similar to numerical calculations presented by the authors (Dey et al. 2013) for upward progressive failure.

As mentioned, a step decrease of s_u to s_{uR} at δ_{95} is used in the previous calculations. In order to show the effect of this assumption, a calculation is also performed with a step decreases of s_u at $2\delta_{95}$, which implies that in the end zone $0\leq\delta\leq2\delta_{95}$ while in the previous cases it was $0\leq\delta\leq\delta_{95}$. The variation of δ and shear stress in the shear band for β=4° at the initiation of shear band propagation are also shown by the red dotted line in Fig. 3.8. The shear band propagation initiates at a slightly higher x_2 (=196 m) than the previous analysis as shown by two vertical arrows on the horizontal axis in Fig. 3.8(a). As expected, the length of the end zone is higher; and, in this particular case, almost the whole length of the shear band is the end zone. Figure 3.8(b) shows that the shear stress gradually decreases almost to s_{uR} while in the previous case the step decrease at s_{u95} is noticeable. In summary, depending upon the strain level at the step decrease of s_u (cc′ in Fig. 3.4), the length of the end zone might vary; however, the length of the shear band required for the initiation of shear band propagation does not vary significantly,

which is the main concern in stability analysis. Therefore, the step decrease of s_u at δ_{95} is used for further analysis.

3.9 Comparison with Linear Post-Peak Softening Model

A linear variation of s_u with δ of sensitive clay has been used for progressive failure analysis (Locat et al. 2011, 2013; Quinn et al. 2011); although the problems analyzed in those studies are different from the problem considered in the present study (Fig. 3.2). Linear strength variation has been also used for stability analysis of submerged offshore slopes of normally consolidated clay and loose sand sediments (Puzrin et al. 2004; Puzrin and Germanovich 2005). Similar to these studies, define the linear variation of s_u as

[27] $$\frac{s_{up} - s_u}{s_{up} - s_{uld}} = \frac{\delta}{\delta_{ld}} \text{ for } \delta \le \delta_{ld}$$

[28] $$s_u = s_{uld} \text{ for } \delta > \delta_{ld}$$

where s_{uld} is the undrained shear strength at large deformation δ_{ld}.

When a linear model is adopted, one of the key questions is how δ_{ld} could be determined. A wide range of δ_{ld}, between 20 mm and 2,000 mm, has been reported in previous studies for sensitive clays (Locat et al. 2011; Quinn et al. 2011). As the present nonlinear model (Eq. (1)) reasonably fits tests data (Figs. 3.3 and 3.5), first assume $s_{uld}=s_{u\mathrm{R}}$ and $\delta_{ld}=\delta_{95}$ and named as model L1, which gives the rightmost dashed linear line in Fig. 3.5. As most of the test data lies in the left side far from this line, also assume two more linear variations with $\delta_{ld}=0.7\delta_{95}$ (Model L2) and $0.5\delta_{95}$ (Model L3) which are also shown by two dashed linear lines in Fig. 3.5.

Now using Eqs. (27) and (28), instead of Eq. (1), Eqs. (8)–(19) are reformulated and solved. The lengths of the shear band and end zones are normalized by another characteristic length defined as $l'_u = \sqrt{hE_u\delta_{ld}/(s_{up}-s_{uR})}$ in which, instead of δ_{95} in Eq. (10) for nonlinear model, δ_{ld} is used for these linear models as Puzrin et al. (2004). The dashed lines in Fig. 3.7 show the variation of $\hat{\omega}_i$ with $\hat{x}_i$ for linear models L1-L3. Although non-normalized end zone length ω_i and shear zone length x_i depend on δ_{ld}, the normalized $\hat{\omega}_i$ vs $\hat{x}_i$ curves are independent of δ_{ld} (see Eq. 19).The following are the key features of these curves.

i) The initiation of shear band propagation with a linear model occurs at a higher normalized shear band length than that with the nonlinear model (compare diamonds and circles); and their difference increases with a decrease in slope angle.

ii) For a given β, the difference between the curves obtained with linear and nonlinear models are negligible at large normalized shear band lengths.

iii) The normalized length of the end zone at the initiation of shear band propagation is higher in a nonlinear model than that with linear models.

The above features of $\hat{\omega}_i$ vs $\hat{x}_i$ curves could be further explained using the non-normalized lengths of the shear band ($x_i = \hat{x}_i l'_u$) and end zone ($\omega_i = \hat{\omega}_i l'_u$), as shown in Fig. 3.10(a) for β=4°. x_i required to initiate shear band propagation for linear model L1 is 220 m which is significantly higher than that required from the nonlinear model (183 m). The reason behind this can be explained using Fig. 3.5, which shows that s_u degradation is faster in a nonlinear model than that of L1. This quick degradation results in the initiation of shear band propagation at low x_i. The calculated length of the end zone is higher with the nonlinear model (83 m) than with L1 (67 m). In other words, the required discontinuity (x_2-ω_2) for the initiation of shear band propagation is

100 m with the nonlinear model and 153 m with L1. The x_2 values required to initiate shear band propagation for linear models L2 and L3 are 184 and 155 m, respectively, with end zone lengths of 56 and 47 m, respectively.

The initiation of shear band propagation is one of the important aspects of submarine slope stability analysis. Figure 3.10(b) shows the variation of δ in the shear band for nonlinear and linear models for β=4° at the initiation of shear band propagation. When $\delta_{ld}=\delta_{95}$ is used (i.e. Model L1), the required displacement δ in the discontinuity is significantly higher than that from the nonlinear model. The δ vs x curves with the nonlinear model and linear model $\delta_{ld}=0.7\delta_{95}$ (i.e. Model L2) are comparable; however, the required length of discontinuity is 100 m for nonlinear but 132 m for Model 2. Calculated δ and shear band lengths are small with Model L3 because a small δ_{ld} is used.

In summary, as Eq. (27) shows that for a given s_{up} and s_{uld}, only one input parameter (δ_{ld}) can be varied to obtain different linear curves. The above comparison shows that it is difficult to match the results (lengths of shear band, end zone and discontinuity, and displacement) using the nonlinear and linear models simply by varying δ_{ld} in the linear model. As the nonlinear model better fits test results (Figs. 3.3 and 3.5), it is expected that calculated results using this model better represent the response. Although mathematical formulation and calculations using a linear model are relatively simple, one of the key input parameters δ_{ld} is very difficult to estimate which might give very different results.

3.10 Global Stability

In the previous sections, it is shown that a relatively small length of discontinuity could cause the propagation of a shear band. It is assumed in this study that the sensitive clay layer parallel to the

slope in Fig. 3.2 is sufficiently long. If the soil properties and geometry meet the conditions for initiation, as discussed before, the shear band propagation will continue and at one stage global failure will occur through the upper glacial clay as shown by the inclined lines in Fig. 3.2. For undrained (ϕ=0) condition, the failure plane should be inclined at 45° (note that this figure is not drawn to scale). Now, using the concept of limit equilibrium and balancing the forces on the soil block above the shear band acting in the *x* direction, the factor of safety (F_s) can be calculated as

$$[29]\quad F_s = \frac{P_p + s_{uR} l}{P_a + \tau_g l}$$

where P_a and P_p are the active and passive forces, respectively, acting at the upper and lower ends. The minimum length (l_f) required to cause the global failure of a slope is then calculated by inserting F_s=1, l=l_f and P_p-P_a=$4\,\bar{s}_u\,h$.

$$[30]\quad l_f = \frac{4\bar{s}_u h}{\tau_g - s_{uR}}$$

For the parameters listed in Table 3.2, l_f is 580 m for the β=4° slope. In other words, if the limit equilibrium method is used, the failure of the slope will be predicted only if the length of the discontinuity is at least 580 m. On the other hand, according to the proposed method, the discontinuity required for shear band propagation can be calculated using Eq. (25) as 200 m. Shear band propagation will continue and once the shear band length becomes 580 m global failure will occur. This implies that the limit equilibrium method significantly overestimates the factor of safety because it does not consider the shear band propagation. If the sensitive clay layer is not sufficiently long (<580 m), shear band propagation will stop, and global failure will not occur. However, the slope might be marginally stable and any additional triggering factor can cause a large-scale failure. It is also to be noted here that after global failure of the soil block

shown in Fig. 3.2, retrogressive failure might occur, which can be simulated using large deformation finite element modeling as presented by the authors in Dey et al. (2015b).

3.11 Parametric Study

The slope angle and soil parameters influence shear band propagation and failure of a slope. A parametric study is conducted using the nonlinear model described above in which only one parameter is varied while the other parameters are kept constant as listed in Table 3.2, unless otherwise mentioned.

Effects of δ_{95}

Table 3.1 shows a wide variation of δ_{95} for different soils. The effects of δ_{95} on total shear band length at which band propagation initiates are shown in Fig. 3.11. Each value of β, $\hat{x}_i$ and $\hat{\omega}_i$ are calculated as shown in Fig. 3.7. Multiplying the normalized shear band length $\hat{x}_i$ by the characteristic length l_u', the values of x_i are calculated which are then used to calculate l^{cr} using Eq. (25). Again, l^{cr} represents the minimum length of discontinuity required for shear band propagation. For example, for β=4° and δ_{95}=70 mm, shear band propagation will initiate only if the length of the shear band is greater than 300 m which is shown by a triangle in Fig. 3.11. Figure 3.11 also shows that l^{cr} increases with δ_{95} because, for a large δ_{95}, the shear strength degradation occurs slowly over a large δ and therefore requires more fracture energy for shear band propagation than that with a small δ_{95}. Moreover, l^{cr} decreases with an increase in β

because τ_g increases with β. In other words, high brittleness (i.e. rapid decrease in s_u with δ) and steeper slopes are more prone to failure.

Effects of s_{up} and Sensitivity

Figure 3.12 shows the $\hat{x}_i$ vs $\hat{\omega}_i$ curves for three values of peak shear strength (s_{up}). With an increase in s_{up} the $\hat{x}_i$ vs $\hat{\omega}_i$ curves shift to the right. As shown by the solid circles, $\hat{x}_i$ required to initiate shear band propagation increases with s_{up}. Figure 3.13 shows the influence of sensitivity on normalized lengths of shear band and corresponding end zone. With an increase in S_t, the $\hat{x}_i$ vs. $\hat{\omega}_i$ curves shift towards the left.

As the length of the shear band is proportional to $\hat{x}_i$ (Eq. (25)), l^{cr} decreases with decreasing s_{up} and increasing S_t. This implies that a submarine slope that has a weak sensitive clay layer parallel to the slope is more susceptible to failure due to shear band propagation if the weak layer is highly sensitive and has low undrained shear strength.

Effects of stress ratio r and Worked example

In order to provide a simple chart for practical application, a set of analyses are performed for different values of r. Figure 3.14 shows the normalized x_i at the initiation of shear band propagation (i.e. at critical length) with r. The normalized form of this curve is independent of slope angle, depth of sensitive clay layer and geotechnical properties of the sensitive clay layer (s_{up}, s_{uR} and δ_{95}), because Eq. (19) is a function of r and $\hat{\delta}$ only. If the values of s_{up}, s_{uR} and τ_g are known, r can be calculated using Eq. (11). Now, using Fig. 3.14 one can easily obtain $\hat{x}_i$ (as

shown by arrows) which can be then used to calculate l^{cr} (Eq. 25) required for the initiation of shear band propagation.

As a worked example, consider an infinite submarine slope inclined at β=4°. A slide-prone weak sensitive clay layer is at depth h=30 m below the seabed. The shear strength properties of the sensitive clay layer are: s_{up}=50 kPa, S_t=6 and δ_{95}= 0.1 m. The geotechnical properties of the upper glacial clay are: $\bar{s}_u$ =60 kPa, γ′=10 kN/m^3 and E_1=20 MPa, E_2=40 MPa. In order to calculate the minimum length of the shear band that initiates shear band propagation, the shear stress on the sensitive clay layer is calculated as τ_g= 20.93 kPa using Eq. (5). Inserting the value of τ_g in Eq. (11), the stress ratio r =0.302 is evaluated. Now from Fig. 3.14, $\hat{x}_i^{cr}$ = 3.25 can be obtained for r =0.302. The characteristics length $l_u^{'}$ for this problem is 53.67 m (Eq. 10). Finally, using Eq. (25) the critical length of the shear band of 298 m can be calculated, which implies that if the length of the shear band exceeds 298 m it will propagate through the sensitive clay layer and could cause a global failure.

3.12 Conclusions

This paper presents a new method to evaluate potential failure mechanisms of submarine slopes having a sensitive clay layer. A discontinuity (weak zone in sensitive clay layer) results in stress concentrations at both ends of the shear band and creates two end zones. When the length of the discontinuity exceeds a critical length the shear band propagation continues through the sensitive clay layer resulting in a large-scale landslide. Significant plastic deformation/strain develops in the shear band that reduced the undrained shear strength. Post-peak degradation of undrained

shear strength of sensitive clay can be better modeled using the proposed nonlinear equation for a wide range of plastic deformations. If the mechanisms of shear band propagation are considered, a much shorter discontinuity (several hundred metres for the cases analyzed in this study) is required for global failure of the slope as compared to that required for failure using the limit equilibrium method. The initiation of shear band propagation depends on slope angle, depth of the sensitive clay layer and undrained shear strength; however, it can be presented in a normalized form using two parameters namely stress ratio r and characteristics length l'_u that combine all these effects. At the initiation of shear band propagation, the end zone length is considerably large as compared to shear band length, and therefore the end zone cannot be neglected as assumed in some previous studies based on the concept of fracture mechanics.

A normalized design chart (Fig. 3.14) is developed which can be easily used to calculate the minimum length of the discontinuity required for shear band propagation that might cause a large-scale landslide. The input parameters required for the analysis are slope angle, location of the weak zone and shear strength properties of soils. Therefore, the proposed solution could be easily used for practical application.

A limitation of this study is that the analytical solution presented above cannot model the retrogressive process after global failure of a soil mass as reported by many researchers. Numerical modeling, such as large deformation FE modeling, is required for that which has been presented by the authors in a separate paper (Dey et al. 2015b).

Acknowledgements

The works presented in this paper have been supported by the Research and Development Corporation of Newfoundland and Labrador, NSERC and C-CORE.

List of symbols

The following symbols are used in this paper:

β	slope angle
h	depth from seabed
τ_g	gravitational shear stress
σ_x	normal stress acting parallel to the slope
$\overline{\sigma}_x$	average normal stress in upper soil layer
σ'_v	vertical effective stress
$\overline{\varepsilon}_x$	average linear strain in upper soil layer
δ	post-peak shear displacement
δ_{95}	δ at which s_u reduced by 95% of (s_{up}-s_{uR})
δ_r	displacement required to obtain residual strength
δ_{50}	δ at which s_u reduced by 50% of (s_{up}-s_{uR})
δ_p	plastic shear displacement
δ_{ld}	large displacement for linear model
$\hat{\delta}$	normalized displacement ($=\delta/\delta_{95}$)
γ'	submerged unit weight
E_1	undrained Young's modulus for loading (x<0)
E_2	undrained Young's modulus for unloading (x>0)
S_t	sensitivity (s_{up}/ s_{uR})

s_u	mobilized undrained shear strength
s_{u50}	s_u mobilized at δ_{50}
s_{up}	peak undrained shear strength
s_{uR}	s_u mobilized at considerable shear displacement
s_{ur}	s_u at completely remoulded state
s_{u95}	s_u mobilized at δ_{95}
s_{uld}	s_u mobilized at δ_{ld}
r	stress ratio $(\tau_g - s_{uR})/(s_{up} - s_{uR})$
l'_u	characteristics length $\left(\sqrt{hE_2\delta_{95}/(s_{up} - s_{uR})}\right)$
$x_{i\ (i=1,2)}$	length of shear band
$\omega_{i\ (i=1,2)}$	length of end zone
x_i -ω_i	length of discontinuity
$\hat{x}_i$	normalized length of shear band (x_i / l'_{ui})
$\hat{\omega}_i$	normalized length of end zone (ω_i / l'_{ui})
l	total length of shear band
l^{cr}	critical length
l_f	global failure length
OCR	overconsolidation ratio
P_a	active force acting at the upper end
P_p	passive force acting at the lower end
F_s	factor of safety

References

Almagor, G., and Wiseman, G. 1991. Analysis of submarine slumping in the continental slope off the southern coast of Israel. Marine Geotechnology, **10**(3-4): 303–342.

Angell, M., Hanson, K., Swan, B., and Youngs, R. 2003. Probabilistic Fault Displacement Hazard Assessment for Flowlines and Export Pipelines, Mad Dog and Atlantis Field Developments, Deepwater Gulf of Mexico. *In* Proc. Off. Tech. Conf., Houston, paper #15202.

Berre, T. 1973. Simple shear tests (CCV) on plastic clay from Onsøy. NGI report No. 50322-3.

Bernander, S. 2000. Progressive failure in long natural slopes: formation, potential extension and configuration of finished slides in strain-softening soils. Licentiate Thesis, Luleå University of Technology.

Biscontin, G., Pestana, J.M., and Nadim, F. 2003. Seismic triggering of submarine slides in soft cohesive soil deposits. Marine Geology, **203**(3-4): 1–14. doi :10.1016/S0025-3227(03) 00314-1.

Bishop, A.W. 1967. Progressive failure — with special reference to the mechanism causing it. *In* Proceedings of the Geotechnical Conference, Oslo, Norway, Vol. 2, pp, 142–150.

Bjerrum, L. 1967. Progressive failure in slopes of overconsolidated plastic clay and clay shales. J. Soil Mech. Found. Engineering Div., ASCE, **93**(SM5): 1–4.

Brink, U.S.T., Lee, H.J., Geist, E.L., and Twichell D. 2009. Assessment of tsunami hazard to the U.S. East Coast using relationships between submarine landslides and earthquakes. Marine geology, **264**(1-2): 65–73.

Bryn, P., Berg, K., Forsberg, C.F., Solheim, A., and Kvalstad, T. 2005. Explaining the Storegga slide. Marine and Petroleum Geology, **22**(1-2): 11–19.

Burland, J. B., Longworth, T. I., and Moore, J. F. A. 1977. A study of ground movement and progressive failure caused by a deep excavation in Oxford Clay. Géotechnique, **27**(4): 557–591.

Canals, M., Lastras, G., Urgeles, R., Casamor, J. L., Mienert, J., Cattaneo, A., Batist, M. De., Haflidason, H., Imbo, Y., Laberg, J. S., Locat, J., Long, D., Longva, O., Masson, D.G., Sultan, N., Trincardi, F., and Bryn, P. 2004. Slope failure dynamics and impacts from seafloor and shallow sub-seafloor geophysical data: case studies from the COSTA project. Marine Geology, **213**(1-4): 9–72. doi:10.1016/j.margeo.2004.10.001.

Conway, K. W., Barrie, J. V., and Thomson, R. E. 2012. Submarine slope failures and Tsunami Hazard in Coastal British Columbia: Douglas Channel and Kitimat Arm. Geological Survey of Canada, Current Research 2012-10, 13 p. doi: 10.4095/291732.

Conte, E., Silvestri, F. and Troncon, A. 2010. Stability analysis of slopes in soils with strain-softening behaviour. Computers and Geotechnics, **37**(5): 710–722.

Dan, G., Sultan, N., and Savoye, B. 2007. The 1979 Nice harbour catastrophe revisited: Trigger mechanism inferred from geotechnical measurements and numerical modelling. Marine Geology, **245**(1-4): 40–64. doi:10.1016/j.margeo.2007.06.011.

DeGroot, D. J., DeJong, J. T., Yafrate, N. J., Landon, M. M., and Sheahan, T. C. 2007. Application of recent developments in terrestrial soft sediment characterization methods to offshore environments. Offshore Tech. Conf. Texas. Paper OTC 18737.

Dey, R., Hawlader, B., Phillips, R., Soga, K. 2015a. Large deformation finite element modeling of progressive failure leading to spread in sensitive clay slopes. Géotechnique (accepted).

Dey, R., Hawlader, B., Phillips, R., Soga, K. 2015b. Numerical modeling of submarine landslides with sensitive clay layers. ASCE Journal of Geotechnical and Geoenvironmental Engineering (under review).

Dey, R., Hawlader, B., Phillips, R., and Soga, K. 2013. Progressive failure of slopes with sensitive clay layers. *In* Proc. of the 18th Int. Conf. on Soil Mech. and Geotech. Eng., Paris.

Dimakis, P., Elverhøi, A., Høeg, K., Solheim, A., Harbitz, C., Laberg, J. S., Vorreng, T. O., and Marr, J. 2000. Submarine slope stability on high-latitude glaciated Svalbard–Barents Sea margin. Marine Geology, **162**(2-4): 303–316. doi:10.1016/S0025-3227(99)00076-6.

Einav, I., and Randolph, M. F. 2005. Combining upper bound and strain path methods for evaluating penetration resistance. Int. J. Num. Methods Engineering, **63**(14): 1991–2016.

Gauer, P., Kvalstad, T. J., Forsberg, C. F., Bryn, P., and Berg, K. 2005. The last phase of the Storegga Slide: simulation of retrogressive slide dynamics and comparison with slide-scar morphology. Marine and Petroleum Geology, **22**(1-2): 171–178.

Gee, M. J. R., Gawthorpe, R.L., and Friedmann, J.S. 2005. Giant striations at the base of a submarine landslide. Marine Geology, **214**(1-3): 287–294.

Hadj-Hamou, T. and Kavazanjian, E. Jr. 1985. Seismic stability of gentle infinite slopes. Journal of Geotechnical Engineering, ASCE, 111(6): 681–697.

Hampton, M.A., Lee, H.J., and Locat, J. 1996. Submarine landslides. Reviews of Geophysics, **34**(1): 33–59.

Jostad, H. P., and Andresen, L. 2002. Bearing capacity analysis of anisotropic and strain-softening clays. *In* Proc. of NUMOG VIII, Rome, Italy, pp. 469–474.

Jostad, H. P., Andresen, L., and Thakur, V. 2006. Calculations of shear band thickness in sensitive clays. Numerical Methods in Geotechnical Engineering–Schweiger (ed.), Taylor & Francis Group, London, pp. 27–32.

Karlsrud, K., and Edgers, L. 1982. Some aspects of submarine slope stability. Marine Slides and Other Mass Movements, Vol. 6, pp. 61-81.

Krastel, S., Wynn, R. B., Hanebuth, T. J. J., Henrich, R., Holz, C., Meggers, H., Kuhlmann, H., Georgiopoulou, A., and Schulz, H. D. 2006. Mapping of seabed morphology and shallow sediment structure of the Mauritania continental margin, North-west Africa: some implications for geohazard potential. Norwegian Journal of Geology, Vol. 86, pp. 163–176.

Kvalstad, T.J., Andresen, L., Forsberg, C.F., Berg, K., and Bryn, P. 2005a. The Storegga Slide: evaluation of triggering sources and slide mechanisms. Marine and Petroleum Geology, **22**(1-2): 245–256.

Kvalstad, T.J., Nadim, F., Kaynia, A.M., Mokkelbost, K.H., and Bryn, P. 2005b. Soil conditions and slope stability in the Ormen Lange area. Marine and Petroleum Geology, **22**(1-2): 299–310.

Lacasse, S., and Nadim, F. 2009. Landslide risk assessment and mitigation strategy. Landslides–Disaster Risk Reduction, pp. 31–61.

Laberg, J.S., Vorren, T.O., Mienert, J., Haflidason, H., Bryn, P. and Lien, R. 2003. Preconditions leading to the Holocene reconditions leading to the holocene trænadjupet slide offshore Norway. *In* Proceedings Submarine Mass Movement and Their Consequences, *Edited by* J. Locat and J. Mienert. pp. 247–254.

Lastras, G., Canals, M., Urgeles, R., Hughes-Clarke, J. E., Acosta, J. 2004. Shallow slides and pockmark swarms in the Eivissa Channel, western Mediterranean Sea. Sedimentology, **51**:1–14.

Lee, H. J., and Edwards, B. D. 1986. Regional method to assess offshore slope stability. Journal of Geotechnical Engineering, **112**(5): 489–509.

Lee, H.J., Schwabb, W.C., Edwardsa, B. D., and Kayena, R. E. 1991. Quantitative controls on submarine slope failure morphology. Marine Geotechnology, **10**(1-2):143–157.

Lee, H.J., and Baraza, J., 1999. Geotechnical characteristics and slope stability in the Gulf of Cadiz. Marine Geology, **155**(1-2): 173–190.

L'Heureux, J. S., Hansen, L., Longva, O., Emdal, A., Grande, L. 2010. A multidisciplinary study of submarine landslides at the Nidelva fjord delta, Central Norway – implications for geohazards assessments. Norwegian Journal of Geology, **90**: 1–20.

L'Heureux, J. S., Longva, O., Steiner, A., Hansen, L., Vardy, M.E., Vanneste, M., Haflidason, H., Brendryen, J., Kvalstad, T.J., Forsbeg, C.F., Chand, S., Kopf, A. 2012. Identification of weak layers and their role for the stability of slopes at Finneidfjord, Northern Norway. Submarine mass movements and their consequences, *edited* by Yamada Y et al., Advances in natural and technological hazards research, **31**: 321–330.

Leynaud, D., Mienert, J., and Nadim, F. 2004. Slope stability assessment of the Helland Hansen area offshore the mid-Norwegian margin. Marine Geology, **213**(1-4): 457–480. doi:10.1016/j.margeo.2004.10.019.

Lo, K.Y. 1972. An approach to the problem of progressive failure. Can. Geotechnical J., **9**(4): 407–429.

Locat, J., and Lee, H. J. 2000. Submarine landslides: advances and challenges. *In* Proceedings 8th Int. Symposium on Landslides, Cardiff, U.K., June, 2000.

Locat, J., and Lee, H. J. 2002. Submarine landslides: advances and challenges. Canadian Geotechnical Journal, **39**(1): 193–212. doi : 10.1139/T01-089.

Locat, A., Leroueil, S., Bernander, S., Demers, D., Locat, J., and Ouehb, L. 2008. Study of a lateral spread failure in an eastern Canada clay deposit in relation with progressive failure: the Saint-Barnabé-Nord slide. *In* Proc. of the 4th Canadian Conf. on Geohazards: From Causes to Management*,* Québec, Que., pp. 89–96.

Locat, J., Lee, H., Brink, U. S., Twichell, D., Geist, E., and Sansoucy, M. 2009. Geomorphology, stability and mobility of the Currituck slide. Marine Geology, **264**(1-2): 28–40. doi:10.1016/j. margeo.20 08.12.0 05.

Locat, A., Leroueil, S., Bernander, S., Demers, D., Jostad, H.P., and Ouehb, L. 2011. Progressive failures in eastern Canadian and Scandinavian sensitive clays. Canadian Geotechnical J., **48**(11): 1696–1712.

Locat, A., Jostad, H. P., and Leroueil, S. 2013. Numerical modeling of progressive failure and its implications for spreads in sensitive clays. Canadian Geotechnical J., **50**: 961–978. dx.doi.org/10.1139/cgj-2012-0390.

Locat, J., Leroueil, S., Locat, A., and Lee, H. 2014. Weak layers: their definition and classification from a geotechnical perspective. Submarine Mass Movements and Their Consequences, *edited* by S. Krastel et al., Advances in Natural and Technological Hazards Research, **37**: 3–12.

Lunne, T., Long, M., and Forsberg, C. F. 2003. Characterisation and engineering properties of Onsøy clay. Characterisation and Engineering Properties of Natural Soils, *Edited by* Tan et al. 2003, Swets & Zeitlinger, Lisse, pp. 395–427.

Lunne, T., Berre, T., Andersen, K.H., Strandvik, S., and Sjursen, M. 2006. Effect of sample disturbance and consolidation procedures on measured shear strength of soft marine Norwegian clays. Can. Geotech. J., **43**(7): 726–750.

Lunne, T., and Andersen, K. H. 2007. Soft clay shear strength parameters for deepwater geotechnical design. *In* Proc. of the 6th Int. Off. Site Investigations and Geotechnics Conf., London, UK. pp. 151–176.

Masson, D. G., Harbitz, C. B., Wynn, R. B., Pedersen, G., and Løvholt, F. A. 2006. Submarine landslides: processes, triggers and hazard prediction. Phil. Trans. R. Soc. A, Vol. 364, pp. 2009–2039. doi: 10.1098/rsta.2006.1810.

McAdoo B. G. 1999. Mapping submarine slope failures. Marine and Coastal Geographical Information Systems, *Edited by* D. J. Wright and D. J. Barlett. pp. 189–205.

Mello, U. T., and Pratson, L. F. 1999. Regional slope stability and slope-failure mechanics from the two-dimensional state of stress in an infinite slope. Marine Geology, **154**(1-4): 339–356.

Mosher, D.C. 2009. Oceans: Submarine landslides and consequent tsunamis in Canada. J. of the Geological Assoc. of Canada, **36**(4): 179–190.

Nadim, F., Krunic, D., and Jeanjean, P. 2003. Probabilistic slope stability analyses of the Sigsbee Esacarpment. *In* Proc. Off. Tech. Conf., Houston, OTC 15203.

Nadim, F., Kvalstad, T. J., and Guttermsen, T. 2005. Quantification of risk associated with seabed instability at Ormen Lange. Marine and Petroleum Geology, **22**(1-2): 311–318.

Nadim, F., and Locat, J. 2005. Risk assessment for submarine slides. Landslide Risk Management – *edited by* Hungr, Fell, Couture & Eberhardt, Taylor & Francis Group, London.

Niedoroda, A. W., Reed, C. W., Hatchett, L., and Das, H. S. 2003. Developing engineering design criteria for mass gravity flows in deep ocean and continental slope environments. Submarine Mass Movements and Their Consequences, *Edited by* J. Locat and J. Mienert, Dordrecht, pp. 85-94.

Nixon, M.F., and Grozic, J.L.H. 2007. Submarine slope failure due to gas hydrate dissociation: a preliminary quantification. Canadian Geotechnical Journal, **44**: 314–325.

Palmer, A. C., and Rice, J. R. 1973. The growth of slip surfaces in the progressive failure of overconsolidated clay. Proc. R. Soc. London, Ser. A, **332**(1591): 527–548.

PLAXIS. 2011. PLAXIS 2D 2010 manuals. PLAXIS bv., Delft, the Netherlands.

Potts, D. M., Dounias, G. T., and Vaughan, P. R. 1990. Finite element analysis of progressive failure of Carsington embankment. Géotechnique, **40**(1): 79–101.

Puzrin, A. M., Germanovich, L. N., and Kim, S. 2004. Catastrophic failure of submerged slopes in normally consolidated sediments. Géotechnique, **54**(10): 631–643.

Puzrin, A.M., and Germanovich, L.N. 2005. The Growth of Shear Bands in the Catastrophic Failure of Soils. Proc. R. Soc. A, **461**(2056): 1199–1228.

Quinn, P. 2009. Large Landslides in Sensitive Clay in Eastern Canada and the Associated Hazard and Risk to Linear Infrastructure. Doctoral thesis, Queen's University.

Quinn, P. E., Diederichs, M. S., Rowe, R. K., and Hutchinson, D. J. 2011. A new model for large landslides in sensitive clay using a fracture mechanics approach. Canadian Geotechnical J., **48**(8): 1151–1162.

Quinn, P. E., Diederichs, M. S., Rowe, R. K., and Hutchinson, D. J. 2012. Development of progressive failure in sensitive clay slopes. Canadian Geotechnical J., **49**(7): 782–795.

Skempton, A.W. 1964. Long-term stability of clay slopes. Géotechnique, **14**(2): 77–102.

Solheim, A., Bryn, P., Sejrup, H.P., Mienert, J., and Berg, K. 2005. Ormen Lange—an integrated study for the safe development of a deep-water gas field within the Storegga Slide Complex, NE Atlantic continental margin; Executive summary. Marine and Petroleum Geology, **22**(1-2): 1–9.

Stark, T., and Contreras, I.A. 1996. Constant volume ring shear apparatus. Geotechnical Testing Journal, **19**(1): 3–11.

Sultan, N., Cochonat, P., Canals, M., Cattaneo, A., Dennielou, B., Haflidason, H., Laberg, J. S., Long, D., Mienert, J., Trincardi, F., Urgeles, R., Vorren, T. O., and Wilson, C. 2004. Triggering mechanisms of slope instability processes and sediment failures on continental margins: a geotechnical approach. Marine Geology, **213**(1-4): 291–321. doi:10.1016/j. margeo.2004.10.011.

Sultan, N., Savoye, B., Jouet, G., Leynaud, D., Cochonat, P., Henry, P., Stegmann, S., and Kopf, A. 2010. Investigation of a possible submarine landslide at the Var delta front (Nice continental slope, southeast France). Canadian Geotechnical J., **47**(4): 486–496. doi:10.1139 /T09-105.

Take, W. A. and Bolton, M. D. 2001. The use of centrifuge modelling to investigate progressive failure of overconsolidated clay embankments. Centrifuge and Constitutive Modelling: Two extremes, Ascona, Switzerland, Springman S.M. (ed.), Balkema, Rotterdam.

Tavenas, F., Flon, P., Leroueil, S., and Lebuis, J. 1983. Remolding energy and risk of slide retrogression in sensitive clays. *In* Proc. of the Symposium on Slopes on Soft Clays, Linköping, Sweden, SGI Report No. 17, pp. 423–454.

Twichell, D.C., Chaytor, J.D., Brink, U. S., and Buczkowski, B. 2009. Morphology of the late Quaternary submarine landslides along the U.S. Atlantic continental margin. Marine Geology, **264**: 4–15. doi: 10.1016/j.margeo.20 09.01.0 09.

Yang, S.L., Solheim, A., Kvalstad, T.J., Forsberg, C.F., and Michael Schnellmann, M. 2006. Behaviour of the sediments in the Storegga Slide interpreted by the steady state concept. Norwegian J. of Geology, **86**(3): 243–253.

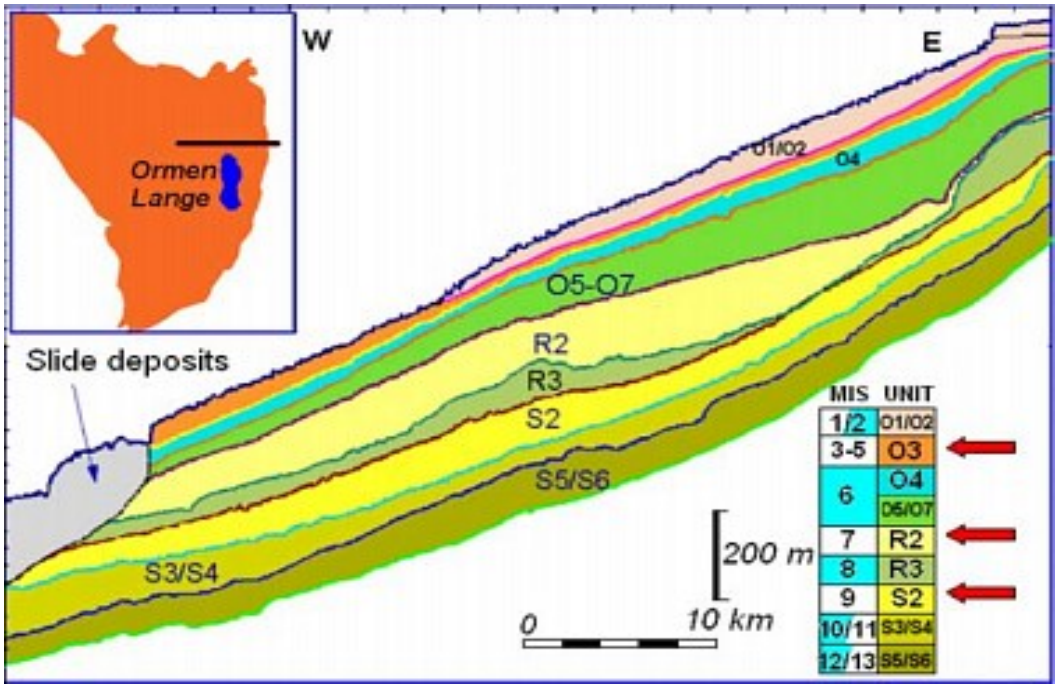

Figure 3.1: Seabed stratigraphy in the Storegga slide area (after Bryn et al., 2005) (Note: red arrows show three main marine sensitive clay layers, i.e. potential failure)

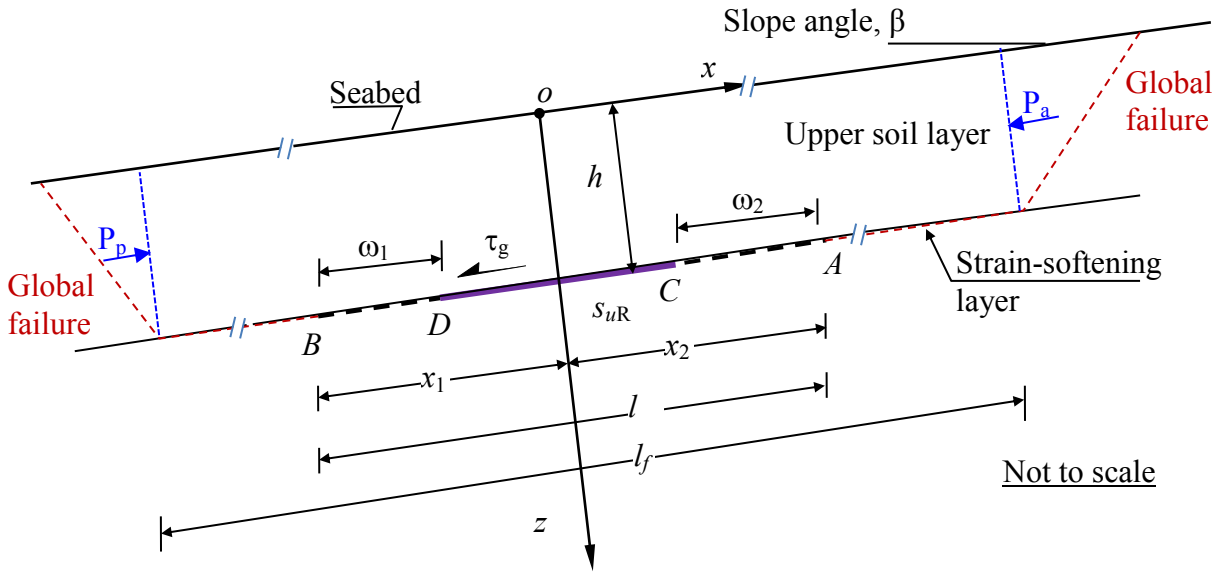

Figure 3.2: Shear band formation in typical submarine slope with a strain softening clay layer

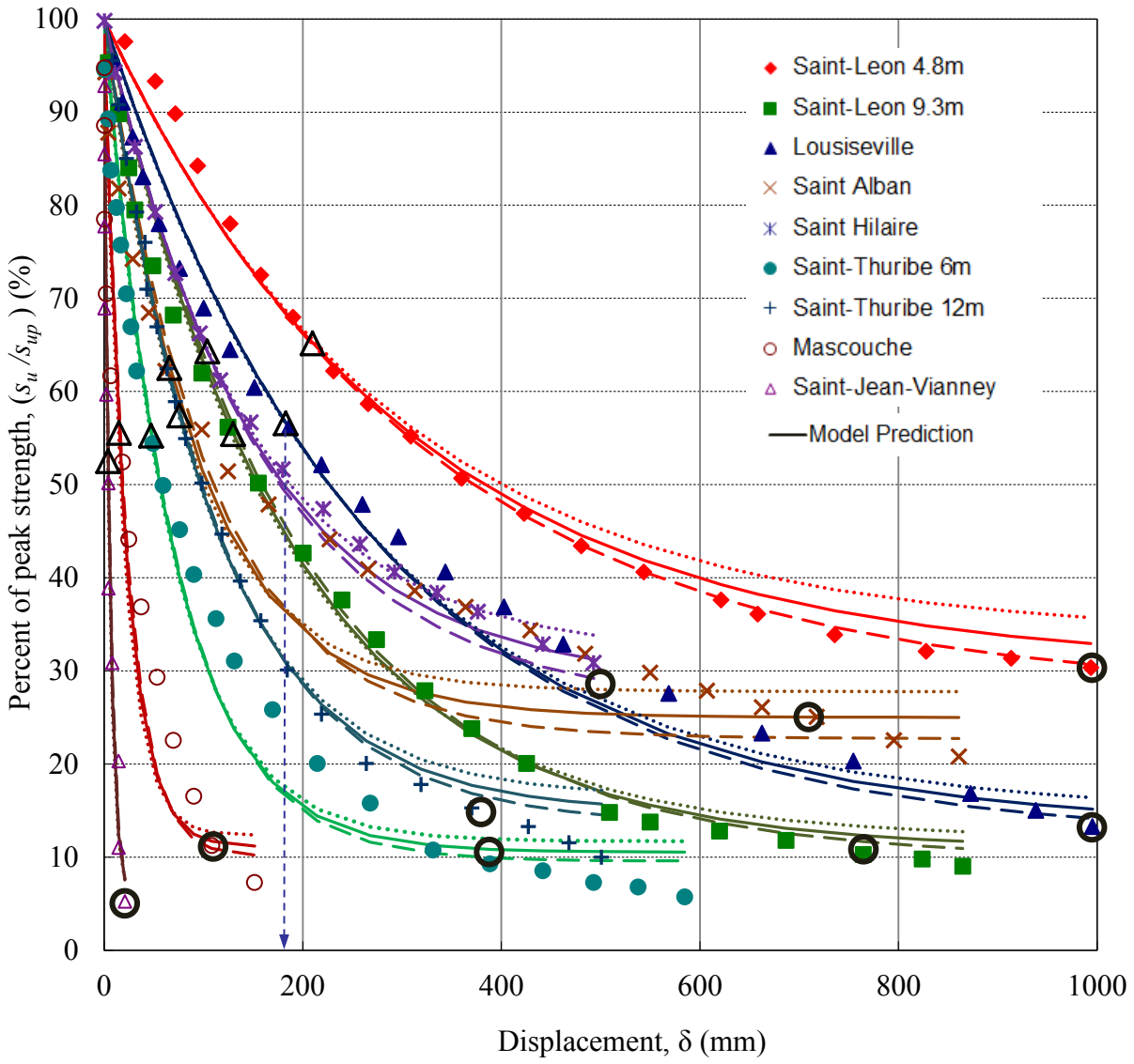

Figure 3.3: Comparison between test results and model predictions of post-peak shear strength

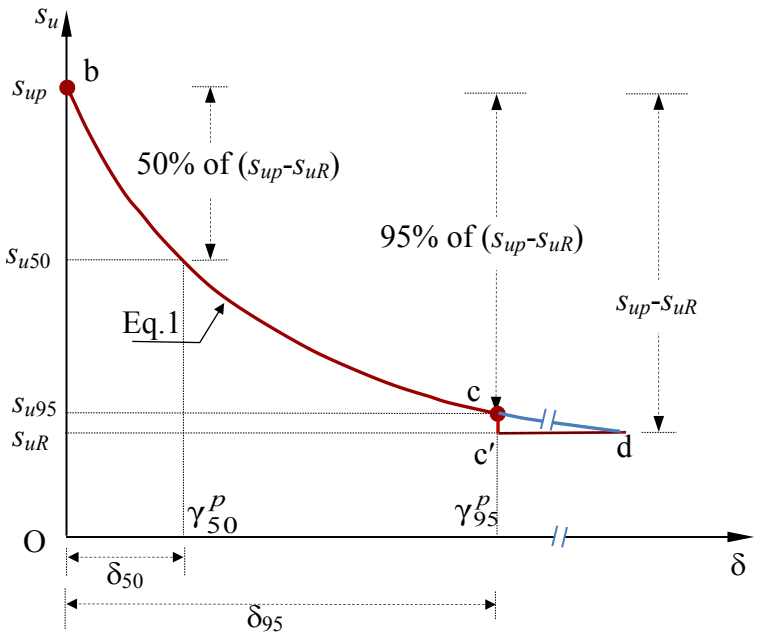

Figure 3.4: Post-peak shear strength degradation model

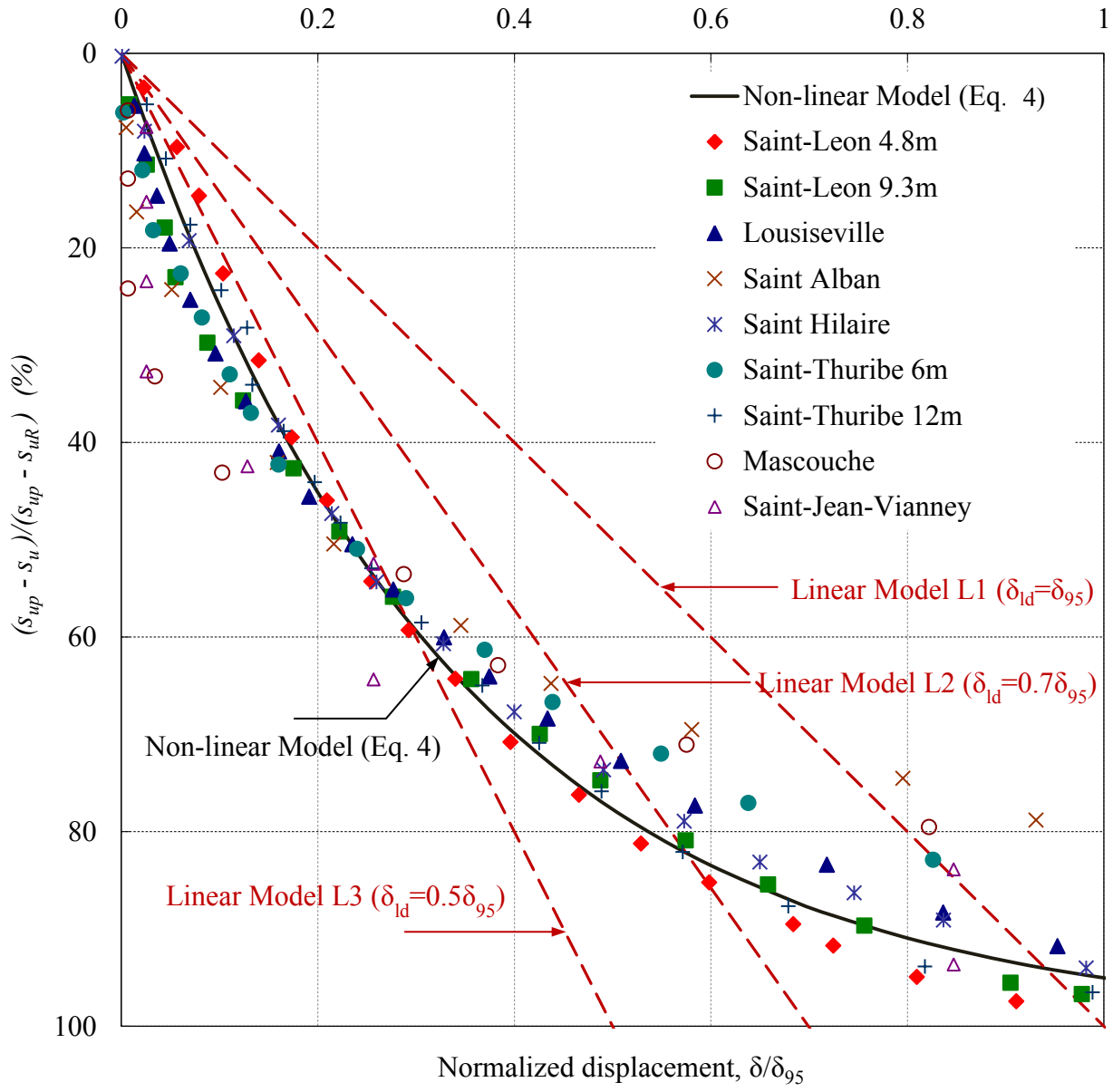

Figure 3.5: Post-peak softening in normalized form

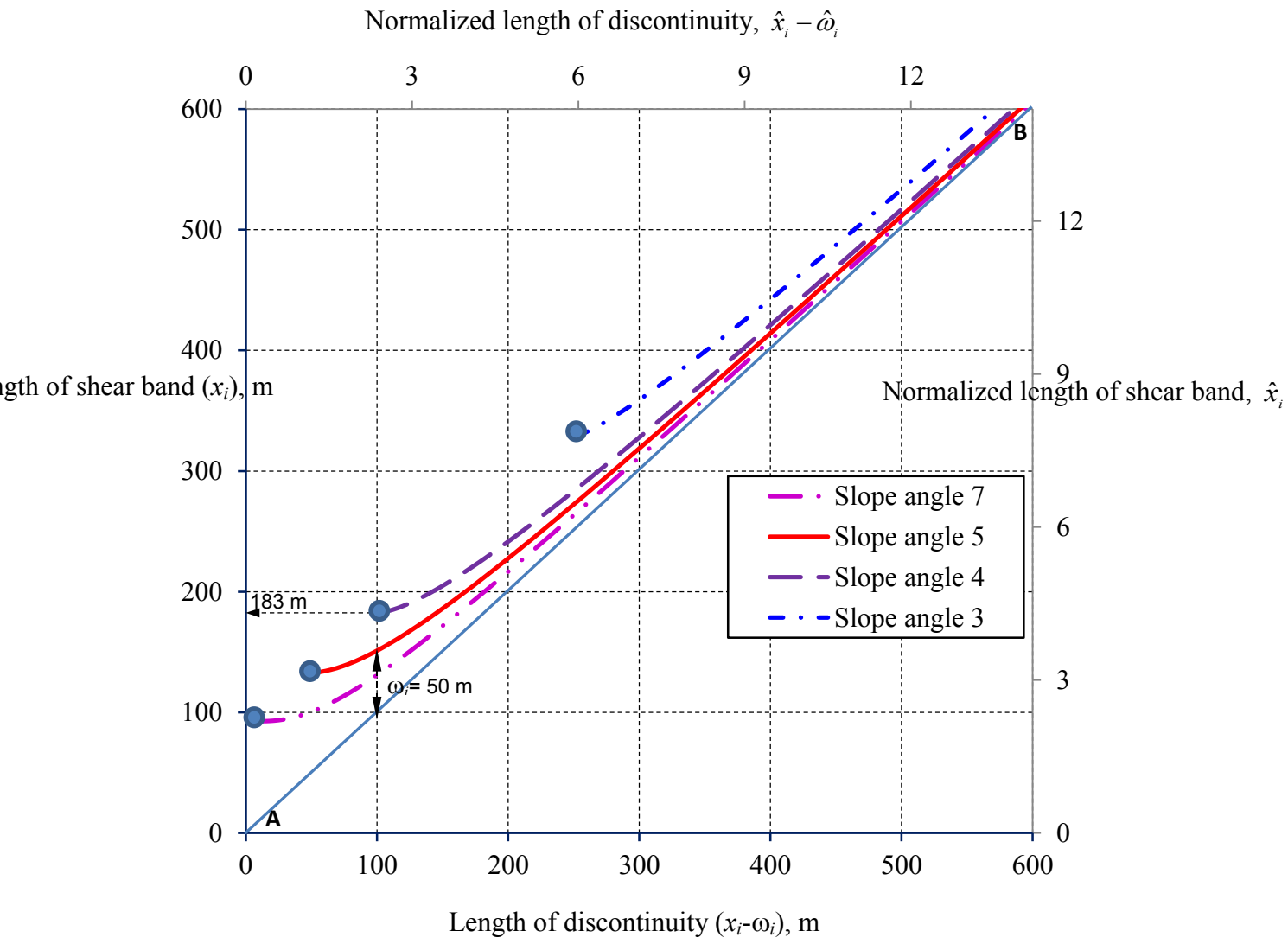

Figure 3. 6: Length of shear band and discontinuity for different slope angle

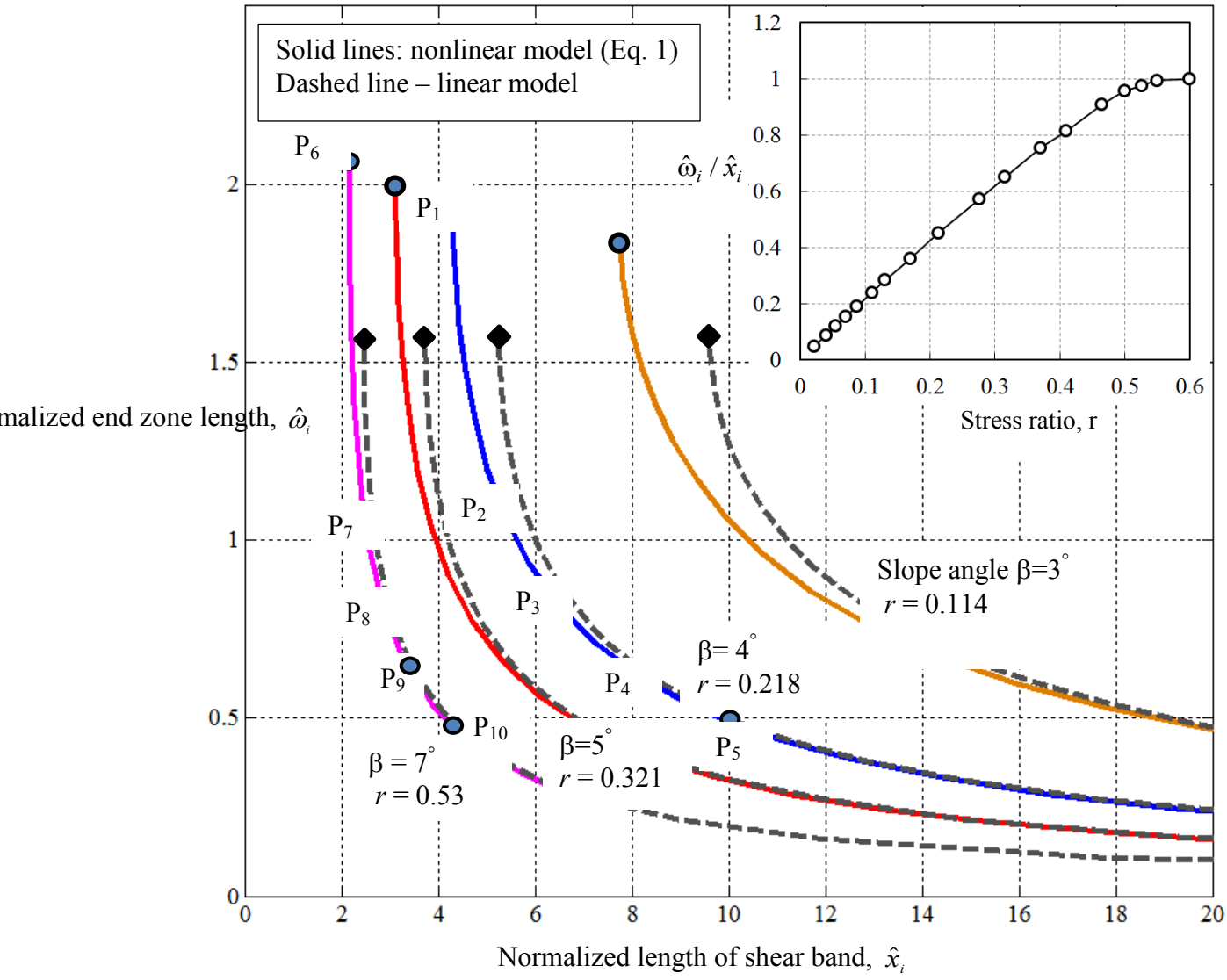

Figure 3. 7: Normalized lengths of shear band ($\hat{x}_2$) and end zone ($\hat{\omega}_2$)

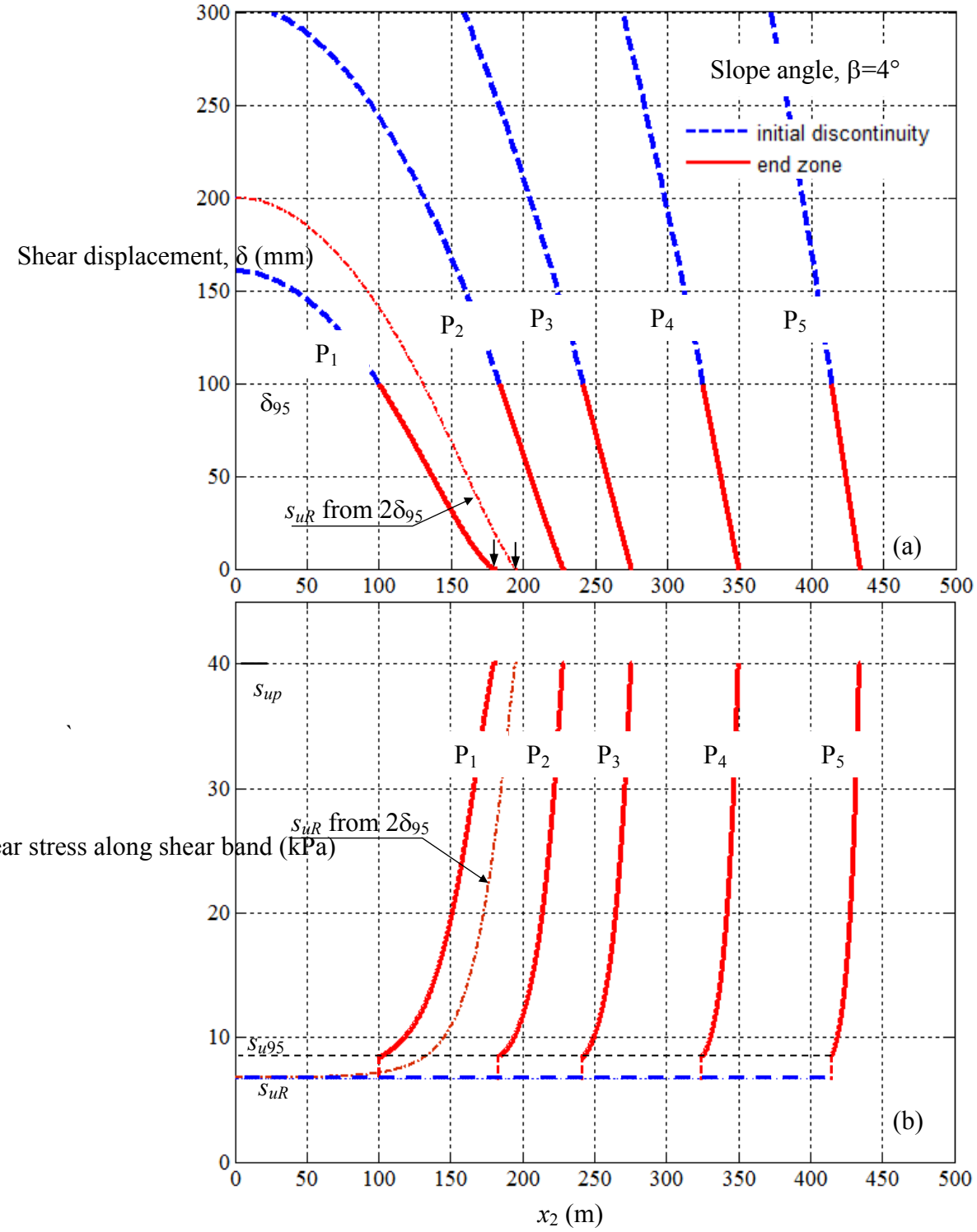

Figure 3. 8: Variation of displacement and shear strength along the shear band for 4° slope angle

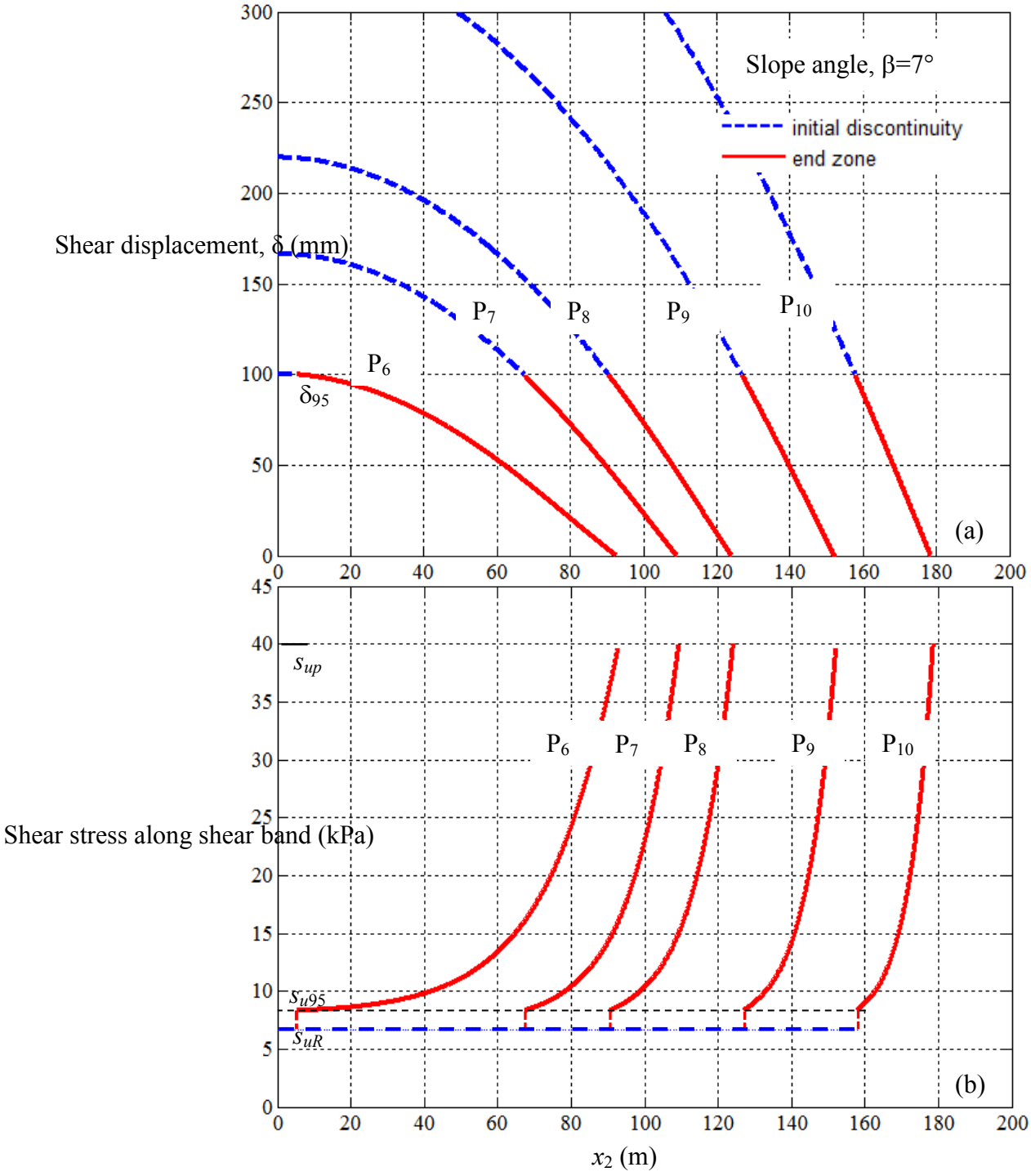

Figure 3. 9: Variation of displacement and shear strength along the shear band for 7° slope angle

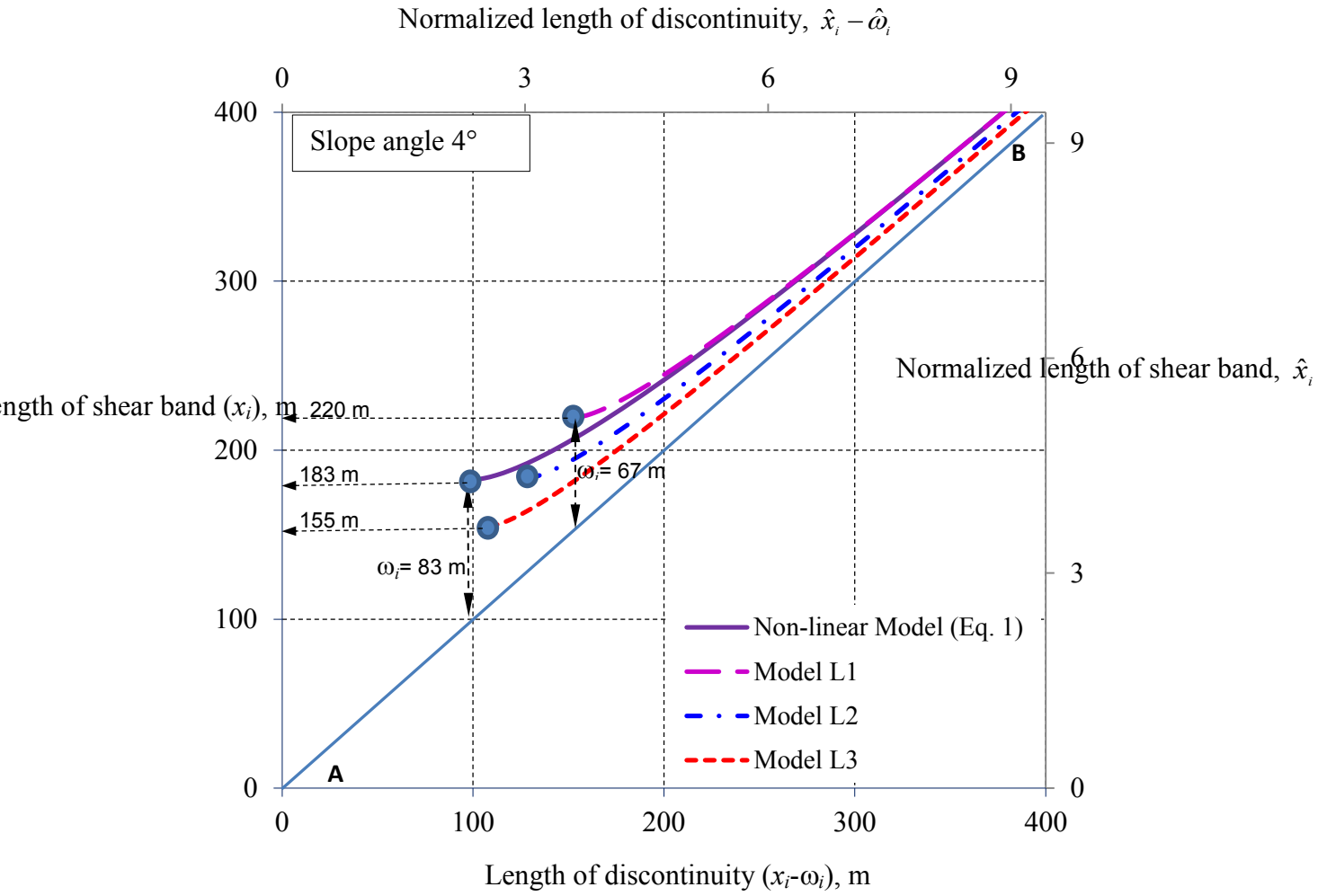

Figure 3.10 (a): Variation of discontinuity and shear band lengths for linear and nonlinear models for β=4°

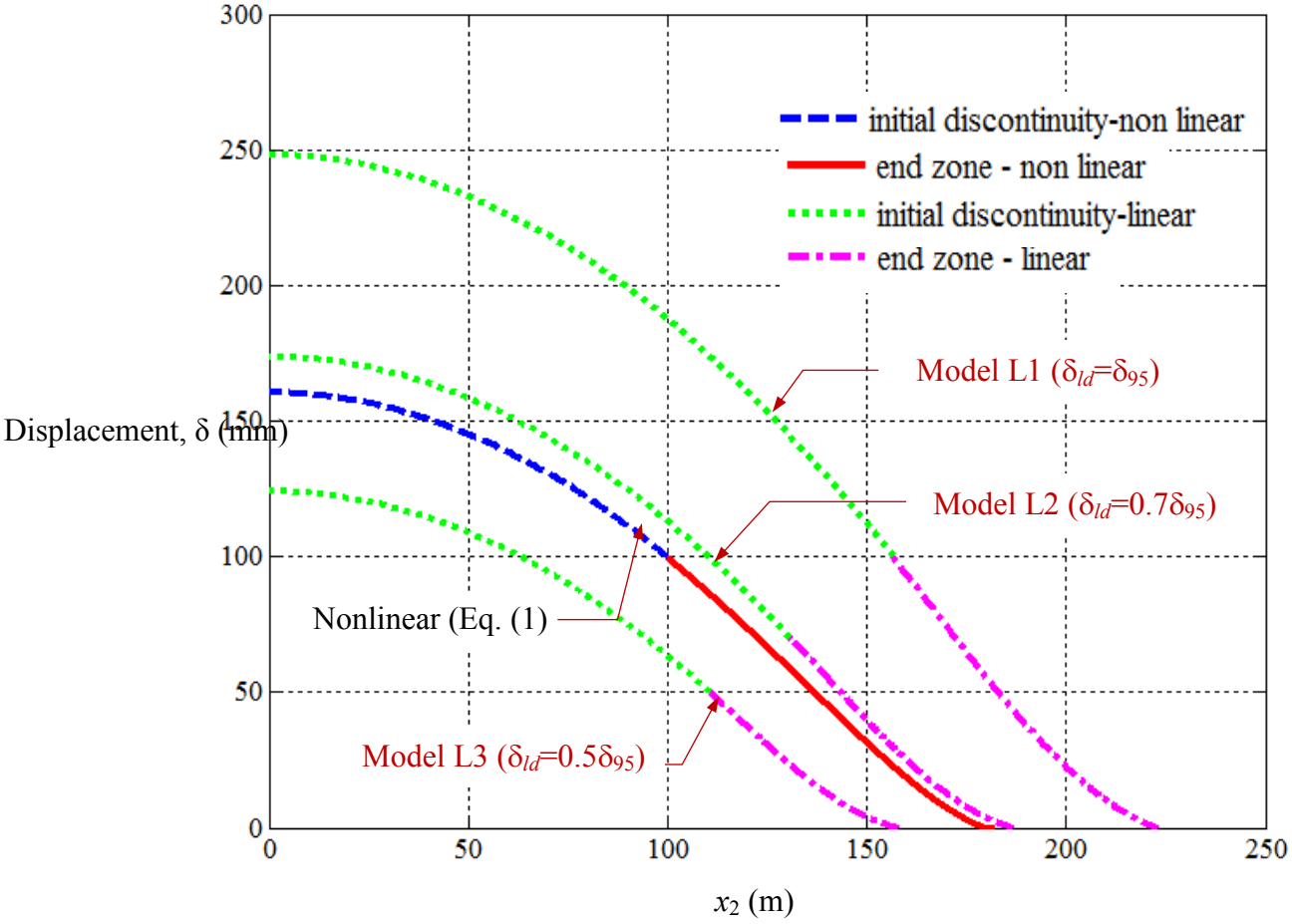

Figure 3.10(b). Comparison of displacement in shear band for linear and nonlinear models at initiation of shear band propagation for β=4°

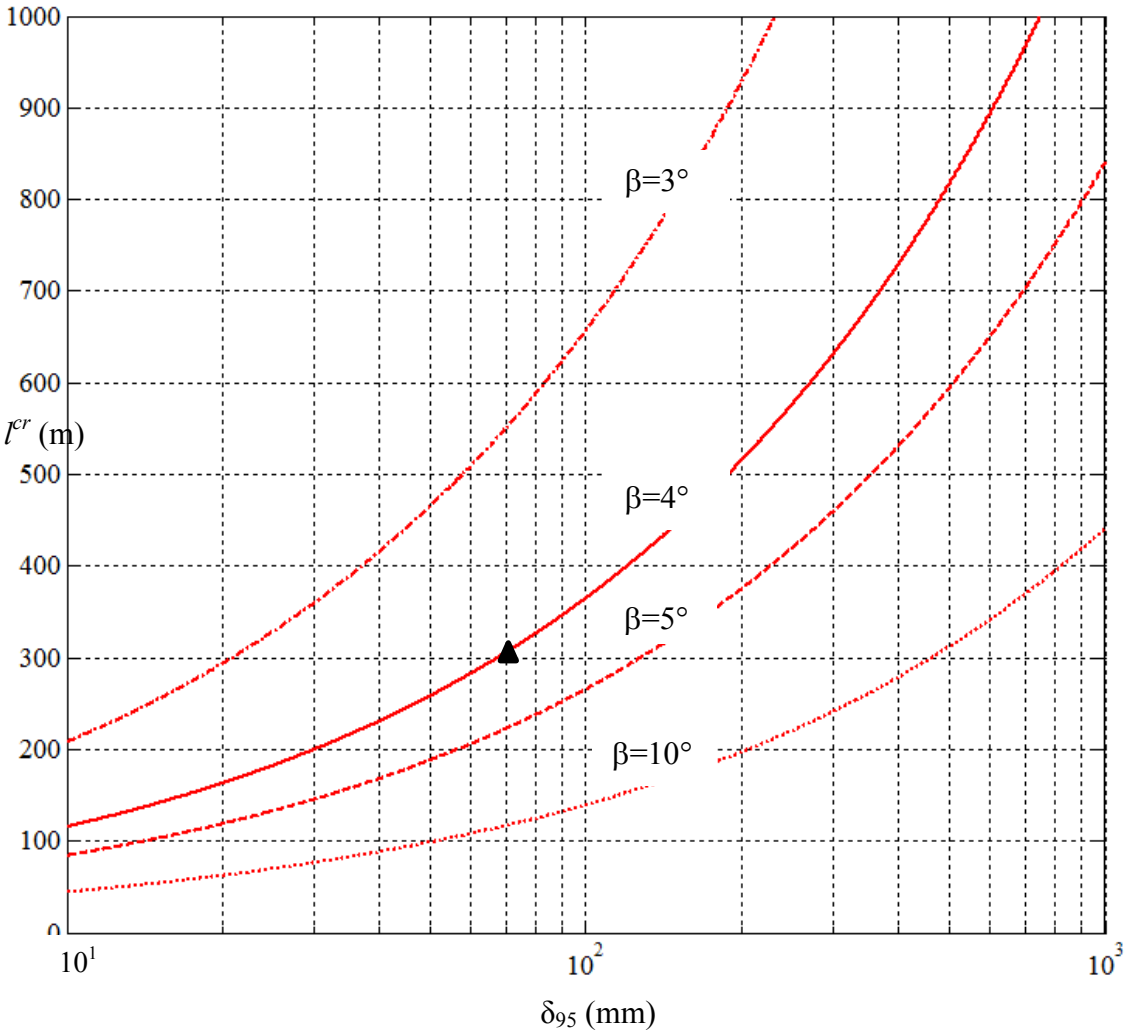

Figure 3.11: Effects of δ_{95} on initiation of shear band propagation

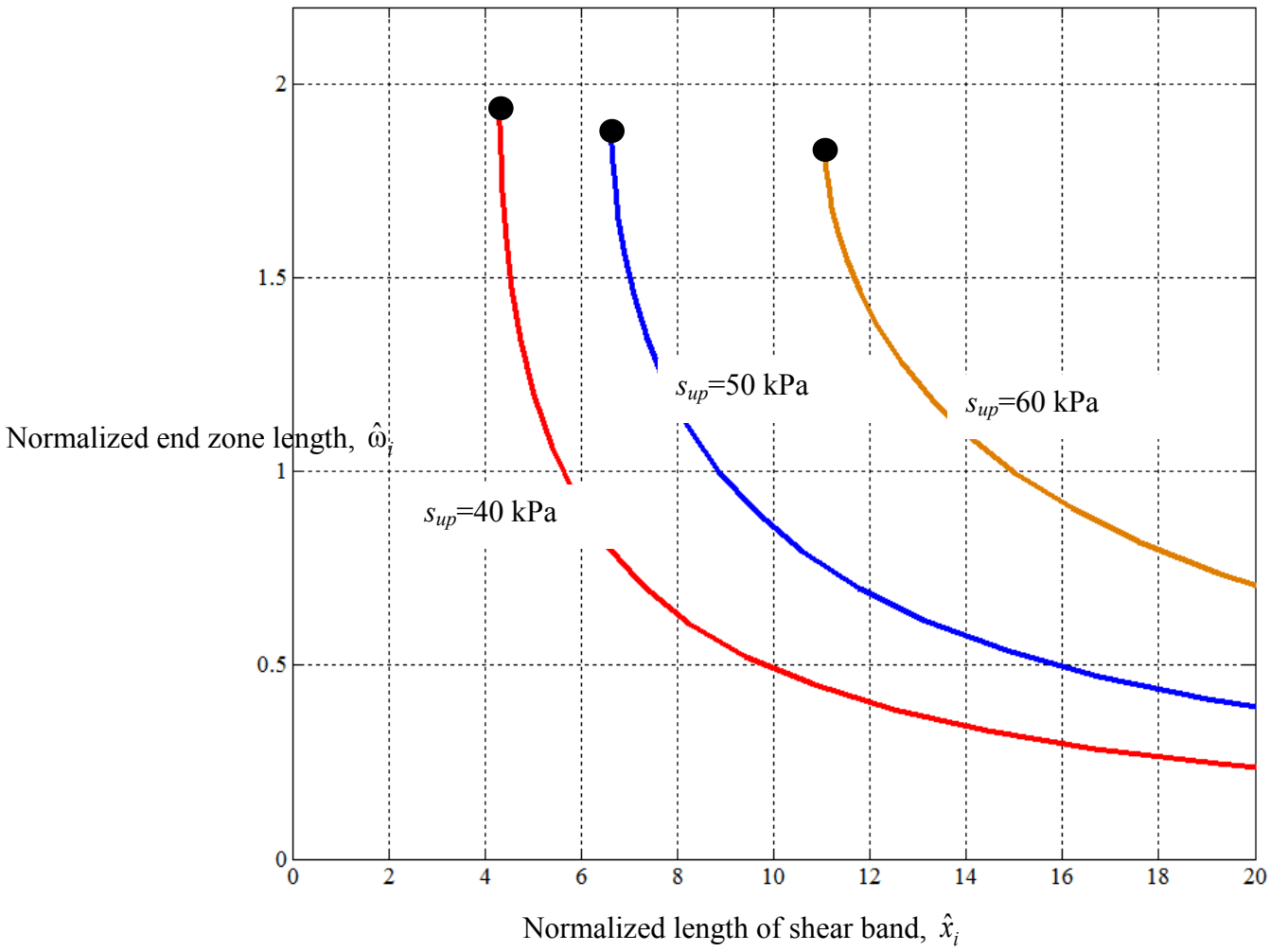

Figure 3. 12: Normalized lengths of shear band and end zone for different peak shear strength

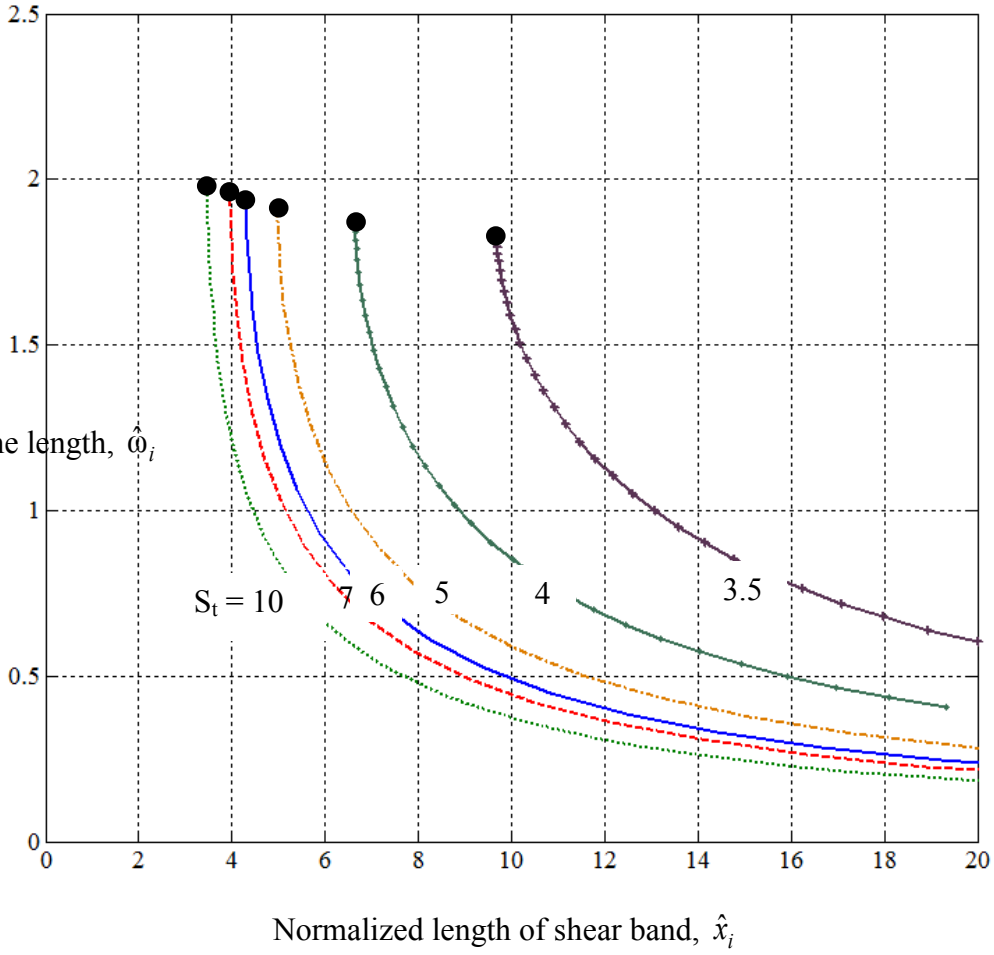

Figure 3. 13: Normalized lengths of shear band and end zone for different sensitivity

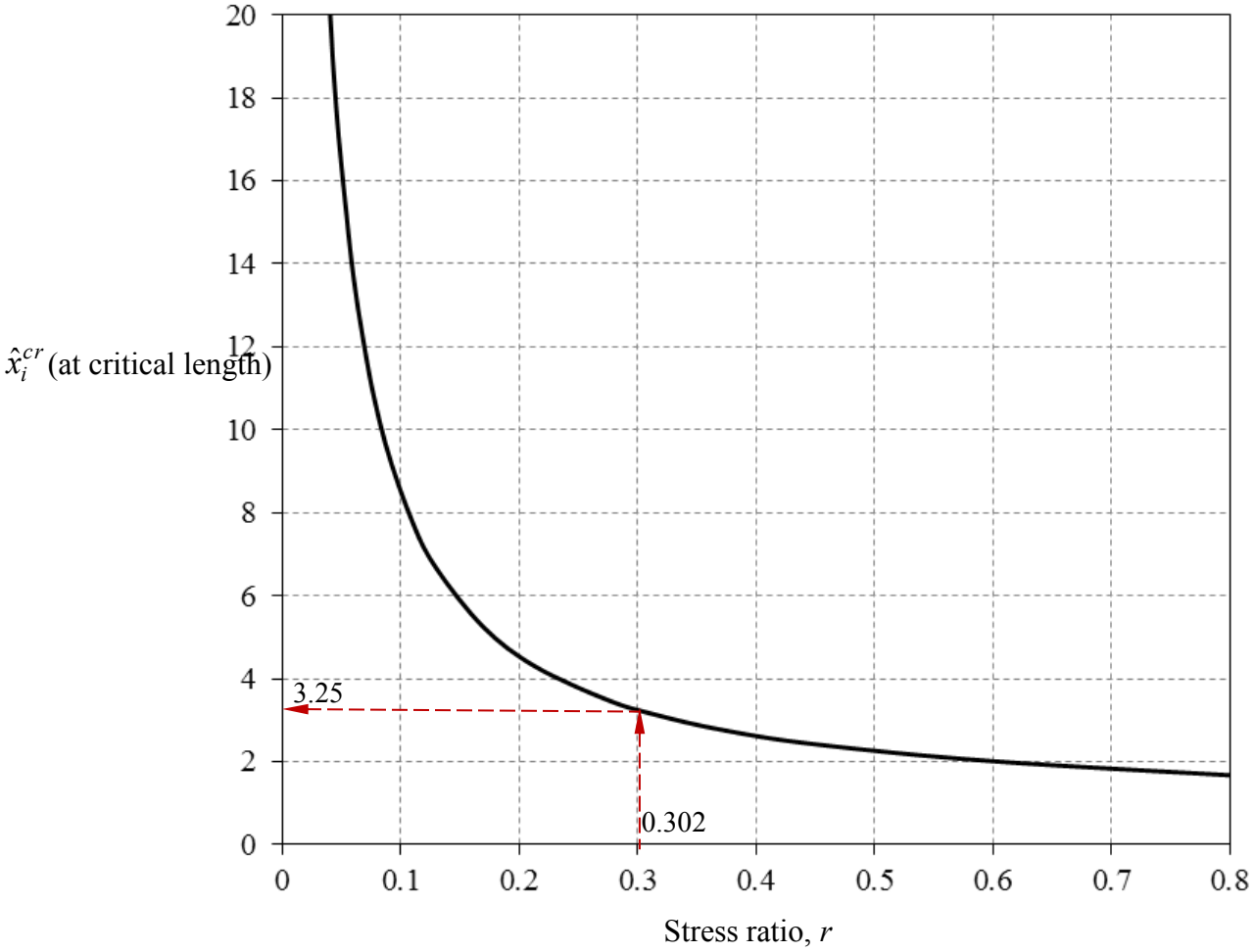

Figure 3. 14: Normalized lengths of shear band and end zone for different stress ratio

Table 3. 1: Calculated values of S_t and δ_{95}

Soil Type & depth (m)	Sensitivity, S_t	δ_{50} (+10%, -10%) (mm)	δ_{95} (+10%, -10%) (mm)
Saint-Leon 4.8m	3.3	210 (220, 198)	909 (952, 857)
Saint-Leon 9.3m	9.25	130 (136, 125)	563 (589, 541)
Lousiseville 6m	7.6	183 (187, 178)	792 (809, 770)
Saint Hilaire 5.6m	3.5	104 (109, 98)	450 (471, 424)
Saint-Thuribe 6m	9.5	47.5 (49, 46)	206 (212, 199)
Saint-Thuribe 12m	6.75	76 (79, 73)	323 (342, 316)
Mascouche 9m	9	15 (16, 13.5)	65 (69, 58)
Saint Alban 6.6m	4	66 (73, 59)	286 (316, 255)
Saint-Jean-Vianney 30m	20	4 (4.25, 3.75)	17 (18, 16)

Table 3. 2: Parameters used in base case analysis

Parameter	Value
Slope angle, β (°)	4
Depth of sensitive clay layer, h (m)	20
Top layer/Glacial clay	
Undrained Young's modulus, $E_1 = E_2$ (MPa)	30
Submerged unit weight of soil, γ' (kN/m^3)	10
Undrained shear strength, $\bar{s}_u$ (kPa)	50
Marine clay layer	
Peak undrained shear strength, s_{up} (kPa)	40
Undrained shear strength, s_{uR} (kPa)	6.67
Sensitivity, $S_t = s_{up}/s_{uR}$	6
δ_{95} (m)	0.1

CHAPTER 4

Large Deformation Finite Element Modeling of Progressive Failure Leading to Spread in Sensitive Clay Slopes

Co-Authorship: This chapter has been accepted for publication as a technical paper in Géotechnique as: Dey, R., Hawlader, B., Phillips, R. and Soga, K. (2015) "Large deformation finite element modeling of progressive failure leading to spread in sensitive clay slopes".
Most of the research work presented in this chapter was conducted by the first author. He also prepared the draft manuscript. The other authors supervised the research and reviewed the manuscript.

4.1 Abstract

The occurrence of large landslides in sensitive clays, such as spreads, can be modeled by progressive development of large inelastic shear deformation zones (shear bands). The main objective of the present study is to preform large deformation finite element (FE) modeling of sensitive clay slopes to simulate progressive failure and dislocation of failed soil mass using the Coupled Eulerian Lagrangian (CEL) approach available in Abaqus FE software. The degradation of undrained shear strength with plastic shear strain (strain-softening) is implemented in Abaqus CEL, which is then used to simulate the initiation and propagation of shear bands due to river bank erosion. The formation of horsts and grabens and dislocation of soil masses that lead to large-scale landslides are simulated. This FE model explains the displacements of different blocks in the failed soil mass and also the remoulding of soil around the shear bands. The main

advantages of the present FE model over other numerical models available in the literature are that it can simulate the whole process of progressive failure leading to spread. The FE results are consistent with previous conceptual models proposed from field observations. The parametric study shows that, depending upon geometry and soil properties, toe erosion could cause three types of shear band formation: (i) only a horizontal shear band without any global failure, (ii) global failure of only one block of soil, (iii) global failure of multiple blocks of soil in the form of horsts and grabens.

Key words: landslides, sensitive clay, progressive failure, large deformation, finite element modeling, shear band, horst and grabens

4.2 Introduction

Large-scale landslides in sensitive clays are common in Eastern Canada and Scandinavia. Most of these slides are progressive in nature. The post-peak softening of sensitive clays is considered as one of the main reasons of progressive failure. The failure occurs quite rapidly, essentially in undrained conditions (Locat et al., 2013). Based on initiation and progression of the sliding surfaces or shear bands, the failure of slopes can be divided into two categories, namely upward and downward progressive failures. Upward progressive failure might be initiated due to excavation, erosion or small slides in the river bank slopes (Quinn et al., 2007; Locat et al., 2008; Demers et al., 2013). On the other hand, downward progressive failure could be triggered by vertical loading or pile driving in the upslope area (Bernander, 2000; Gylland et al, 2010). The numerical modeling of upward progressive failure is presented in this paper. It is to be noted here

that the propagation of a shear band has been identified as one of the key factors for modelling different types of failure, such as catastrophic failure of mild submarine slopes and progressive failure of embankments (Potts et al., 1990; Puzrin et al., 2004; Puzrin and Germanovich, 2005; Gauer et al., 2005; Kvalstad et al., 2005). The focus of the present study is to analyze the failure of sensitive clay slopes under undrained conditions.

Landslides in sensitive clays could be in the form of multiple retrogressive, translational progressive or spreads (Tavenas, 1984; Karlsrud et al., 1984). According to Fortin et al. (2008), 42% of large landslides which occurred in Eastern Canada can be categorized as spreads. Many spread failures such as Sköttorp landslide in Sweden (Odenstad, 1951) and the landslides that occurred in Quebec including the 1989 Saint-Liguori landslide (Grondin and Demers, 1996), Saint-Ambroise-de-Kildare landslide (Carson, 1977), Saint-Barnabé-Nord slide (Locat et al., 2008) are reported to be triggered by erosion at the toe of the slope (Bernander, 2000; Locat et al., 2008; Quinn et al., 2007; Locat et al., 2011), even though it is very difficult to identify the true triggering mechanisms. The spread type of failures could be explained by the progressive failure mechanisms (Locat et al., 2013).

Field observations show that the progressive failure propagating in the upslope direction is initiated by formation of a quasi-horizontal shear band from the toe of the slope (Locat et al., 2011; 2013). Due to significant displacement, the soil layer above this shear band might dislocate into a number of soil blocks in the form of horsts and grabens (Fig. 4.1). The shear strains are mainly concentrated around the surfaces of the horsts and grabens with minimal strains inside these blocks. Moreover, once the failure surfaces are developed, the horsts and grabens displace almost laterally on the initially developed quasi-horizontal shear band that results in spread. This

process is shown schematically in Figure 4.2. Very large strains and displacements are developed around the shear bands and therefore it should be modeled as a large deformation problem.

To explain upward progressive failure and spreads, the presence of a horizontal weak layer/surface was recognized by researchers several decades ago (Odenstad, 1951; Carson, 1977). Examining field evidences, in the recent studies (e.g. Locat et al., 2008; 2011; 2013; Quinn et al., 2011) it is shown that the initial horizontal shear band might form due to erosion, excavation or small slides near the bank. Locat et al. (2011) demonstrated the mechanisms of quasi-horizontal shear band formation for an idealized condition in an infinite slope. An external force parallel to the ground surface is applied near the toe above the predefined shear zone. The variation of shear stress, in relation to shear strength, with distance from the point of load is discussed. Locat et al. (2013) extended their work (Locat et al., 2011) through numerical modeling using PLAXIS 2D (PLAXIS, 2011) and BIFURC (Jostad and Andresen, 2002) FE programs. In this decoupled modeling, the initial stresses of soil are calculated using the PLAXIS 2D with the Mohr-Coulomb model. The calculated stresses from PLAXIS are then used in BIFURC to simulate the initiation and progression of a quasi-horizontal shear band, simply by pulling the top of the predefined shear zone at the toe of slope. While these initial attempts partly explain the mechanisms involved in shear band formation, the complete failure processes were not simulated. These studies have some limitations. They could simulate the formation of quasi-horizontal shear band only, because the soil above the shear zone is assumed to be elastic. With the applied force, the length of the shear band increases along the predefined shear zone. However, in reality another shear band might form from the horizontal shear band that might propagate to the ground surface resulting in global failure of the slope as discussed in the following sections. As it is not possible to model this with elastic soil properties above the shear

zone, they assumed that the global failure occurs when it reaches the active failure condition. With their numerical techniques, the formation of subsequent horsts and grabens could not be simulated.

Quinn et al. (2011) used the concepts of linear elastic fracture mechanics (FM) and proposed a model for development of shear bands in a simplified slope with a vertical cut. The critical length required to initiate the propagation of the shear band was calculated using the approach of Palmer and Rice (1973). They hypothesize that the failure of the slope would occur when the length of the shear band is sufficiently large such that the downward unbalanced force causes active shear failure. The authors also used the same concept to analyze the slope with additional stresses due to earthquake loading (Quinn et al., 2012). They also conducted elastic FE analysis to validate some of their assumptions.

Norwegian Geotechnical Institute (NGI) (Jostad and Andresen, 2002; Andresen and Jostad, 2004; Andresen and Jostad, 2007; Gylland et al., 2010) also analyzed progressive failure of slopes developing the computer program BIFURC. However, none of these numerical techniques could simulate the complete process of upward progressive failure.

Recognizing the fact that the progressive failure of slopes involves large deformation, the Coupled Eulerian Lagrangian (CEL) approach in Abaqus FE software is used in the present FE analyses. The paper is organized in the following way. First, the FE modeling in Abaqus CEL is presented. A model that represents the variation of undrained shear strength (s_u) with shear strain is presented in the second part. In the third part, the formation of shear bands and horsts and grabens is presented. Finally, a parametric study is conducted to show the effects of some soil parameters and the slope geometry.

4.3 Problem Definition

The geometry of the 'base case' slope considered in this study is shown in Fig. 4.3. The river bank has a slope, β of 30° and the ground surface is horizontal. There is a crust of overconsolidated clay near the face of the slope and below the ground surface. The thickness of the crust below the level ground surface is H_c. Under the crust there is a thick layer of sensitive clay (thickness H_{st}) followed by a base layer of stiff clay. It is assumed that the base layer is very thick; however, in the FE analyses only 3 m of this layer is modeled as it does not have significant effect on the results, which has been verified by an analysis with a 10 m thick base layer. The geometry considered here is an idealized section of river banks in Eastern Canada where spread failures have occurred (Locat et al., 2011; Quinn et al., 2012). Note that change in geometry and soil properties, including the property of base layer, might alter the failure pattern. For simplicity the groundwater table is assumed to be located at the ground surface and the river is full. Potential long-term failure of the riverbank is not considered. It is assumed that the upward progressive failure is initiated by erosion and/or excavation of the river bank. In the FE analyses, the erosion or excavation is modeled by removing a block of soil near the toe of the slope as shown by the shaded zone in Fig. 4.3. In the following sections this block will be referred as the "eroded block." It is also assumed that the erosion or excavation occurs relatively fast such that the deformation/failure of the remaining soil occurs in undrained condition. The length of the soil domain in the present FE model is 200 m and therefore no significant effects on the results are expected from the right boundary.

4.4 Finite Element Modeling

The elasto-plastic FE analysis is a powerful alternative approach for slope stability analysis over conventional limit equilibrium methods. Most of the FE models available in the literature for slope stability analysis are developed in a Lagrangian framework (e.g. Griffith and Lane, 1999; Loukidis et al., 2003). One of the main disadvantages of this type of model is that a significant mesh distortion occurs around the failure planes. The non-convergence of the solution due to significant mesh distortion is considered as one of the conditions of failure in some studies (e.g. Griffith and Lane, 1999). In order to overcome these issues, the CEL approach in Abaqus 6.10 EF1 is used in this study. In CEL, the mesh is fixed and soil as Eulerian material flows through the fixed mesh. Therefore, numerical issues related to mesh distortion or mesh tangling, even at very large strains, are not expected anywhere including the zones around the failure planes. Note that Abaqus CEL has been used in previous studies for other applications such as quasi-static penetration of spudcan foundations and offshore pipelines (Qiu et al., 2011; Tho et al., 2012; Dutta et al., 2014). Its performance has also been validated by comparing the results with the remeshing and interpolation technique with small strain (RITSS) for static and dynamic problems (Tian et al., 2011; Wang et al., 2013)

The CEL framework allows only three-dimensional modeling, and therefore the analyses are performed with only one element length in the out of plane direction. For the 'base case' analysis, 0.5 m × 0.5 m mesh is used. However, analyses are also performed for different mesh sizes and a mesh independent modeling technique is presented. The FE model consists of three parts: (i) soil, (ii) eroded block and (iii) void space. The eroded block is modeled as a rigid body in the Lagrangian framework, which makes the model computationally efficient, while the soil is modeled as an Eulerian material using EC3D8R 8-noded brick elements. A void space (efghij) is

created above the soil as shown in Fig. 4.3 to accommodate displaced soil. The soil and voids for the initial condition are created using the Eulerian Volume Fraction (EVF) tool available in Abaqus. For clay, EVF=1 meaning that the elements are filled with Eulerian material (clay) while EVF=0 for the void space. Zero velocity boundary conditions are applied normal to the bottom and all the vertical faces of the domain. No velocity boundary condition is applied at the soil-void interface (efgh in Fig. 4.3) so that the soil can move into the void space when needed. Unbonded smooth interface condition between the eroded block and clay is used.

The numerical analysis consists of two steps of loading. Keeping the eroded block fixed, the geostatic load is applied in the first step to bring the soil to an in-situ stress condition under K_0=1. The initial effective stresses influence the failure of the slope (Lo and Lee, 1973; Locat et al., 2013) and therefore analyses with different initial effective stress conditions need to be performed. The slope is stable in the geostatic step for the conditions analyzed here, even though some shear stress (less than peak undrained shear strength) develops especially near the river bank. In the second step, the eroded block is displaced laterally (Δ) up to 30.75 m at a constant speed (v_e) of 0.05 m/s to the left applying a displacement boundary condition at the reference point of the rigid body. The speed 0.05 m/s is low enough to maintain quasi-static conditions during the analyses with the 0.5-m mesh, as the analysis at a slower speed (v_e=0.01 m/s) does not show any significant change in the failure pattern. However, the computational time for this slow speed is very high and therefore all the analyses presented in the following sections are performed at v_e=0.05 m/s unless otherwise mentioned. Note that, analyses are also performed by replacing the eroded block with soil of same properties of the crust and sensitive clays and found that the slope is stable after the geostatic step. This implies that the movement of the eroded block represents the effect of erosion on a stable slope.

4.5 Undrained Shear Strength of Soil

Laboratory tests (e.g. Tavenas et al., 1983; Bjerrum and Landva, 1966; Bernander, 2000) show that the undrained shear strength of sensitive clay decreases with plastic shear strain. Following Anastasopoulos et al. (2007), it is assumed that equal shear strains develop throughout the whole depth of the soil specimen until the peak. After that, the shear strain is localized in a very small region along the shear band. The shear strain could be calculated if the thickness of the shear band is known; however, the proper estimation of shear band thickness is very difficult in laboratory experiments or in the field. Therefore, shear displacement is used to define the post-peak softening curve while shear strain is used in the pre-peak region. It is to be noted here that previous authors (e.g. Quinn et al., 2011) also recommended to use relative displacement along the shear band after the peak and the strain concepts for the pre-peak elastic part of the stress-strain curve.

Figure 4.4 shows the stress-strain behaviour of sensitive clay used in the present FE analysis. The linear elastic pre-peak segment (line *oa* in Fig. 4.4) is defined by undrained Young's modulus (E_u) and Poisson's ratio (ν_u). The peak undrained shear strength (s_{up}) is mobilized at point *a* and remains constant up to point *b* for a displacement of δ_{pc} from point *a*. The undrained shear strength at completely remoulded (stirred) condition (s_{ur}) can be measured in laboratory. However, Bernander (2000) could not find relevance of s_{ur} in post-slide investigations and therefore recommended an undrained shear strength s_{uR} ($>s_{ur}$) for progressive failure analysis that mobilizes in shear bands at a considerable shear displacement.

The shear strength degradation curve (*bcd*) is defined by the following exponential function.

$$s_u = \left[\frac{1}{S_t} + \left(1 - \frac{1}{S_t} \right) e^{-3\delta / \delta_{95}} \right] s_{up} \quad (1)$$

where s_u is the mobilized undrained shear strength; $\delta=\delta_t-(\delta_e+\delta_{pc})$ with δ_e and δ_t are the elastic and total shear displacements, respectively; δ_{95} is the value of δ at which the undrained shear strength is reduced by 95% of (s_{up}-s_{uR}) and $S_t = s_{up}/s_{uR}$. Equation (1) is a modified form of the strength degradation equation proposed by Einav and Randolph (2005), but in terms of displacement along the shear band. As it is an exponential curve, s_u up to $2\delta_{95}$ is defined by Eq. (1). After that a linear relationship (line *de*) is used to decrease s_u to a constant $s_{u(ld)}$ at δ_{ld}. Assuming simple shear condition, the plastic shear strain (γ^p) can be calculated as $(\delta_t-\delta_e)/t$, where t is the thickness of the soil element. In FE analysis, the variation of yield strength ($=2s_u$) is defined as a function plastic shear strain, which is calculated assuming $t=t_{FE}$, where t_{FE} is the thickness of the cubical EC3D8R elements. The von Mises yield criterion is adopted.

Table 4.1 shows the geotechnical parameters used in this study. These parameters are estimated from laboratory tests, interpretation of test data, constitutive model development and numerical studies on landslides in sensitive clays available in the literature (e.g. Tavenas et al., 1983; Bernander, 2000; Leroueil, 2001; Locat et al., 2008; Quinn, 2009; Quinn et al., 2011; Locat et al., 2011 and 2013). Tavenas et al. (1983) presented experimental results of undrained shear strength behaviour of Champlain sea clays from 7 different sites in Quebec, Canada. Equation (1), with the model parameters in Table 4.1, fits these experimental results well (Dey et al., 2015).

The presence of fissures might affect the apparent shear strength of the crust. The distribution of fissures and their continuity would govern the shear resistance in a slope stability analysis. In the

present study, the effects of fissures are not modeled rather an average undrained shear strength is assumed for the crust.

4.6 Results of Base Case Analysis

Propagation of shear band

The strain localization and formation of shear bands are the key issues in landslides in sensitive clays. Figure 4.5 shows the development of shear stress (τ_c) and equivalent plastic shear strain (PEEQVAVG) with displacement of eroded block (Δ). PEEQVAVG represents the integration of plastic deviatoric strain rate tensor over the period of analysis, which is related to plastic shear strain in simple shear condition (γ^p) as PEEQVAVG=$\gamma^p/\sqrt{3}$. The shear strain concentrates mainly in one layer elements and a shear band is formed that propagates horizontally with increasing Δ. Figure 4.5a shows the variation of PEEQVAVG when Δ=0.1 m. For the parameters listed in Table 4.1, $s_u=s_{u95}$ at PEEQVAVG=0.035 (see Eq. 1, and definition of strain discussed above). For the ease of discussion, let us define the zone where PEEQVAVG≥0.035 (i.e. $s_u \leq s_{u95}$, Section c-d-e in Fig. 4.4) as 'residual shear band' because significantly large plastic strain accumulates in this zone. The zone where $s_{u95}<s_u< s_{up}$ (Section b-c in Fig. 4.4) is defined as 'softening zone.' Figure 4.5(a) shows that a 21.5 m long horizontal residual shear band is formed when Δ=0.1 m.

Figure 4.5(b) shows the variation of shear stress (τ_c) along the shear band for Δ=0.05, 0.06, 0.075 and 0.1 m. In order to explain the process, consider the variation of τ_c for Δ=0.1 m. The maximum τ_c of 37.5 kPa (i.e. s_{up}) is mobilized at 25 m from the vertical face of the eroded block.

Between 0 and 25 m, $\tau_c \leq 37.5$ kPa (i.e. $\tau_c \leq s_{up}$), meaning that the s_u along this length is in the post-peak softening zone (Section be in Fig. 4.4), because $\gamma^p \geq \gamma_c^p$ as shown in Fig. 4.5(a). In the first 21.5 m length of residual shear band $\tau_c \leq s_{u95}$. The left side of the peak (21.5–25 m) where τ_c increases from s_{u95} to s_{up} represents the softening zone. After 25 m, τ_c is again less than s_{up}. In this zone the yield strength is not mobilized and it represents the pre-yield behaviour (line oa in Fig. 4.4). At a very large distance, τ_c reduces to zero as the ground surface is horizontal. The pattern of τ_c for other values of Δ is similar, although the location of maximum τ_c moves to the right with increasing Δ. As an example, for Δ=0.1 m the maximum τ_c is at 25 m while it is at 11 m for Δ=0.06 m.

In the following sections, the discussion is mainly focused on residual shear band ($\gamma^p \geq \gamma_{95}^p$) formation and propagation.

Development of spread failure

Figure 4.6 shows the formation of shear bands for six values of Δ during the displacement of the eroded block to Δ=30.75 m. A horizontal shear band f_1 is formed when Δ=0.5 m. The maximum PEEQVAVG is developed near the toe, which gradually decreases with horizontal distance. The initiation of a shear band near the toe and its propagation in sensitive clays almost in the horizontal direction are reported in previous studies (Locat, 2007; Locat et al., 2008 and 2013; Fortin-Rhéaume, 2013). At Δ=0.65 m, a curved shear band f_2 starts to form from point P_1 when the length of f_1 is 88.5 m. The band f_2 propagates up to the ground surface at Δ=0.75 m (Fig. 4.6b). With further displacement of the eroded block, the soil mass M1 slides along a failure plane formed by the shear bands f_1 and f_2. At this same time, M1 also rotates in the clockwise

direction and therefore a gap is formed between M1 and the eroded block near the top as shown in Fig. 4.6(c). Because of this lateral displacement and rotation of M1, settlement occurs where f_2 intersects the ground surface. As significant deformation occurs, the extent of the plastic shear strain zone around the failure plane also increases (compare PEEQVAVG in Figs. 4.6b and 4.6c). Near the toe of the slope, multiple surfaces of high plastic shear strain develop. At Δ=4.5 m, another shear band f_3 starts to form in the sensitive clay layer from the intersection of f_2 and the bottom of the crust (point P_2). The band f_3 propagates further toward deeper depths and at Δ=5.95 m it joins the initially developed shear band f_1. At this stage, a soil mass (M2) bounded by the shear bands f_1, f_2 and f_3 forms a horst. As undrained (ϕ=0) condition is used, the tip of the simulated horst is approximately 90° although in the field this angle is typically close to 60° (Carson, 1979; Locat et al., 2011). A better soil model might be able to simulate this shape.

As the displacement continues, another shear band f_4 starts to form from point P_3 on f_1 at Δ=10.5 m. The shear band f_4 reaches to the ground surface at Δ=12.15 m (Fig. 4.6d). Another soil mass M3 bounded by the shear bands f_1, f_3 and f_4 fails, which is commonly known as a graben. This process will be continued (Figs. 4.6e & f) until: (i) strong or less sensitive soil layers are encountered in the upward (right) direction, (ii) the movement of the soil mass M1 is obstructed in the downward (left) side, and/or (iii) length of f_1 is not sufficient for formation of another horst. Let us define the extent of failure (L_{ex}) as the lateral distance between the initial position of the crest of the slope and the point where the last shear band intersects the ground surface. In this case, the displacement of the eroded block is stopped at Δ=30.75 m and L_{ex}=73 m is obtained (see Fig. 4.6f).

Figure 4.7 shows the instantaneous velocity vectors of soil elements for four different stages. As shown in Fig. 4.6(b), a complete failure plane is developed when the shear band f_2 propagates up to the ground surface at Δ=0.075 m. After that the soil mass M1 slides on this failure plane. The instantaneous velocities of soil particles at Δ=9.15 m are shown in Fig. 4.7(a). The velocities of soil particles near the face of the slope are less than those of the particles near the failure plane, which causes the rotation of M1 as discussed above. Due to movement of M1, the lateral support on the remaining soil is reduced. Moreover, s_u in the shear bands f_1 under the block M2 in Fig. 4.6(c) is significantly reduced because of an increase in plastic shear strain. The combined effects of these two factors results in formation of shear band f_3 and the horst M2 at Δ=5.95 m (Fig. 4.6c). The velocities of soil elements at Δ=11.15 m are shown in Fig 4.7b. As expected, the velocities of the soil elements in M1 are higher than those in M2. The soil particles in M1 slides on the shear band f_2 and a crater is formed. On the other hand, the horst M2 moves laterally to the left. The lateral movement of M2 reduces the support on remaining soil that results in formation of the shear band f_4 and the graben M3. The velocity vectors at Δ=12.55 m are shown in Fig. 4.7(c). The velocities of soil particles gradually decrease from M1 to M3. This process is continued with increasing Δ, and the mechanism involved in formation of each horst and graben can be explained in the same way. For a large value of Δ=25.35 m (Fig. 4.7d), the movements of soil masses M1 to M4 are almost horizontal, while the graben M5 moves downward left. Moreover, as expected, the velocity of M1 is the highest and M5 is the lowest at this stage. Figure 4.7(d) also shows that the graben M3 sinks with an increase in Δ forming another crater on the right side of the horst M2. In other words, the rate of reduction of height of the graben is

higher than that of the horst. Many field observations (e.g. Locat et al., 2011) show that the horsts projected up over the grabens after failure, as depicted in Fig. 4.1.

Conceptual models have been proposed in the past to explain the mechanisms of spread and retrogressive landslides (Odenstad, 1951; Carson, 1977, Carson, 1979b). These models describe the dislocation of the soil mass based on analysis of forces acting on the surfaces of horsts and grabens. Odenstad (1951) assumed that a horizontal weak surface or layer exists in the clay soil, and the strength of this weak layer is almost completely destroyed when the failure is initiated due to stress concentration. This model does not explain the formation and propagation of this horizontal shear band. In a recent study, Locat et al. (2013) took an initiative to model the propagation of the horizontal shear band. As mentioned in the introduction, although their FE models can simulate the propagation of a quasi-horizontal shear band, they could not simulate the whole process including the formation and displacement of horsts and grabens.

In the present FE model, the formation and propagation of shear bands are successfully simulated. The horizontal shear band (e.g. f_1 in Fig. 4.6) forms along the interface between the basal and sensitive clay layers. The other failure planes (e.g. f_2-f_6 in Fig. 4.6f) are not predefined, and therefore shear band formation occurs through stress concentrations and/or weaker zones due in part to stress redistribution and reduction of shear strength along the shear bands. At large Δ, a number of shear bands are formed above the initial horizontal shear band, which causes global failure of the slope and formation of horsts and grabens and finally spread failure. The simulation results suggest that the initial development and the extent of the horizontal shear band are important features to generate horsts and grabens in a progressive manner. The use of large deformation FE modeling technique coupled with strain/deformation dependent undrained shear

strength model is one of the main advantages of the present FE model over the existing numerical models available in the literature.

4.7 FE Mesh Size

The size of the FE mesh has a significant influence on simulation results when the analyses involved with post-peak softening behavior of soil defined as a function of shear strain. Generally, for the given relative displacements between two faces, the finer mesh calculates higher shear strain. Element size scaling rules have been proposed in the past to reduce the effects of mesh dependency (Pietruszczak and Mróz, 1981; Moore and Rowe, 1990; Andresen and Jostad, 2004; Anastasopoulos et al., 2007). In addition to the base case discussed in previous sections, analyses are also performed for two different mesh sizes (1.0 m and 0.25 m), again with uniform cubical elements in the whole domain. For FE input, γ^p is calculated scaling by element size; for example, s_{u95} mobilizes at $\gamma_{95}^{p} = \delta_{95}/t_{FE}$ of 3%, 6% and 12% for mesh size 1.0, 0.5 and 0.25 m, respectively, for same δ_{95}=0.03 m. The orientation of the shear band is not considered in the scaling rule, which might induce some mesh dependency.

Figure 4.8 shows the shear bands, together with plastic shear strains, for three Δ values. Higher shear strains are calculated with finer mesh because $\gamma^p=\delta/t_{FE}$. Note that, for a better presentation of the shear bands, the adopted vertical scale is twice the horizontal scale in all the figures presented in the following sections. As shown in Figs. 4.8(a-c) for Δ=0.45 m, the length of the horizontal shear band is almost the same (~68 m) for all three mesh sizes when the element size scaling rule is used. Analyses are also performed with the same value of $\gamma_{95}^{p} = 6\%$ (without

element size scaling), which give 55, 68 and 88.5 m shear band length for the 1.0, 0.5 and 0.25 m meshes, respectively, at Δ=0.45 m. This shows that element size scaling significantly improves the simulation although the results are not strictly the same for these three mesh sizes. The shear bands at Δ=0.75 m are shown in Figs. 4.8(e-g). Again, the length of the shear bands and the location where the curved failure surface intersects the ground surface are consistent. Finally, Figs. 4.8(i-k) show the simulation results for a very large Δ (=17.25 m). The formation of shear bands with Δ shown in Figs. 4.8(i) and 4.8(j) is very similar, and has been discussed further in previous sections using Figs. 4.6 and 4.7. However, Fig. 4.8(k) shows that the 1.0 m mesh could not maintain the shape of the horsts and grabens at large displacements. From a close examination of the results it is found that the quasi-static conditions could not be maintained properly at this speed of the eroded block (v_e=0.05 m/s) in 1.0 m mesh. The effect is significant at large values of Δ because a large soil mass displaces at this stage resulting in an increase of the kinetic energy. Therefore, in order to maintain quasi-static conditions, a simulation is also performed at a slower speed of the eroded block of v_e=0.01 m/s, and the results are shown in the last row of Fig. 4.8. As shown in Fig. 4.8(l), the shear bands formation at this v_e with 1.0 m coarse mesh is very similar to the shear bands formed in finer meshes (Figs. 4.8i & 4.8j). In other words, when the element size scaling is used, the results with these three different mesh sizes are comparable in terms of strain, displacement and shape of the displaced horst and grabens provided the quasi-static conditions are maintained. Analyses are also performed at a slower speed (v_e=0.01 m/s) for 0.25 m and 0.5 m mesh and the results are very similar to the first two rows in Fig. 4.8, which confirms that v_e=0.05 m/s is low enough to maintain quasi-static conditions for these two mesh sizes. It is to be noted here that this type of large deformation FE

analysis is computationally expensive. Therefore, all the analyses presented in the previous and following sections are conducted with 0.5 m mesh and v_e=0.05 m/s.

4.8 Parametric Study

The geometry of the slope and soil parameters influence the shear band formation/propagation and spread failure. A parametric study is conducted using the above base case FE model in which only one parameter is varied while the other parameters are kept constant as listed in Table 4.1, unless otherwise mentioned.

Post-peak strength degradation parameter (δ_{95})

The undrained shear strength degradation occurs quickly if the value of δ_{95} in Eq. 1 is reduced. The analyses presented in the previous sections are for δ_{95}=0.03 m. In order to examine the effects of δ_{95}, analyses are also performed for δ_{95}=0.045, 0.1 and 0.15 m. Figure 4.9 shows the results for three different values of Δ. For δ_{95}=0.03, 0.045 and 0.1 m, a horizontal shear band forms with displacement of the eroded block as presented before in Fig. 4.6. A curved shear band is then formed, propagates upward and reaches the ground surface as shown in Figs. 4.9(a–c). Comparison of Figs. 4.9(a–c) shows that, for a given Δ, the length of the horizontal shear band increases with a decrease in δ_{95}. The shear bands propagate faster for lower values of δ_{95} because of faster reduction of s_u. For example, at Δ=22.35 m, two horsts and one graben are formed for δ_{95}=0.03 m (Fig. 4.9i) while only one horst and one graben are formed for δ_{95}= 0.1 m (Fig. 4.9k). The last row of Fig. 4.9 shows that the shear band formation with δ_{95}=0.15 m is different from the other three rows. For δ_{95}=0.15 m, a curved shear band forms from the end of the horizontal

shear band resulting in global failure of a large soil mass (Fig. 4.9d) as compared to other three cases (Figs. 4.9a–c). With further displacement of the eroded block, the failed soil mass disintegrated into smaller soil blocks as shown in Figs. 4.9(h) and 4.9(l), instead of formation of horst and grabens shown in Figs. 4.9(i–k). In summary, high brittleness (i.e. rapid decrease in s_u with δ) is required for formation of horsts and grabens. This is consistent with Locat et al. (2013) who also showed that brittle soils are more susceptible to progressive failure.

Slope angle (β)

The susceptibility and extent of progressive failure is high in steep slopes (Lo and Lee, 1973; Locat et al., 2013). In order to understand the mechanisms, analyses are performed for three different slope angles and the results are presented in Fig. 4.10. The thicknesses of the crust in all three cases are the same as the base case shown in Fig. 4.3. As the value of β is different, the size of the eroded block is the largest for β=15° even though the maximum depth of the excavation is same (10 m) in all three cases. Figure 4.10 shows the plastic strain contour for Δ=30.75 m. For β=15°, a horizontal shear band is formed that ended at 91 m from the crest. However for β=25°, a slightly shorter (89 m) horizontal shear band than that of β=15° is formed. In addition, some plastic shear strain accumulation above the horizontal shear band occurs as shown by the shaded zone near point A. It shows that there is a tendency to form another shear band even though it is not fully formed up to the ground surface to cause a global failure as in the previous cases (e.g. failure of soil mass M1 in Fig. 4.6b). In both cases (β=15° and 25°), global failure of the slope does not occur, even though a large horizontal shear band is developed. It is to be noted here that

additional triggering factors, such as construction in the upslope area, may cause a global failure as shown by the authors (Dey et al., 2014).

Unlike Figs. 4.10(a) and 4.10(b), a global failure occurs for β=30° (Fig. 4.10(c)) because the shear stress along the potential failure plane increases with the slope angle, β. The formation of horizontal shear band and subsequent horsts and grabens are discussed in detail in the previous sections. Based on this analysis, it can be concluded that the slope angle and the potential to initiate the first circular failure are the key factors for spread failure.

Sensitivity (S_t)

Figure 4.11 shows the effects of S_t on shear band formation. For a low S_t (=3), the post-peak reduction of s_u is not sufficient to cause global failure of the slope (Fig. 4.11a). With displacement of the eroded block a small horizontal shear band is formed and at one stage the eroded block separates from the remaining soil. For S_t=5 and 7, global failure and subsequent formation of horst and grabens occurs (Figs. 4.11(b) and 4.11(c)). The extent of failure increases with S_t because of higher reduction of s_u (compare Figs. 4.11b and 4.11c). However, the failure pattern is different if S_t is very high as shown in Fig. 4.11(d). In this case a large horizontal shear band is formed first with displacement of the eroded block. However, once the global failure has occurred by the formation of a curved shear band, strain concentration mainly occurs along the global failure plane instead of formation of horsts and grabens as shown in Figs. 4.11(b) and 4.11(c). Figure 4.11(d) also shows that, although a large horizontal shear band is formed, the extent of failure is not visible at the ground surface, at least for the maximum displacement of the eroded block simulated in this case.

Thickness of crust and sensitive clay layer

In the analyses presented in the previous sections, the thickness of the crust (H_c) and sensitive clay (H_{st}) are 3.0 m and 16.0 m, respectively (Fig. 4.3). Keeping the total thickness of soil same above the base (H_c+H_{st}=19.0 m), the effects of H_c and H_{st} on slope failure are investigated. Figure 4.12(a) shows that global failure of the slope does not occur when H_{st}=10.0 m because of the existence of a thick crust (9.0 m) of higher shear strength, although a long horizontal shear band is formed. When H_{st}=14 or 16 m, global failure and subsequent formation of horst and grabens occur (Figs. 4.12(b) and 4.12(c)). Figure 4.12(b) shows the formation of shear bands f_1–f_6 in chronological order. Unlike Fig. 4.12(c), a shear band f_5 is formed in the sensitive clay layer just below the crust. The failure pattern shown in Fig. 4.12(d) for a very thin crust (H_c=1 m and H_{st}=18 m) is different from Figs. 4.12(b) or 4.12(c). In this case, although a large horizontal shear band is formed initially, horst and grabens do not form with displacement of the eroded block. Instead, large strain concentration mainly occurs around the global failure plane and only one block of failed soil mass follow the eroded block, at least, up to the maximum displacement of the eroded block simulated.

Shear strength of crust

Figure 4.13 shows that a horizontal shear band is formed initially for all three different values of undrained shear strength of the crust (s_{uc}). After the formation of the first global failure plane, large deformation through the segment of the failure plane in the crust could occur easily for low s_{uc} (Fig. 4.13a) as compared to the simulations with high s_{uc} (e.g. Figs. 4.13(b) and 4.13(c)). Therefore, only one block of soil moves with the eroded block for s_{uc}=40 kPa. When the crust is

relatively strong (e.g. s_{uc}=60 or 80 kPa), the higher shear resistance in the segment of the failure plane in the crust results in formation of inclined downward shear bands in the sensitive clay layer (e.g. f_3 in Fig. 4.13c) and subsequent formation of horst and grabens (Figs. 4.13(b) and 4.13(c)). Similar to Fig. 4.12(b), a shear band f_5 is formed below the crust when s_{uc}=80 kPa, which suggest that the formation of such shear band depends upon thickness and strength of the crust.

4.9 Conclusions

Post slide field investigations of spreads in sensitive clay slopes show that in many cases a number of horst and graben blocks of almost intact clay displace laterally on a long flat horizontal failure plane. Early researchers assumed the presence of a hypothetical horizontal weak plane, and used this postulated failure plane to develop the conceptual models for spreads. In more recent studies, the formation of shear band due to disturbance at the toe of the slope and its propagation in the horizontal direction are modeled analytically and numerically for simplified conditions.

In the present study, the large deformation FE modeling technique in Abaqus CEL is used to simulate progressive failure. The development of a horizontal shear band due to river bank erosion or excavation and its propagation in sensitive clay layer are simulated using a constitutive model that considers post-peak softening behaviour. In addition, successive formation of horsts and grabens with displacement of failed soil masses is successfully simulated. Very large displacement of the failed soil mass are simulated using Abaqus CEL without any numerical issues due to mesh distortion as encountered in typical FE modeling in

Lagrangian framework. The parametric study shows that toe erosion does not always create horsts and grabens rather their formation depends on soil properties and geometry. The following conclusions can be drawn from this study:

i) Due to erosion or excavation near the toe of the slopes, a shear band could be formed and propagated horizontally in the sensitive clay to a large distance. The slope might be globally stable but the shear resistance in the band decreases to a low value.

ii) For the base case analysis, the first global failure occurs after the formation of a shear band above the initial horizontal shear band. The horsts and grabens are formed when the previous failed soil masses move a sufficiently large distance. Large plastic shear strains develop on the surfaces of horst and grabens, which reduces the undrained shear strength.

iii) When the stress-strain behaviour is defined by element size scaling rule, the simulation results are almost independent of mesh size, provided the quasi-static conditions are properly maintained during the analysis. Low speed of the eroded block is required to maintain quasi-static conditions for coarse mesh.

iv) The susceptibility and extent of progressive failure increase with decrease in δ_{95} because of quick post-peak reduction of undrained shear strength.

v) For the ground profile and soil properties considered in the bases case, a global failure does not occur for slope angles up to 25°, even though a large shear band develops. However, for a slope angle of 30°, global failure and subsequent formation of horsts and grabens are simulated.

vi) For low values of S_t of sensitive clay layer, only a small horizontal shear band is formed by toe erosion. On the other hand, only one block of soil near the slope fails

when S_t is very high. For intermediate values of S_t (5 and 7 in the present study) a number of horst and grabens are formed and the failure is extended over a large distance.

vii) Toe erosion creates only a horizontal shear band when the crust is thick. For a thin crust, global failure of only one soil block occurs. Horst and graben formation occurs only for intermediate thicknesses of the crust and sensitive clay layer. In addition to thickness, sufficiently high shear strength of the crust is required for the formation of horsts and grabens.

Finally, although a parametric study is performed for a number of soil parameters and geometry, the effects of other factors such as initial effective stress conditions, slope height, inclination of the ground surface, and the size and shape of the eroded block need to be investigated further.

Acknowledgements

The works presented in this paper have been supported by the Research and Development Corporation of Newfoundland and Labrador, NSERC and C-CORE. The authors also express their sincere thanks to Sujan Dutta, Biswajit Saha and John Barrett for their valuable suggestions and help with FE modeling.

List of symbols

The following symbols are used in this paper:

β slope angle

δ post-peak shear displacement

Δ displacement of the eroded block

δ_{95} δ at which s_u reduced by 95% of (s_{up}-s_{uR})

τ_c shear stress along the shear band

δ_e elastic shear displacement

δ_p plastic shear displacement

δ_{pc} plastic shear displacement at point b in Fig. 4.4

δ_t total shear displacement

ν_u undrained Poisson's ratio

L_{sb}^{r} length of residual shear band where $\delta_p \geq (\delta_{pc}+\delta_{95})$

L_{sb}^{s} Length of softening zone where $\delta_{pc}<\delta<\delta_{95}$

E_u undrained modulus of elasticity

γ^p plastic shear strain

H_c thickness of crust (Fig. 4.3)

H_{st} thickness of sensitive clay layer (Fig. 4.3)

H_b thickness of the base (Fig. 4.3)

L_{ex} lateral extent of failure

S_t s_{up}/ s_{uR}

s_u mobilized undrained shear strength

s_{uc} undrained shear strength of crust

$s_{u(ld)}$ s_u at large displacements

s_{up} peak undrained shear strength

s_{uR} s_u mobilized in shear band at considerable shear displacement

s_{ur} s_u at completely remoulded state

t shear band thickness

t_{FE} finite element mesh size

v_e speed of eroded block

References

Anastasopoulos, I., Gazetas, G., Bransby, M. F., Davies, M. C. R. and Nahas, A. El. (2007). Fault rupture propagation through sand: finite-element analysis and validation through centrifuge experiments. *J. of the Geotech. and Geoenviron. Eng.*, *ASCE*, **133**, No. 8, 943–958.

Andresen, L. and Jostad, H.P. (2004). Analyses of progressive failure in long natural slopes. *In Proc. of the 9th Symp. on Num. Models in Geomech. - NUMOG IX*, *Ottawa*, Ont., 603–608.

Anderson, L. and Jostad, H.P. (2007). Numerical modeling of failure mechanisms in sensitive soft clays — application to offshore geohazards. *Off. Technology Conf.*, *Texas,* OTC 18650.

Bernander, S. (2000). *Progressive failure in long natural slopes: formation, potential extension and configuration of finished slides in strain-softening soils*. Licentiate Thesis, Luleå University of Technology.

Bjerrum, L. and Landva, A. (1966). Direct simple-shear tests on a Norwegian quick clay. *Géotechnique*, **16,** No. 1, 1–20.

Carson, M. A. (1977). On the retrogression of landslides in sensitive muddy sediments. *Canadian Geotechnical J.*, **14**, No. 4, 582–602.

Carson, M. A. (1979b). On the retrogression of landslides in sensitive muddy sediments: Reply. *Canadian Geotechnical J.*, **16**, No. 2, 431–444.

Demers, D., Robitaille, D., Locat, P., and Potvin, J. (2013). Inventory of large landslides in sensitive clay in the province of Quebec, Canada: preliminary analysis. *In Proc. of the 1st Int. Workshop on Landslides in Sensitive Clays,* Landslides in Sensitive Clays –From Geosciences to Risk Management, Québec, Que.

Dey, R., Hawlader, B., Phillips, R. and Soga, K. (2014). Stability analysis of a river bank slope with an existing shear band. *6th Canadian GeoHazards Conf.*, Kingston, Ontario.

Dey, R., Hawlader, B., Phillips, R. and Soga, K. (2015). Modeling of large deformation behaviour of marine sensitive clays and its application to submarine slope stability analysis. (in preparation).

Dutta, S., Hawlader, B. and Phillips, R. (2014). Finite element modeling of partially embedded pipelines in clay seabed using Coupled Eulerian–Lagrangian method. *Canadian Geotechnical Journal*, 10.1139/cgj-2014-0045.

Einav, I. and Randolph, M.F. (2005). Combining upper bound and strain path methods for evaluating penetration resistance. *Int. J. Num. Methods Engineering,* **63**, No. 14, 1991–2016.

Fortin, A., Ouellet, D., P aradis, S. and Demers, D. (2008). Développement au Ministère des Transports du Québec d'un porail informatique pour l'accès à des bases de données géotechnique. *In Proc. of the 4th Canadian Conf. on Geohazards*: F*rom Causes to Management, Québec*. Edited by J. Locat, D. Perret, D. Turmel, D. Demers, and S. Leroueil. Presses de l 'Université Laval, Québec, 169–174.

Fortin-Rhéaume, A.-A. (2013). *Étude de l'étalement latéral de 1988 et des autresglissements de terrain le long de la vallée a` Brownsburg-Chatham, Québec*. M.Sc. thesis, Département de génie civil, Université Laval, Québec.

Griffiths, D. V. and Lane, P. A. (1999). Slope stability analysis by finite elements. *Géotechnique*, **49**, No. 3, 387–403.

Grondin, G., and Demers, D. (1996). The Saint-Liguori flake slide: characterization and remedial works. *In Proc. of the 7th Int. Symposium on Landslides*, *Trondheim, Norway*. Edited by K. Senneset. Balkema, Rotterdam, the Netherlands, **2**, 743–748.

Gauer, P., Kvalstad, T. J., Forsberg, C. F., Bryn, P., and Berg, K. (2005). The last phase of the Storegga Slide: simulation of retrogressive slide dynamics and comparison with slide-scar morphology. *Marine and Petroleum Geology*, **22**(1-2): 171–178.

Gylland, A. S., Sayd, M. S., Jostad, H. P., and Bernander, S. (2010). Investigation of soil property sensitivity in progressive failure. *In Proc. of the 7th European Conf. on Num. Methods in Geotech. Eng.*, Trondheim, Norway, 515–520.

Jostad, H. P., and Andresen, L. (2002). Capacity analysis of anisotropic and strain-softening clays. *In Proc. of NUMOG VIII*, Rome, Italy, 469–474.

Karlsrud, K., Aas, G. and Gregersen, O. (1984). Can we predict landslide hazards in soft sensitive clays? Summary of Norwegian practice and experiences. *In Proc. of the 4th Int. Symposium on Landslides,* Toronto, Ont., **1**, 107–130.

Kvalstad, T.J., Andresen, L., Forsberg, C.F., Berg, K., and Bryn, P. (2005). The Storegga Slide: evaluation of triggering sources and slide mechanisms. Marine and Petroleum Geology, **22**(1-2): 245–256.

Leroueil, S. (2001). Natural slopes and cuts: movement and failure mechanisms. *Géotechnique,* **51**, No. 3, 197–243.

Lo, K.Y., and Lee, C.F. (1973). Stress analysis and slope stability in strain-softening soils. *Géotechnique*, **23**, No. 1, 1–11.

Locat, A. (2007). *Étude d'un étalement latéral dans les argiles de l'Est du Canada et de la rupture progressive, Le cas du glissement de Saint-Barnabé-Nord*. M.Sc. thesis, Département de génie civil, Université Laval, Québec, Que.

Locat, A., Leroueil, S., Bernander, S., Demers, D., Locat, J. and Ouehb, L. (2008). Study of a lateral spread failure in an eastern Canada clay deposit in relation with progressive failure: the Saint-Barnabé-Nord slide. *In Proc. of the 4th Canadian Conf. on Geohazards: From Causes to Management,* Québec, Que., 89–96.

Locat, A., Leroueil, S., Bernander, S., Demers, D., Jostad, H.P. and Ouehb, L. (2011). Progressive failures in eastern Canadian and Scandinavian sensitive clays. *Canadian Geotechnical J.,* **48**, No. 11, 1696–1712.

Locat, A., Jostad, H. P. and Leroueil, S. (2013). Numerical modeling of progressive failure and its implications for spreads in sensitive clays. *Canadian Geotechnical J.*, **50**, 961–978.

Loukidis, D., Bandini, P., and Salgado, R. (2003). Stability of seismically loaded slopes using limit analysis. *Géotechnique*, **53**, No. 5, 463–479.

Moore, I. D. and Rowe, R. K. (1990). Scaling rule for localized plasticity in strain-softening continua. *Proc. of 1st Int. Conf. on Computer Aided Assessment of Localized Damage, Portsmouth*, **2**, 99–112.

Odenstad, S. (1951). The landslide at Sköttorp on the Lidan River, February 2, 1946. *Royal Swedish Institute Proceedings*, **4,** 1–38.

Palmer, A. C., and Rice, J. R. (1973). The growth of slip surfaces in the progressive failure of overconsolidated clay. *Proc. R. Soc. London, Ser. A*, **332**, No. 1591, 527–548.

Pietruszczak, St. and Mróz, Z. (1981). Finite element analysis of deformation of strain-softening materials. *Int. Journal for Numerical Methods in Engineering*, **17**, 327–334.

PLAXIS. (2011). PLAXIS 2D 2010 manuals. PLAXIS bv., Delft, the Netherlands.

Potts, D. M., Dounias, G. T., and Vaughan, P. R. (1990). Finite element analysis of progressive failure of Carsington embankment, *Géotechnique,* **40**, No. 1, 79–101.

Puzrin, A. M., Germanovich, L. N. and Kim, S. (2004). Catastrophic failure of submerged slopes in normally consolidated sediments. *Géotechnique,* **54**, No. 10, 631–643.

Puzrin, A. M. and Germanovich, L. N. (2005). The Growth of Shear Bands in the Catastrophic Failure of Soils. *Proc. R. Soc. London, Ser. A*, **461**, No. 2056, 1199–1228.

Qiu G, Henke S, Grabe J. (2011). Application of a Coupled Eulerian–Lagrangian approach on geomechanical problems involving large deformations. *Computers and Geotechnics*, **38** No. 1, 30–39.

Quinn, P., Diederichs, M.S., Hutchinson, D.J. and Rowe, R.K. (2007). An exploration of the mechanics of retrogressive landslides in sensitive clay. *In Proc. of the 60th Canadian Geotechnical Conf*., Ottawa, Ontario, 721–727.

Quinn, P. (2009). *Large Landslides in Sensitive Clay in Eastern Canada and the Associated Hazard and Risk to Linear Infrastructure*. Doctoral thesis, Queen's University.

Quinn, P. E., Diederichs, M. S., Rowe, R. K. and Hutchinson, D. J. (2011). A new model for large landslides in sensitive clay using a fracture mechanics approach. *Canadian Geotechnical J.*, **48**, 1151–1162.

Quinn, P. E., Diederichs, M. S., Rowe, R. K., and Hutchinson, D. J. (2012). Development of progressive failure in sensitive clay slopes. *Canadian Geotechnical J.*, **49**, No. 7, 782–795.

Tavenas, F., Flon, P., Leroueil, S. and Lebuis, J. (1983). Remolding energy and risk of slide retrogression in sensitive clays. *Proc. of the Symposium on Slopes on Soft Clays,* Linköping, Sweden, SGI Report No. **17,** 423–454.

Tavenas, F. (1984). Landslides in Canadian sensitive clays — a state-of the-art. *In Proc. of the 4th Int. Symposium on Landslides*, Toronto, Ont., **1,** 141–153.

Tho, K. K., Leung, C. F., Chow, Y. K., and Swaddiwudhipong, S. (2012). Eulerian finite element technique for analysis of jack-up spudcan penetration. *ASCE International Journal of Geomechanics*, **12**, No. 1, 64–73.

Tian, Y., Wang, D., and Cassidy, M. J. (2011). Large deformation finite element analysis of offshore penetration tests. *Proc 2nd Int Symp Comput Geomech, Cavtat-Dubrovnik*, 925–933.

Wang, D., Randolph, M. F. and White, D. J. (2013). A dynamic large deformation finite element method based on mesh regeneration. *Computers and Geotechnics*, **54**, 192–201.

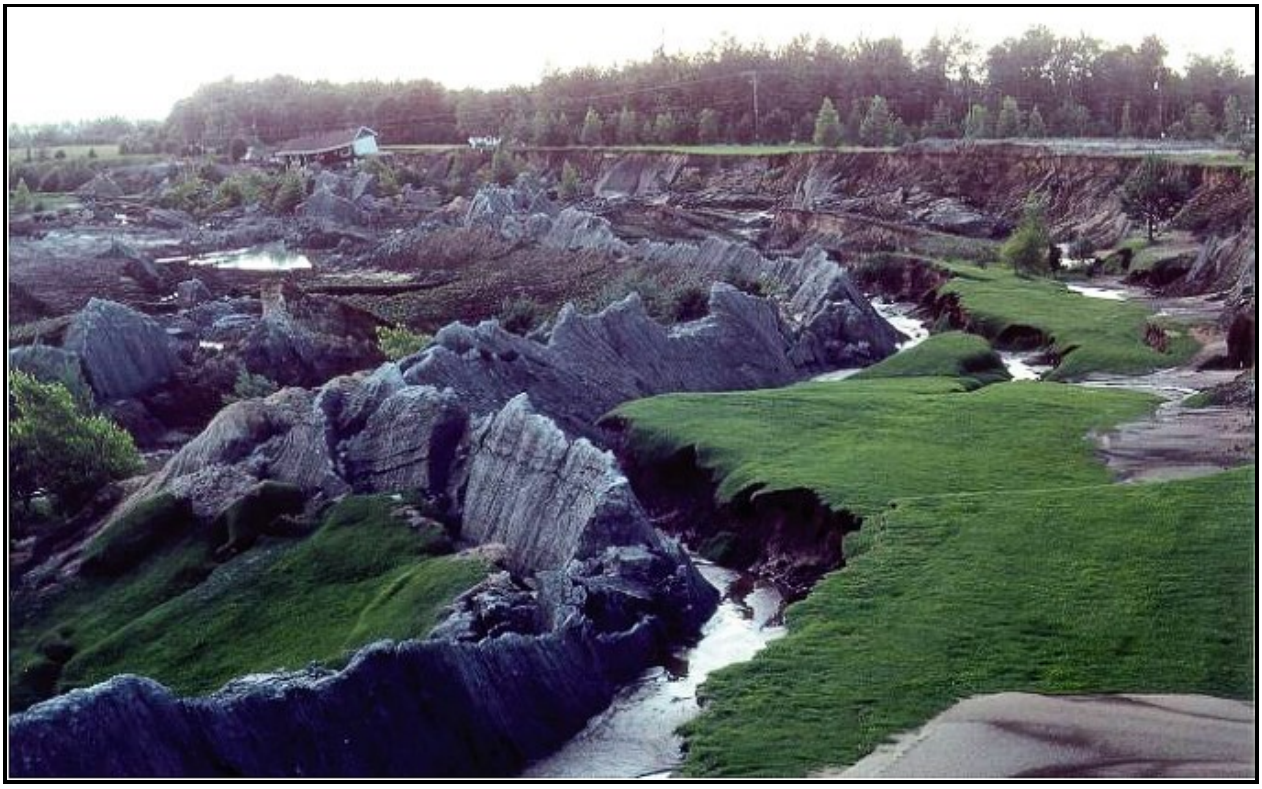

Figure 4. 1: Typical morphology of spreads – The 1989 landslide at Saint-Liguori, Quebec (Locat et al., 2011)

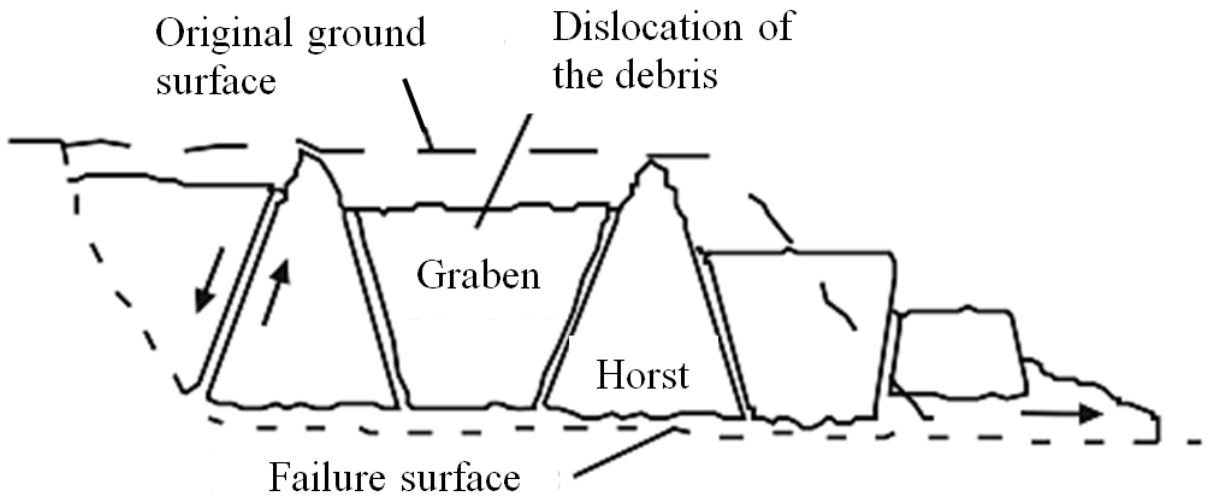

Figure 4. 2: Sketch of spread type landslide in sensitive clay (after Locat et al. 2013)

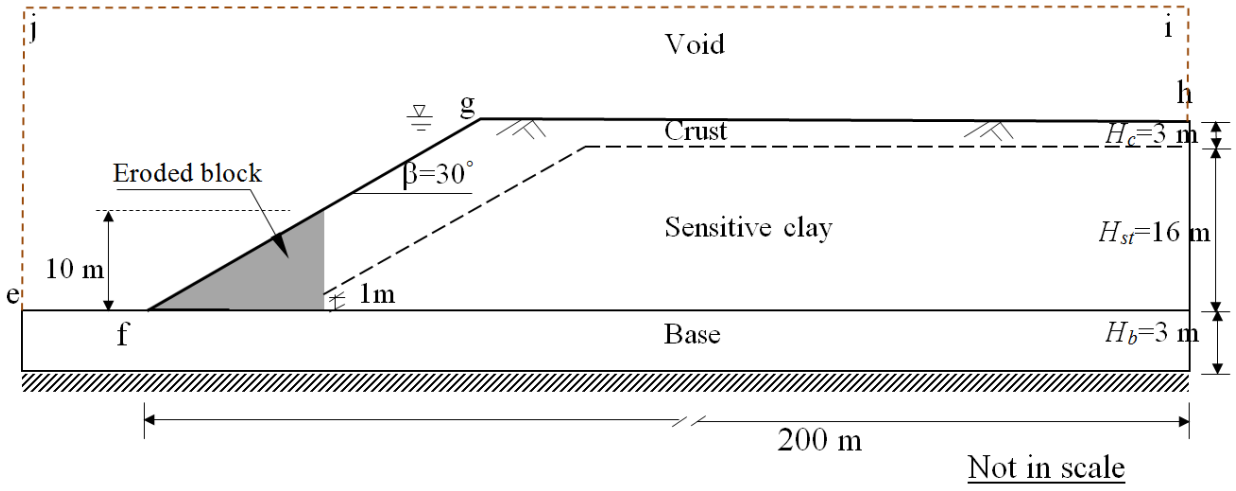

Figure 4. 3: Geometry of the "base case" slope used in numerical analysis

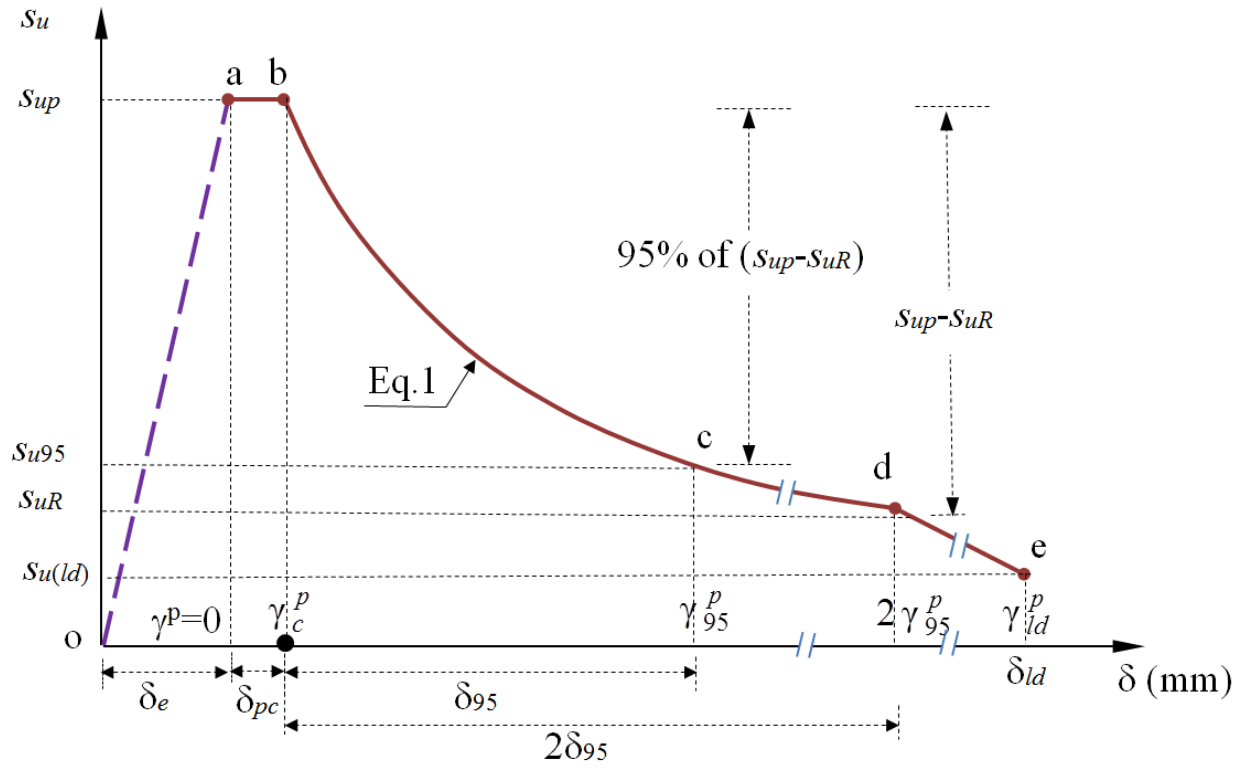

Figure 4. 4: Stress-strain behavior used in finite element modeling

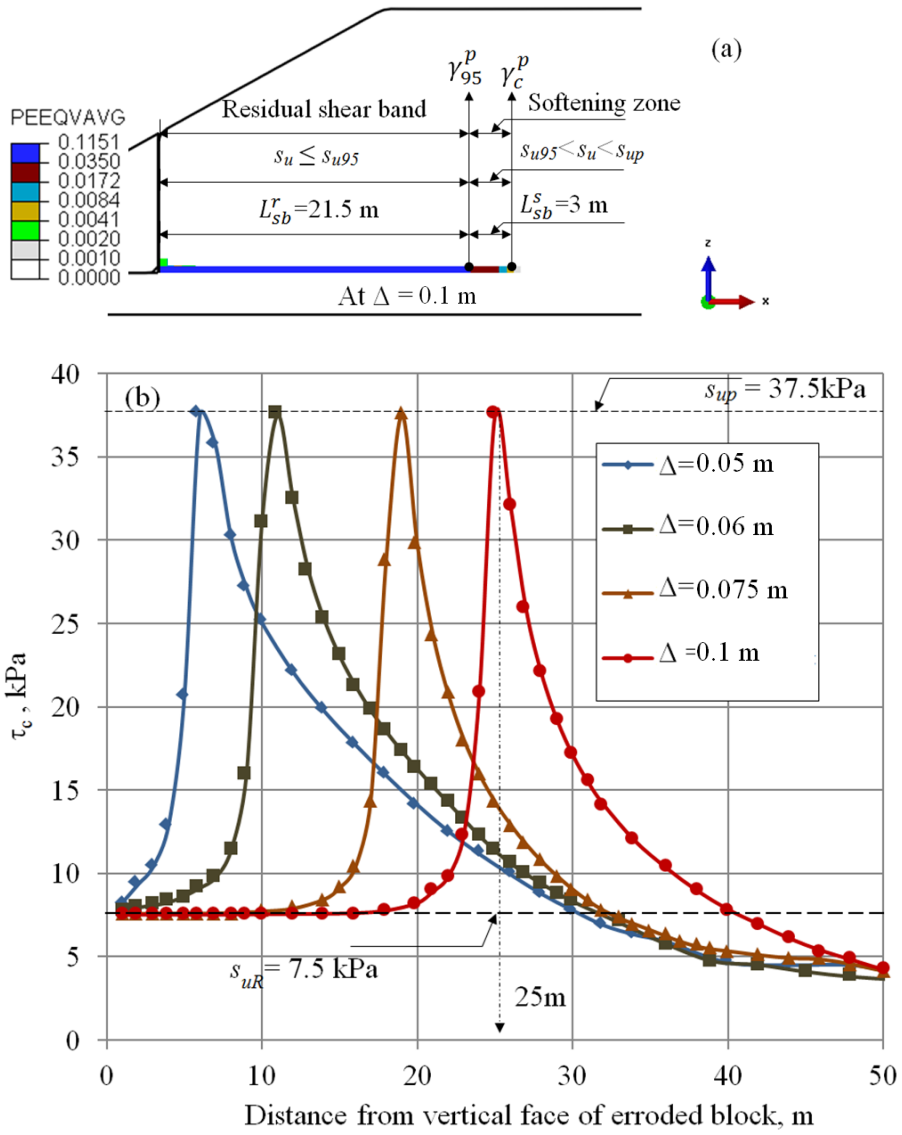

Figure 4. 5: Mobilized stress and strain in shear band: (a) equivalent plastic shear strain at Δ=0.1 m, (b) Shear stress

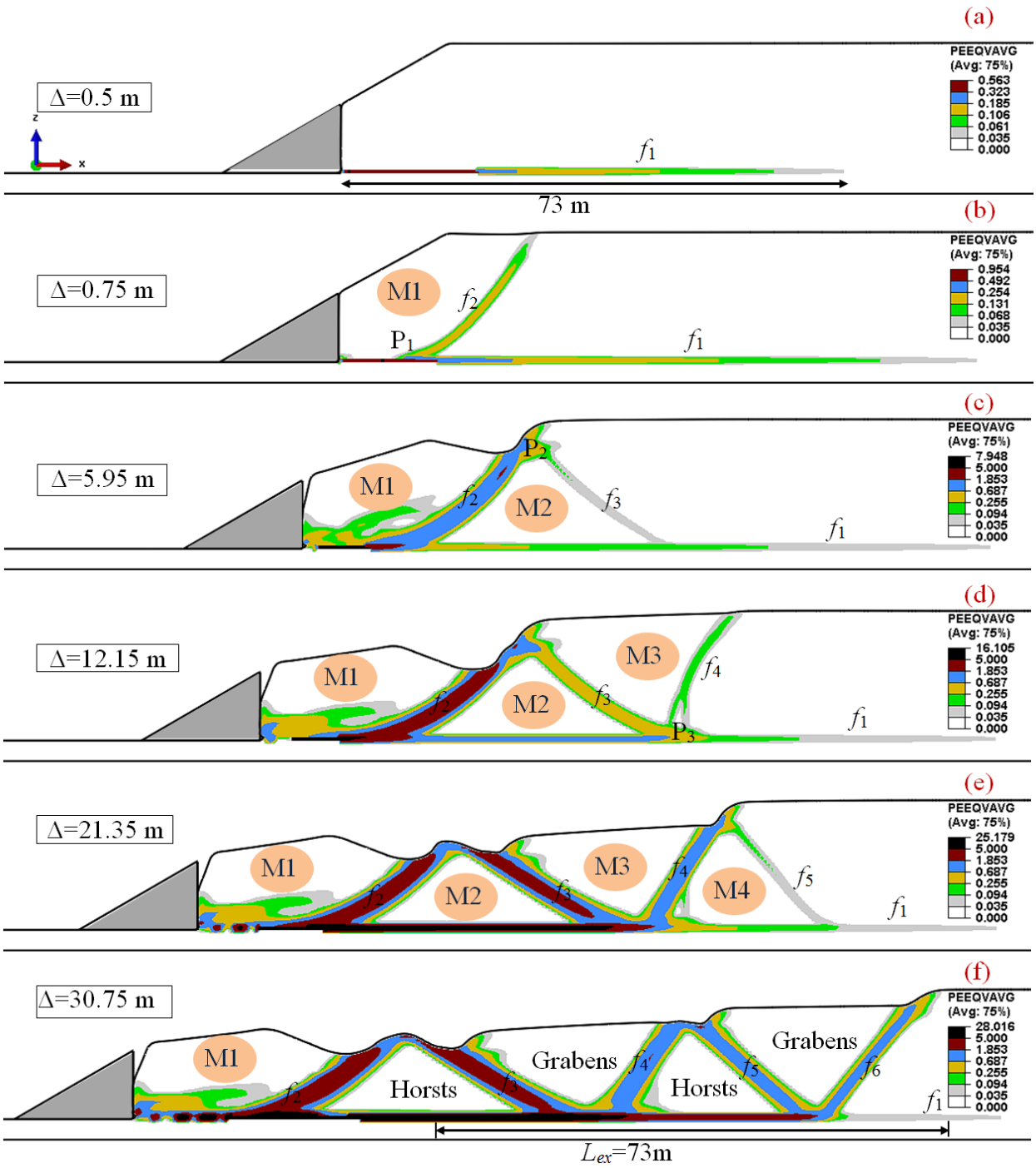

Figure 4. 6: Formation of horsts and grabens leading to spread

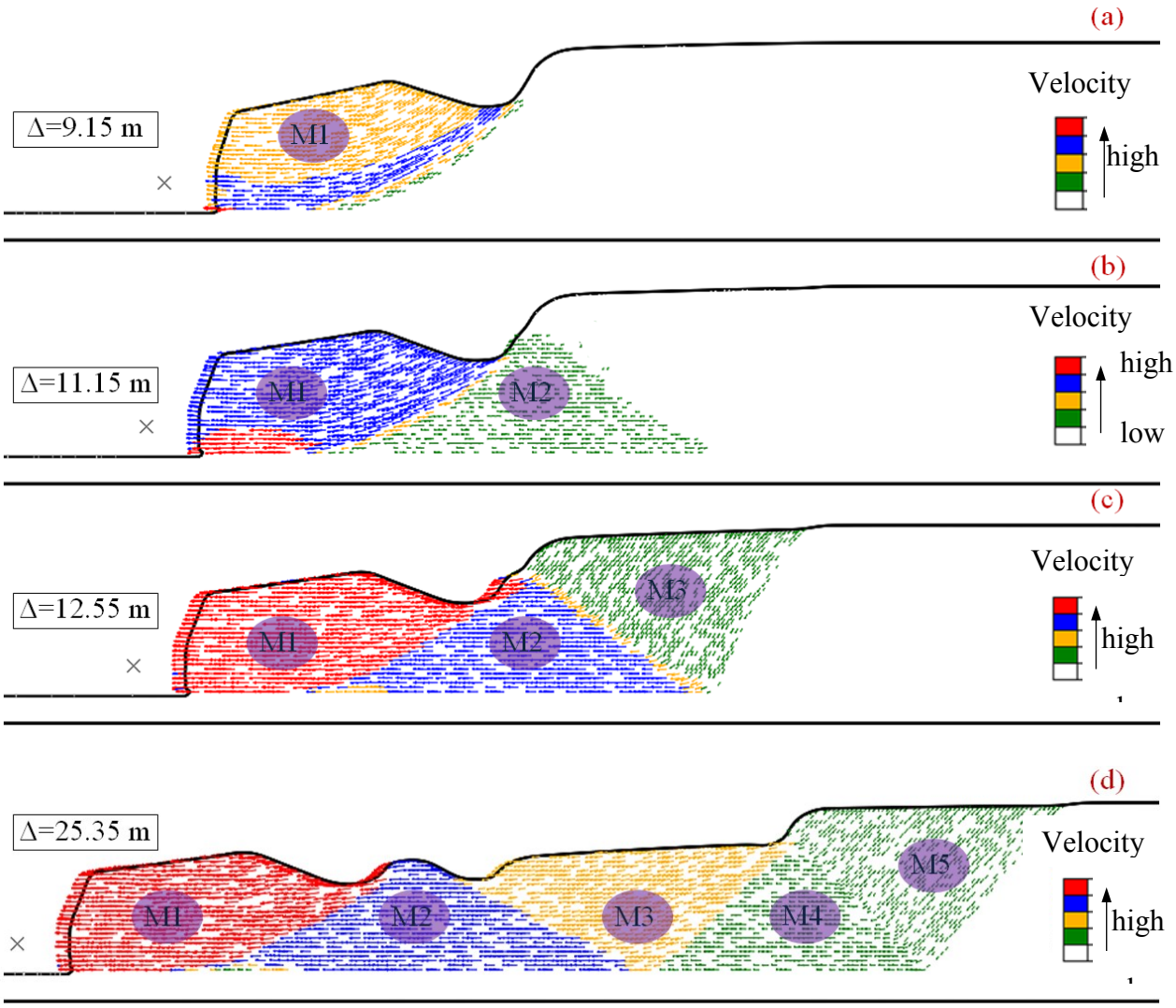

Figure 4. 7: Velocity vectors of soil elements

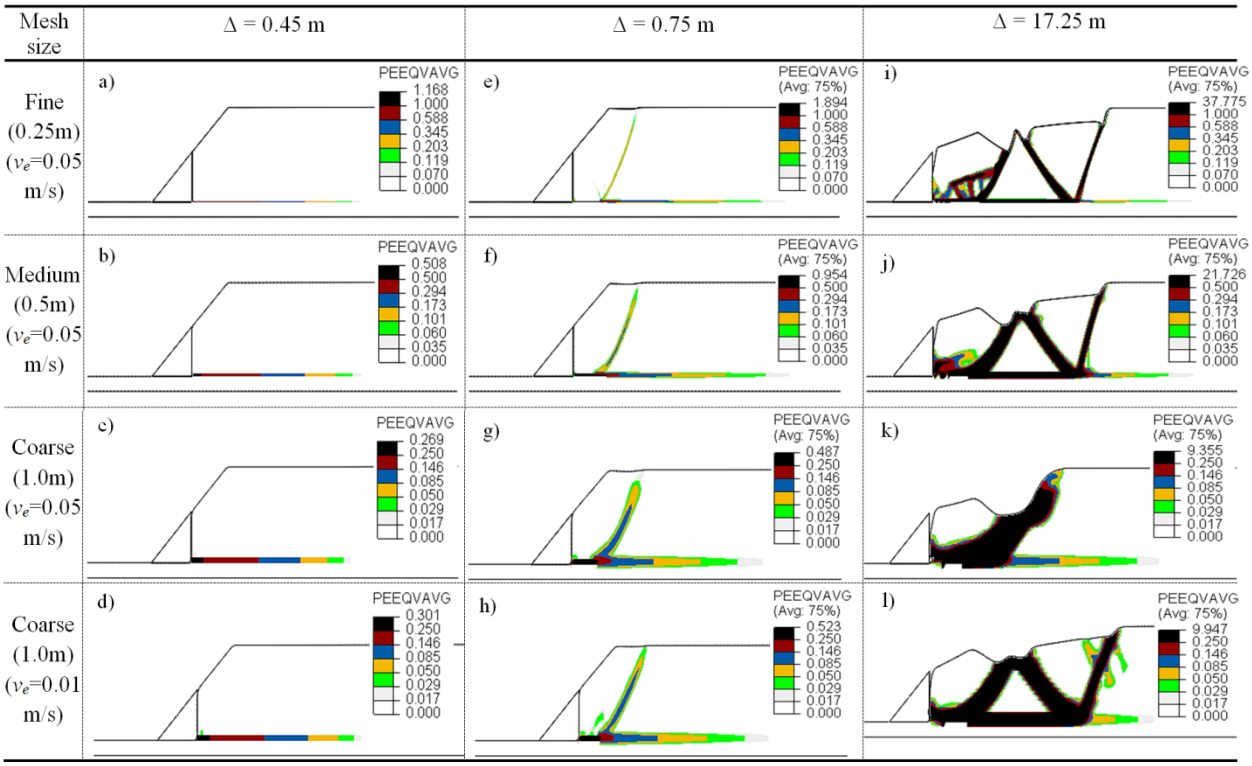

Figure 4. 8: Effects of mesh size on development of shear bands

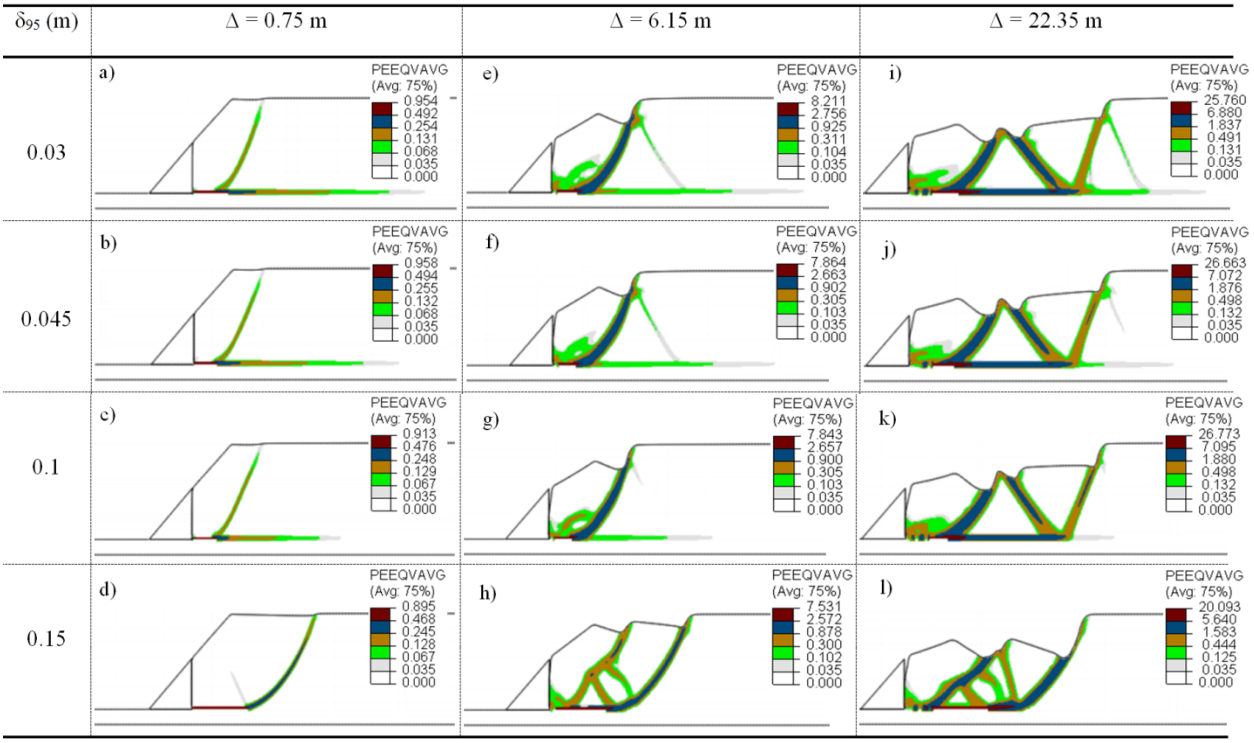

Figure 4. 9: Effect of δ_{95}

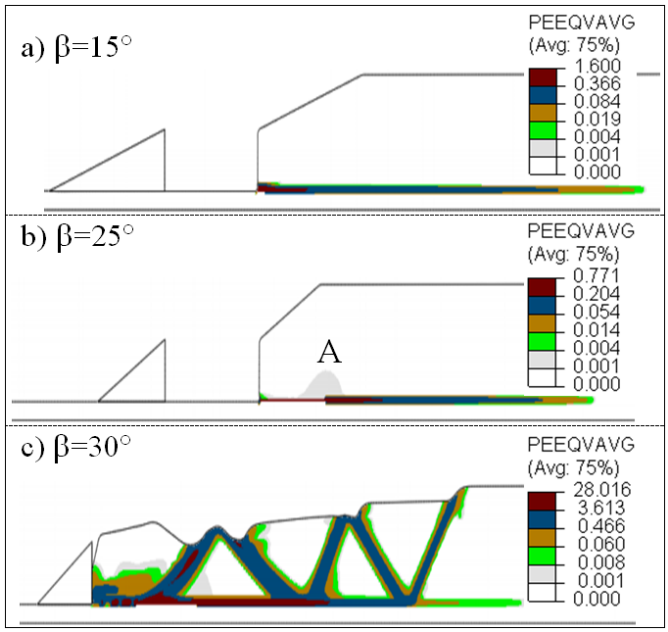

Figure 4. 10: Effect of river bank slope angle (β) at Δ=30.75 m

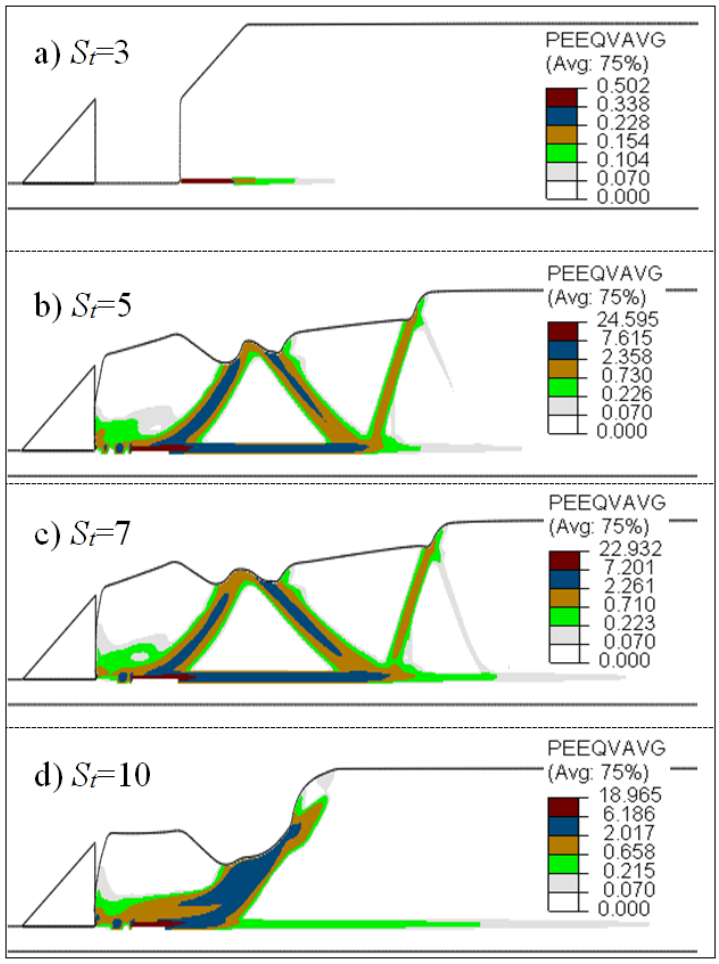

Figure 4. 11: Effects of sensitivity at Δ=20.5 m

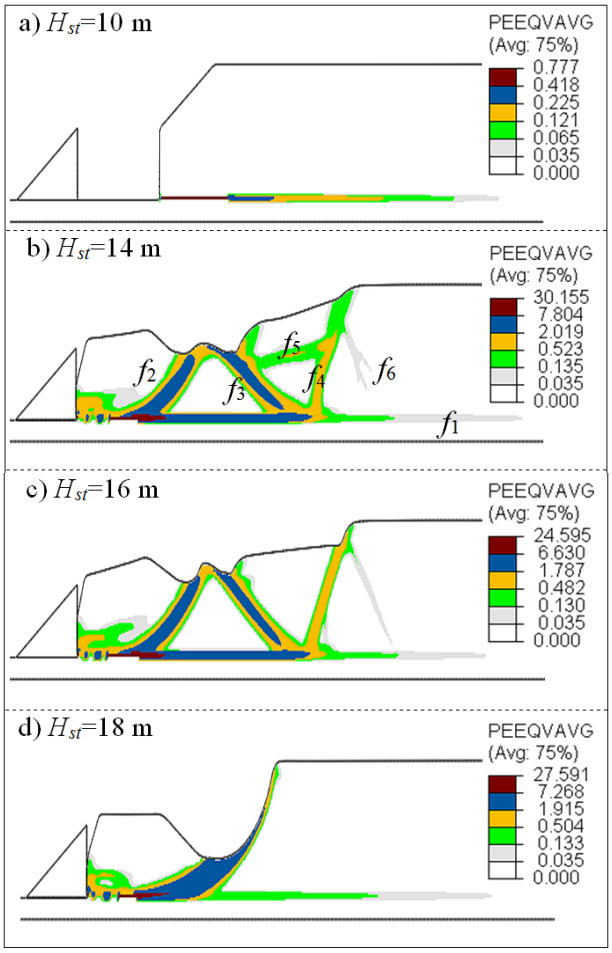

Figure 4. 12: Effect of crust and sensitive clay layer thickness at Δ=20.55 m

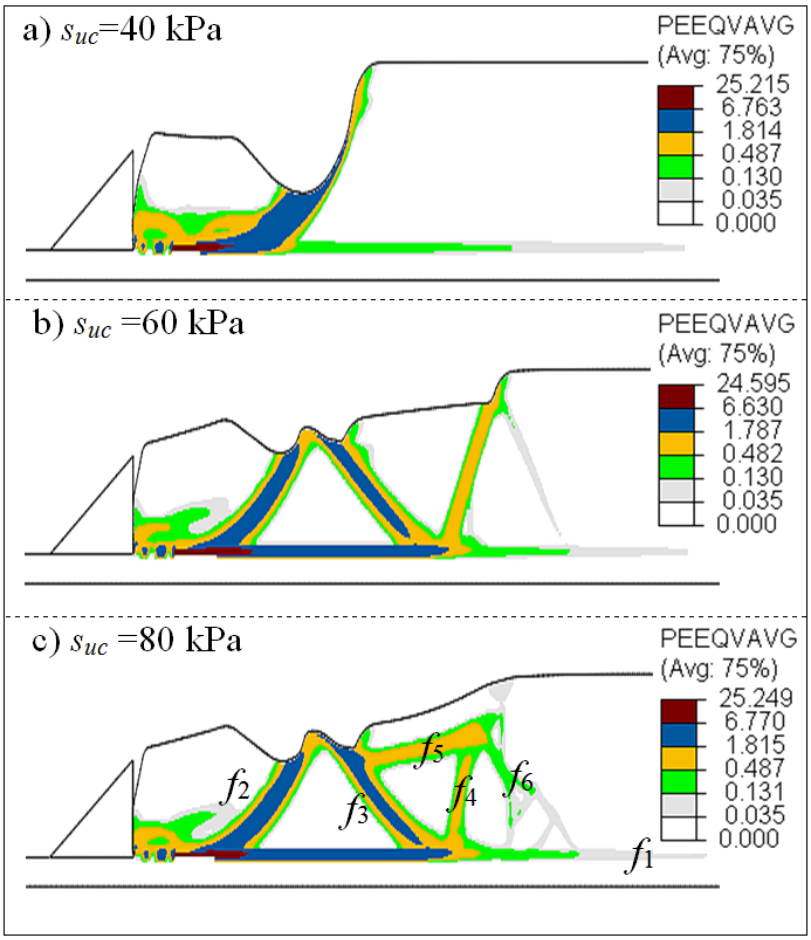

Figure 4. 13: Effect of undrained shear strength of the crust (s_{uc}) at Δ=20.55 m

Table 4. 1: Parameters used for finite element modeling

Parameters	Values		
	Sensitive clay	Crust	Base
Undrained Young's modulus, E_u (MPa)	7.5	10	100
Poisson's ratio, ν_u	0.495	0.495	0.495
Peak undrained shear strength, s_{up} (kPa)	37.5	60*	-
Undrained shear strength, s_{uR} (kPa)	7.5	-	-
Large displacement undrained shear strength, $s_{u(ld)}$ (kPa)	2.0	-	-
δ_{pc} (m)	0.004	-	-
δ_{95} (m)	0.03	-	-
δ_{ld} (m)	2.0	-	-
Submerged unit weight, γ' (kN/m^3)	8.0	9.0	11

*crust is modeled as elastic-perfectly plastic without softening

CHAPTER 5

Numerical Modeling of Combined Effects of Upward and Downward Propagation of Shear Bands on Stability of Slopes with Sensitive Clay

Co-Authorship: This chapter has been submitted for publication as a technical paper in a journal as: Dey, R., Hawlader, B., Phillips, R. and Soga, K. (2015) "Numerical Modeling of Combined Effects of Upward and Downward Propagation of Shear Bands on Stability of Slopes with Sensitive Clay".

Most of the research work presented in this chapter was conducted by the first author. He also prepared the draft manuscript. The other authors supervised the research and reviewed the manuscript.

5.1 Abstract

Many large-scale landslides in sensitive clays cannot be explained by limit equilibrium methods generally used for slope stability analysis. Modeling of progressive development of zones of large inelastic shear deformation (shear band) that results from the strain-softening behaviour of sensitive clays, could explain the failure mechanisms of these large landslides. Different triggering mechanisms for slope failure have been identified; among them the effects of toe erosion and surcharge loading are simulated in this study. Due to toe erosion, a shear band can be initiated and propagated upward (inward) from the river bank. On the other hand, upslope surcharge loading (e.g. the placement of fill) could generate shear bands that might propagate down towards the river bank. In the present study, upward and downward propagation of shear

bands and failure of the slope are modeled using the Coupled Eulerian Lagrangian (CEL) approach in Abaqus finite element (FE) software. It is shown that the formation and propagation of shear bands are significantly influenced by kinematic constraints that change with displacements of the soil masses, and therefore the propagation of an existing shear band might be stopped and new shear band(s) could be formed. The main advantages of the present FE modeling are: (i) extremely large strains in the shear bands can be successfully simulated without numerical issues, (ii) postulated definition of shearing zones with special mesh and/or element type is not required to tackle severe strains in the shear bands, and (iii) the FE program automatically identify the location of critical shear band formation and direction of propagation. Toe erosion could significantly increase the slope failure potential due to surcharge loading. FE analyses with a thick and thin sensitive clay layers show that the global failure could occur at lower surcharge loads in the former as compared to the latter cases.

Key words: sensitive clay slope, landslides, shear band, large deformation, finite element modeling, progressive failure

5.2 Introduction

Many engineering structures, such as foundations, embankments or fills, are required to be placed near the crest of a slope. Such structures might create sufficiently large bearing pressure which could be one of the potential causes of failure of the slope and structures foundation. Among these types of problems, the foundations systems near the slope have been studied by a number of researchers in which the ultimate bearing capacity of the foundation and the stability of the slopes under surcharge loads are investigated [1–6]. The stability analysis of a slope with a

surcharge load becomes further complicated when the soil has strain softening behavior [7]. While these studies significantly advanced the modeling of slopes under surcharge load, a class of problems that need to be investigated further is the effects of surcharge loads on the stability of sensitive clay slopes in which unloading occurs near the toe of the slope due to erosion or small slides as commonly observed in Eastern Canada [8,9]. The main objective of the present study is to present large deformation finite element (FE) modeling of sensitive clay slopes to simulate progressive failure due to combined effects of toe erosion followed by surcharge loading.

The strain-softening behaviour of soil is the main cause of progressive failure [7,10,11]. Depending upon the location of disturbing agents, the progressive failure can be divided into two categories: *upward* and *downward*. In the upward progressive failure the disturbing agents are located downslope and therefore shear band formation or local failure initiates near the toe of the slope and it propagates towards upslope areas (Fig. 5.1a). Previous researchers explained the upward progressive failure assuming an existing horizontal weak layer [12,13]. Examination of field evidence in recent studies [8,14–16] shows that a horizontal shear band might be formed due to toe erosion, excavation or small slides near the bank. Depending upon geometry and soil properties, the shear band could reach to the ground surface causing a global failure of the slope, which might even lead to large landslides with formation of horsts and grabens [8,15,17]. The authors presented similar FE simulations of horsts and grabens in Dey et al. [18]. Without causing any global failure, toe erosion or excavation could simply create a shear band (Fig. 5.1a) which may not be visible or detected during geotechnical investigation even though it might be a

segment of the critical failure plane because the shear strength in the shear band might be significantly reduced due to strain softening behaviour of the soil.

In the downward progressive failure, the disturbing agents (e.g. embankment construction) are in upslope areas and the shear band formation initiates in upslope. Depending upon soil properties and loading conditions, shear band propagation might be limited in the vicinity of surcharge loading as the one shown by type-I or continues towards the initially developed shear band due to toe erosion as Type-II in Fig. 5.1(b). The combined effects of these two triggering factors may or may not cause global failure of the slope as shown in Fig. 5.1(c) and 5.1(b), respectively. Therefore, the combined effects of upward and downward propagation of shear bands need to be analyzed properly.

Numerical models available in the literature for upward progressive failure in sensitive clay for undrained conditions are based on a number of simplifying assumptions. Locat et al. [8] explains the mechanism of progressive failure and formation of a shear band parallel to an infinite slope. In their study, a disturbing force parallel to the slope is applied on the soil layer above the predefined shear zone. The soil above the shear zone is assumed to be linear elastic. Locat et al. [15] conducted numerical modeling using the PLAXIS 2D [19] and BIFURC [20] FE programs. In this decoupled modeling, the initial stresses are calculated using the PLAXIS 2D, which were then used in BIFURC to simulate the initiation and progression of a quasi-horizontal shear band, by applying an external load on the top of the predefined shear zone near the toe. Quinn et al. [16] used the concepts of linear elastic fracture mechanics (LEFM) and proposed a model for development of a shear band in an infinite slope with a vertical step cut. The critical length required to initiate the propagation of the shear band is calculated using the LEFM approach proposed by Palmer and Rice [21]. They showed that the failure of the slope would occur when

the length of the shear band is sufficiently large such that the downward unbalanced force causes active shear failure. Quinn et al. [22] further conducted FE analysis to demonstrate the effects of erosion on propagation of shear bands through a weak predefined shear zone. As a number of simplifying assumptions have been made, the authors admitted that their analyses are only for illustrative purpose.

The downward progressive failure could be initiated by various triggering activities, such as placement of fill in the upslope areas. These activities can increase shear stresses along the potential failure planes. Shear bands may start to develop near the loaded area and propagate further leading to downward progressive failure. Gylland [23] listed a number of landslides in sensitive clays where the downward progressive failure is believed to be the dominating mechanism.

Studies on modeling of downward progressive failure are very limited. Bernander [24,25] presented a finite difference method to simulate the downward progressive failure of long infinite slopes. The effect of fill in the upslope area was idealized as a downward force (N_x) acting parallel to a predefined failure plane. The failure zone was defined as a sensitive clay layer with strain softening behaviour, while the soil above the failure plane was assumed to be elastic. The post-peak softening behaviour of the sensitive clay in the failure zone was modeled by decreasing linearly the mobilized undrained shear strength (s_u) with shear displacement. Increasing N_x with time, the propagation of shear band and the variation of shear stress along the predefined failure plane were examined. This model was further used by Locat et al. [8] to explain some features of downward progressive landslides. Andresen and Jostad [26] modeled downward progressive failure using the BIFURC FE program [20] where the strain softening behaviour of the predefined failure zone was modeled using a finite thickness interface element.

Gylland et al. [27] extended this work further and showed the effects of some key input parameters. Further discussion on FE modeling of slopes is provided in the following sections.

In summary, the numerical modeling techniques available in the literature for progressive failure are limited to idealized conditions, such as infinite slopes, predefined shear zone, ideal triggering effects (such as concentrated force) and elastic behaviour outside the shear bands. One of the main challenges in numerical modeling is that the progressive failure of slopes involved with large deformation that result in significant mesh distortion around the failure plane in the conventional FE modeling in Lagrangian framework. In order to overcome these issues, the Coupled Eulerian Lagrangian (CEL) approach available in Abaqus FE software is used in this study to model progressive failure of slopes in the undrained condition (ϕ=0).

The paper is organized in the following way. First, the performance and advantages of CEL in modeling shear band formation and its propagation is shown from the simulation of a large shear box problem. In the second part, the shear band formation due to toe erosion is presented. Finally, the downward progressive failure due to placement of a fill in the upslope areas is simulated with and without toe erosion.

5.3 Problem Definition

Large Shear Box:

In previous studies, the propagation of a shear band through a predefined weak layer between two idealized soil layers (mainly elastic) has been studied analytically and numerically [21,28,29]. In order to show the performance of the present large deformation FE modeling

technique, simulations are performed for an idealized case similar to the aforementioned studies [28], which is a large shear box of 500 m length (Fig. 5.2a). The total thickness of the soil layer is 6 m with a top layer of 3.0 m. The thickness of the sensitive clay layer is varied from 0.25 m to 1.0 m. Similar to the aforementioned studies, the top and bottom soil layer is assumed to be elastic. The left side of the top soil layer (*ab*) is displaced laterally to form a shear band near point *b* which propagates along the sensitive clay layer.

River Bank:

Figure 5.2(b) shows the geometry of the river bank slope analyzed in this study. The effects of following three factors on stability of the slope are analyzed: (i) toe erosion, (ii) placement of fill, and (iii) thickness of the sensitive clay layer. The erosion is modeled by displacing a block of soil near the toe as shown by the shaded triangular zone in Fig. 5.2(b), which is referred as the "eroded block." The height of eroded block is H_e. The placement of fill is modeled by displacing vertically a 20 m wide rigid block placed at a distance x from the crest. This block is referred as the "load block." Analyses are performed for 'thin' and 'thick' sensitive clay layers for the model shown in Fig. 5.2(b). The lower boundary of the sensitive clay is the top of the base layer for both thin and thick conditions, while the upper boundaries for thin and thick conditions are shown by dashed lines in Fig. 5.2(b). In other words, for the thin condition the areas *mnqgh* and *klmn* are the non-sensitive upper clay and sensitive clay layers, respectively; while for the thick condition the areas *nophgq* and *klpon* are the upper clay and sensitive clay layers, respectively. The upper clay layer is modeled as elastic-perfectly plastic material while the base is assumed to be very stiff and modeled as elastic material. It is assumed that the base layer is very thick;

however, in the FE analyses only 3 m of this layer is modeled to make it computationally efficient. Analysis is also performed with a 10 m thick base layer and similar results are obtained. FE analyses are performed for the following conditions (see Fig. 5.2b for dimensions).

(i) Model-I: Effect of toe erosion is simulated by displacing an eroded block of H_e=10 m for a slope with a thin sensitive clay layer. The thickness of the thin sensitive clay layer is varied from 0.25 m to 1.0 m.

(ii) Model-II: A 0.5 m thin sensitive clay layer is considered. Toe erosion is simulated by displacing an eroded block of H_e=7.5 m and then a vertical load is applied from the load block. Analyses are also performed only for vertical loading without toe erosion.

(iii) Model-III: This is similar to Model-II but with a 16 m thick sensitive clay layer.

5.4 Finite Element Modeling

In a state-of the-art report, Duncan [30] showed the advantages of FE analysis over limit equilibrium methods for slope stability analysis. Griffiths and Lane [31] also showed that FE method is a powerful alternative approach because, unlike limit equilibrium methods, fewer suppositional assumptions are required and the failure occurs naturally through the zones where shear stress reaches the shear strength of the soil. Most of the FE models developed at that time for slope stability analysis were in the purely Lagrangian framework [32–36]. One of the main disadvantages of this type of FE models is that a significant mesh distortion occurs around the failure planes and the solutions generally suffer from mesh dependency, numerical instabilities and lack of convergence. The non-convergence to the solution due to significant mesh distortion is considered as one of the conditions of onset of failure in some studies [31,34]. The application

of FE method becomes further complex in stability analysis of slopes in soils with strain softening behaviour because large strain concentration occurs in narrow zones forming shear bands. The propagation of shear bands has been identified as one of the key factors of many slides involved with strain softening materials [10,11,37–39]. In order to model the large strains along the shear band a number of attempts have been taken in the past. The Norwegian Geotechnical Institute (NGI) [20,26,27,40] modeled shear band propagation using interface elements of finite thickness along the potential failure planes. They also claimed that finite thickness interface elements better model the behaviour than zero thickness interface elements. Mohammadi and Taiebat [41,42] presented FE analysis based on adaptive mesh refinement algorithm using the updated Lagrangian formulation; however, it is applicable to limited deformation even though it performs better than the purely Lagrangian formulation. The extended finite element method (X-FEM), which was originally developed to model growth of cracks without remeshing, has been used in some studies for stability analysis of joined rock slopes [43]. Thakur [29] demonstrated its potential application to slope stability problems from some preliminary analysis. In X-FEM, the shear band is treated as a strong discontinuity instead of a band of finite thickness. Nonconventional definitions of the continuum, such as the Cosserat model [44,45], model based on gradient or nonlocal theories [7,46–50], have also been used to simulate strain localization. Gylland [23] provided a brief summary of advantages and limitations of available techniques for modeling shear band/discontinuity. In the present study, the CEL approach in Abaqus FE software is used to analyze stability of sensitive clay slopes. In CEL, the mesh is fixed and soil as Eulerian material flows through the fixed mesh; therefore, numerical issues related to mesh distortion are not expected even at very large strains in the shear band.

Abaqus CEL allows only three-dimensional modeling, and therefore the analyses are performed with only one element length in the out of plane direction in order to simulate plane strain condition. Uniform mesh of 0.5 m × 0.5 m is used except for the mesh sensitivity analyses. The large shear box simulation consists of soil and a void space (left of Fig. 5.2a) to accommodate the displaced soil. However, the river bank problem consists of soil, eroded block, load block and void space (Fig. 5.2b). The eroded block and load block are modeled as rigid bodies in the Lagrangian framework. The soil is modeled as an Eulerian material using EC3D8R 8-noded brick elements.

As the soil is modeled as Eulerian material, velocity boundary conditions are applied. In the large shear box problem, zero velocity boundary conditions are applied normal to the top, all the vertical faces of the domain and the vertical face *cd*, which prevent any flow of soil through these boundaries. At the bottom, zero velocity boundary conditions are applied in all three directions. At the vertical face *ab* a velocity v (0.05 mm/s) is applied to displace this face laterally to the left to a given distance Δ_1.

In the river bank problem, zero velocity boundary conditions are applied normal to all vertical faces of the domain. However, at the bottom, zero velocity boundary conditions are applied in all three directions. No velocity boundary condition is applied at the soil-void interface (efgh in Fig. 5.2b) so that the soil can move into the void space when needed. Unbonded and smooth interface conditions are used between both the eroded and load blocks against the clay.

The numerical analyses consist of the following steps of loading. Keeping the eroded block fixed, the geostatic load is applied in the first step to bring the soil to an in-situ stress condition. The slope is stable in the geostatic step for the conditions analyzed here. Although some shear stresses develop especially near the river bank, it is less than the maximum undrained shear

strength and therefore no plastic shear strain or shear band forms. In the second step, the eroded block is displaced laterally (Δ) up to 0.65 m at a constant speed of 0.05 m/s to the left applying a displacement boundary condition on the rigid eroded block. In the no erosion condition, analyses are performed by replacing the eroded block with soil of the same properties as the crust. It is found that the slope is stable at the end of the geostatic step. This implies that the movement of the eroded block simulates the effect of erosion on an initially stable slope. In the third step, the load block is displaced vertically downward without any rotation. Authors understand that the time lag between toe erosion and surcharge loading might change the undrained shear strength; however, such issues are not considered in this study.

5.5 Undrained Shear Strength of Sensitive Clay

Whether the analyses should be performed for drained or undrained conditions depends on drainage characteristics of soil and the time allowed for pore water pressure dissipation. A small slide near the toe of the slope can generate a shear band quickly in an undrained condition. Similar to previous studies [e.g. 25,51], analysis for surcharge loading is also performed for undrained conditions. Abaqus CEL is limited to only single-phase analysis; therefore, total stress analysis is performed which is applicable only to undrained conditions. Further discussion on effective stress and total stress analysis of slopes can be found in Duncan [52].

Laboratory tests were conducted in the past to understand undrained stress-strain behaviour of sensitive clays [24,53,54]. Test results show that during shearing shear stress gradually increases, reaches the peak undrained shear strength (s_{up}), remains almost constant at s_{up} for some strains

and then decreases resulting in post-peak softening. The pre-peak stress-strain behaviour is assumed to be elastic.

In the post-peak zone, strains are localized in the shear band [8,15,29,55]. Based on four different types of laboratory tests, Tavenas et at. [53] reported the variation of s_u with strain energy for sensitive Champlain clays collected from 7 different sites in Quebec in eastern Canada. Quinn et al. [16] reanalyzed those data and presented the post-peak s_u degradation as a function of plastic shear displacement. The following are the key features of the post-peak softening behaviour: (i) s_u decreases nonlinearly with post-peak plastic deformation (δ) and the rate of decrease is high at the beginning and very low at large values of δ; (ii) the rate of decrease of s_u with δ is not the same for all clays tested, (iii) the percentage of reduction from s_{up} is not the same for all clays, which depends upon sensitivity (S_t) of the clay.

The localized shear strain could be calculated if the thickness of the shear band is known; however, proper estimation of shear band thickness is very difficult. Therefore, similar to previous authors [16] shear displacement is used to define the post-peak softening curve while shear strain is used in the pre-peak region.

Figure 5.3 shows the stress-strain behaviour used to model sensitive clay. The linear elastic pre-peak (line *oa* in Fig. 5.3) behavior is defined by the elastic properties (E_u, and ν_u). The peak undrained shear strength (s_{up}) is mobilized at point *a* and remains constant up to point *b* for a displacement of δ_{pc} from point *a*. The completely remoulded (stirred) undrained shear strength (s_{ur}) can be measured in the laboratory. However, post-slide investigations does not show relevance of s_{ur} and therefore Bernander [24] recommended an undrained shear strength s_{uR}

($>s_{ur}$) for progressive failure analysis that mobilizes in shear bands as a result of considerable shear displacement.

The shear strength degradation curve (*bcd*) is defined by the following exponential function.

$$s_u = \left[\frac{1}{S_t} + \left(1 - \frac{1}{S_t}\right) e^{-3\delta/\delta_{95}}\right] s_{up} \quad (1)$$

where s_u is the mobilized undrained shear strength; $\delta=\delta_t-(\delta_e+\delta_{pc})$ with δ_e and δ_t are the elastic and total shear displacements, respectively; δ_{95} is the value of δ at which the undrained shear strength is reduced by 95% of (s_{up}-s_{uR}) and $S_t=s_{up}/s_{uR}$. Plastic shear deformation δ_p ($=\delta_t-\delta_e$) initiates from point *a*, although s_u degradation occurs after point *b*. Equation (1) is similar to the strength degradation equation proposed by Einav and Randolph [56], but in terms of δ. As it is an exponential curve, s_u up to $2\delta_{95}$ is defined by Eq. (1). After that a linear relationship (line *de*) is used to decrease s_u to a constant $s_{u(ld)}$ at δ_{ld}. Equation (1) fits well with post-peak stress-displacement behaviour of sensitive clays reported from laboratory tests [9,53], which has been presented elsewhere [57]. Assuming a simple shear condition, the plastic shear strain is calculated as δ_p/t, where t is the thickness of the soil element. In FE analysis, the variation of yield strength ($=2s_u$) is defined as a function of plastic shear strain, which is calculated assuming $t=t_{FE}$, where t_{FE} is the thickness of the cubical EC3D8R element. The von Mises yield criterion is adopted, which represents a right cylinder in the three-dimensional stress space. Therefore, the plastic volumetric strain is zero for compression and shearing. Moreover, elastic volumetric strain is zero for total stress analysis because the undrained bulk modulus is infinite.

Table 5.1 lists the geotechnical parameters used in this study. Based on experimental results of sensitive clays, Quinn et al. [16] suggested $E_u/s_{up}\cong$90–300, which is also comparable with the range of values used by Bernander [24]. In this study E_u/s_{up}=187.5 is used. Based on laboratory

stress-strain behaviour [24,29,54,58] δ_{pc}=4 mm is selected. Smaller values of δ_{95} give faster reduction of s_u in the softening zone that result in higher potential for shear band propagation. Locat et al. [15] assumed complete strength degradation at displacements between 62.5 and 260 mm for a 0.5 m thick shear zone. In this study, it is assumed that 95% strength degradation occurs at 90 mm displacement. Note that, for a given δ, the shear strain for FE input depends on t_{FE} as discussed later. It is also assumed that $s_{u(ld)}$=2 kPa mobilizes at a very large displacement of 3 m; however, these two parameters do not have any significant influence on initiation of failure. Other soil parameters in Table 5.1 are estimated from typical soil properties [59]. The parameters in Table 5.1 are consistent with previous studies on landslides in sensitive clays [8,9,14–16,24,53,60].

5.6 FE Results

Large shear box

As mentioned before, shear bands form because of plastic shear strain concentration. In order to examine the development of strains in the shear band, the equivalent plastic strain (PEEQVAVG) is obtained from Abaqus. Here PEEQVAVG represents the integration of plastic deviatoric strain rate tensor ($\dot{\epsilon}_{ij}^{p}$) over the period of analysis (i.e. $\int_0^t \sqrt{\frac{2}{3}\dot{\epsilon}_{ij}^{p}\dot{\epsilon}_{ji}^{p}}dt$). In other words, PEEQVAVG is a scalar variable to represent generalized plastic deformation. If the plastic shear strain in simple shear condition is γ^p, then PEEQVAVG=$\gamma^p/\sqrt{3}$. When PEEQVAVG is greater than zero, the stresses in that element reach the yield strength and plastic deformation occurs. When PEEQVAVG is zero, only undrained elastic deformation occurs.

Figure 5.4(a) shows the equivalent plastic strain (PEEQVAVG) at Δ_1=0.2 m for 0.5 m mesh. The strain concentration in the sensitive clay layer starts from the left side and propagates to the right with increase in horizontal displacement Δ_1. Figure 5.4(b) shows the plastic shear displacement ($\delta_p=\delta_t-\delta_e$) of the top of the sensitive clay layer (see Fig. 5.2a) at different locations along the clay layer. Plots are given for different horizontal displacements (Δ_1 = 0.06, 0.1, 0.2, 0.28 and 0.4 m). From Abaqus PEEQVAVG is obtained from which γ^p ($=\sqrt{3}$ PEEQVAVG) is calculated. The plastic shear displacement is then calculated as $\delta_p=\gamma^p \times t$, where t is the thickness of the finite element mesh. In order to explain the results, consider the results with 0.5 m mesh size (dashed lines with square symbols in Fig. 5.4b). For a given Δ_1, δ_p gradually decreases with distance from point *b* in Fig. 5.2(a) and becomes zero at a certain distance. For example, when Δ_1=0.2 m, δ_p=0 at a distance of 201.5 m. In other words, plastic deformation occurs up to this distance. In this analysis, $s_u=s_{u95}$ at $\delta=\delta_{95}$=0.09 m (i.e. $\delta_p=\delta_{pc}+\delta_{95}$=0.094 m), which is shown by a horizontal dashed line. The section of the shear band where $\delta_p \geq (\delta_{pc}+\delta_{95})$ (i.e. $s_u \leq s_{u95}$) is referred as the *residual shear band* because significant plastic strain accumulates in this zone (Section c-d-e in Fig. 3). For example, when Δ_1=0.2 m, the residual shear band of 104 m develops from the left boundary as shown in Figs. 5.4(a) and 5.4(b). The section of the shear band where $\delta_{pc}<\delta_p<(\delta_{pc}+\delta_{95})$ (Section b-c in Fig. 5.3) is defined as "softening zone" as shown in Fig. 5.4(a). No strength degradation occurs in a small segment near the right end where $\delta_p \leq \delta_{pc}$ (Section a-b Fig. 5.3), and therefore is not considered as a shear band. Hence, the term shear band in the following sections represents the residual and softening zones only. For Δ_1=0.2 m, the lengths of the residual shear band (L_{sb}^r) and softening zone (L_{sb}^s) are 104 m and 90.5 m, respectively. The length of the shear band ($L_{sb} = L_{sb}^r + L_{sb}^s$) increases with Δ_1.

The success of FE modeling of strain-softening response depends on reliable calculation of localized plastic strains, which is strongly related to FE mesh size and shape as well as orientation and thickness of the shear bands. Several authors [40,61–63] proposed an element scaling rule to reduce the effects of mesh dependency on results. In this study, uniform cubical elements are used in the whole domain. In order to show the effects of mesh size on results and advantages of element size scaling, the following two sets of analyses are performed.

i) With element size scaling: Analyses are performed for four different mesh sizes of 0.25, 0.5, 0.75 and 1.0 m in which γ^p for FE input is calculated scaling by element size. For example, s_{u95} mobilizes at $\gamma_{95}^{p} = \delta_{95}/t_{FE}$ of 18% and 9% for mesh size 0.5 and 1.0 m, respectively, for the same value of δ_{95}=0.09 m.

ii) Without element size scaling: Analyses are performed for three different mesh sizes (0.25, 0.5, and 1.0 m) using the same s_u vs plastic shear strain curve used in 0.5 m mesh without considering any effect of element size on γ^p for FE input. For example, s_{u95} mobilizes at $\gamma_{95}^{p} = 18\%$ irrespective of the mesh size.

The orientation of the shear band is not considered in the scaling rule. This might induce some mesh dependency when shear band in river bank slope develops in an inclined direction, as discussed later.

Figure 5.4(b) shows a very small difference between calculated δ_p for different mesh sizes when the element size scaling rule is used. Figure 5.4(c) shows the comparison of calculated δ_p with and without element size scaling. For clarity, calculated δ_p with 0.25 m and 1.0 m mesh sizes at Δ_l= 0.1 and 0.2 m are shown in Fig. 5.4(c). As shown, 0.25 m mesh gives higher and 1.0 m mesh gives lower δ_p as compared to the values obtained with element size scaling. The difference is

higher in the softening zone because of a higher rate of reduction of s_u with δ when $\delta<\delta_{95}$. The length of the shear band is also different if element size scaling is not used. Hence, the use of the element size scaling significantly improves the simulation of a shear band.

River Bank

Model-I:

Similar to Fig. 5.4(a), the plastic shear strain in the sensitive clay layer in the river bank slope is shown in Fig. 5.5(a) when the eroded block is displaced to Δ=0.45 m. The plastic shear strains accumulate only in this horizontal shear band. For Δ=0.45 m, L_{sb}^{r}=44.5 m and L_{sb}^{s}=13.5 m, where the parameters L_{sb}^{r} and L_{sb}^{s} are defined above. The shear bands for other values of eroded block displacement Δ are very similar to this one except for their length. The larger the eroded block movement is, the longer the plastic zone L_{sb} becomes.

Figure 5.5(b) shows the variation plastic shear displacement (δ_p) along the top of the thin sensitive clay layer under the river bank slope. As discussed, δ_p is calculated using PEEQVAVG obtained from Abaqus. At a given distance from the vertical face of the eroded block, δ_p increases with an increase in block movement Δ. The eroded block separates from the main soil body when Δ=0.5 m, therefore δ_p does not increase after Δ=0.5 m. The length of the shear band increases with block movement until Δ=0.5 m.

Analyses are also performed for different mesh sizes (0.25, 0.5, 0.75 and 1.0 m) with element size scaling as discussed above. The calculated values of δ_p for different block movements are all similar, which implies that the scaling rule works well for horizontal shear band formation and propagation due to toe erosion. In order to show the advantages of scaling, analyses are also

performed with 0.25, 0.75 and 1.0 m mesh sizes but with s_u vs plastic strain curve of 0.5 m mesh. The results are shown in Fig. 5.5(c). Again for clarity, calculated values of δ_p for Δ=0.45 m are shown. Unlike Fig. 5.5(b), results are significantly mesh dependent as 0.25 m mesh gives higher and 1.0 m mesh gives lower δ_p than the values obtained with element size scaling. The difference between δ_p with and without element size scaling is higher in this case than the shear box problem presented in Fig. 5.4(c). The length of the shear band also varies widely if scaling is not used. This again highlights the importance of element size scaling for shear band modelling in FE analysis.

In a recent study, Locat et al. [15] numerically simulated horizontal propagation of a shear band. They applied an external nodal load at the point of intersection on top of the sensitive clay layer and the vertical excavation face. The load is then gradually increased to simulate the propagation of a shear band. Uniform displacements of soil above the shear zone were assumed. In the present study, the unloading due to toe erosion is simulated using an eroded block instead of applying an external force like Locat et al. [15]. The FE program calculates the deformation of the soil in the whole domain and therefore there is no need to impose any assumed deformation conditions. Furthermore, shear band propagation will stop if the vertical face of the eroded block separates from the soil, which is successfully simulated in the present study. On the other hand, if the external force is applied as Locat et al. [15] did, shear band propagation will continue with an increase in applied force until failure occurs. Therefore, the present FE model better simulates the process of shear band propagation due to toe erosion. It is noted that the variation of shear stress along the shear band has been also successfully simulated as presented in Dey et al. [64].

Influence of soil properties on shear band length, L_{sb}

Some soil parameters (e.g. E_u of the crust, S_t and δ_{95} of the sensitive clay layer) have significant influence on the length of the shear band. The effects of these parameters are examined varying only one of these parameters while keeping all other parameters the same as listed in Table 5.1. The eroded block is displaced laterally until it separates from the main soil body. In the analysis, S_t is varied by changing the value of s_{uR} keeping s_{up} constant. Figure 5.6(a) shows that L_{sb} increases with S_t. On the other hand, L_{sb} decreases with δ_{95} (Fig. 5.6b). The increase in S_t and/or decrease in δ_{95} increase the rate of softening (i.e. more brittle) and therefore L_{sb} increases. Moreover, as shown in Fig. 5.5(a), no plastic strain develops in the soil above the sensitive clay layer during the propagation of the shear band, which implies that the deformation of this soil at this stage is governed by elastic properties. Figure 5.6(c) shows that L_{sb} decreases nonlinearly with an increase in undrained Young's modulus of soil above the sensitive clay layer.

Although these parameters influence the results, the soil parameters listed in Table 5.1 are used in the FE analyses presented in the following sections.

Model-II:

In this case, analyses are performed for 5 different vertical loading conditions and they are named as: TE-X40-TN, TE-X70-TN, TE-X150-TN, NE-X70-TN and NE-X150-TN, where TE represents toe erosion, NE represents no erosion, X represents the distance of the vertical loading from the crest (e.g. X40 represents 40 m horizontal distance (see Fig. 5.2b), and TN represents thin layer of sensitive clay (i.e. a thick layer case is presented in the next section). The vertical load is applied in displacement controlled conditions. The variation of bearing pressure (q) under the load block with its vertical displacement (Δy) for these five cases is shown in Fig. 5.7. For a

given Δy, the reaction force (R) at the reference point of the rigid load block is obtained from Abaqus, which is then used to calculate $q=R/wl$, where w and l are the width (=20 m) and length (=0.5 m) of the load block, respectively.

In TE-X40-TN and TE-X70-TN, q gradually increases with Δy and reaches the peak (q_{max}) at $\Delta y \approx 250$ mm (Fig. 5.7). The value of q_{max} in TE-X70-TN is approximately 14 kPa higher than that of in TE-X40-TN. At a first glance, the q-Δy curves of these two simulations look similar to a typical force-displacement curve of a shallow foundation in elastic-perfectly plastic soil. However, the failure mechanism in this case is different from the shallow foundation alone because the thin sensitive clay layer plays a significant role on the shape of the force-displacement curve as discussed below.

To explain the mechanisms involved in the observed load-displacement response, first consider the simulation TE-X40-TN. Because of toe erosion, plastic shear strains accumulate in a horizontal shear band AB of 76 m length (Fig. 5.8a). In this figure PEEQVAVG ≥0.0046 represents the shear band where s_u degradation occurs (i.e. $\delta_p \geq \delta_{pc}$ in Fig. 5.3). With an increase in vertical displacement of the load block Δy, the shear band AB propagates further to point F and also two new shear bands generate from the two ends of the load block (Fig. 5.8b). At Δy=213 mm, a triangular wedge CDE is formed and also the shear band CE extends to the horizontal shear band AF (Fig. 5.8c). Due to a further increase in Δy, instead of curving upward as general or local shear failure of shallow foundations (i.e. failure type-I in Fig. 5.1b), the plastic shear zone spreads downward to the horizontal shear band AF (Figs. 5.8d & 5.8e). The soil mass in the left side of the load block displaces laterally to the left as there is kinematically less restraint than the soil in the right side. The plastic shear strain increases in the horizontal

shear band AB (compare PEEQAVAG in Figs. 5.8a and 5.8e). The shear bands under the load block are not symmetric and also very different from general or local shear failure surfaces that typically develop under shallow foundations. The instantaneous velocity vectors (Fig. 5.8f) at Δy=392 mm shows that the soil elements in the left side of the load block move almost horizontally while in the right side there is negligible movement.

The shear band formation mechanism in TE-X70-TN (not shown) is very similar to TE-X40-TN.

As shown in Fig. 5.7, the load-displacement behaviour in TE-X150-TN, in which the vertical load block is placed at 150 m from the crest, is different from the previous two cases. In this case, the bearing stress q increases with vertical displacement Δy to a peak at Δy=210 mm and then decreases. This shape of the q-Δy curve could be explained from the formation of shear band and its propagation (Figs. 5.9a-e). Similar to TE-X40-TN, the horizontal shear band AB of 76 m is initially formed due to erosion prior to the vertical loading. At Δy= 141 mm, two shear bands start to form under the load block (Fig. 5.9a). With an increase in Δy, the shear bands from C and D propagate down and form the triangular wedge CDE and also a horizontal shear band FG in the thin sensitive clay layer (Fig. 5.9b). With a further increase in Δy, another horizontal shear band forms in the right side of the load block in the sensitive clay layer (Fig. 5.9c). The shear bands AB and FG propagate further with Δy and merge together forming a long horizontal shear band ABGF. At this stage, the plastic shear strain in the major portion of the developed shear band ABGF is less than γ_{95}^{p} (=18%). With a further increase in Δy, the soil mass above ABFG displaces laterally, which increases the plastic shear strain in the horizontal shear band reducing its shear strength. Therefore, q reduces from the peak as shown in Fig. 5.7. When Δy is approximately 445 mm, the plastic shear strain in the major portion of the horizontal shear

band exceeds $2\gamma_{95}^{p}$ where $s_u \approx s_{uR}$. As the rate of reduction of s_u after s_{uR} is very low (Fig. 5.3), q is almost constant for $\Delta y \geq 450$ mm. Figure 5.9(d) shows that, at large Δy (=685 mm), plastic shear strain spreads over a wide area under the load block in the elastic-perfectly plastic upper clay layer, while in the sensitive clay the strain accumulation occurs only in the narrow horizontal shear band. Similar to Fig. 5.8(f), the instantaneous velocity vectors in Fig. 5.9(e) show that the soil elements displace to the left almost horizontally at this Δy.

The effects of toe erosion are examined by conducting analyses without toe erosion (NE-cases). The q vs Δy curve of NE-X70-TN, which has no toe erosion, is similar to that of TE-X150-TN, but the failure mechanism is slightly different. In NE-X70-TN, there is no horizontal shear band from the toe of the slope prior to the vertical loading. As the vertical loading continues, two shear bands form under the load block (Fig. 5.10a). With an increase in Δy, a triangular wedge CDE and a horizontal shear band FG in the sensitive clay layer is formed (Fig. 5.10b). The length of the shear band FG increases with Δy, which is accompanied by the reduction in q as shown in Fig. 5.7. The instantaneous velocity vectors for Δy=232 mm as presented in Fig. 5.10(c) show that the soil elements in the triangular wedge below the load block move downward and left. A block of soil above the horizontal shear band FG moves almost laterally. Most of the soil elements above the left side of this block displace upward to the left. This displacement pattern changes with Δy. With an increase in Δy, the length of the horizontal shear band FG increases and at Δy=283 mm it reaches the toe of the slope. Figure 5.10(d) shows that large plastic shear strains develop in the horizontal shear band that reduce s_u to values lower than s_{uR}. At this stage the soil elements move almost laterally as shown in Fig. 5.10(e).

In both aforementioned cases (TE-X150-TN & NE-X70-TN), the vertical load resistance begins to decrease when the horizontal shear band in the sensitive clay layer starts to develop. The resistance then becomes more or less steady state when a continuous horizontal shear band is formed between the toe and the vertical load block location.

When the load block is placed far from the crest of the slope without any toe erosion (NE-X150-TN), the load-displacement behaviour is different from those discussed in the previous four cases. The q vs Δy curve in NE-X150-TN does not show any peak, rather the value of q continuously increases with Δy (Fig. 5.7). Similar to the previous cases, shear bands and a triangular wedge are formed below the load block with an increase in Δy (Fig. 5.11). After reaching the sensitive clay layer, the shear band propagates horizontally. Unlike NE-X70-TN, the kinematical restraint of the soil mass in the left side of the load block is similar to the right side and therefore the horizontal shear bands propagate almost symmetrically to both sides, which gives more shear resistance than the cases when a horizontal shear band develops towards the slope. Also, even at the maximum Δy (=740 mm), the shear band does not reach the toe of the slope.

Figure 5.7 shows that the slopes of the initial segment of the q-Δy curves of TE-X40-TN and TE-X70-TN (i.e. the former two cases which are influenced by toe erosion) are smaller than those of the latter three cases. In the former two cases, the load block is placed near the slope and the horizontal shear band due to toe erosion propagates close to the load block. Therefore, the soil in the left side could slide easily to the left.

It is noted that extremely large shear strains develop in the shear band at large displacements. For example, Fig. 5.9(b) shows that the PEEQVAVG as high as 180% is developed, however it has

been successfully simulated without any numerical issues using the present FE modeling techniques, which may not be possible using the typical FE programs in the Lagrangian framework due to significant mesh distortion.

In summary, with an increase in distance of the vertical loading from the slope, the shape of the load-displacement curve changes from post-peak softening to hardening type, depending upon the formation and propagation of shear bands. Post-peak softening behavior leads to catastrophic failure. Massive ground movement or failure occurs when the shear band from the upslope loading reaches the toe or merges with the shear band due to toe erosion. The present FE analyses explain the combined effects of these two triggering factors.

Model III:

A total of seven more simulations are performed with a thick sensitive clay layer (TH, as compared to the TN thin layer cases) and they are named: TE-X60-TH, TE-X90-TH, TE-X120-TH, TE-X150-TH, NE-X60-TH, NE-X90-TH and NE-X150-TH. Similar to Model-II, TE represents toe erosion, NE represents no erosion, and X represents the distance of the load block. TH represents a 16 m thick sensitive clay layer below the 3 m crust as shown in Fig. 5.2(b).

Figure 5.12 shows that the bearing stress q increases with vertical displacement Δy until a peak value and then decreases at large Δy. The shapes of the q-Δy curves are different from those shown in Fig. 5.7 with a thin sensitive clay layer. Similar to the previous cases, the mechanisms involved in the observed load-displacement behaviour can be explained using shear band formation/propagation and instantaneous velocity vectors of soil elements.

In TE-X60-TH, the vertical load is applied relatively close to the crest of the slope at x=60 m. Figure 5.13(a) shows that at the end of toe erosion a 73 m horizontal shear band AB is formed.

However, the slope is globally stable. With increases in vertical load, the existing shear band AB propagates horizontally further to point F below the load block (Fig. 5.13b). With a further increase in vertical load, two shear bands appear from points C and D. However, a shear band from point F propagates up at a faster rate than the propagation of shear bands from C and D (Fig. 5.13c), and a complete shear band CF, approximately at a 45° angle with the horizontal, is formed as shown in Fig. 5.13(d). As the soil mass ABFC in the left side of the load block is kinematically less restrained, it moves laterally to the left. With an increase in Δy, another shear band forms from point F (Fig. 5.13e) and reaches the ground surface at point H (Fig. 5.13f), which is 10 m further than the right edge of the load block. The shear band FH makes an angle of 45° with the horizontal which represents the active failure plane for ϕ=0 condition. Once the complete failure surface ABFH is developed, the failed soil mass moves laterally, except for the soil elements in the triangular block where they move downward left (Fig. 5.13g).

Figure 5.14 shows the formation of shear bands and movement of the soil block when the load block is placed 90 m from the crest (TE-X90-TH). Similar to Fig. 5.13(a), prior to the vertical loading, a horizontal shear band AB of 73 m length is formed due to toe erosion only (Fig. 5.14a). When the vertical load is increased, two shear bands form from points C and D and the existing shear band AB propagates horizontally to point F (Fig. 5.14b). With an increase in Δy, an additional shear band forms from point F and propagates up and merges with the shear band that forms form point D (Fig. 5.14c). Due to further displacement of the load block, shear band DE reaches the horizontal shear band and the failure plane DEGBA is formed (Fig. 5.14d). Finally, the shear band GH forms at large Δy (>348 mm) propagating up from point G (Fig.

5.14e). At this condition (Δy=690 mm), the soil mass above the horizontal shear band moves almost laterally as shown by the instantaneous velocity vectors in Fig. 5.14(f).

Figure 5.15 shows simulation results when the load block is placed at x=120 m (TE-X120-TH). The triangular wedge CDE forms at $\Delta y \approx$150 mm (Fig. 5.15a), accompanied by the peak resistance (Fig. 5.12). Then a horizontal shear band develops under the triangular wedge and propagates to the left due to less kinematic restraint in the left (Fig. 5.15b). With an increase in Δy, the shear band EF propagates further to the left but at a shallower depth than that obtained in TE-X60-TH and TE-X90-TH. Because the load block is placed sufficiently far from the slope, there is a tendency to form a curved upward shear band from E as the one shown in Fig. 5.16(b). However, after propagating a certain distance, the lateral kinematic restraint becomes smaller because of existence of shear band AB. The length of the shear bands AB and EF increase with vertical loading and at Δy=242 mm they cross each other as they are at different depths. When Δy is between 242 and 263 mm, four additional small shear bands are formed in order to connect the upward (AB) and downward (EF) progressive shear bands as shown in Fig. 5.15(c). The instantaneous velocity vectors at Δy=440 mm (Fig. 5.15d) show that the soil elements above the shear bands move almost horizontally at large displacement. Until $\Delta y \approx$385 mm, the shear strains mainly increase in the horizontal shear bands and along DE, and therefore q decreases as the lateral restraint is reduced (Fig. 5.12). When Δy=385–535 mm, the shear strains in the four small shear bands mainly increase, which reduces s_u. As they do not have significant influence on the lateral restraint, q remains almost constant when Δy=385–535 mm. At very large displacements, q again decreases because s_u gradually decreases to $s_{u(ld)}$.

Figure 5.16 shows the results of the simulations when the load block is placed significantly far away from the crest at x=150 m (TE-X150-TH). The response is very different from the previous conditions. In this case, a triangular wedge CDE is formed when $\Delta y \approx 158$ mm (Fig. 5.16a). With an increase in Δy, a shear band from point E continues to grow and reaches to the ground surface at point H (Fig. 5.16b). The length of the shear band AB that formed due to toe erosion also slightly increases from 73 m at Δy=0 to 81 m at Δy=348 mm. The curved shear band forms only to the left, because the left side has still less kinematic restraint than the right side. The instantaneous velocity vectors in Fig. 5.16(c) show that only the soil elements above the shear band DEH displace at this stage. Because the shear band from the vertical load block does not merge with the horizontal shear band formed due to toe erosion, the lateral restraint is not significantly reduced like in the previous cases. Therefore, the reduction of q after the peak is relatively small, which is mainly due to the reduction of s_u in the shear band DEH where it passes through the sensitive clay layer.

Analyses presented in Figs. 5.12-5.16 can be divided into two groups. In the first group (TE-X60-TH, TE-X90-TH and TE-X120-TH) the upslope surface loading triggers global failure of the slope. In these cases, q decreases significantly after reaching a peak developing a complete failure plane, potentially leading to catastrophic failure. The lower vertex of the triangular wedge formed by surface loading (point E in Figs. 5.14 and 5.15) is well above the shear band (AB) formed due to toe erosion. However, because of less kinematic restraint to the left, the shear band propagates towards AB. Moreover, during the development of the complete failure plane and also during the displacement of failed soil mass, a number of shear bands form in different locations and orientations because the kinematic restraints of soil blocks change with displacement and reduction of s_u with plastic strain. Therefore, results show that a shear zone

cannot be easily defined (using interface elements or fine mesh) prior to analysis. However, the present FE model could successfully simulate this complex process.

In the second group (TE-X150-TH, NE-X60-TH, NE-X90-TH and NE-X150-TH) the surface load does not cause global failure of the slope, rather the shear bands form only in the vicinity of the loaded area because the slope or the shear band due to toe erosion is far away from the vertical loading block. However, a slight difference in kinematic restraint results in the formation of a failure plane only on one side of the load block at large Δy (Figs. 5.16).

For the thin sensitive clay layer cases (Figs. 5.8-5.10), the plastic shear strains spread over a wide area, especially at large Δy, in the upper clay layer because this soil is modeled as elastic-perfectly plastic material without any softening. However, for the thick sensitive clay layer cases (Figs. 5.13-5.16), the shearing occurs in the narrow shear bands because of post-peak degradation of s_u with plastic shear displacement. Comparison of Figs. 5.7 and 5.12 shows that slope failure or significant vertical displacement of the load block occur at low q values in the thick sensitive clay layer cases as compared to thin sensitive clay layer cases of similar loading conditions.

Another key question in progressive failure analysis is whether the failure progress from one or both ends. It has been generally assumed that, for natural and cut slopes only under gravity loading, failure generally initiates from the toe of the slope and progress back to the crest [60,65,66]. However, in the present study the process is further complex because it involves the combined effects of toe erosion, loading in the upslope and strain softening behavior of soil. Failure occurs in those soil elements which are overstressed in relation to strain dependent mobilized s_u. Therefore, with an increase in vertical loading, the shear band can propagate from the load block (e.g. Fig. 5.15b), or from the tip of the horizontal shear band formed due to toe

erosion (e.g. Fig. 5.13b) or from both sides (5.14b), which depends upon location of vertical load, amount of toe erosion, soil properties and the thickness of the sensitive clay layer.

5.7 Discussions and Conclusions

Modeling of progressive failure of a slope can be broadly classified into two categories. In the first category, the location of the potential shear zone (e.g. existence of thin weak or strain-softening layers between competent soil strata) is known prior to analysis. Most of the models available in the literature are of this category [15, 22]. In the second category, the location and direction of propagation of potential shear bands are not known prior to analysis. Moreover, for modeling shear bands, several approaches have been used in the past such as zero or finite thickness interface elements and re-meshing techniques. When the location of the potential shear band is not known, it is very difficult to assign the interface elements because kinematic restraint changes with progress of analysis that influences the formation and propagation of shear bands. NGI [20,40] manually implemented the interface element which seems to be cumbersome and less accurate for the type of complex problem presented in this study. They also suggested that automated mesh refinement would be a better option. Automated remeshing is generally computationally very expensive. Therefore, considering the geometry of the slope, the analysis would be computationally extremely expensive. Moreover, if different sizes of elements are used in an analysis, numerically it would be difficult to adopt the element size scaling rule as mentioned before.

In the present study a large deformation FE modeling technique is developed using Abaqus CEL to simulate shear bands in progressive failure of slopes. A model for the variation of

undrained shear strength with plastic deformation is proposed and implemented in Abaqus CEL. Very large displacements were simulated using this FE modeling technique.

At first, the simulation is performed for an idealized large shear box problem. And then a river bank slope is simulated for a thin and a thick sensitive clay layers. Two types of triggering agents are considered for initiation and propagation of shear bands. The effects of these two triggering agents are simulated by displacing an eroded and a load block. The FE program identifies the critical locations and propagation directions of shear bands depending upon kinematic restraints. The toe erosion generates a horizontal shear band that propagates upward and an upslope fill creates shear bands that propagate in the downward direction. The combined effects of these two triggering factors on stability of slope are examined. Analyses are also performed only for fill placement without toe erosion. Most of the cases analyzed in this study show that the placement of fill causes further propagation of the initially developed shear band due to toe erosion. The shear bands generated by fill placement may merge with the horizontal shear band created by toe erosion, resulting in global failure.

After the formation of a horizontal shear band due to toe erosion the slope is globally stable but s_u in the shear band decreases. Note that depending upon geometry and soil properties, global failure might occur due to toe erosion only as shown by the authors in Dey et al. [64]. Three types of q-Δy curves are obtained from the simulation of the effects of upslope fill in Model-II with a thin sensitive clay layer above the base: (i) when the upslope load is placed relatively close to the crest of the slope (x=40 and 70 m), the shear band due to toe erosion affects q from the very beginning, (ii) for an intermediate value of x, the load-displacement curves exhibit post-peak softening behaviour, indicating the possibility of catastrophic failure of the slope if the

applied vertical stress is greater than the peak value, (iii) if the load is placed far from the slope it does not cause global failure of the slope and q increases gradually without any peak.

In Model-III with a thick sensitive clay layer, the q-Δy curves exhibits post-peak softening for all the cases analyzed because the shear bands pass through the thick sensitive clay layer where strength degradation occurs with an increase in plastic strain. Mainly two types of responses are obtained. In the first category, global failure occurs when the upslope load is placed close to the slope. The post-peak degradation of q-Δy curves is significantly higher than that of in Model-II with a thin sensitive clay layer. In the second category, the post-peak softening is not very significant and global failure of the slope does not occur. The post-peak reduction of q is because of strength degradation in the section of the shear band passing through the thick sensitive clay layer.

In summary, a number of limitations in previous FE modeling techniques to simulate progressive failure of slope could be overcome using the present FE modeling technique. However, a parametric study is required for different geometries, location of sensitive clay layer, initial earth pressure at rest and soil parameters.

Acknowledgements

The works presented in this paper have been supported by the Research and Development Corporation of Newfoundland and Labrador, NSERC and C-CORE.

List of symbols

The following symbols are used in this paper:

β slope angle

δ post-peak shear displacement ($\delta=\delta_t-(\delta_e+\delta_{pc})$)

Δ displacement of the eroded block

Δ_l displacement of the left side of upper soil in large shear box

δ_{95} δ at which s_u reduced by 95% of (s_{up}-s_{uR})

τ_c shear stress along the shear band

δ_e elastic shear displacement

δ_p plastic shear displacement ($\delta=\delta_t-\delta_e$)

δ_{pc} plastic shear displacement at point b in Fig. 5.3

δ_t total shear displacement

ν_u undrained Poisson's ratio

L_{sb}^r length of residual shear band where $\delta_p \geq (\delta_{pc}+\delta_{95})$

L_{sb}^s length of softening zone where $\delta_{pc}<\delta<\delta_{95}$

E_u undrained modulus of elasticity

γ^p plastic shear strain

q bearing pressure under the load block

S_t $s_{up}/\ s_{uR}$

s_u mobilized undrained shear strength

$s_{u(ld)}$ s_u at large displacements

s_{up} peak undrained shear strength

s_{uR} s_u mobilized in shear band at considerable shear displacement

s_{ur} s_u at completely remoulded state

t shear band thickness

t_{FE} FE mesh size

References

[1] Sokolovski VV. Statics of granular media. Butterworth Scientific Publications, London. Transaction of Royal Society of London, Series A, vol. 254; 1960. p. 1–45.

[2] Meyerhof GG. The ultimate bearing capacity of foundations on slopes. Proc 4th Int Conf on Soil Mechanics and Foundation Engineering, vol. 1; 1957. p. 384–386.

[3] Narita K, Yamaguchi H. Bearing capacity analysis of foundations on slopes by use of log-spiral sliding surfaces. Soils and Foundations 1990; 30(3):144–152.

[4] de Buhan P, Garnier D. Analysis of the bearing capacity reduction of a foundation near a slope by means of the yield design theory. Revue Française de Géotechnique, vol. 68; 1994. p. 79–101.

[5] de Buhan P, Garnier D. Bearing capacity analysis of foundations on slopes by use of log-spiral sliding surfaces. Soils and Foundations 1998; 38(3):153–163.

[6] Shiau J, Merifield R, Lyamin A, Sloan S. Undrained Stability of Footings on Slopes. Int J Geomech (ASCE) 2011; 11(5):381–390.

[7] Conte E, Silvestri F, Troncon A. Stability analysis of slopes in soils with strain-softening behaviour. Computers and Geotechnics 2010; 37(5): 710–722.

[8] Locat A, Leroueil S, Bernander S, Demers D, Jostad HP, Ouehb L. Progressive failures in eastern Canadian and Scandinavian sensitive clays. Can Geotech J, 2011; 48(11):

1696–1712.

[9] Quinn P. Large Landslides in Sensitive Clay in Eastern Canada and the Associated Hazard and Risk to Linear Infrastructure. PhD thesis, Queen's University, 2009.

[10] Potts DM, Dounias GT, Vaughan, PR. Finite element analysis of progressive failure of Carsington embankment. Géotechnique 1990; 40(1):79–101.

[11] Puzrin AM, Germanovich LN, Kim S. Catastrophic failure of submerged slopes in normally consolidated sediments. Géotechnique 2004; 54(10): 631–643.

[12] Odenstad S. The landslide at Sköttorp on the Lidan River, February 2, 1946. Royal Swedish Institute Proceedings, vol. 4; 1951. p. 1–38.

[13] Carson MA. On the retrogression of landslides in sensitive muddy sediments. Canadian Geotechnical J 1977; 14(4): 582–602.

[14] Locat A, Leroueil S, Bernander S, Demers D, Locat J, Ouehb L. Study of a lateral spread failure in an eastern Canada clay deposit in relation with progressive failure: the Saint-Barnabé-Nord slide. In Proc. of the 4th Canadian Conf. on Geohazards: From Causes to Management, Québec, 2008. p. 89–96.

[15] Locat A, Jostad HP, Leroueil S. Numerical modeling of progressive failure and its implications for spreads in sensitive clays. Canadian Geotechnical J, 2013; 50:961–978.

[16] Quinn PE, Diederichs MS, Rowe RK, Hutchinson DJ. A new model for large landslides in sensitive clay using a fracture mechanics approach. Can Geotech J, 2011; 48(8):1151–1162.

[17] Demers D, Robitaille D, Locat P, Potvin J. Inventory of large landslides in sensitive clay in the province of Québec, Canada: preliminary analysis. Proc of the 1st Int Workshop on

Landslides in Sensitive Clays, Landslides in Sensitive Clays –From Geosciences to Risk Management, Québec, 2013. p. 77–89.

[18] Dey R, Hawlader B, Phillips R, Soga K. Large deformation finite element modeling of progressive failure leading to spread in sensitive clay slopes. Géotechnique 2015 (submitted).

[19] PLAXIS, PLAXIS 2D 2010 manuals. PLAXIS bv., Delft, the Netherlands, 2011.

[20] Jostad HP, Andresen L. Bearing capacity analysis of anisotropic and strain-softening clays. In Proc. of NUMOG VIII, Rome, Italy, 2002. p. 469–474.

[21] Palmer AC, Rice JR. The growth of slip surfaces in the progressive failure of overconsolidated clay. Proc. R. Soc. London, Ser. A, 1973; 332(1591): 527–548.

[22] Quinn PE, Diederichs MS, Rowe RK, Hutchinson DJ. Development of progressive failure in sensitive clay slopes. Canadian Geotechnical J, 2012; 49(7): 782–795.

[23] Gylland AS. Material and slope failure in sensitive clays. PhD thesis, Norwegian University of Science and Technology; 2012.

[24] Bernander S. Progressive failure in long natural slopes: formation, potential extension and configuration of finished slides in strain-softening soils. Licentiate Thesis, Luleå University of Technology; 2000.

[25] Bernander S. Down-hill progressive landslides in soft clays, triggering disturbance agents, slide propagation over horizontal or gently sloping ground, sensitivity related to geometry. Research report, Luleå University of Technology, Luleå, Sweden; 2008.

[26] Andresen L, Jostad HP. Numerical modeling of failure mechanisms in sensitive soft clays – application to offshore geohazards. Off. Technology Conf., Texas, 2007; OTC 18650.

[27] Gylland AS, Sayd MS, Jostad HP, Bernander S. Investigation of soil property sensitivity in progressive failure. In Proc. of the 7th European Conf. on Num. Methods in Geotech. Eng., Benz & Nordal (eds), Trondheim, Norway, 2010. p. 515–520.

[28] Chowdhury RN. Propagation of failure surfaces in natural slopes. J Geophysical Res, 1978; 83(B12): 5983–5988.

[29] Thakur V. Strain localization in sensitive soft clays. PhD thesis, Norwegian University of Science and Technology, Trondheim and Norwegian Centre of Excellence: International Centre for Geohazards, 2007.

[30] Duncan JM. State of the art: limit equilibrium and finite element analysis of slopes. J of Geotechnical and Geoenvironmental Engineering (ASCE) 1996; 122(7):577–596.

[31] Griffiths DV, Lane PA. Slope stability analysis by finite elements. Géotechnique, 1999; 49(3): 387–403.

[32] Dawson EM, Roth WH, Drescher A. Slope stability analysis by strength reduction. Géotechnique 1999; 49(6):835 – 840.

[33] Swan CC, Seo YK. Limit state analysis of earthen slopes using dual continuum/fem approaches. Int J Numer Anal Meth Geomech, vol. 23; 1999. p.1359–1371.

[34] Zheng H, Liu DF, Li CG. Slope stability analysis based on elasto-plastic finite element method. Int J Numer Meth Eng 2005; 64(14):1871–88.

[35] Cheng YM, Lansivaara T, Wei WB. Two-dimensional slope stability analysis by limit equilibrium and strength reduction methods. Comput Geotech 2007; 34(3):137–50.

[36] Liu SY, Shao LT, Li HJ. Slope stability analysis using the limit equilibrium method and two finite element methods. Computers and Geotechnics, vol. 63; 2015. p. 291–298.

[37] Puzrin AM, Germanovich LN. The Growth of Shear Bands in the Catastrophic Failure of Soils. Proc R Soc A, 2005; 461(2056):1199–1228.

[38] Kvalstad TJ, Nadim F, Kaynia AM, Mokkelbost KH, Bryn P. Soil conditions and slope stability in the Ormen Lange area. Marine and Petrol Geology 2005; 22(1-2):299–310.

[39] Gauer P, Kvalstad TJ, Forsberg CF, Bryn P, Berg K. The last phase of the Storegga Slide: simulation of retrogressive slide dynamics and comparison with slide-scar morphology. Marine and Petroleum Geology 2005; 22(1-2): 171–178.

[40] Jostad HP, Andresen L. Modeling of shear band propagation in clays using interface elements with finite thickness. In Proc. of the 9th International Symposium on 'Numerical Models in Geomechanics - Numog IX', Ottawa, Canada, 2004.

[41] Mohammadi S, Taiebat HA. A large deformation analysis for the assessment of failure induced deformations of slopes in strain softening materials. Computer and Geotechnics, vol. 49; 2013. p. 279– 288.

[42] Mohammadi S, Taiebat HA. H-adaptive updated Lagrangian approach for large-deformation analysis of slope failure. Int J Geomech (ASCE), 2014. p. 1943–5622.

[43] Bian HB, Zheng LF, Shao JF. A numerical model for the long-term stability of jointed rock slope. Com Meth Recent Adv in Geomechanics-Oka, Murakami, 2015. p. 249–254.

[44] de Borst R. Simulation of strain localization: A reappraisal of the Cosserat continuum. Engineering Computations, vol. 8; 1991. p. 317–332.

[45] de Borst R, Sluys L, Mulhaus H, Pamin J. Fundamental issues in finite element analyses of localization of deformation. Engineering Computations, vol. 10; 1993. p. 99–121.

[46] Aifantis EC. On the microstructural origin of certain inelastic models. J Eng Mater

Technol (Trans ASME), vol. 106; 1984. p. 326–330.

[47] Vardoulakis I, Aifantis EC. Gradient-Dependent dilatancy and its implications in shear banding and liquefaction. Ingenieur—Archive 59; 1989. p. 197–208.

[48] Pijaudier-Cabot G, Bažnt ZP. Nonlocal damage theory. J Eng Mech (ASCE), vol. 113; 1987. p. 1512–1533.

[49] Troncone A. Numerical analysis of a landslide in soils with strain-softening behaviour. Géotechnique 2005; 55(8): 585–596.

[50] Vardoulakis I, Sulem J. Bifurcation Analysis in Geomechanics. Second-grade plasticity theory for geoaterials, ed. Blackie Academic & Professional, 1995. p. 382–425.

[51] Gylland AS, Nordal S, Jostad HP, Mehli M. Pragmatic approach for estimation of slope capacity in soft sensitive clay, Electronic J Geotech Eng, vol. 16F; 2011. p. 575–590.

[52] Duncan, JM, Wright, SG, Brandon, TL. Soil Strength and Slope Stability. 2nd edition, John Wiley & Sons, Inc. 2014.

[53] Tavenas F, Flon P, Leroueil S, Lebuis J. Remolding energy and risk of slide retrogression in sensitive clays. In Proc of the Symposium on Slopes on Soft Clays, Linköping, Sweden, 1983. SGI Report No. 17, p. 423–454.

[54] Bjerrum L, Landva A. Direct simple-shear tests on a Norwegian quick clay. Géotechnique, 1966; 16(1): 1–20.

[55] Lo KY, Lee CF. Stress analysis and slope stability in strain-softening soils. Géotechnique 1973; 23(1):1–11.

[56] Einav I, Randolph MF. Combining upper bound and strain path methods for evaluating penetration resistance. Int J Num Methods Engineering, 2005; 63(14): 1991–2016.

[57] Dey R, Hawlader B, Phillips R Soga K. Modeling of large deformation behaviour of marine sensitive clays and its application to submarine slope stability analysis. (2015 - in preparation).

[58] Stark T, Contreras IA. Constant volume ring shear apparatus. Geotechnical Testing Journal, 1996; 19(1): 3–11.

[59] Kulhawy FH, Mayne PW. Manual on estimating soil properties for foundation design. Research Project 1493-6, Cornell University, New York, 1990.

[60] Leroueil S. Natural slopes and cuts: movement and failure mechanisms. Géotechnique, 2001; 51(3): 197–243.

[61] Anastasopoulos I, Gazetas G, Bransby MF, Davies MCR, Nahas AEl. Fault rupture propagation through sand: finite-element analysis and validation through centrifuge experiments. J of the Geotech and Geoenviron Eng, ASCE, 2007; 133(8): 943–958.

[62] Pietruszczak St, Mróz Z. Finite element analysis of deformation of strain-softening materials. Int Journal for Numerical Methods in Engineering, 1981; 17:327–334.

[63] Moore ID, Rowe RK. Scaling rule for localized plasticity in strain-softening continua. Proc of 1st Int Conf on Computer Aided Assessment of Localized Damage, Portsmouth, vol. 2; 1990. p. 99–112.

[64] Dey R, Hawlader B, Phillips R, Soga K. Progressive failure of slopes with sensitive clay layers. In Proc of the 18th Int Conf on Soil Mech and Geotech Eng, Paris, 2013.

[65] Duncan JM, Chang CY. Non linear analysis of stress and strain in soils. J Soil Mech Found Div (ASCE) 1970; 96(5): 1629–1653.

[66] Chowdhury R, Flentje P, Bhattacharya G. Geotechnical Slope Analysis. CRC Press,

Taylor & Francis Group, 2010.

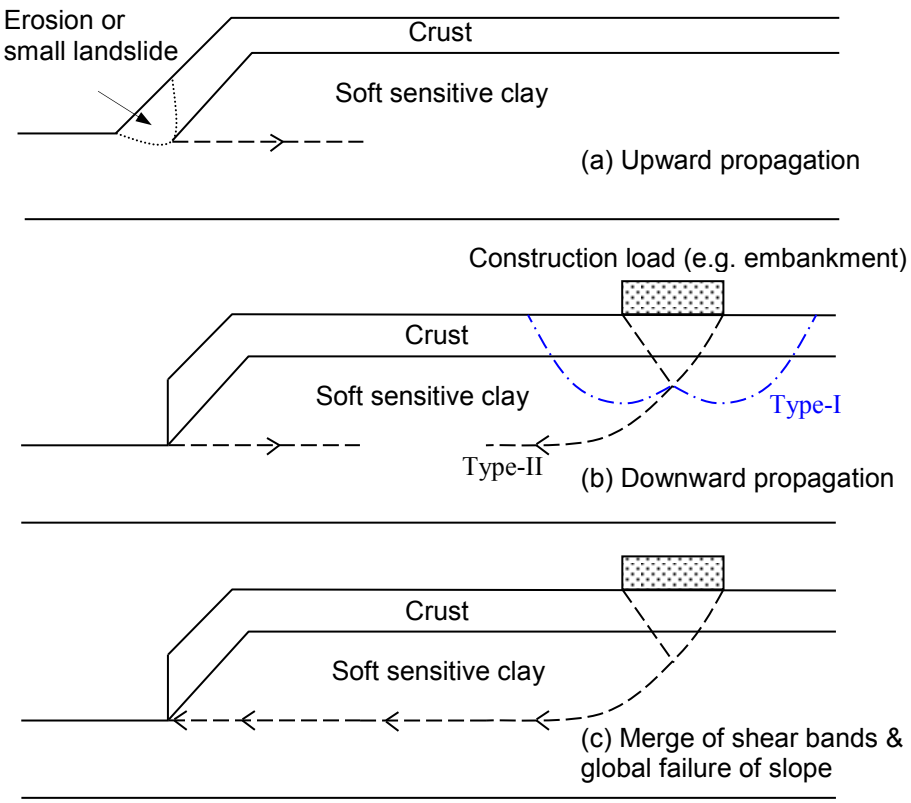

Figure 5. 1: Schematics of upward and downward propagation of shear bands

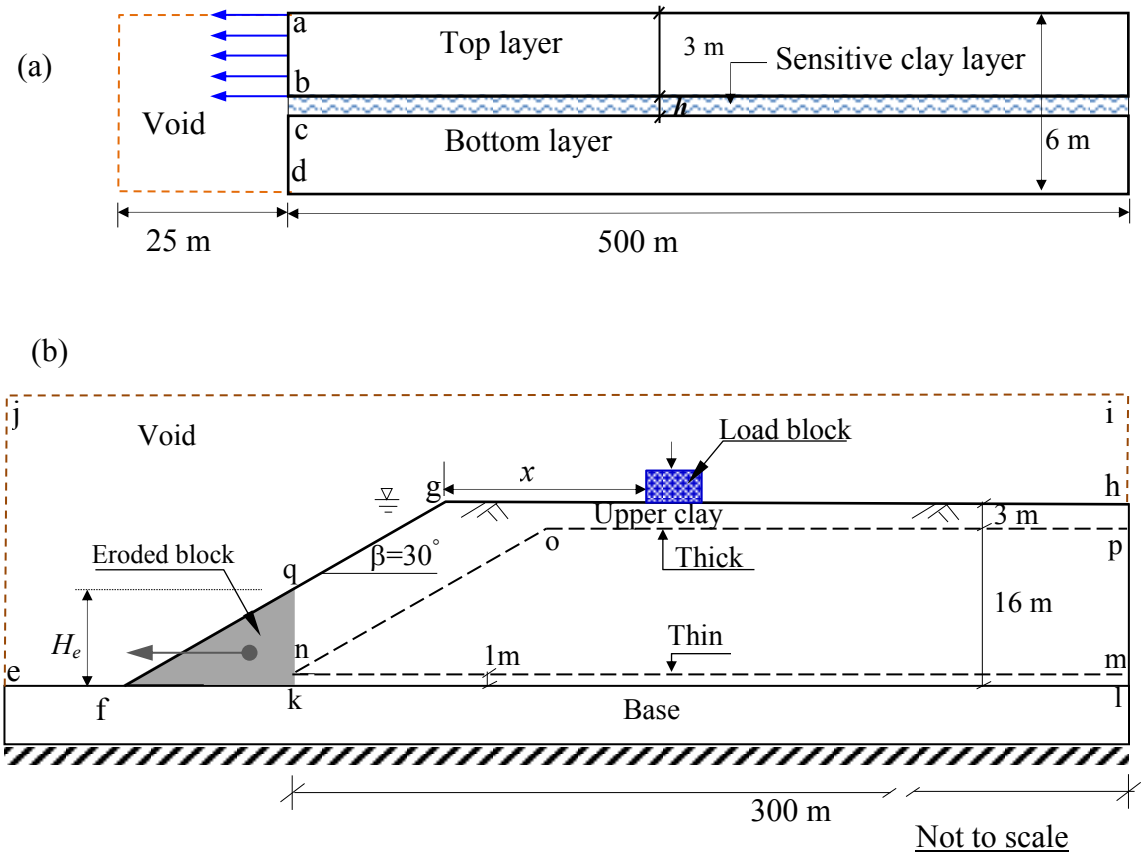

Figure 5. 2: Model geometry: (a) Large shear box (b) River bank

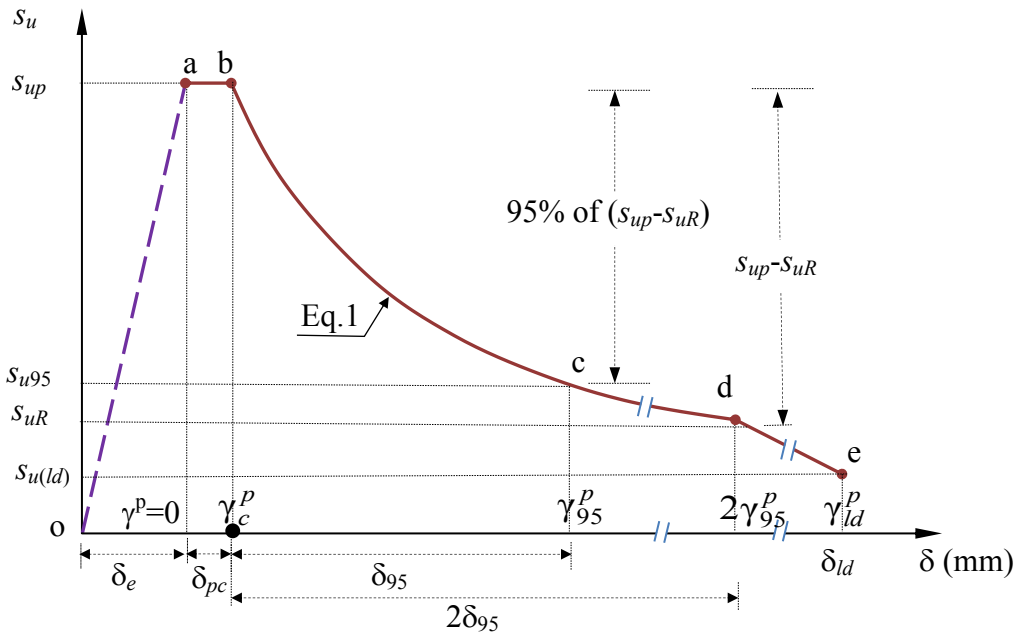

Figure 5. 3: Stress-strain behavior used in finite element modeling

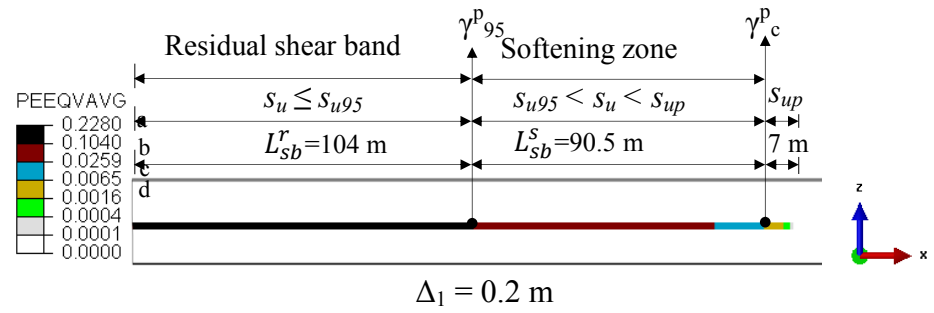
Residual shear band
γ^p_{95}
Softening zone
γ^p_c
PEEQVAVG
0.2280
0.1040
0.0259
0.0065
0.0016
0.0004
0.0001
0.0000
$s_u \leq s_{u95}$
$s_{u95} < s_u < s_{up}$
s_{up}
L^r_{sb}=104 m
L^s_{sb}=90.5 m
7 m
a
b
c
d
z
x

(a)

Δ_1 = 0.2 m

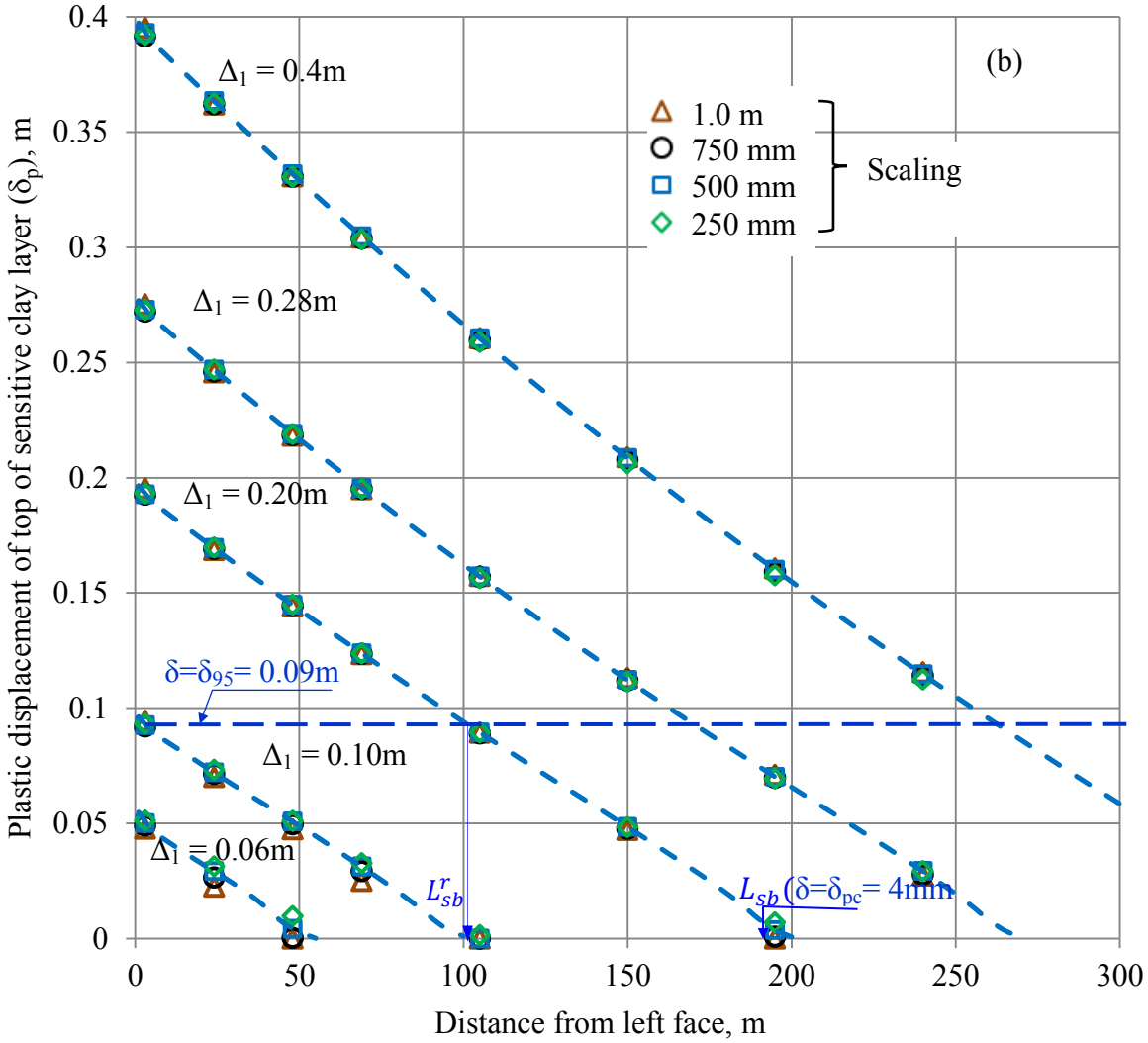
(b)
Δ_1 = 0.4m
Δ_1 = 0.28m
Δ_1 = 0.20m
Δ_1 = 0.10m
Δ_1 = 0.06m
1.0 m
750 mm
500 mm
250 mm
Scaling
$\delta=\delta_{95}$= 0.09m
L^r_{sb}
L_{sb} ($\delta=\delta_{pc}$= 4mm
Plastic displacement of top of sensitive clay layer (δ_p), m
Distance from left face, m
0
0.05
0.1
0.15
0.2
0.25
0.3
0.35
0.4
0
50
100
150
200
250
300

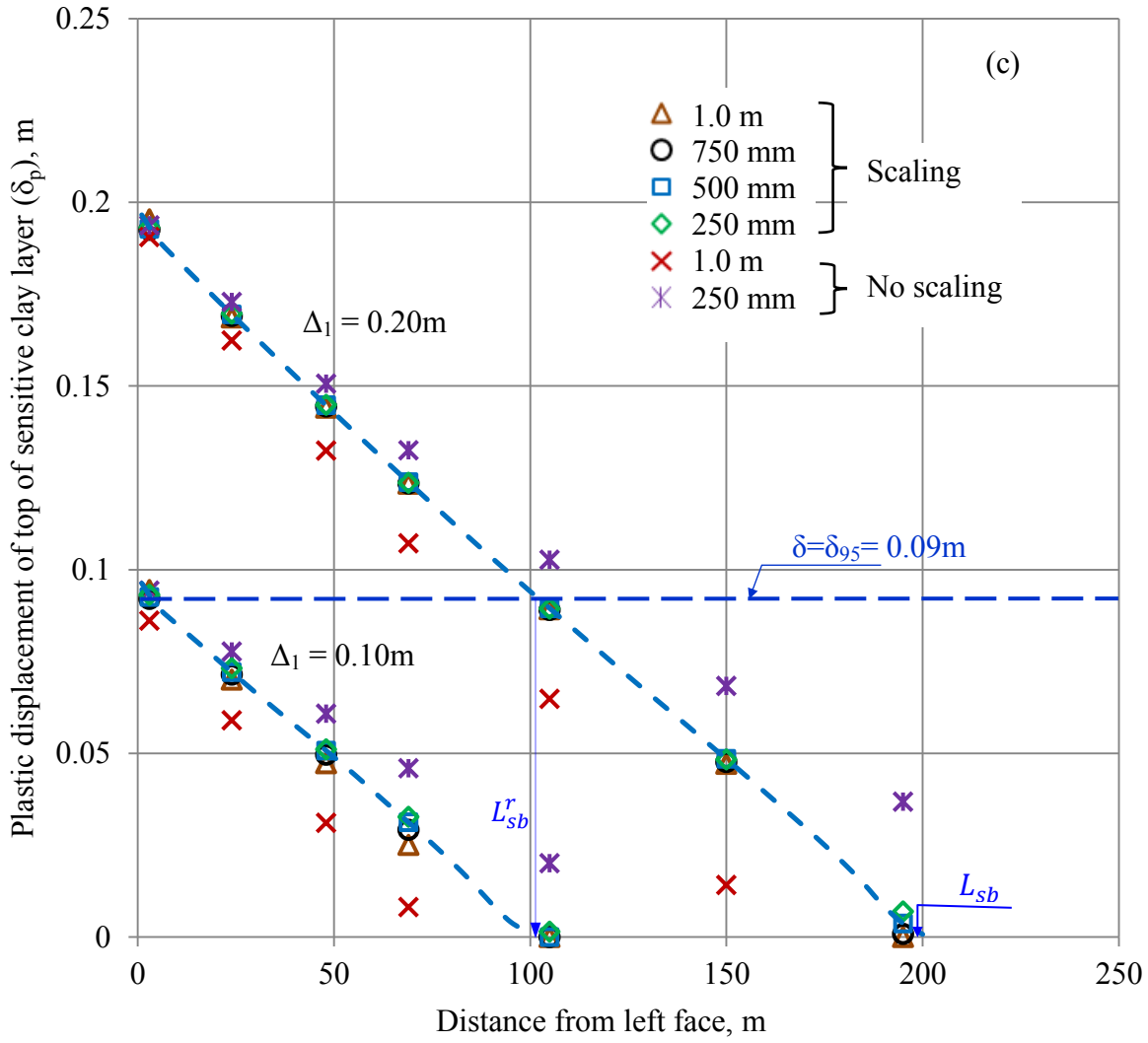

Figure 5. 4: Large shear box: (a) plastic strain at Δ_1=200 mm, (b) Plastic displacement of top of the sensitive clay layer, (c) effect of element size scaling

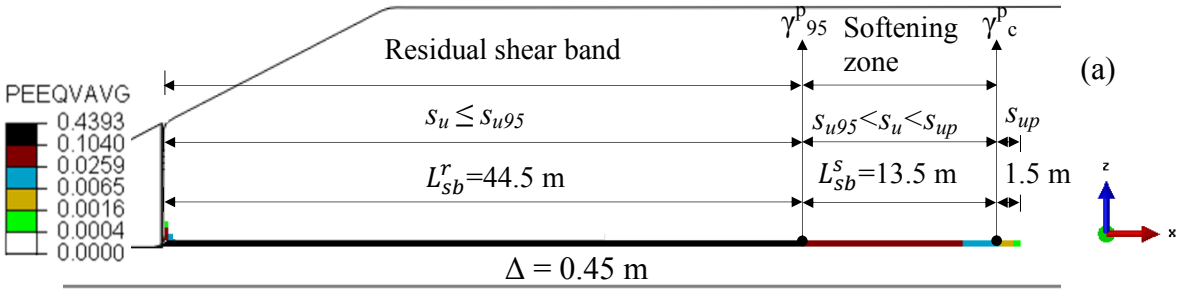
PEEQVAVG
0.4393
0.1040
0.0259
0.0065
0.0016
0.0004
0.0000
Residual shear band
γ^p_{95}
Softening zone
γ^p_c
(a)
$s_u \leq s_{u95}$
$s_{u95} < s_u < s_{up}$
s_{up}
L^r_{sb}=44.5 m
L^s_{sb}=13.5 m
1.5 m
Δ = 0.45 m

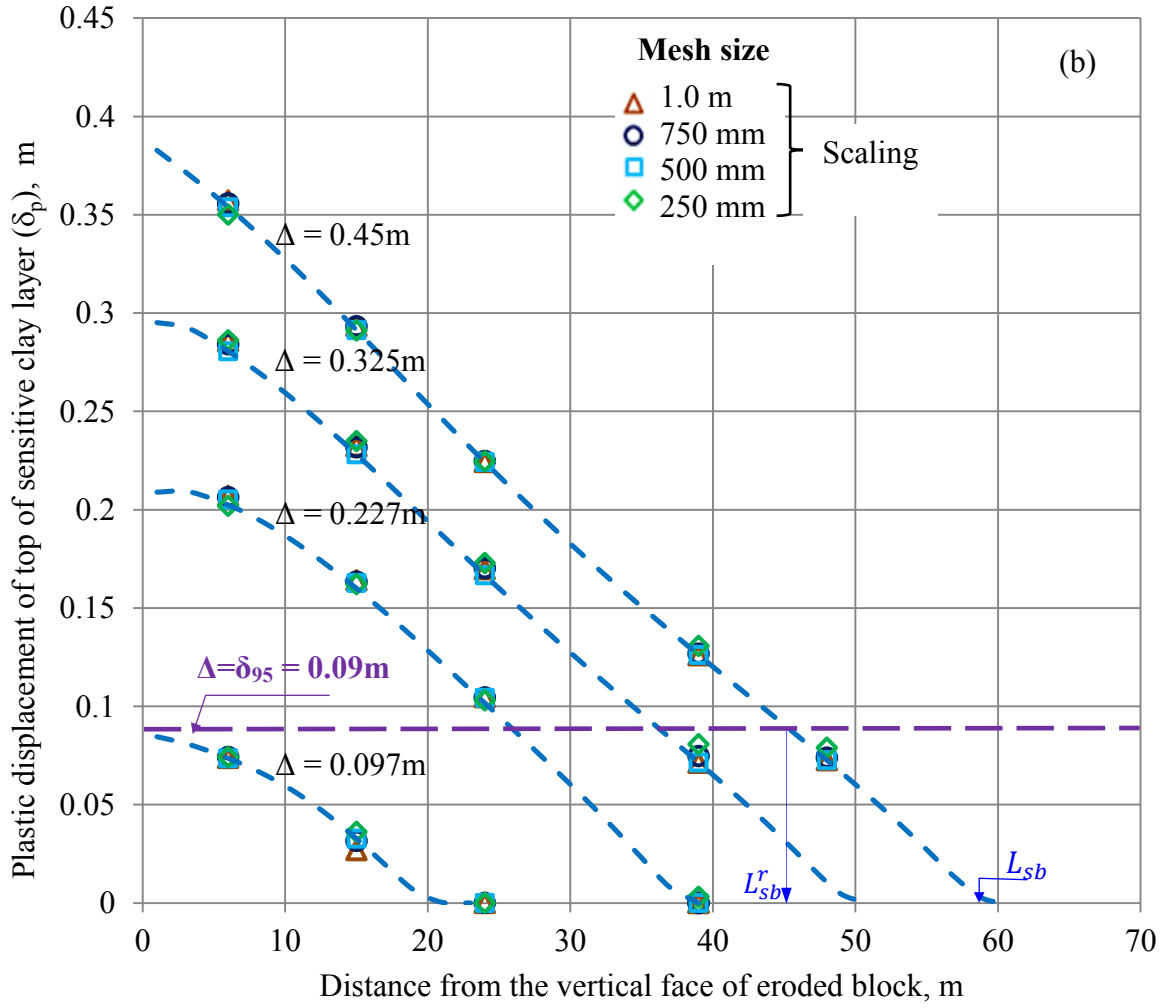
Mesh size
1.0 m
750 mm
500 mm
250 mm
Scaling
(b)
Δ = 0.45m
Δ = 0.325m
Δ = 0.227m
Δ=δ95 = 0.09m
Δ = 0.097m
L^r_{sb}
L_{sb}
Plastic displacement of top of sensitive clay layer (δp), m
Distance from the vertical face of eroded block, m
0
0.05
0.1
0.15
0.2
0.25
0.3
0.35
0.4
0.45
0
10
20
30
40
50
60
70

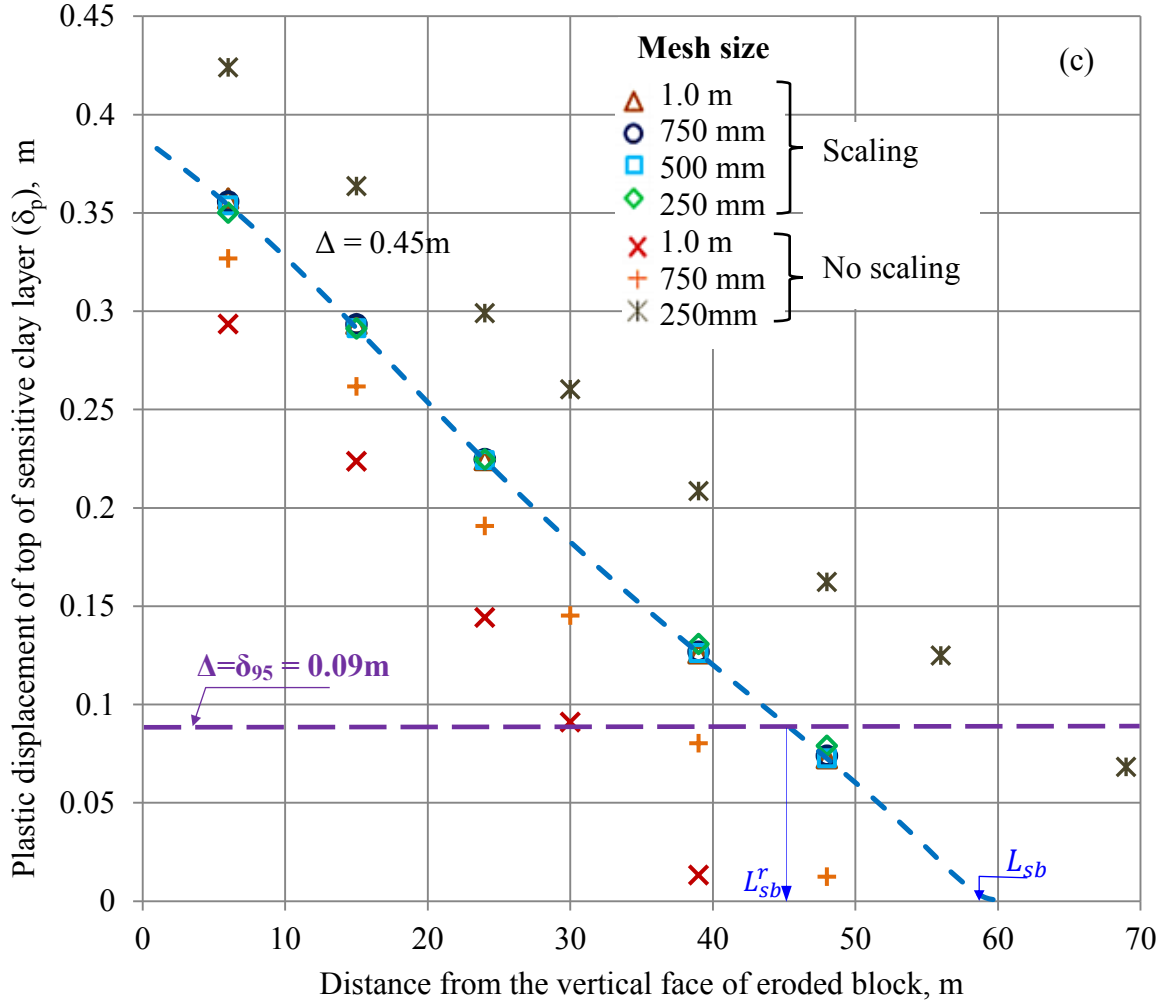

Figure 5. 5: Thin sensitive clay layer in river bank slope: (a) plastic strain at Δ=450 mm, (b) Plastic displacement of top of the sensitive clay layer, (c) effect of scaling

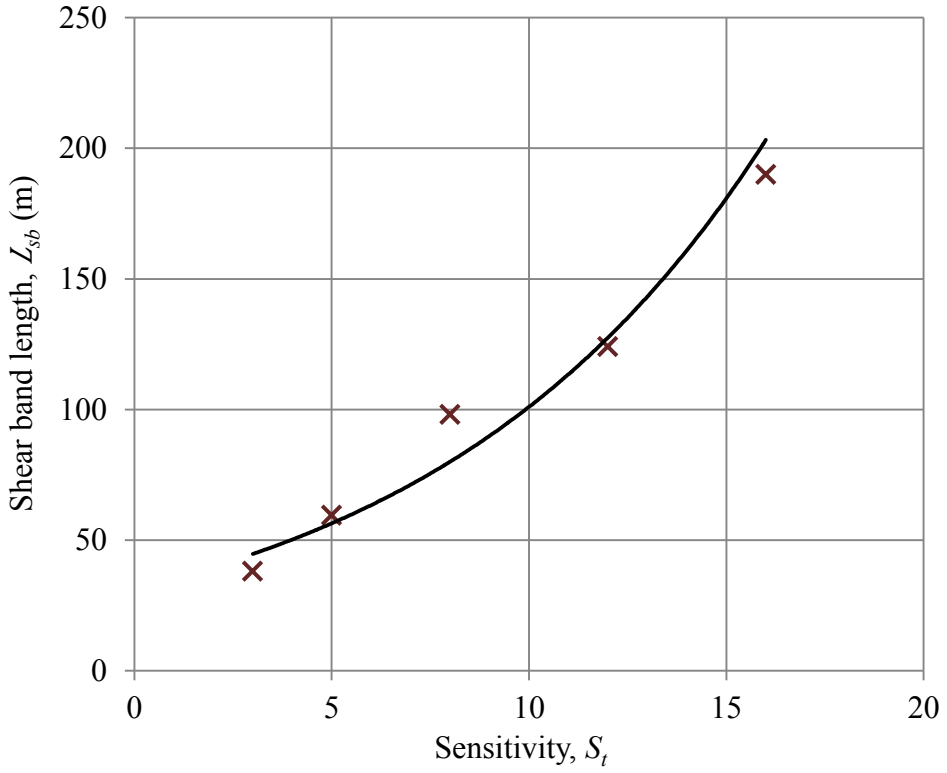
250
200
150
100
50
0
0
5
10
15
20
Shear band length, L_{sb} (m)
Sensitivity, S_t

(a)

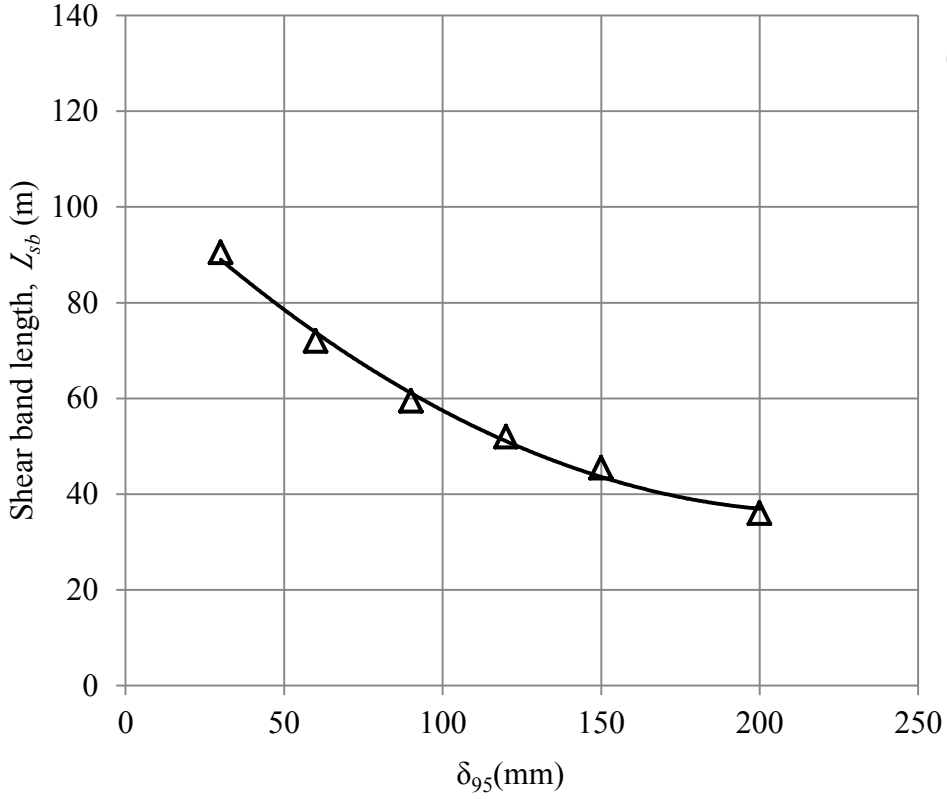
140
120
100
80
60
40
20
0
0
50
100
150
200
250
Shear band length, L_{sb} (m)
δ_{95}(mm)

(b)

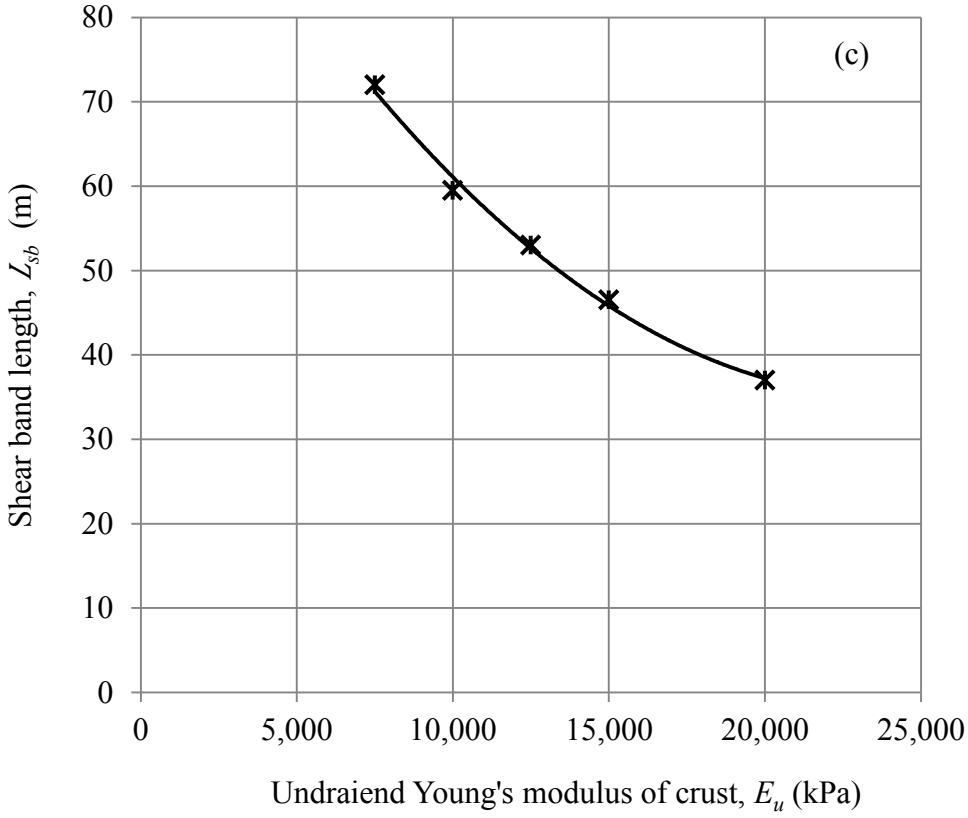

Figure 5. 6: Effects of soil parameters on shear band length with L_{sb}

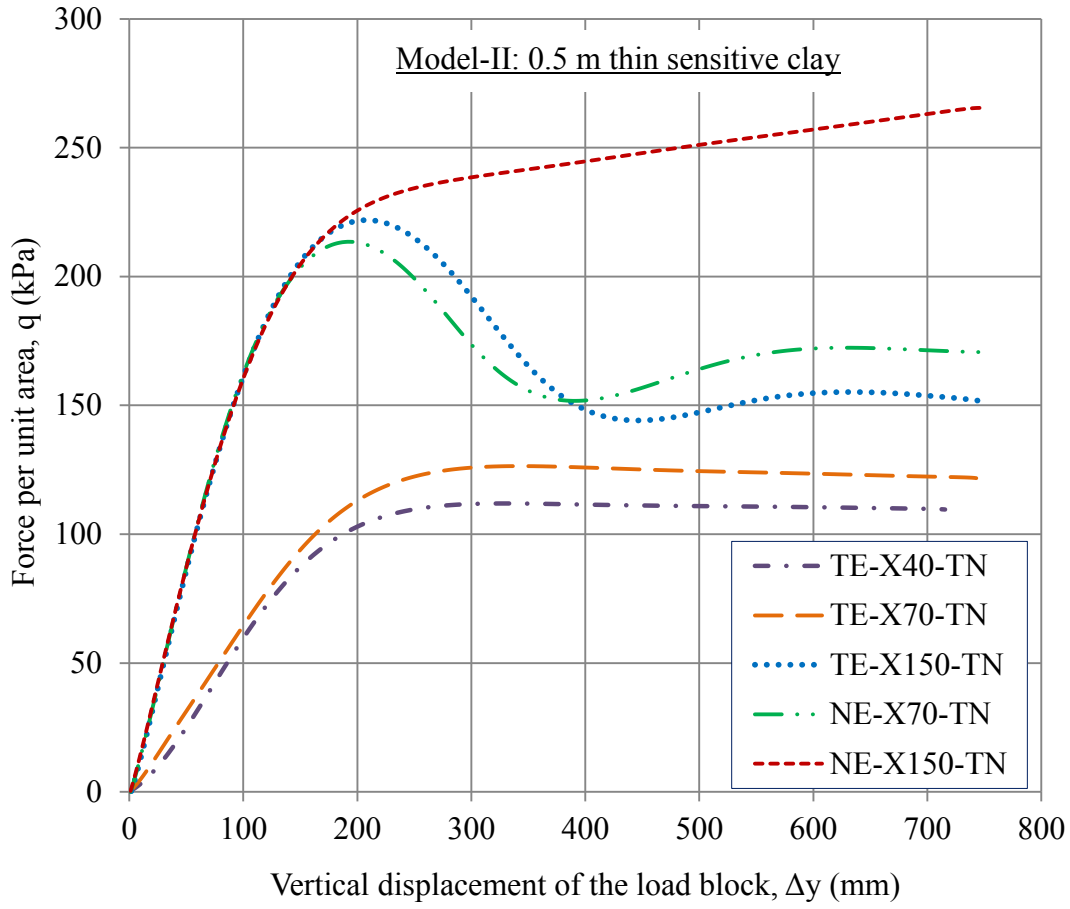

Figure 5. 7: Model-II: Vertical pressure under the load block

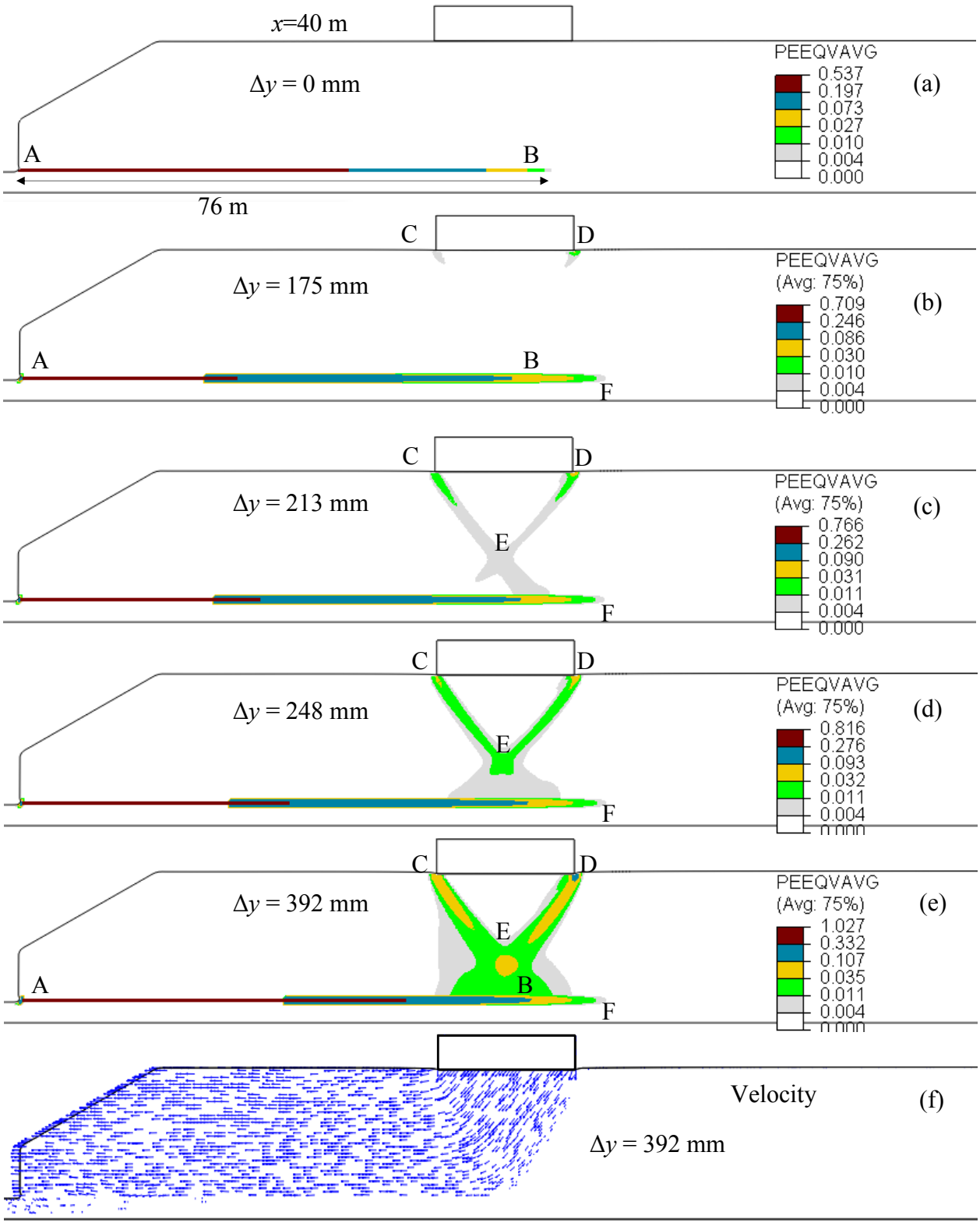

Figure 5. 8: Simulation TE-X40-TN: Shear band formation and instantaneous velocity of soil elements

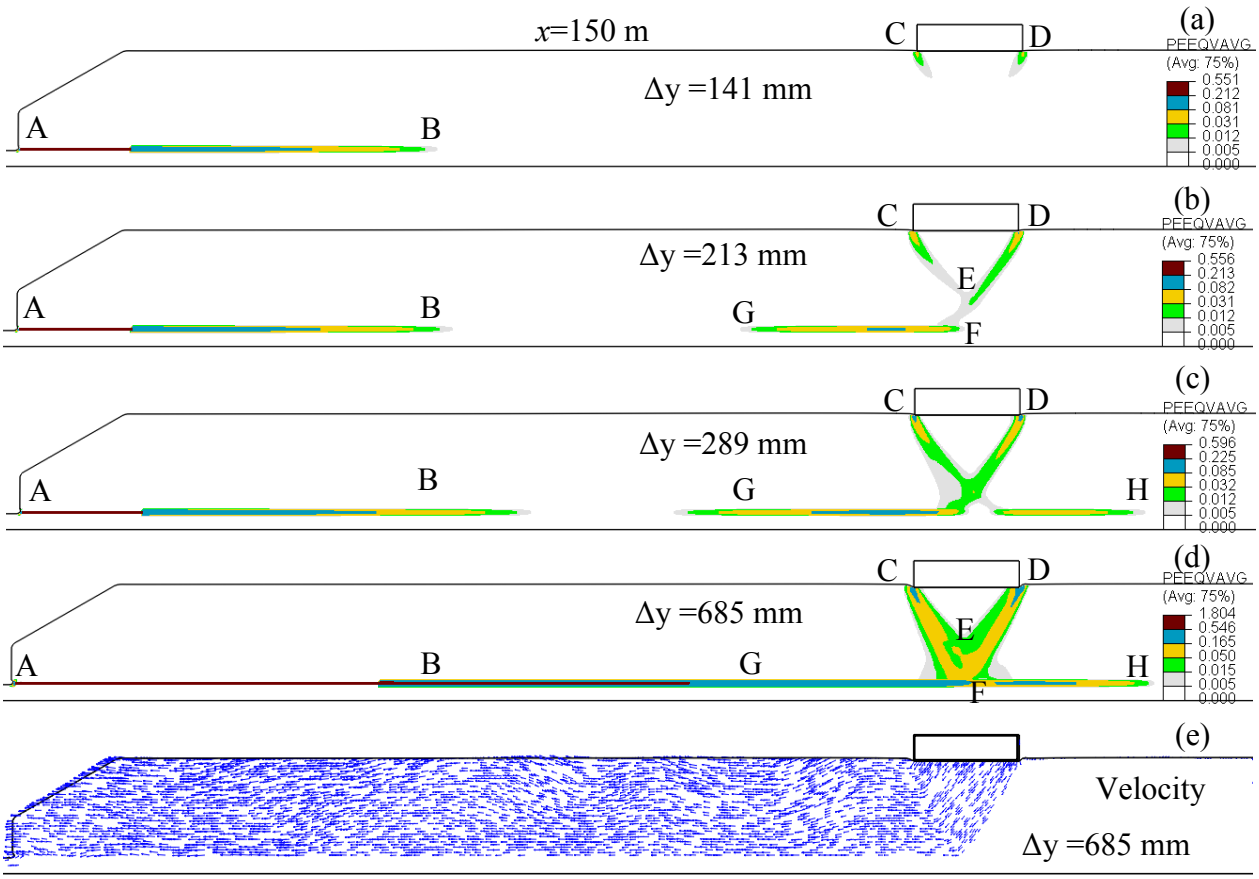

Figure 5. 9: Simulation TE-X150-TN: Shear band formation and instantaneous velocity of soil elements

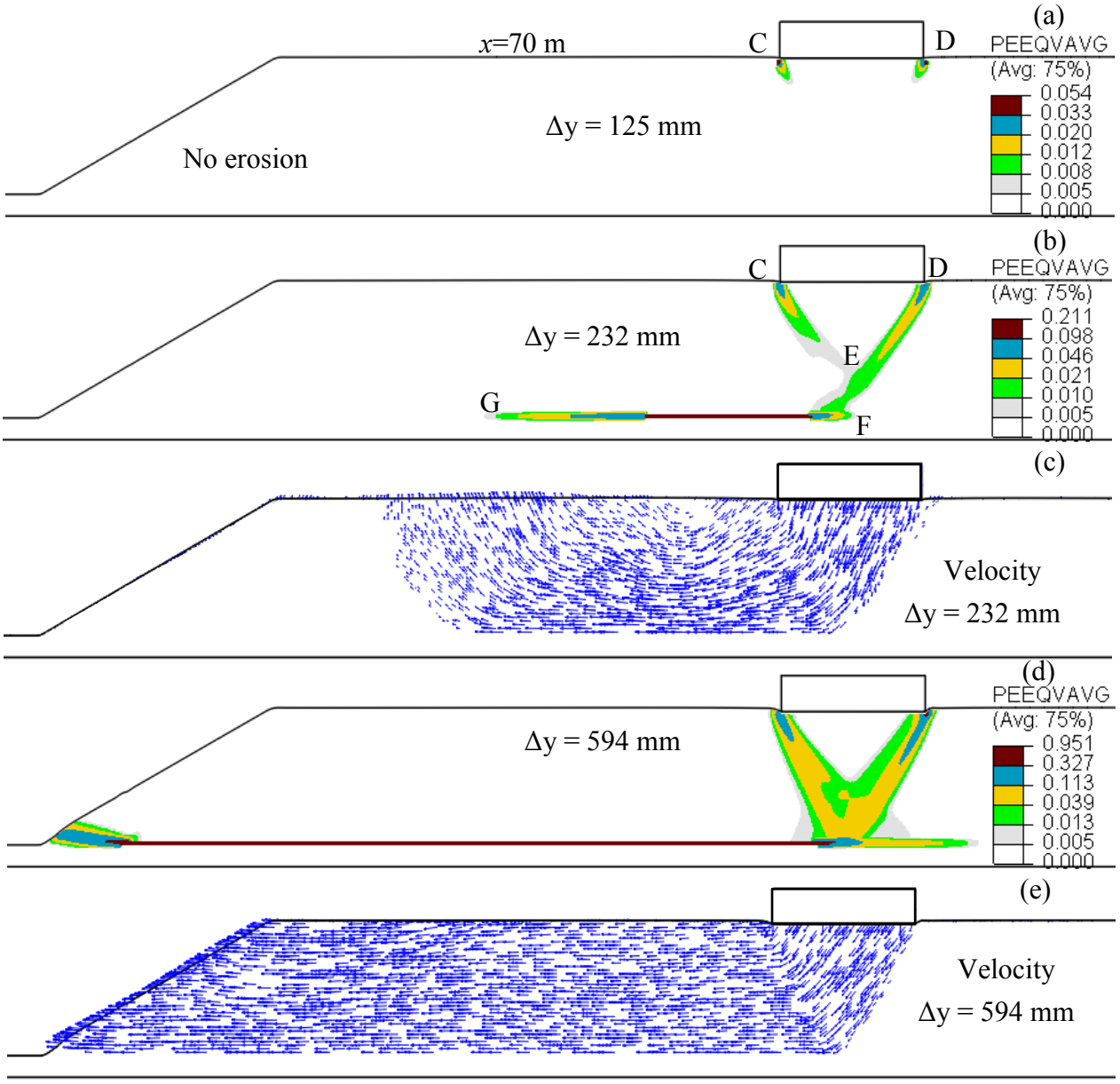

Figure 5. 10: Simulation NE-X70-TN: Shear band formation and instantaneous velocity of soil elements

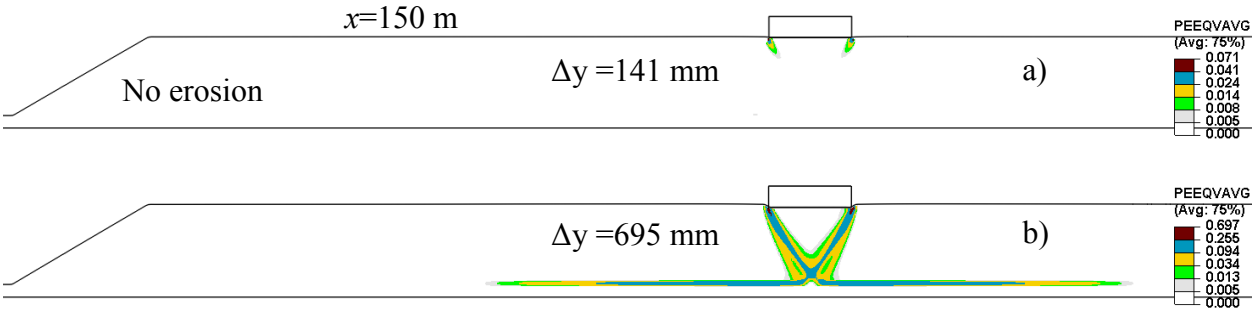

Figure 5. 11: Simulation NE-X150-TN: Shear band formation and instantaneous velocity of soil elements

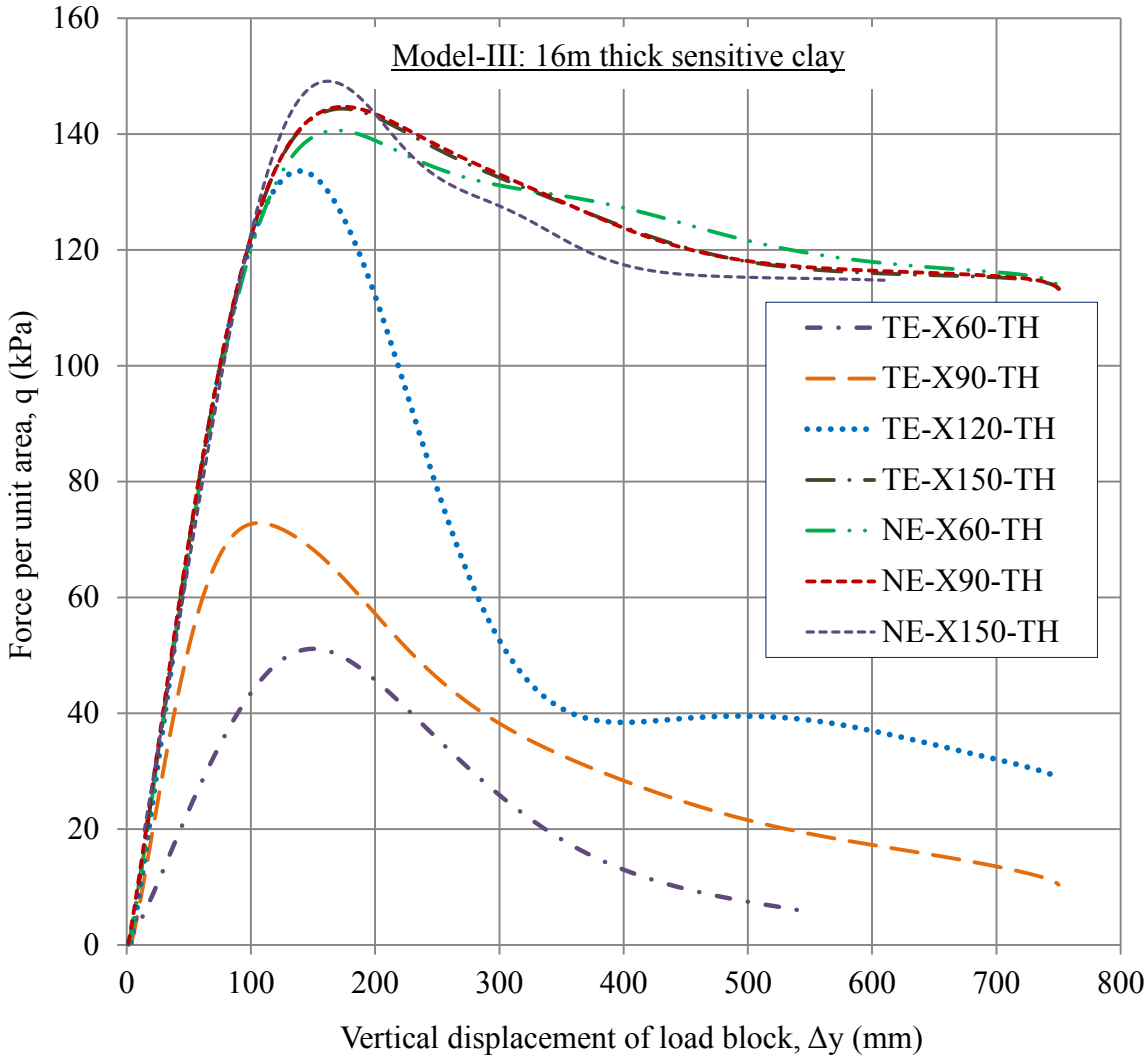

Figure 5. 12: Model-III: Vertical pressure under the load block

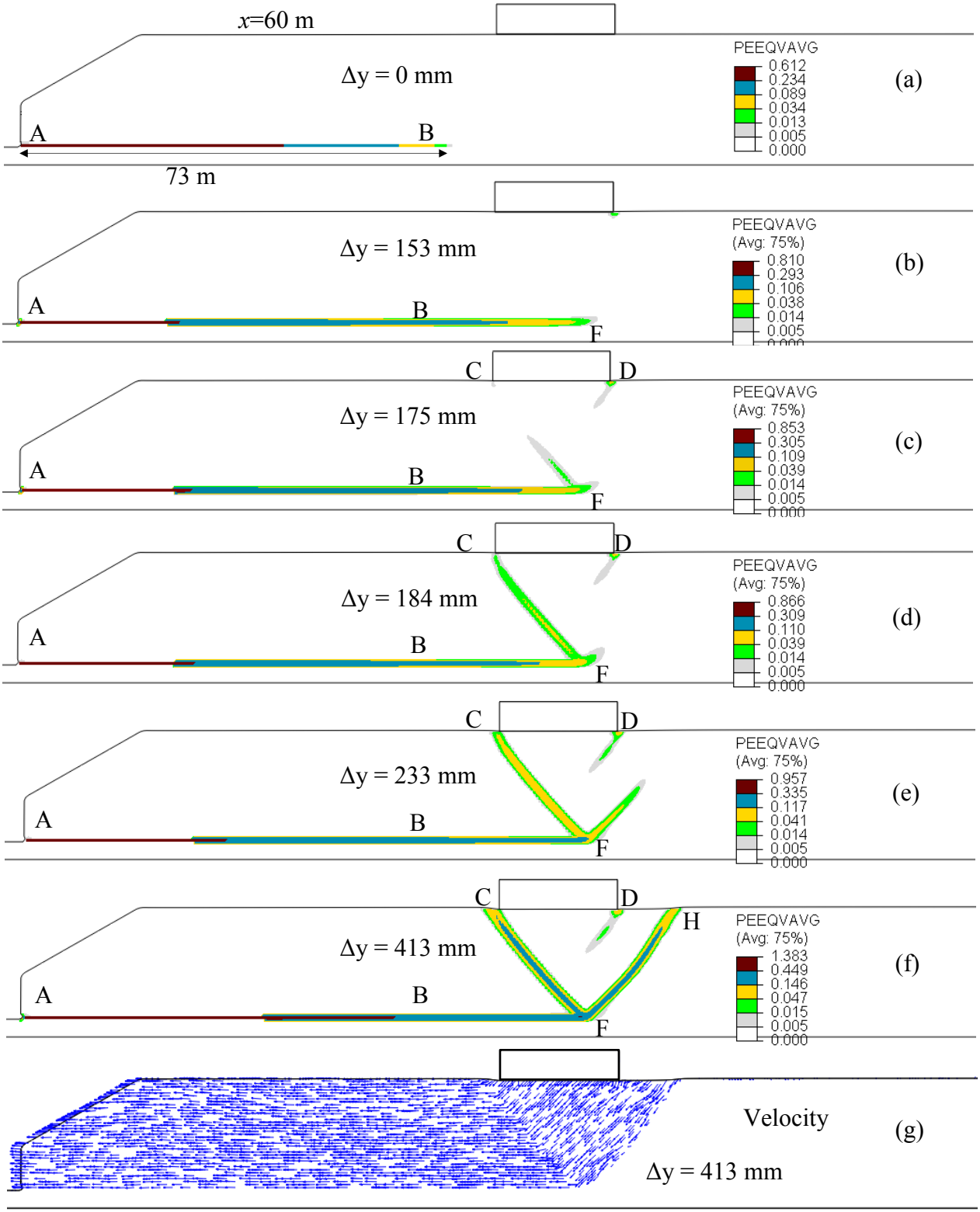

Figure 5. 13: Simulation TE-X60-TH: Shear band formation and instantaneous velocity of soil elements

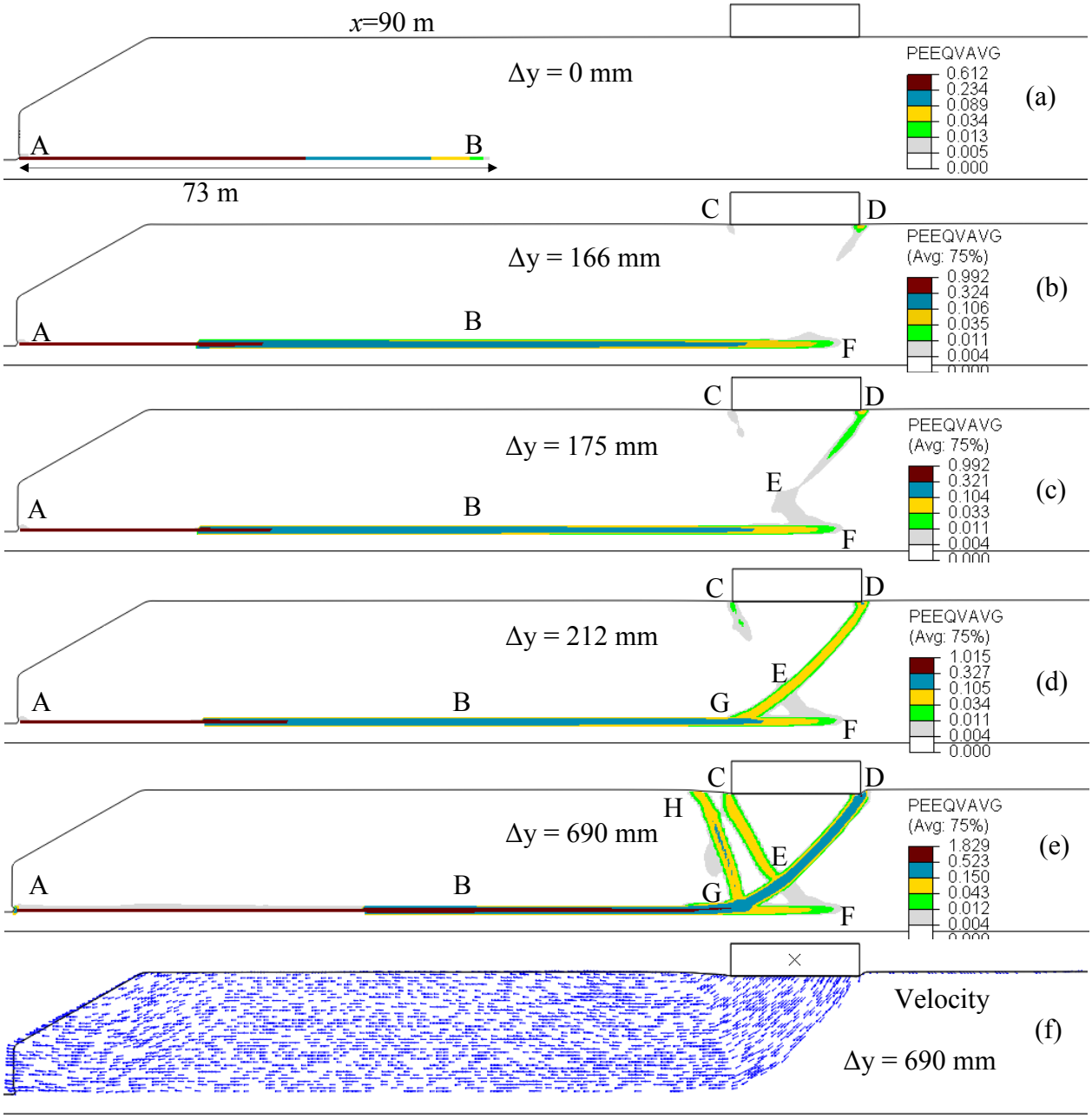

Figure 5. 14: Simulation TE-X90-TH: Shear band formation and instantaneous velocity of soil elements

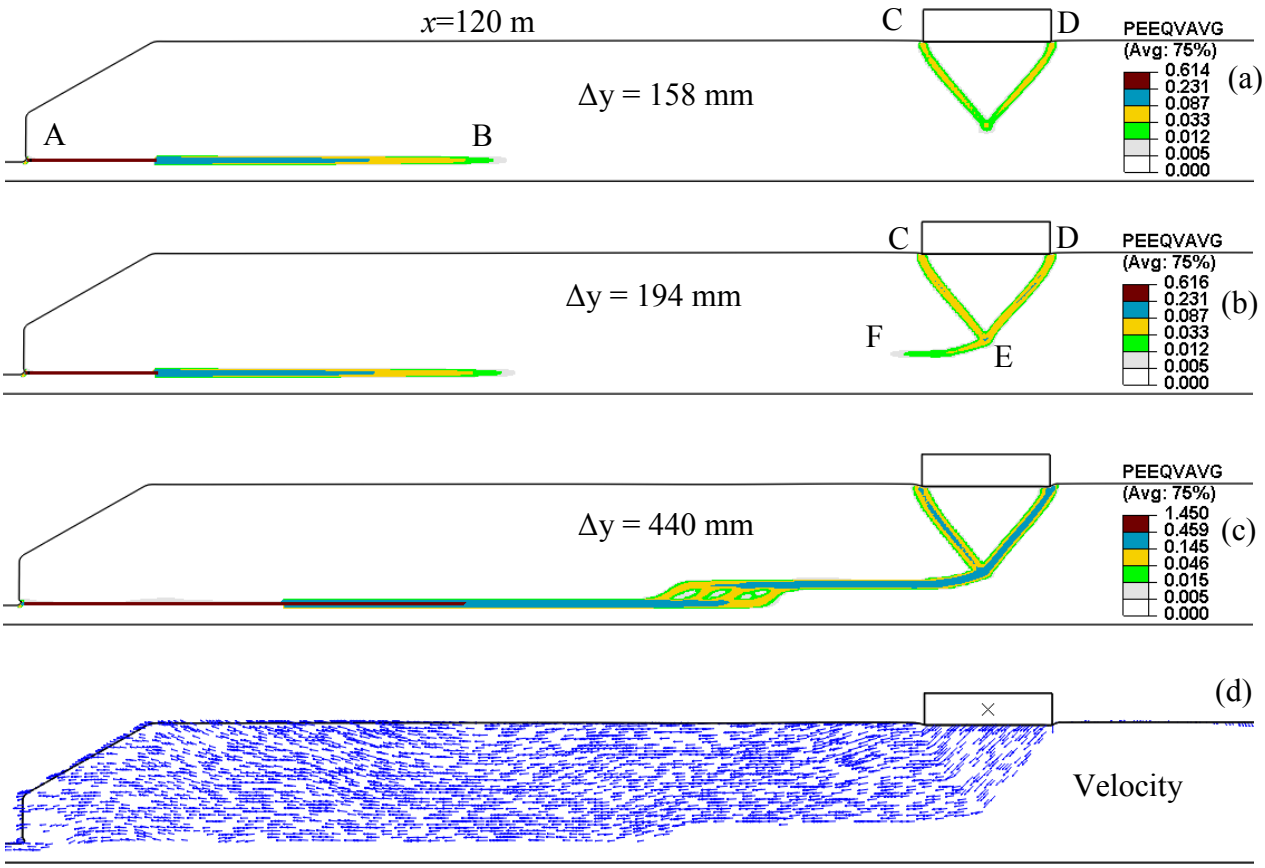

Figure 5. 15: Simulation TE-X120-TH: Shear band formation and instantaneous velocity of soil elements

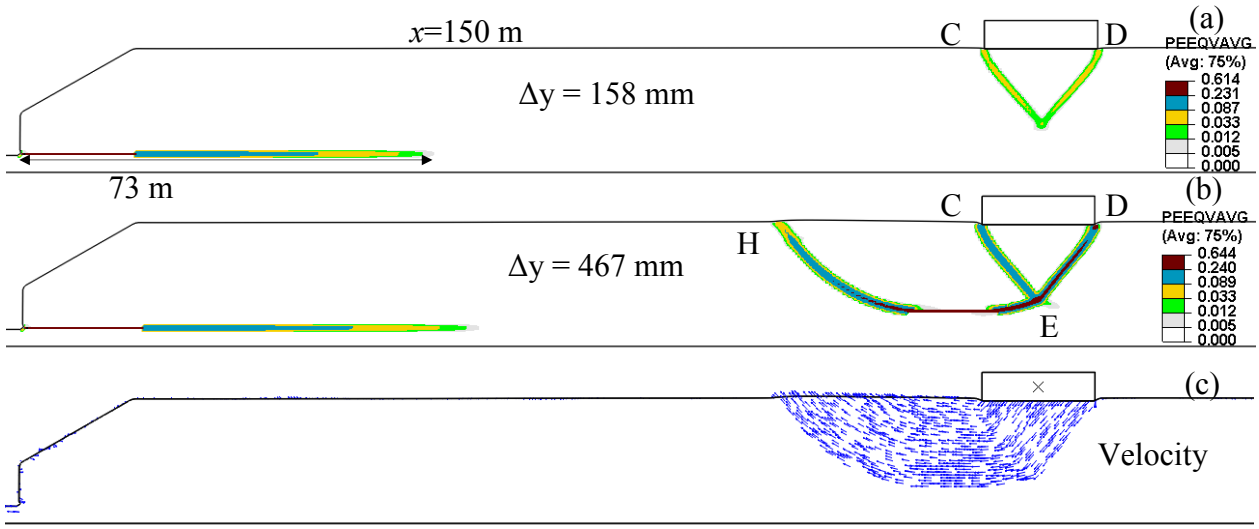

Figure 5. 16: Simulation TE-X150-TH: Shear band formation and instantaneous velocity of soil elements

Table 5. 1: Parameters used in "base case" finite element modeling

Crust (Elastic-perfectly plastic)	
Undrained modulus of elasticity, E_u (kPa)	10,000
Submerged unit weight of soil, γ' (kN/m^3)	9.0
Poisson's ratio, ν_u	0.495
Undrained shear strength, s_u (kPa)	60
Sensitive clay layer	
Undrained modulus of elasticity, E_u (kPa)	7,500
Poisson's ratio, ν_u	0.495
Peak undrained shear strength, s_{up} (kPa)	37.5
Undrained shear strength, s_{uR} (kPa)	7.5
Large displacement undrained shear strength, $s_{u(ld)}$ (kPa)	2.0
Rate of shear strength degradation, m	3.0
Submerged unit weight of soil, γ' (kN/m^3)	8.0
δ_{pc} (mm)	4
δ_{95} (mm)	30
δ_{ld} (mm)	2,000
Base	
Undrained modulus of elasticity, E_u (kPa)	100,000
Submerged unit weight of soil, γ' (kN/m^3)	11.0
Poisson's ratio, ν_u	0.495

CHAPTER 6

Numerical Modeling of Submarine Landslides with Sensitive Clay Layers

Co-Authorship: This chapter has been submitted as a technical paper for publication in a journal as: Dey, R., Hawlader, B., Phillips, R. and Soga, K. (2015) "Numerical modeling of submarine landslides with sensitive clay layers".

Most of the research work presented in this chapter was conducted by the first author. He also prepared the draft manuscript. The other authors supervised the research and reviewed the manuscript.

6.1 Abstract:

Geohazards associated with submarine landslides are one of the most significant considerations in offshore oil and gas development on or near the foot of the continental slope. Offshore infrastructure such as pipelines might be located in such areas where small- to large-scale submarine landslides occurred in the past as inferred from geophysical and geotechnical data. Such failure mechanisms could be better understood from advanced numerical modeling. In the present study, a large deformation finite element (FE) modeling technique is presented to model submarine landslides. As the presence of a strain softening clay layer has been identified as one of the potential causes of many submarine landslides, a strain softening model for undrained shear strength of marine clay is incorporated in this FE modeling. The development of large plastic shear strain concentrated zones (shear bands) and their propagation with displacement of

soil mass are simulated. These numerical simulations show that the existence of a weak layer might result in the initiation and propagation of a shear band leading to large-scale landslides together with the formation of subsequent shear bands and failure planes within the failed soil mass. Such progressive development of failure planes cannot be simulated using the limit equilibrium method of slope stability analysis. Depending upon the geometry and soil properties, a number of failure patterns are identified which are comparable with morphologic features seen in field observations. Based on this type of FE analysis and compared with seabed morphology, the developed failure planes could be identified where the shear strengths are expected to be lower because of pre-shearing than the shear strengths of the soil outside these zones, which could be then implemented in the modeling of seabed for offshore development projects in the areas where failure occurred in the past.

Key words: large deformation; finite element modeling; submarine landslides; sensitive clay; shear band.

6.2 Introduction

Numerous submarine landslides have been reported in the literature from various parts of the world. Submarine landslides occur in different seabed settings and are often considered one of the major offshore geohazards to offshore developments on or near the continental slope. With increasing offshore developments for oil and gas and technological advancement, the quality of mapping of the seabed surface has been improved significantly. A large number of such studies are available in the literature where high quality seafloor mapping have been presented (e.g. Hampton et al. 1996; Gardner et al. 1999; McAdoo 1999; Canals et al. 2004; Solheim et al.

2005; Gee et al. 2005; Greene et al. 2006; Micallef et al. 2007; Mountjoy et al. 2009; Locat et al. 2009; Twichell et al. 2009; Harders et al. 2011; Li et al. 2014). Most of these studies closely examined the morphology of the area for signs, e.g. features or scars that might have potentially developed from previous landslides, and potential models for some of these slides (e.g. Gee et al. 2005; Kvalstad et al. 2005a). Figure 6.1 shows some of the failure patterns compiled from different sources, which shows a wide range of failure surfaces in the failed soil mass. In the Storegga slide (Fig. 6.1a), retrogressive failure occurred along a basal failure plane with the formation of a series of grabens and ridges (Kvalstad et al. 2005). Figure 6.1(b) shows a complex slide feature in the Tuaheni South landslide in which the failure is assumed to have initiated locally and progressed towards head scarps together with compressional and extensional distortion and formation of shear surfaces in the sediment above the basal failure zone (Mountjoy et al. 2009). In the Tampen slide (Fig. 6.1c), a large sediment block slid over the glide plane through a fine grained marine sediment layer parallel to the slope together with a number of rotational slides near the headwall with formation of curved shear planes (Solheim et al. 2005). In the landslide off Angola (Fig. 6.1d), a tabular block slid over a weak basal shearing layer which then disintegrated into a number of smaller blocks (Gee et al. 2005). The Currituck slide shown in Fig. 6.1(e) is also assumed to be a retrogressive slide over a large basal glide plane with formation of steep and high head scarps (Locat et al. 2009). The common features of these slides are: (i) failure occurs along a basal plane, (ii) in many cases slides initiate locally and then retrogress further and (iii) different types of failure planes develop in the soil mass above the basal failure plane. While some conceptual models have been proposed in the past, very few numerical studies are available in the literature that explain the complete process of development of failure using the concept of soil mechanics.

Some of the previous studies used the limit equilibrium method to assess the stability of submarine slopes assuming an infinite slope (e.g. Karlsrud and Edgers 1982; Lee and Edwards 1986; Hampton et al. 1996; Leynaud et al. 2004; Kvalstad et al. 2005a; Brink et al. 2009). Computer programs, such as Slope/W, have been also used in some studies in order to accommodate complex geometry and soil properties (Almagor and Wiseman 1991; Mello and Pratson 1999; Dimakis et al. 2000; Leynaud et al. 2004; Kvalstad et al. 2005b). However, the limit equilibrium method cannot explain the mechanics for many submarine landslides. For example, one of the main causal factors of many offshore landslides is the existence of marine/glaciomarine sensitive clay layers of moderate sensitivity which have strain-softening behaviour (Dan et al. 2007; Sultan et al. 2010). Post-slide indicators (e.g. slide scars and debris formation) show that the failure pattern of some of these slopes is very similar to onshore large-scale landslides through marine sensitive clays as encountered in Eastern Canada and Scandinavia (e.g. Bryn et al. 2005; Gauer et al. 2005; Kvalstad et al. 2005a). Locat et al. (2014) discussed the formation and role of a weak layer on submarine landslides and highlighted that the strain softening behaviour of this weak layer could be the cause of many large-scale progressive failures in mild submarine slopes.

The Ormen Lange gas field project in offshore Norway developed analytical/numerical methods for progressive failure analysis of submarine slopes in order to assess the risks associated with these geohazards as such tools were not then available. Based on mesh distortion in FE analysis, Kvalstad et al. (2005a) showed a wedge type failure of the slope due to unloading that contains a sensitive clay layer. Instead of conducting FE simulations for retrogressive slide development, they proposed a simplified tri-block/wedge model for retrogressive spreading in which calculations have been performed using the energy principle (upper bound solution). Gauer et al.

(2005) used the concept of computational fluid dynamics and predicted retrogressive development of this slide.

In the recent years, further attempts have been taken to model progressive failure of slopes in onshore environments (e.g. Locat et al. 2011, 2013; Quinn et al. 2011). Using the concepts of linear elastic fracture mechanics (LEFM) (Palmer and Rice 1973), Quinn et al. (2011) proposed an analytical model for development of a shear band in an infinite slope with a vertical step cut. Quinn et al. (2012) conducted FE analysis to demonstrate the effects of toe erosion on propagation of a shear band through a weak predefined shear zone. Locat et al. (2011) demonstrate the mechanisms of shear band formation for an idealized condition in an infinite slope by applying an external force parallel to the ground surface near the toe above a predefined shear zone. Locat et al. (2013) extended their work (Locat et al. 2011) through numerical modeling using PLAXIS 2D (PLAXIS 2011) and BIFURC (Jostad and Andresen 2002) FE programs. Authors of the present study discussed the advantages and limitations of these studies elsewhere (Dey et al. 2015a).

Kvalstad et al. (2005a) assumed that unloading occurs because of an initial instability at the lower end (e.g. at continental slope or steeper part of the slope), which causes progression of a shear band through the weak layer. While the weak layer could be several kilometers long, many studies reported that the failure initiates locally in a section of the weak zone and then propagates further because of strain softening behaviour of the weak layer. The shear strength of the section from where failure initiates might be decreased due to various reasons such as geological activities, pore pressure generation, earthquake and plastic shear deformation (Lastras et al. 2004; L'Heureux et al. 2012; Locat et al. 2014), which could create a "discontinuity." If the shear stress along the discontinuity is greater than the reduced shear strength, stress will be

transferred to the surrounding soil elements through which shear band propagation might occur if the soil has strain-softening behaviour.

Puzrin and Germanovich (2005) showed that the existence of a weak layer might result in propagation of a shear band leading to failure of the slope. They also developed an analytical model that can be used to calculate the length of the weak zone required for initiation of shear band propagation through a strain softening weak layer in an infinite slope leading to global failure. The authors of the present study extended this work implementing nonlinear softening behaviour of sensitive clays (Dey et al. 2015b). However, these analytical solutions cannot be used for retrogressive failure or any geometry other than an infinite slope, and therefore numerical modeling is warranted. FE modeling of this type of problem is challenging because: (i) very large plastic strains/displacements occur in the shear band, (ii) the location of the shear band is not known permitting interface elements to pre-defined, and (iii) appropriate post-peak softening model need to be implemented, which is not available in the commercially available software packages. The large deformation FE modeling technique presented in this study for simulation of submarine slope addresses these issues. The FE simulations are performed for a number of possible cases where the failed soil mass displaces over large distance. The failure patterns obtained from the present FE analysis are compared with field observations.

6.3 Problem Definition

Two model geometries are considered in this study as shown in Fig. 6.2. Models-I and -II are without and with a steeper slope, respectively (Fig. 6.2). As the seabed slope is very mild, the slope geometry is presented with an exaggerated vertical scale for clarity. Figure 6.2(a) shows an

infinite offshore slope inclined at an angle β=4°. The upper soil layer (19 m) represents a relatively strong soil such as glacial clay. A 1 m thick marine clay layer of moderate sensitivity is assumed at 19 m depth. Although multiple layers of marine clay might be encountered in the field, only one layer is considered in this study. A strong base layer is assumed below the marine clay layer. A 1.2 km long slope is modeled. In the upper and lower ends a 100 m strong soil layer without any sensitive clay layer is assumed, which in the field might represent an overconsolidated glacial clay. A discontinuity of length l_d is placed at the middle of the sensitive clay layer.

The geometry of the second model (Fig. 6.2b) is similar to the first model (Fig. 6.2a) except for the existence of a 15° slope in the lower end and a strong soil layer only in the upslope area. Analyses are performed by placing a discontinuity of length l_d at different locations in the sensitive clay layer. The position of the discontinuity is indicated by the distance between the crest g and left end of the discontinuity, denoted as x_d.

Laboratory tests show that offshore glacial clay might be also slightly sensitive (Kvalstad et al. 2005a, 2005b; Yang et al. 2006). Therefore, analyses are also performed using slight sensitivity of the upper glacial clay layer. The effects of the thickness of marine clay layer are also examined.

6.4 Finite Element Modeling

Most of the FE models available in the literature for slope stability analysis are developed in the Lagrangian framework. One of the main disadvantages of this type of FE models is that significant mesh distortion occurs around the failure planes and the solutions generally suffer

from mesh dependency, numerical instabilities and lack of convergence. The non-convergence to a solution due to significant mesh distortion has been considered as one of the conditions of failure in some studies (e.g. Griffiths and Lane 1999). FE analysis becomes more complex if the soil has strain softening behaviour because large strain concentrations occur in narrow zones forming shear bands. Various attempts have been made in the past to model large strains in the shear band. The Norwegian Geotechnical Institute (NGI) (Jostad and Andresen 2002, 2004; Andresen and Jostad 2007; Gylland et al. 2010) modeled shear band propagation using interface elements of finite thickness along the potential failure plane. Mohammadi and Taiebat (2013, 2014) conducted FE analysis based on an adaptive mesh refinement algorithm using the updated Lagrangian formulation; however, it is applicable to limited deformation even though it performs better than the purely Lagrangian formulation. Thakur (2007) demonstrated the potential application of an extended finite element method to slope stability problems from some preliminary analysis. Nonconventional definitions of the continuum, such as the Cosserat model (de Borst 1991; de Borst et al. 1993), model based on gradient or nonlocal theories (Aifantis 1984; Pijaudier-Cabot and Bažnt 1987; Vardoulakis and Aifantis 1989; Vardoulakis and Sulem 1995; Troncone 2005; Conte et al. 2010), have also been used to simulate strain localization. A brief summary of advantages and limitations of these techniques for modeling strain localization are available in Gylland (2012).

In the present study, the CEL approach in Abaqus 6.10 EF1 is used in which the mesh is fixed and soil as Eulerian material flows through the fixed mesh. Therefore, numerical issues related to mesh distortion are not expected. Note that Abaqus CEL has been used in previous studies for other applications such as quasi-static penetration of the spudcan foundations and offshore pipelines (Qiu et al. 2011; Tho et al. 2012; Dutta et al. 2015). Its performance has also been

validated by comparing the results with the remeshing and interpolation technique with small strain (RITSS) for static and dynamic problems (Tian et al. 2011; Wang et al. 2013).

This CEL framework allows only three-dimensional modeling, and therefore the analyses are performed with only one element length in the out of plane direction. Analyses are performed with 1 m × 1 m uniform mesh due to the large size of FE model. All the simulations consist of a soil and a void space (efgh and efghij in Figs. 6.2a and 6.2b, respectively) to accommodate any displaced soil. The soil is modeled as an Eulerian material using EC3D8R 8-noded brick elements. Eulerian Volume Fraction (EVF) tool available in the Abaqus is used to create the soil and voids for initial condition.

Zero velocity boundary conditions are applied normal to the bottom and along all the vertical faces of the domain. No velocity boundary condition is applied at the soil-void interface, so that the soil can move into the void space when needed.

The numerical analyses contain the following loading steps. In the first step, geostatic load is applied to bring the soil into an in-situ stress condition. The slope is stable at the end of the geostatic step for the conditions analyzed here. In the second step, the discontinuity is created by reducing the undrained shear strength gradually in the sensitive clay layer. Previous studies (Puzrin and Germanovich 2005; Dey et al. 2015b) show that, when the length of the discontinuity is greater than a critical length (l^{cr}), the shear band propagates under the gravitational shear stress in the sensitive clay layer without any additional triggering factors. As the focus of the present study is to examine the potential mechanisms involved in the failure of submarine slopes, $l_d \geq l^{cr}$ is assigned in all simulations. The slope is stable if $l_d < l^{cr}$, which is not the focus of the present study. In the third step, the analysis is continued without changing any inputs. In this step, as the shear band propagation continues, the length of the shear band

increases. A new shear band forms and failure planes develop until it is stopped by the upper and lower strong soil layer in Model-I or by the user in Model-II.

6.5 Undrained Shear Strength Behaviour of Seabed Sediments

Two types of soil are considered in this study. The marine clay layer is sensitive, while the glacial clay may be insensitive or slightly sensitive (Kvalstad et al. 2005a, 2005b; Yang et al. 2006, 2007; Lunne and Andersen 2007). Laboratory tests on sensitive clays (e.g. Tavenas et al. 1983; Bjerrum and Landva 1966; Stark and Contreras 1996; Bernander 2000; Locat et al. 2015) show that the mobilized undrained shear strength (s_u) is a function of plastic shear displacement or strain. During shearing, more or less uniformly distributed shear strains develop throughout the whole depth of the soil specimen until the peak strength is mobilized (Anastasopoulos et al. 2007). However, the post-peak strains are localized in a shear band. The shear strain could be calculated if the thickness of the shear band is known; however, proper estimation of shear band thickness is very difficult. Therefore, similar to previous studies (Quinn et al. 2011, 2012), shear displacement is used to define the post-peak softening curve while shear strain is used in the pre-peak region.

Figure 6.3 shows the variation of undrained shear strength, s_u used in the present study. The linear elastic pre-peak (line *oa* in Fig. 6.3) behavior is defined by the elastic properties (E_u, and ν_u). The peak undrained shear strength (s_{up}) is mobilized at point *a* and remains constant up to point *b* for a displacement of δ_{pc} from point *a*. The remoulded undrained shear strength (s_{ur}) can be measured in the laboratory. However, post-slide investigations do not show any significant relevance of s_{ur} and therefore Bernander (2000) recommended an undrained shear strength s_{uR}

($>s_{ur}$) for progressive failure analysis that mobilizes in shear bands as a result of considerable shear displacement.

The shear strength degradation curve (*bcd*) is defined by the following exponential function.

$$s_u = \left[\frac{1}{S_t} + \left(1 - \frac{1}{S_t} \right) e^{-3\delta / \delta_{95}} \right] s_{up} \quad (1)$$

where s_u is the mobilized undrained shear strength; $\delta=\delta_t-(\delta_e+\delta_{pc})$ with δ_e and δ_t are the elastic and total shear displacements, respectively; δ_{95} is the value of δ at which the undrained shear strength is reduced by 95% of (s_{up}-s_{uR}) and sensitivity $S_t = s_{up}/s_{uR}$. Plastic shear deformation δ_p ($=\delta_t-\delta_e$) initiates from point *a* with s_u degradation past point *b*. The sensitivity S_t of marine clay and glacial clay are denoted as $S_{t(m)}$ and $S_{t(g)}$, respectively. Equation (1) is similar to the strength degradation equation proposed by Einav and Randolph (2005), but in terms of δ. In FE implementation, s_u up to $2\delta_{95}$ is defined by Eq. (1) and after that s_u remains constant (line *de*) which is denoted as $s_{u\infty}$. The difference between $s_{u\infty}$ and s_{uR} is very small. Equation (1) fits well the post-peak stress-displacement behaviour of sensitive clays reported from laboratory tests (Quinn 2009; Tavenas et al. 1983), which has been presented elsewhere (Dey et al. 2015b). Assuming simple shear condition, the plastic shear strain is calculated as $(\delta_t-\delta_e)/t_s$, where t_s is the thickness of the soil element. In FE analysis, the variation of von Mises yield strength ($=2s_u$) is defined as a function of plastic shear strain, which is calculated assuming $t_s=t_{FE}$, where t_{FE} is the thickness of the cubical EC3D8R element. The von Mises yield criterion is adopted.

When the glacial clay is considered to be slightly sensitive, a similar shape of stress-strain curve to that shown in Fig. 6.3 is used; meaning that Eq. (1) is used to define post-peak softening of glacial clay using the sensitivity $S_{t(g)}$. When insensitive, s_u remains constant at s_{up} without any post-peak degradation.

The geotechnical parameters used in this study are listed in Table 6.1. Most of these parameters are estimated from Kvalstad et al. (2005a, b) who reported a wide range of geotechnical properties of offshore sediments from an extensive site investigation program for the Ormen Lange gas development project. The marine clays have a high clay content (45–65%), plasticity index (PI>25%) and sensitivity (3–6) as compared to glacial clay having clay content of about 30–40%, PI of 12 to 25% and sensitivity (1.5–3.0). As E_u/s_{up} decreases with increasing PI (Duncan and Buchignani 1976), E_u/s_{up} of 600 and 375 are used for glacial and marine clay, respectively.

For marine clays, Kvalstad et al. (2005a, b) showed that s_{up} increases with vertical effective stress (σ'_v) as $s_{up} \approx 0.2\sigma'_v$ in direct simple shear (DSS) condition that represents better the basal failure through the sensitive clay layer shown in Fig. 6.2. Now, using γ' of the upper glacial clay layer, the value of σ'_v at the depth of sensitive clay layer can be calculated, which gives s_{up} of 40 kPa. Based on laboratory stress-strain behaviour (Bjerrum and Landva 1966; Stark and Contreras 1996; Bernander 2000; Thakur 2007), δ_{pc}=3 mm is selected for marine sensitive clay. Locat et al. (2013) assumed complete strength degradation at displacements between 62.5 and 260 mm. In the present study, it is assumed that 95% strength degradation occurs at δ_{95}=100 mm. A detailed discussion on estimation of δ_{95} from laboratory tests is provided in Dey et al. (2015b).

For the upper glacial clay, Gauer et al. (2005) assumed s_u=25 kPa at the seabed increasing linearly at 2.4 kPa per metre depth. An average value of s_{up} of 50 kPa is assumed in this study for the upper clay layer. Kvalstad et al. (2005b) also showed that post-peak degradation of s_u occurs in glacial clays at larger strains than in marine clays. Therefore, higher values of δ_{pc} and δ_{95} are

used for glacial clays. Moreover, relatively higher values of δ_{pc} are used for glacial clay of lower sensitivity. The base, upper and lower strong layers are modeled as elastic material.

6.6 Finite Element Results

Plastic shear strain concentration occurs in the shear band. In order to examine the development of strains in the shear band, the equivalent plastic strain (PEEQVAVG) is obtained from Abaqus, which represents the integration of plastic deviatoric strain rate tensor ($\dot{\epsilon}_{ij}^{p}$) over the period of analysis (i.e. $\int_0^t \sqrt{\frac{2}{3}\dot{\epsilon}_{ij}^{p}\dot{\epsilon}_{ji}^{p}}dt$). In other words, PEEQVAVG is a scalar variable to represent generalized plastic deformation. When PEEQVAVG is greater than zero, the stresses in that element reach the yield strength and plastic deformation occurs. When PEEQVAVG is zero, only undrained elastic deformation occurs. Note that, PEEQVAVG is related to plastic shear strain (γ^p) as $\gamma^p = \sqrt{3}$ PEEQVAVG. Assuming simple shear condition and the thickness of shear band equal the thickness of finite element t_{FE}, the plastic shear displacement can be calculated as $\delta_p=\gamma^p \times t_{FE}$. For the soil parameter used in Table 6.1 for marine clay and t_{FE}=1 m, $s_{u\infty}$ will be mobilized at $\delta_p=\delta_{pc}+2\delta_{95}$=203 mm (point d in Fig. 6.3), which gives γ^p=0.2 and PEEQVAVG=0.12. In other words, in the section of the shear band where PEEQVAVG≥0.12 the mobilized $s_u=s_{u\infty}$ while in other sections of the shear band $s_u > s_{u\infty}$. As the focus of the study is to show the failure pattern, the zones of PEEQVAVG≥0.12 are shown by only one color (dark blue) in the following sections.

<u>Model-I</u>

Figure 6.4 shows the progressive development of failure planes in Model-I. As $l_d \geq l^{cr}$ and τ_g is greater than the shear strength in the discontinuity ($s_{u\infty}$), shear band propagation continues under gravitational force. For example, the shear band length is 400 m at t=7.2 sec (Fig. 6.4a), while it propagates to form a 1000 m long shear band at step t=11 sec (Fig. 6.4b). Further discussion on failure planes is provided below.

Figure 6.5 shows the typical variation of horizontal stress, σ_{xx} in the upper soil layer for three time increments during the propagation of the shear band. Note that for small values of β (4° in this case), σ_{xx} is approximately equal to the normal stress parallel to the slope. The horizontal line at the middle represents σ_{xx} at the end of the gravitational step and before formation of the discontinuity, denoted as σ_{xx0}. With propagation of the shear band, σ_{xx} decreases to the right and increases to the left side. The blue and red vertical arrows show the end of the discontinuity and shear band, respectively. σ_{xx} varies almost linearly in the middle of the shear band. In the end zone, a transition occurs and σ_{xx} gradually approaches to σ_{xx0} with distance. The rate of change of σ_{xx} is higher for a shorter shear band. A similar pattern could be shown for other depths, and σ_{xx0} increases with depth.

In the formulation of an analytical model for shear band propagation, Puzrin et al. (2004) and Puzrin and Germanovich (2005) assumed an average normal stress in the upper soil layer acting parallel to the slopes ($\overline{\sigma}_p$) to calculate strain and then the shear deformation along the sliding plane. It was shown that $\overline{\sigma}_p$ increases and decreases linearly in the left and right sides respectively, with downward displacement of the upper soil layer above the shear band. From Figure 6.5, it can be concluded that the assumption of linear variation of stress parallel to the

slope used in the development of analytical models is reasonable until the first global failure occurs by formation of the two failure planes MN and PR through the upper soil layer (Fig. 6.4b). However, for progression of the failure, as discussed in the following sections, numerical analysis is required. The instantaneous velocity vectors at t=11s (Fig. 6.4c) show that, except for the soil elements near the ends, most of the soil elements move at a constant velocity.

Soil deformation continues even after the formation of MN and PR planes in Figure 6.4b. Using an analytical solution, this process cannot be modeled; that is, the analytical solutions (Puzrin et al. 2004; Dey et al. 2015b) are applicable only up to the first global failure. As shown in Figs. 6.4(d)–6.4(f), triangular shear surfaces progressively develop in the upper soil layer both in the right and left ends. Shear surfaces form at the end first and then propagate towards the middle. Passive failure occurs in the left end while active failure occurs to the right. As an undrained model (ϕ=0) is used, the failure planes looks similar at both ends.

Figures 6.4(d)–6.4(f) also show successive head scarps in the upslope and corresponding heave in the downslope areas with further displacements of the upper soil layer. The driving force gradually reduces due to the undercut of the upslope while the resistance increases due to heave downslope. This process continues until the development of a sufficient amount of downslope heave and upslope settlement such that the downward force can be resisted (Fig. 6.4g). At the end of the analysis, a maximum of 8 m heave is calculated near the lower end in the Model I case.

Downslope heave and upslope head scarps have been reported in many offshore slopes (e.g. Greene et al. 2006; Mountjoy et al. 2009). As it is extremely difficult to identify exact reasons,

various possible factors have been inferred from interpretation of seabed profile. For example, Gardner et al. (1999) suggested that the Humboldt Slide was initiated by subsidence of the middle section followed by downslope compression and upslope retrogressive failure. The Tuaheni South Landslide also follows a similar pattern (Mountjoy et al. 2009). The present numerical modeling shows that these features might be developed due to shear band propagation through a strain softening weak layer. Unlike many previous studies, such as Kvalstad et al. (2005a), the present numerical modeling technique can simulate the large deformation behaviour, which is essential for modeling the features of failed seabed profile.

Model II

A total of 8 different cases are analyzed using Model II. Four of them are performed with a discontinuity at the middle of the slope as shown in Fig. 6.2(b) and are named as NS-G19-M1, LS-G19-M1, NS-G5-M15 and M20, where NS and LS represent no softening and little softening of the upper glacial clay (S_t=S_{tg}=1.5), the number after the letter G represents the thickness of glacial clay from mudline (top surface) and the number after M represents the thickness of the marine clay layer. For example LS-G19-M1 represents a 1 m thick marine sensitive clay layer underlain by a 19 m thick glacial clay of little sensitivity.

To explain the slope failure mechanisms, the simulation NS-G19-M1 is first considered and the results are shown in Fig. 6.6. The mechanisms involved in discontinuity formation and initiation of shear band propagation are similar to Model-I as shown in Fig. 6.4. At the initial stage, the rate of shear band propagation is the same in the left and right directions. However, when the shear band reaches under the crest of the steeper slope, the downward propagation is slightly higher than the upward propagation because of less kinematic restraint in the downslope. The

shear band reaches the toe and also propagates to the right until it reaches the strong layer in the upslope. At this stage, a 1 km long failure surface PABRQ is developed and the soil above this layer moves downward as shown by the instantaneous velocity vectors in Fig. 6.6(c). The instantaneous velocity of the failed soil mass located above the failure plane PABRQ is different; the frontal portion has a maximum velocity which gradually decreases with distance. A number of successive triangular wedges (V- and Λ-shaped) are formed in the upslope area with displacement of the failed soil mass. The zone of plastic strains around the failure plane in the upslope expands and subsides. During downward movement of the failed soil mass, additional shear surfaces develop in the glacial clay as shown in Figs. 6.6(d)–6.6(i) because the frontal soil mass moves at a faster rate. In between these failure surfaces, the deformation of soil is primarily elastic. Based on sonar data, displacement of intact soil glide blocks have been reported in the past (Gee et al. 2005; Harders et al. 2011). The present large deformation FE modeling appears to simulate this process.

Figure 6.7 shows the progressive development of the shear band with time for LS-G19-M1. Compared to the previous case, this case introduces little softening to the upper glacial clay. The initial development of the shear band and the formation of a complete failure surface MABN are very similar to the previous case NS-G19-M1, except for the formation of shear surface at the right end which occurs more quickly in this case because of the sensitivity of the upper soil layer. With downward displacement of the upper soil layer, a number of shear surfaces form in the upper end and also at the middle of the slope. In between the shear surfaces, the plastic deformation of the soil is negligible and therefore these blocks move almost as intact blocks. Comparison of the failure pattern in this case (Fig. 6.7) with the previous case (Fig. 6.6) shows that more shear surfaces are formed in LS-G19-M1. Plastic shear strain in the shear band is

concentrated in narrow zones in LS-G19-M1, while it is more dispersed in NS-G19-M1. The seismic profile through the Storegga slide (Fig. 6.1a) shows very similar triangular wedges to those shown in the upper end of the slope (Gauer et al. 2005). However, the size of the triangular wedge in Storegga slide is larger than this because the slide occurs at greater depth (approximately at 100 m depth). If the analysis is not stopped, the number of triangular wedges will increase. It is also expected that some blocks in between these wedges might be completely detached and move as independent tabular blocks as mentioned by Gee et al. (2005) in their conceptual model.

The effects of thickness of the sensitive clay layer are examined from the simulations NS-G5-M15 (a 15 m thick sensitive clay layer) and M20 (a 20 m thick sensitive clay layer). Similar to NS-G19-M1and LS-G19-M1, an initial failure surface with a V-shape failure wedge at the head of the slide is formed in NS-G5-M15 (Figs. 6.8a–6.8d). This is followed by the development of multiple shear surfaces (Figs. 6.8f–6.8i) in the slide mass during its downward displacement. A number of large slide masses remain almost intact but displace on the basal failure plane (Figs. 6.8g-6.8j). A few grabens are formed between the previously developed shear surfaces (Fig. 6.8i). Formation of some successive ribs and ridges is also observed (Fig. 6.8j). The present FE simulation also indicates that the slide mass could split into multiple soil blocks during its downward movement. A comparison with two previous cases shows that the active failure planes develop more frequently in this case because of higher sensitivity of the clay layer above the basal failure plane. These active failure planes are very similar to the slide features interpreted from the seismic profile of the Tampen Slide located in the Storegga region (Fig. 6.1c, Solheim et al. 2005).

The progressive development of failure planes for M20 (only sensitive clay above the base) is shown in Fig. 6.9. In this case, after formation of a shear bands parallel to the slope, the failure plane MXN is formed first at a distance of 325 m from the toe of the slope before formation of failure plane near the upper strong layer as occurred in the previous cases (Figs. 6.6-6.8). After that, shear surfaces formed at the end (Fig. 6.9d). A number of active failure surfaces and V-shaped failure wedges are formed with displacement of failed soil blocks. Finally, the head of the slide mass seems to separate from the upper strong layer.

6.7 Location of Discontinuity

The effects of the location of discontinuity are examined with 4 more simulations (Cases I-IV) where the geometry is similar to LS-G19-M1 (i.e. 1 m thick marine sensitive clay layer below a 19 m thick glacial clay, as shown in Fig. 6.2b); however, the discontinuity is located near the crest (*g*) of the 15° slope. In other words, the discontinuity CD in Fig. 6.2(b) is placed further left in the marine clay layer. These four simulations are performed for the following conditions.

Case-I: 30 m discontinuity (i.e. l_d=30 m) under the 15 degrees slope located on the left side of the crest *g* in Fig. 6.2b (i.e. x_d=-30 m) (see also Fig. 6.10 at t=4.6 s) and the glacial clay has sensitivity $S_{t(g)}$=1.5, and δ_{pc}=20 mm.

Case-II: l_d=30 m, x_d=-30 m (Fig. 6.11), $S_{t(g)}$=3.0 and δ_{pc}=10 mm.

Case-III: l_d=150 m, x_d=0 (Fig. 6.12), $S_{t(g)}$=1.5 and δ_{pc}=20 mm.

Case-IV: l_d=150 m, x_d=0 (Fig. 6.13), $S_{t(g)}$=3.0 and δ_{pc}=10 mm.

Figures 6.10–6.13 show the failure planes developed from the propagation of shear bands for these four cases. In all cases, the shear band starts to propagate through the marine sensitive clay

layer. Because of less lateral restraint at the left side, the rate of shear band propagation towards the toe of the 15 degree slope is higher than to the right side. After reaching the toe, the shear band propagates to the upslope areas and at one stage failure surfaces develop through the upper glacial clay.

Comparison of failure surfaces presented in Figs. 6.10–6.13 shows that, if the sensitivity of the upper glacial clay is low (=1.5, Fig. 6.10: Case-I and Fig 6.12: Case-III), the plastic shear strains develop over a large area instead of forming clear shear bands (see S_t = 3.0, Fig. 6.11: Case-II and Fig. 6.13: Case-IV). The basal shear band propagates up to the head wall and then settlement occurs over a large zone forming a head scarp. The length of the discontinuity required for initiation of shear band propagation increases with its distance from the toe of the 15 degree slope (30 m, 150 m and 400 m for cases analyzed above).

When $S_{t(g)}$=3.0, strain localization occurs in a narrow zone and clear shear bands form (Figs. 6.11 and 6.13). In these cases, the active failure planes develops first, which is followed by development of a number of other internal shear bands with displacements of the upper failed soil mass. Some of the shear surfaces cross each other. Post-slide investigation of many submarine landslides show the development of such internal shear surfaces (Micallef et al. 2007).

In summary, depending upon geometry, location of the discontinuity and shear strength parameters, different types of shear surfaces might be formed in the failed soil mass. When the soil is sensitive, the shear strength in these failure planes might be decreased significantly which should be considered in the modeling of the seabed for any development in the zone where such failure occurred in the past. The large deformation FE modeling presented in this study can

simulate the deformed shape of the seabed after failure and also can explain many of the failure mechanisms.

6.8 Morphologic Features and Failure Planes

Various conceptual failure mechanisms have been inferred to explain large-scale offshore landslides from close examination of morphologic features obtained from bathymetry (Kvalstad et al. 2005a; Solheim et al. 2005; Gee et al. 2005; Mountjoy et al. 2009; Locat et al. 2009; Greene et al. 2006; Micallef et al. 2007). Although these conceptual models correspond with observed features, they could be better explained using large deformation FE modeling. Based on the FE results presented above, at least the following 7 types of failure surfaces development could be identified (Fig. 6.14), which depends on geometry and soil properties.

1. Horst and graben type (Fig. 6.14a) - These occurs mainly in the upslope areas near the head wall. During downward displacements of failed soil mass, the height of the graben reduces at a faster rate than that of the horst and therefore the horsts project above the graben (Figs. 6.7, 6.10 & 6.12). This type of failure pattern has been reported in many studies (e.g. Kvalstad et al. 2005a; Gauer et al. 2005; Bryn et al. 2005; Micallef et al. 2007; Wang et al. 2013) (see also Fig. 6.1a).

2. Compression type (Fig. 6.14b) - Formation of a number of triangular wedges occurs near the lower end if the movement is obstructed in the downslope (Fig. 6.4g). With displacement of the failed soil mass, the V-shaped block is pushed up at a faster rate than Λ-shaped block. Several studies reported this type of failure pattern. (Mountjoy et al. 2009; Gardner et al. 1999; Greene et al. 2006) (see also Figs. 6.1a and 6.1b).

3. Multiple scarps (Fig. 6.14c) - When the upper soil layer in the downslope areas moves at a relatively higher velocity, longitudinal tension develops that creates this type of failure surfaces (Figs. 6.8 and 6.9). It is very similar to Fig. 6.1(c). For the cases analyzed in this study, this type of failure surfaces encountered when the failure is initiated from the toe of the slope and upper soil layer is also sensitive.

4. Large plastic zone (Fig. 6.14d) - When the upper soil layer is insensitive or with low sensitivity, the shear surface is not distinct and the plastic shear deformation occurs over a large area (Figs. 6.6, 6.10, 6.12).

5. Tabular block (Fig. 6.14e) - At a very large displacement, a number of tabular glide blocks might be formed, which might displace downward independently over the basal shear zone (Figs. 6.8, 6.9, 6.11 & 6.13). The potential for tabular block formation increases with an increase in sensitivity and rate of post peak softening. A number of internal shear surfaces might be also formed in the tabular block. Several studies (e.g. Gee et al. 2005; Harders et al. 2011) reported this type of failure, one of them is shown in Fig. 6.1(d).

6. Multiple shear surfaces (Fig. 6.14f) - These failure surfaces are observed when the upper soil layer is sensitive and shear band propagation initiates near the steeper slope. In this case, in addition to active failure surfaces shown in Fig. 6.14(c), a number of shear bands form which sometime cross each other (Figs. 6.11 and 6.13). Micallef et al. (2007) interpreted this type of failure in Storegga Slide.

7. Polished head scarp (Fig. 6.14g) - When there is a strong clay layer in the upslope, the soil mass above the basal failure plane might displace significantly leaving polished head scarps (Fig. 6.9), similar to Fig. 6.1(e).

6.9 Conclusions

Many offshore facilities are located, or planned, in locations where submarine landslides occurred in the past. While geophysical and geotechnical information provide valuable information for interpretation of seabed morphology at the time of investigation, numerical modeling can better explain potential mechanisms involved in the process of failure that brought the slope to the current post-failure state. However, numerical modeling is challenging because most of these large-scale submarine landslides are progressive in nature and significant large shear deformation occurs along the failure planes.

This study developed a large deformation FE modeling technique to simulate progressive failure of submarine slopes. Analyses are performed for undrained condition using Abaqus CEL FE program where the clay is modeled as Eulerian material that flows through the fixed mesh and therefore numerical issues related to mesh distortion are avoided. As encountered in many offshore environments, the existence of a moderately sensitive marine clay layer is considered in this study. A model for strain softening behaviour of marine clay in undrained loading is implemented in Abaqus CEL and the simulations are performed for different soil properties and slope geometries with a weak clay layer. The following conclusions are drawn from the present numerical study.

a) An existence of a discontinuity could initiate the propagation of a shear band along the marine clay layer. If the shear band propagates a sufficiently long distance, failure surfaces form through the upper soil layer that leads to global failure of the slope.
b) When a strong soil layer exists in both upslope and downslope areas and the discontinuity is located in the marine clay layer somewhere in between them, as in Model I, the

compressive failure in the downslope creates heave and tensile failure in the upslope causing settlement.

c) The variation of stress in the direction parallel to the slope obtained from the present numerical analysis is similar to the assumption made in the development of an analytical solution (Puzrin and Germanovich 2005). However, the analytical solution cannot model the formation of subsequent shear band/failure planes in the upper soil layer as presented in this study, which might be important in the modeling of previously failed seabed.

d) Clear shear bands form when the upper soil layer is sensitive; while plastic deformation occurs over a large area of the upper soil layer if it is not sensitive.

e) The failure pattern of seabed is significantly influenced by a relatively steep slope in the downslope areas. When the discontinuity is located closer to the steep downslope, mainly active failure planes are developed in the upper soil layer during the displacement of failed soil mass.

f) FE simulated failure patterns are comparable with interpreted failure patterns from field investigations.

To the best knowledge of the authors, this is the first attempt at large deformation FE modeling of the complete process of submarine slope failure resulting from a discontinuity. One of the main advantages of the present numerical modeling is that extremely large deformations could be simulated and the performance is more robust than previous attempts. Although the simulations are performed only for a discontinuity, the present numerical modeling technique could be used for modeling of failure in undrained conditions triggered by other factors.

While the present numerical modeling shows some promising results which are comparable with many field observations, it has some limitations. Analyses are performed for undrained

conditions without considering shear strain rate effects on undrained shear strength. Drainage and creep behaviour of soil, which might also influence the failure of a slope, are not considered in this study. Moreover, the analyses are performed for idealized soil profiles and geotechnical properties and the effects on failure patterns need to be examined further.

Acknowledgements

The work presented in this paper has been supported by the Research and Development Corporation of Newfoundland and Labrador, NSERC and C-CORE.

List of symbols

The following symbols are used in this paper:

β slope angle

h depth of marine clay

τ_g gravitational shear stress

$\overline{\sigma}_p$ average normal stress in the upper soil layer acting parallel to the slopes

σ_{xx} horizontal stress

δ post-peak shear displacement

δ_{95} δ at which s_u reduced by 95% of (s_{up}-s_{uR})

δ_e elastic shear displacement

δ_p plastic shear displacement

δ_{pc} plastic shear displacement at point b in Fig. 6.3

δ_t total shear displacement

E_u undrained Young's modulus

γ^p plastic shear strain

S_t sensitivity, s_{up}/s_{uR}

$S_{t(g)}$ sensitivity of glacial clay

$S_{t(m)}$ sensitivity of marine clay

s_u mobilized undrained shear strength

s_{up} peak undrained shear strength

s_{uR} s_u mobilized in shear band at considerable shear displacement

s_{ur} s_u at completely remoulded state

s_{u95} s_u mobilized at δ_{95}

$s_{u\infty}$ s_u mobilized after $2\delta_{95}$

t_s soil element thickness

t FE analysis time

t_{FE} FE mesh size

l_d length of discontinuity

l^{cr} critical length

References

Aifantis, E. C. (1984). "On the microstructural origin of certain inelastic models." *J. Eng. Mater. Technol.* (Trans ASME), 106, 326–330.

Almagor, G., and Wiseman, G. (1991). "Analysis of submarine slumping in the continental slope off the southern coast of Israel." *Marine Geotechnology*, 10(3-4), 303–342.

Anastasopoulos, I., Gazetas, G., Bransby, M. F., Davies, M. C. R., and Nahas, A. El. (2007). "Fault rupture propagation through sand: finite-element analysis and validation through centrifuge experiments." *J. Geotech. and Geoenviron. Eng.* (*ASCE*), 133(8), 943–958.

Andresen, L., and Jostad, H. P. (2007). "Numerical modeling of failure mechanisms in sensitive soft clays – application to offshore geohazards." *Off. Technology Conf.*, OTC 18650.

Bernander, S. (2000). *Progressive failure in long natural slopes: formation, potential extension and configuration of finished slides in strain-softening soils*, Licentiate Thesis, Luleå University of Technology.

Bjerrum, L., and Landva, A. (1966). "Direct simple-shear tests on a Norwegian quick clay." *Géotechnique*, 16(1), 1–20.

Brink, U. S. T., Lee, H. J., Geist, E. L., and Twichell, D. (2009). "Assessment of tsunami hazard to the U.S. East Coast using relationships between submarine landslides and earthquakes." *Marine geology*, 264(1-2), 65–73.

Bryn, P., Berg, K., Forsberg, C. F., Solheim, A., and Kvalstad, T. (2005). "Explaining the Storegga slide." *Marine and Petroleum Geology*, 22(1-2), 11–19.

Canals, M., Lastras, G., Urgeles, R., Casamor, J. L., Mienert, J., Cattaneo, A., Batist, M. De., Haflidason, H., Imbo, Y., Laberg, J. S., Locat, J., Long, D., Longva, O., Masson, D.G., Sultan, N., Trincardi, F., and Bryn, P. (2004). "Slope failure dynamics and impacts from seafloor and shallow sub-seafloor geophysical data: case studies from the COSTA project." *Marine Geology*, 213(1-4), 9–72.

Conte, E., Silvestri, F., and Troncon, A. (2010). "Stability analysis of slopes in soils with strain-softening behaviour." *Computers and Geotechnics*, 37(5), 710–722.

Dan, G., Sultan, N., and Savoye, B. (2007). "The 1979 Nice harbour catastrophe revisited: Trigger mechanism inferred from geotechnical measurements and numerical modelling." *Marine Geology*, 245(1-4), 40–64.

Dimakis, P., Elverhøi, A., Høeg, K., Solheim, A., Harbitz, C., Laberg, J. S., Vorreng, T. O., and Marr, J. (2000). "Submarine slope stability on high-latitude glaciated Svalbard–Barents Sea margin." *Marine Geology*, 162(2-4), 303–316.

de Borst, R. (1991). "Simulation of strain localization: A reappraisal of the Cosserat continuum." *Engineering Computations*, 8, 317–332.

de Borst, R., Sluys, L., Mulhaus, H., and Pamin, J. (1993). "Fundamental issues in finite element analyses of localization of deformation." *Engineering Computations*, 10, 99–121.

Dey, R., Hawlader, B., Phillips, R., and Soga, K. (2015a). "Large deformation finite element modeling of progressive failure leading to spread in sensitive clay slopes." *Géotechnique* (accepted).

Dey, R., Hawlader, B., Phillips, R., and Soga, K. (2015b). "Modeling of large deformation behaviour of marine sensitive clays and its application to submarine slope stability analysis." (submitted for review).

Dutta, S., Hawlader, B., and Phillips, R. (2015). "Finite element modeling of partially embedded pipelines in clay seabed using Coupled Eulerian–Lagrangian method." *Canadian Geotechnical Journal*, 52(1), 58–72.

Duncan, J.M., and Buchignani, A. L. (1976). "An engineering manual for settlement studies." *The Earthquake Engineering Online Archive (NISEE e-Library)*, Department of Civil Engineering, University of California, Berkley.

Einav, I., and Randolph, M. F. (2005). "Combining upper bound and strain path methods for evaluating penetration resistance." *Int. J. Num. Methods Engineering*, 63(14), 1991–2016.

Gauer, P., Kvalstad, T. J., Forsberg, C. F., Bryn, P., and Berg, K. (2005). "The last phase of the Storegga Slide: simulation of retrogressive slide dynamics and comparison with slide-scar morphology." *Marine and Petroleum Geology*, 22(1-2), 171–178.

Gardner J.V., Prior, D. B., and Field, M. E. 1999. Humboldt Slide– a large shear-dominated retrogressive slope failure. Marine Geology, **154:** 323–338.

Gee, M. J. R., Gawthorpe, R.L., and Friedmann, J.S. (2005). "Giant striations at the base of a submarine landslide." *Marine Geology*, 214(1-3), 287–294.

Griffiths, D. V., and Lane, P. A. (1999). "Slope stability analysis by finite elements." *Géotechnique*, 49(3), 387–403.

Greene, H.G., Murai, L. Y., Watts, P., Maher, N. A., Fisher, M. A., Paull, C. E., and Eichhubl, P. (2006). "Submarine landslides in the Santa Barbara Channel as potential tsunami sources." *Natural Hazards and Earth System Sciences*, 6, 63–88.

Gylland, A. S., Sayd, M. S., Jostad, H. P., and Bernander, S. (2010). "Investigation of soil property sensitivity in progressive failure." *Proc. of the 7th European Conf. on Num. Methods in Geotech. Eng.*, Benz & Nordal eds., Trondheim, Norway, 515–520.

Gylland, A. S. (2012). *Material and slope failure in sensitive clays*. PhD thesis, Norwegian University of Science and Technology.

Hampton, M.A., Lee, H.J., and Locat, J. (1996). "Submarine landslides." *Reviews of Geophysics*, 34(1), 33–59.

Harders, R., Ranero, C. R., Weinrebe, W., and Behrmann, J. H. (2011). "Submarine slope failures along the convergent continental margin of the Middle America Trench." *Geochemistry, Geophysics and Geosystems*, 12(6), 1–26.

Jostad, H. P., and Andresen, L. (2002). "Bearing capacity analysis of anisotropic and strain-softening clays." *Proc. of NUMOG VIII*, Rome, Italy, 469–474.

Jostad, H. P., and Andresen, L. (2004). "Modeling of shear band propagation in clays using interface elements with finite thickness." *Proc. of the 9th International Symposium on 'Numerical Models in Geomechanics - Numog IX'*, Ottawa, Canada.

Karlsrud, K., and Edgers, L. (1982). "Some aspects of submarine slope stability." *Marine Slides and Other Mass Movements*, 6, 61–81.

Kvalstad, T.J., Andresen, L., Forsberg, C.F., Berg, K., and Bryn, P. (2005a). "The Storegga Slide: evaluation of triggering sources and slide mechanisms." *Marine and Petroleum Geology*, 22(1-2), 245–256.

Kvalstad, T.J., Nadim, F., Kaynia, A.M., Mokkelbost, K.H., and Bryn, P. (2005b). "Soil conditions and slope stability in the Ormen Lange area." *Marine and Petroleum Geology*, 22(1-2), 299–310.

Lastras, G., Canals, M., Urgeles, R., Hughes-Clarke, J. E., and Acosta, J. (2004). "Shallow slides and pockmark swarms in the Eivissa Channel, western Mediterranean Sea." *Sedimentology*, 51, 1–14.

Li, W., Wu, S., Völker, D., Zhao, F., Mi, L., and Kopf A. (2014). "Morphology, seismic characterization and sediment dynamics of the Baiyun Slide Complex on the northern South China Sea margin." *Journal of the Geological Society*, London.

Lee, H. J., and Edwards, B. D. (1986). "Regional method to assess offshore slope stability." *Journal of Geotechnical Engineering*, 112(5), 489–509.

Lee, H.J., and Baraza, J., (1999). "Geotechnical characteristics and slope stability in the Gulf of Cadiz." *Marine Geology*, 155(1-2), 173–190.

Leynaud, D., Mienert, J., and Nadim, F. (2004). "Slope stability assessment of the Helland Hansen area offshore the mid-Norwegian margin." *Marine Geology*, 213(1-4), 457–480.

L'Heureux, J. S., Longva, O., Steiner, A., Hansen, L., Vardy, M.E., Vanneste, M., Haflidason, H., Brendryen, J., Kvalstad, T.J., Forsbeg, C.F., Chand, S., and Kopf, A. (2012). "Identification of weak layers and their role for the stability of slopes at Finneidfjord, Northern Norway." *Submarine mass movements and their consequences*, Yamada Y et al. eds., Advances in natural and technological hazards research, 31, 321–330.

Locat, J., Lee, H., Brink, U. S., Twichell, D., Geist, E., and Sansoucy, M. (2009). "Geomorphology, stability and mobility of the Currituck slide." *Marine Geology*, 264(1-2), 28–40.

Locat, A., Leroueil, S., Bernander, S., Demers, D., Jostad, H. P., and Ouehb, L. (2011). "Progressive failures in eastern Canadian and Scandinavian sensitive clays." *Canadian Geotechnical Journal*, 48(11), 1696–1712.

Locat, A., Jostad, H. P., and Leroueil, S. (2013). "Numerical modeling of progressive failure and its implications for spreads in sensitive clays." *Canadian Geotechnical J.*, 50, 961–978.

Locat, J., Leroueil, S., Locat, A., and Lee, H. (2014). "Weak layers: their definition and classification from a geotechnical perspective." *Sub. Mass Movements and Their Conseq.*, S. Krastel et al. eds., Advances in Natural and Technological Hazards Research, 37, 3–12.

Locat, A., Leroueil, S., Fortin, A., Demers, D., and Jostad, H.P. (2015). "The 1994 landslide at Sainte-Monique, Quebec: geotechnical investigation and application of progressive failure analysis." *Canadian Geotechnical Journal*, 52, 490–504.

Lunne, T., and Andersen, K. H. (2007). "Soft clay shear strength parameters for deepwater geotechnical design." *Proc. 6th Int. Off. Site Investigations and Geotech. Conf.*, UK, 151–176.

McAdoo, B. G. (1999). "Mapping submarine slope failures." *Marine and Coastal Geographical Information Systems*, D. J. Wright and D. J. Barlett eds., 189–205.

Micallef, A., Masson, D. G., Berndt, C., and Stow, D. A. V. (2007). "Morphology and mechanics of submarine spreading: A case study from the Storegga Slide." *Journal of Geophysical Research*, Vol. 112, F03023.

Mello, U. T., and Pratson, L. F. (1999). "Regional slope stability and slope-failure mechanics from the two-dimensional state of stress in an infinite slope." *Mar. Geol.*, 154(1-4), 339–356.

Mohammadi, S., and Taiebat, H. A. (2013). "A large deformation analysis for the assessment of failure induced deformations of slopes in strain softening materials." *Computer and Geotechnics*, 49, 279– 288.

Mohammadi, S., and Taiebat, H. A. (2014). "H-adaptive updated Lagrangian approach for large-deformation analysis of slope failure." *Int. J. Geomech.,* ASCE, 1943–5622.

Mountjoy, J. J., McKean, J., Barnes, P. M., and Pettinga, J. R. (2009). "Terrestrial-style slow-moving earth flow kinematics in a submarine landslide complex." *Mar. Geol.,* 267, 114–127.

Palmer, A. C., and Rice, J. R. (1973). "The growth of slip surfaces in the progressive failure of overconsolidated clay." *Proc. R. Soc. London*, Ser. A, 332(1591), 527–548.

Pijaudier-Cabot, G., and Bažnt, Z. P. (1987). "Nonlocal damage theory." *J. Eng. Mech.* (ASCE), 113, 1512–1533.

PLAXIS. (2011). *PLAXIS 2D 2010 manuals*. PLAXIS bv., Delft, the Netherlands.

Puzrin, A. M., Germanovich, L. N., and Kim, S. (2004). "Catastrophic failure of submerged slopes in normally consolidated sediments." *Géotechnique,* 54(10), 631–643.

Puzrin, A. M., and Germanovich, L. N. (2005). "The Growth of Shear Bands in the Catastrophic Failure of Soils." *Proc. R. Soc. London*, Ser. A, 461(2056), 1199–1228.

Qiu, G., Henke, S., and Grabe, J. (2011). "Application of a Coupled Eulerian–Lagrangian approach on geomechanical problems involving large deformations." *Computers and Geotechnics*, 38(1), 30–39.

Quinn, P. (2009). *Large Landslides in Sensitive Clay in Eastern Canada and the Associated Hazard and Risk to Linear Infrastructure*. Doctoral thesis, Queen's University.

Quinn, P. E., Diederichs, M. S., Rowe, R. K., and Hutchinson, D. J. (2011). "A new model for large landslides in sensitive clay using a fracture mechanics approach." *Canadian Geotechnical J.*, 48(8), 1151–1162.

Quinn, P. E., Diederichs, M. S., Rowe, R. K., and Hutchinson, D. J. (2012). "Development of progressive failure in sensitive clay slopes." *Canadian Geotechnical J.*, 49(7), 782–795.

Solheim, A., Berg, K., Forsberg, C. F., and Bryn, P. (2005). "The Storegga slide complex: repetitive large scale sliding with similar cause and development." *Marine and Petroleum Geology*, 22(1-2), 97–107.

Sultan, N., Savoye, B., Jouet, G., Leynaud, D., Cochonat, P., Henry, P., Stegmann, S., and Kopf, A. (2010). "Investigation of a possible submarine landslide at the Var delta front (Nice continental slope, southeast France)." *Canadian Geotechnical J.*, 47(4), 486–496.

Stark, T., and Contreras, I. A. (1996). "Constant volume ring shear apparatus." *Geotechnical Testing Journal*, 19(1), 3–11.

Tavenas, F., Flon, P., Leroueil, S., and Lebuis, J. (1983). "Remolding energy and risk of slide retrogression in sensitive clays." *Proc. of the Symposium on Slopes on Soft Clays*, Linköping, Sweden, SGI Report No. 17, 423–454.

Thakur, V. (2007). *Strain localization in sensitive soft clays*. Doctoral thesis, Norwegian University of Science and Technology, Trondheim and Norwegian Centre of Excellence: International Centre for Geohazards.

Tho, K. K., Leung, C. F., Chow, Y. K., and Swaddiwudhipong, S. (2012). "Eulerian finite element technique for analysis of jack-up spudcan penetration." *International Journal of Geomechanics*, ASCE, 12(1), 64–73.

Tian, Y., Wang, D., and Cassidy, M. J. (2011). "Large deformation finite element analysis of offshore penetration tests." *Proc. Int. Symp. Com. Geomech*., Cavtat-Dubrovnik, 925–933.

Troncone, A. (2005). "Numerical analysis of a landslide in soils with strain-softening behaviour." *Géotechnique*, 55(8), 585–596.

Twichell, D.C., Chaytor, J.D., Brink, U. S., and Buczkowski, B. (2009). "Morphology of the late Quaternary submarine landslides along the U.S. Atlantic continental margin." *Marine Geology*, 264, 4–15.

Vardoulakis, I., and Aifantis, E. C. (1989). "Gradient-Dependent dilatancy and its implications in shear banding and liquefaction." Ingenieur—*Archive* 59, 197–208.

Vardoulakis, I., and Sulem, J. (1995). "Bifurcation Analysis in Geomechanics." *Second-grade plasticity theory for geomaterials*, Blackie Academic & Professional eds., 382–425.

Wang, D., Randolph, M. F., and White, D. J. (2013). "A dynamic large deformation finite element method based on mesh regeneration." *Computers and Geotechnics*, 54, 192–201.

Yang, S.L., Solheim, A., Kvalstad, T.J., Forsberg, C.F., and Michael Schnellmann, M. (2006). "Behaviour of the sediments in the Storegga Slide interpreted by the steady state concept." *Norwegian J. of Geology*, 86(3), 243–253.

Yang, S.L., Kvalstad, T.J., Solheim, A., and Forsberg, C.F. (2007). "Slope Stability at Northern Flank of Storegga slide." *Proc. 16th Int. Off. and Polar Eng. Conf*., Lisbon, Portugal, 1524–1529.

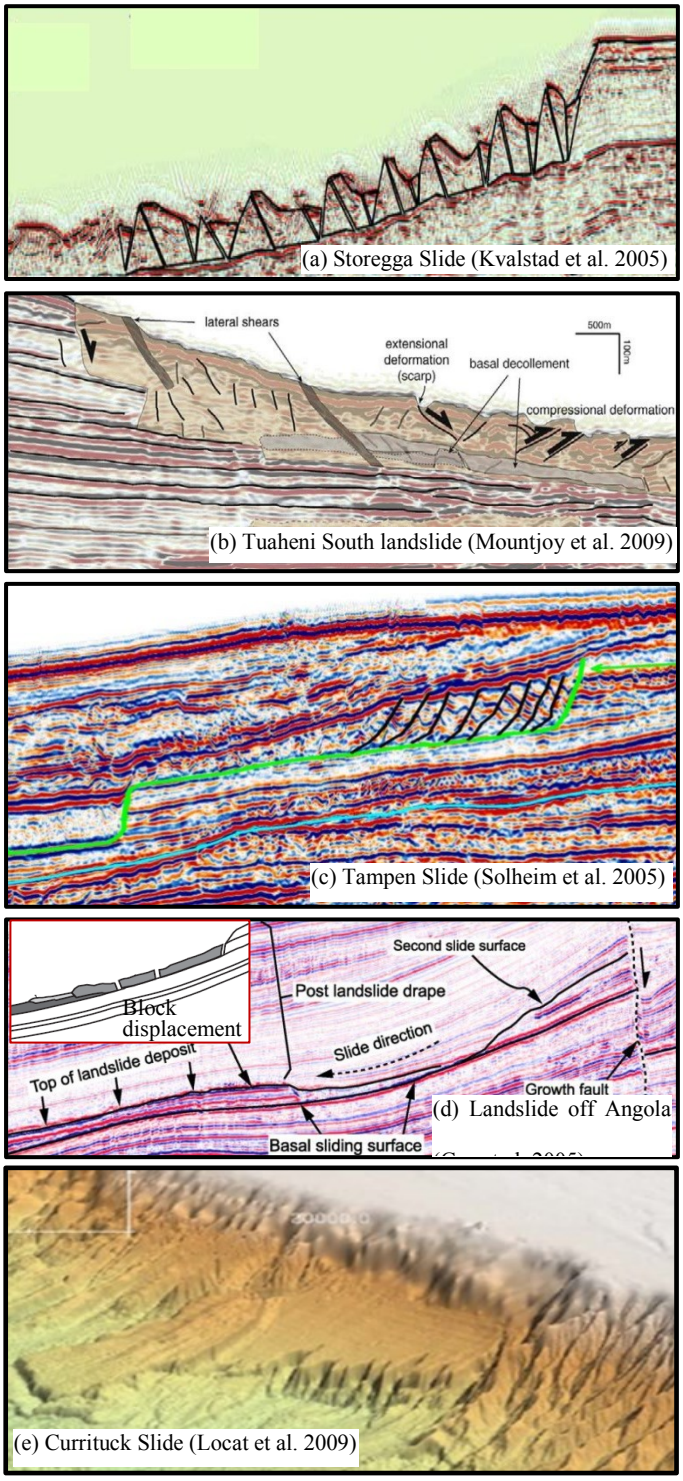

Figure 6. 1. Interpreted shear zones and deformation in seismic profiles of different landslides

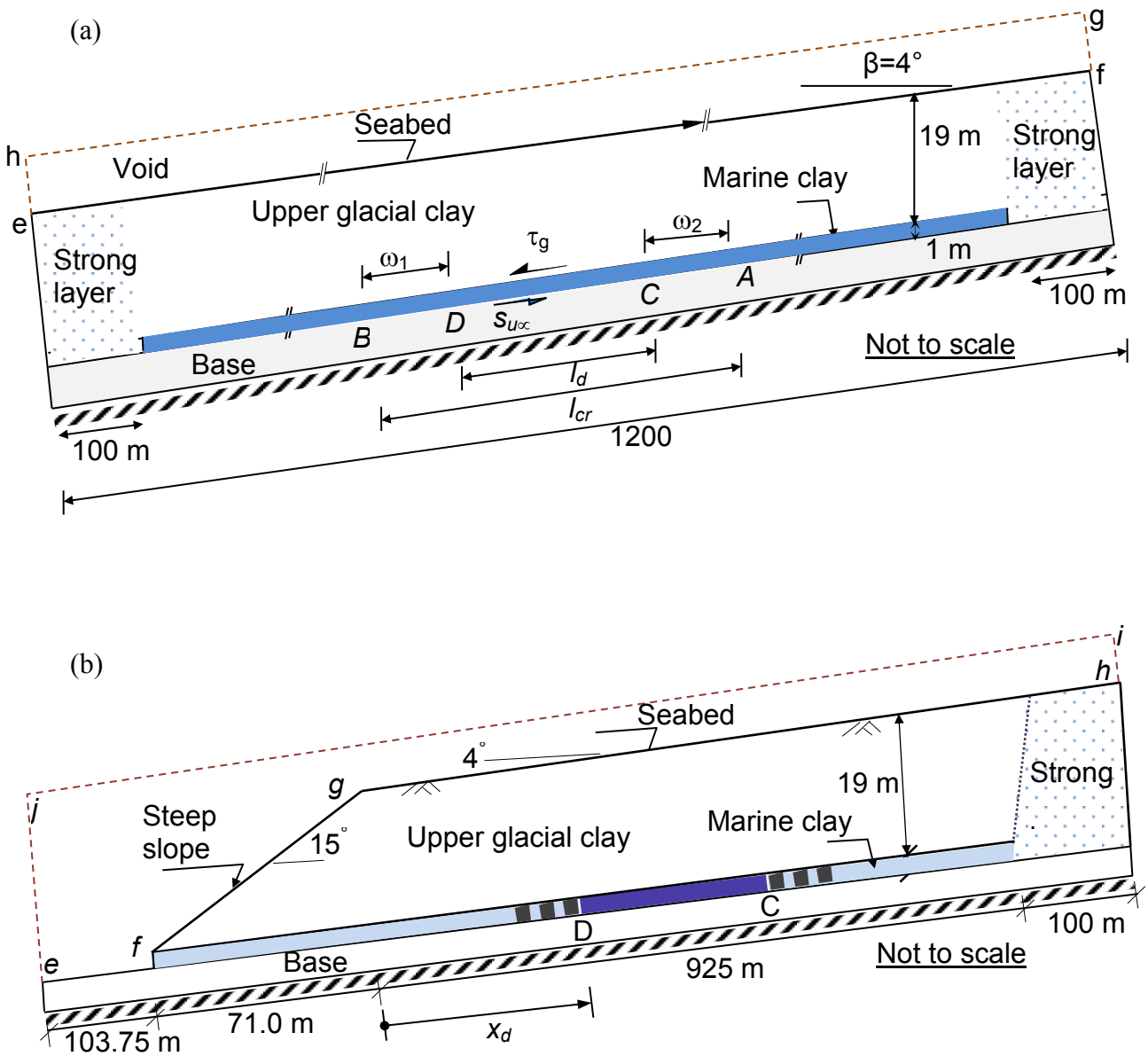

Figure 6. 2: Model geometry: (a) Model I: without steep slope (b) Model II: with a steep slope

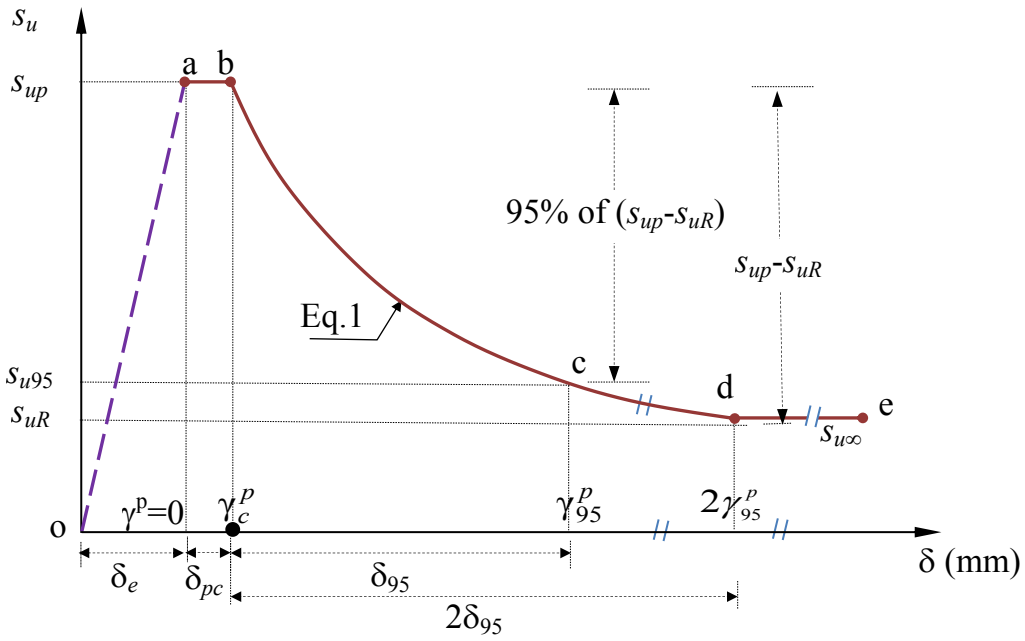

Figure 6. 3: Stress-strain behavior used in finite element modeling

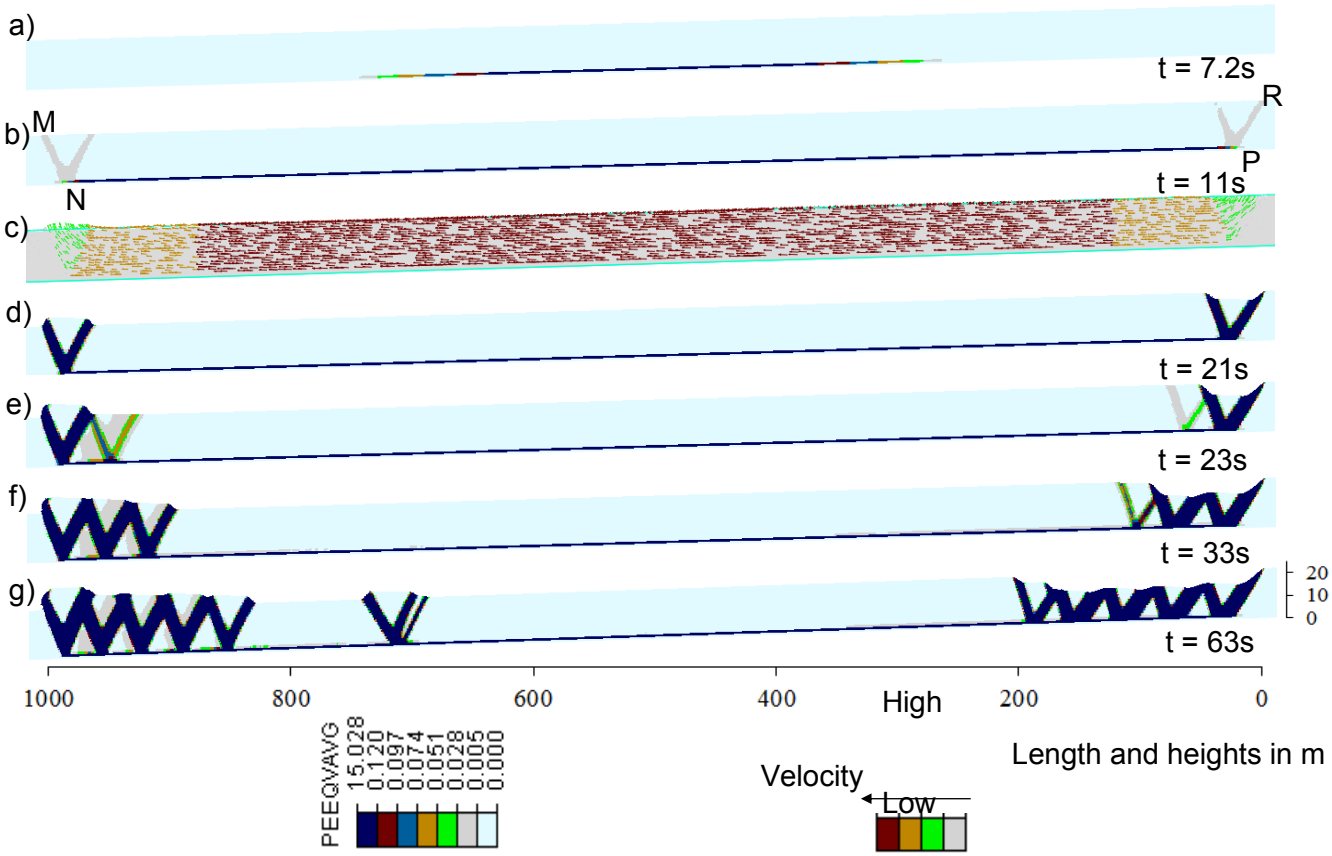

Figure 6. 4: Development of failure surfaces in Model-I

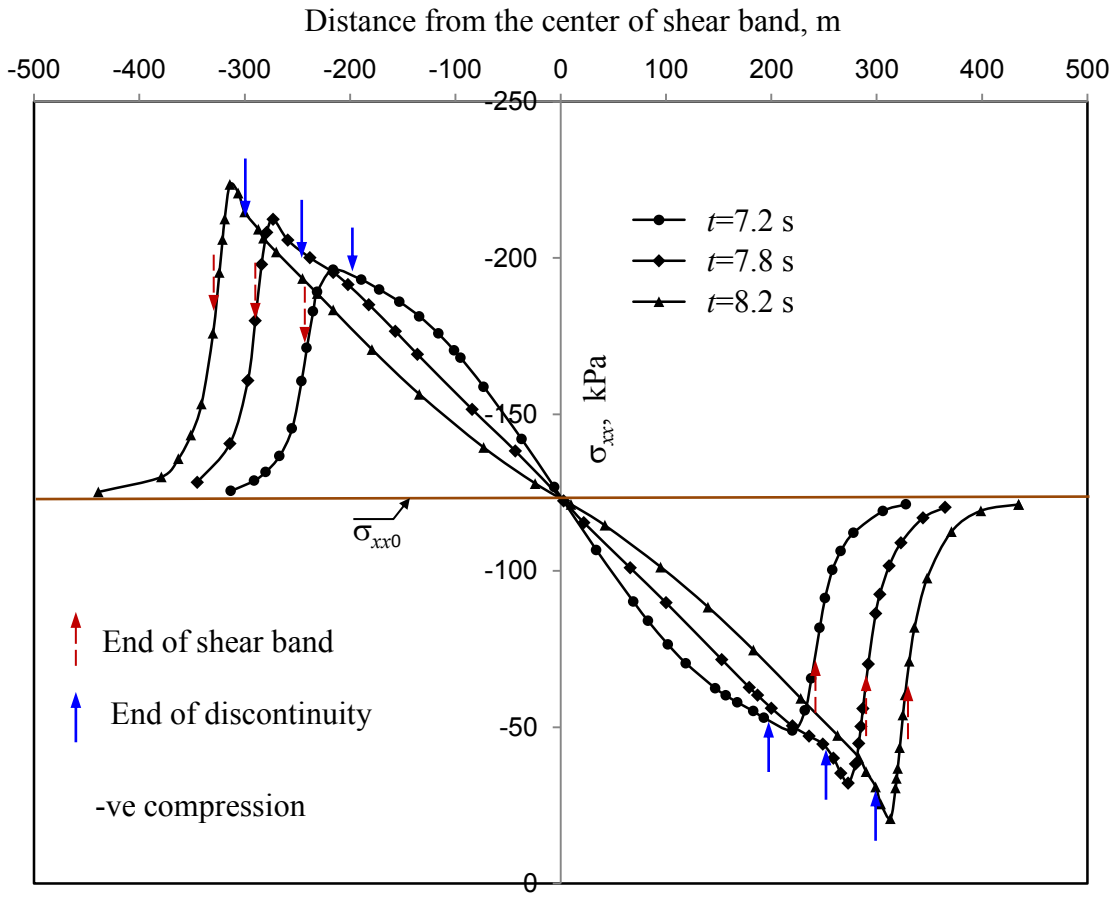

Figure 6. 5: Variation of σ_{xx} at depth 12.5 m in the upper soil layer

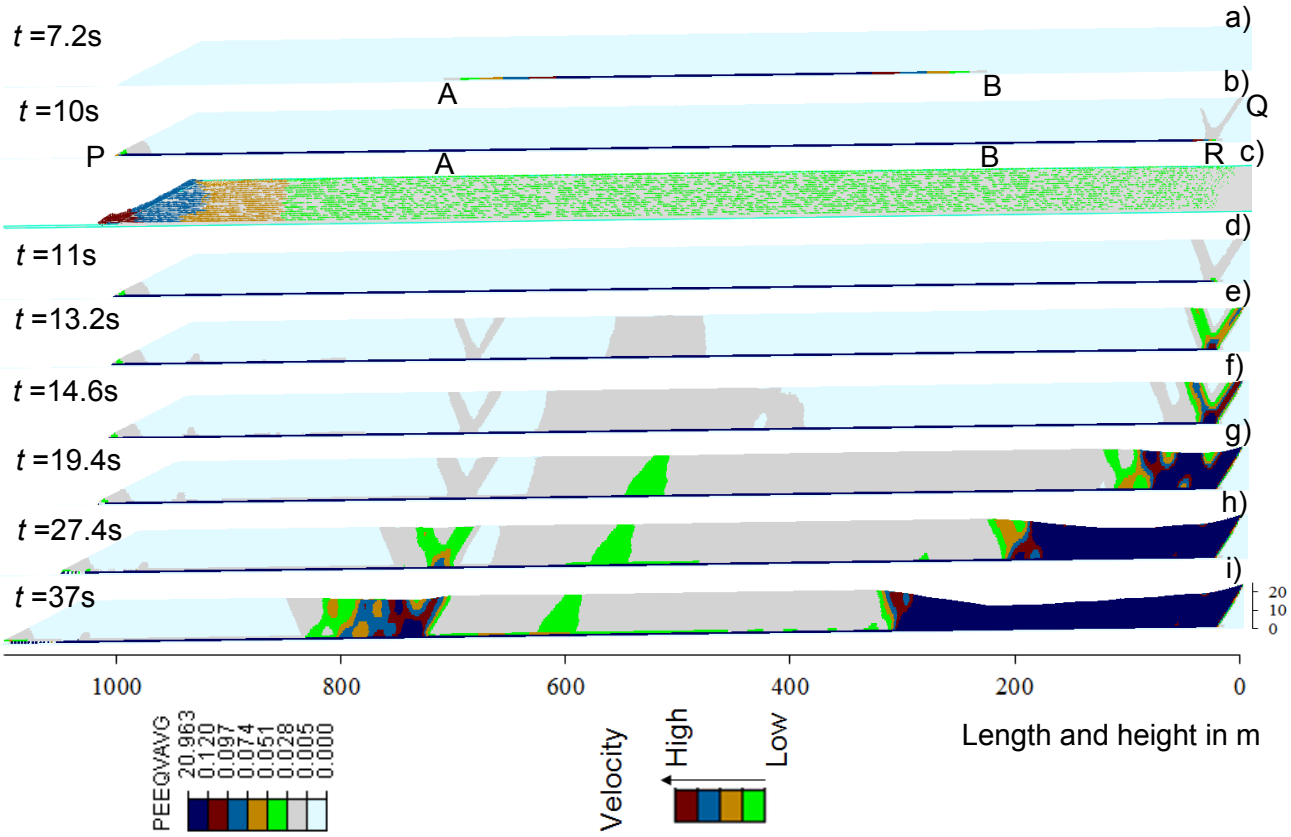

Figure 6. 6: Simulation NS-G19-M1: Shear band formation and instantaneous velocity of soil elements

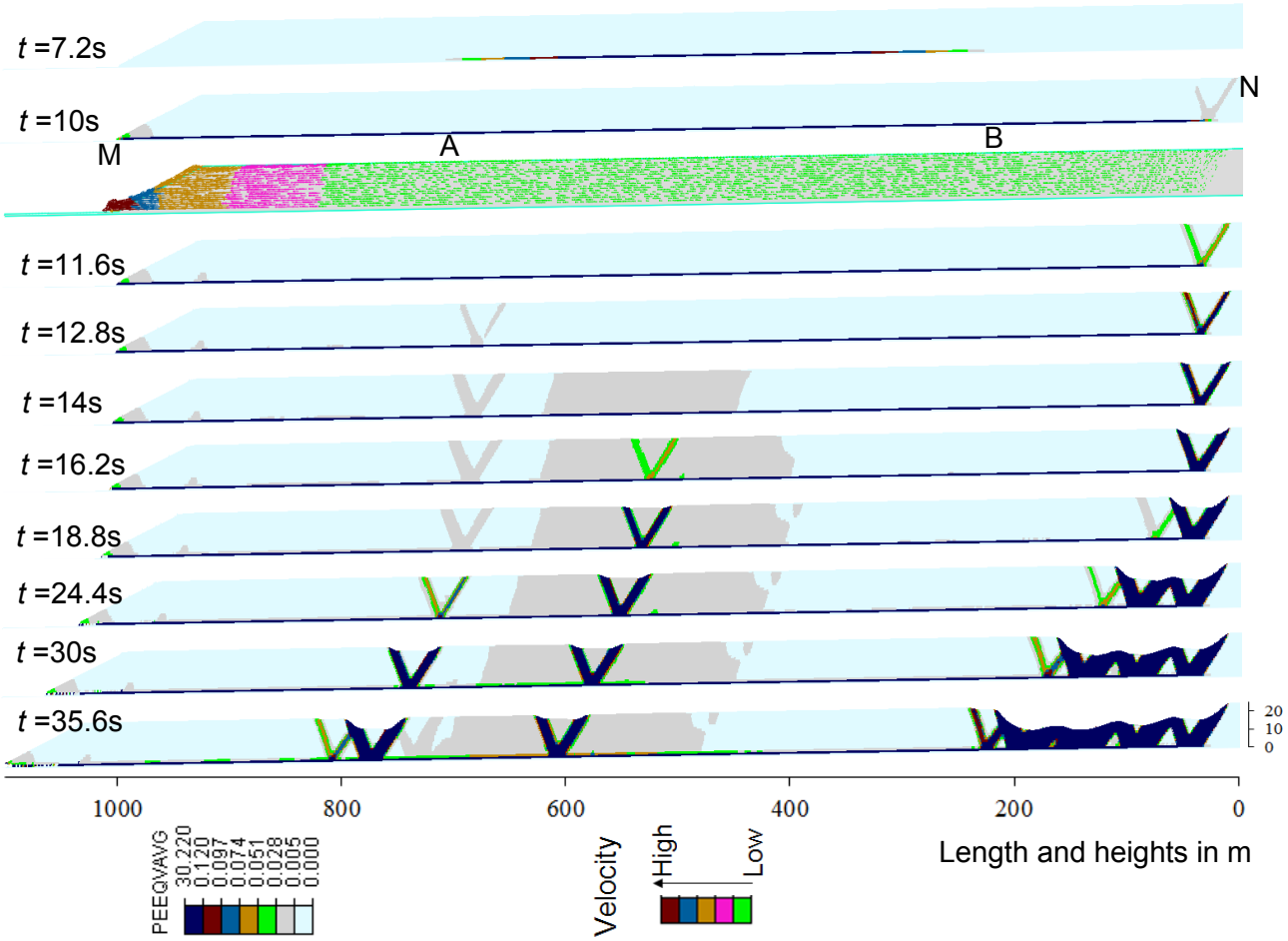

Figure 6. 7: Simulation LS-G19-M1: Shear band formation and instantaneous velocity of soil elements

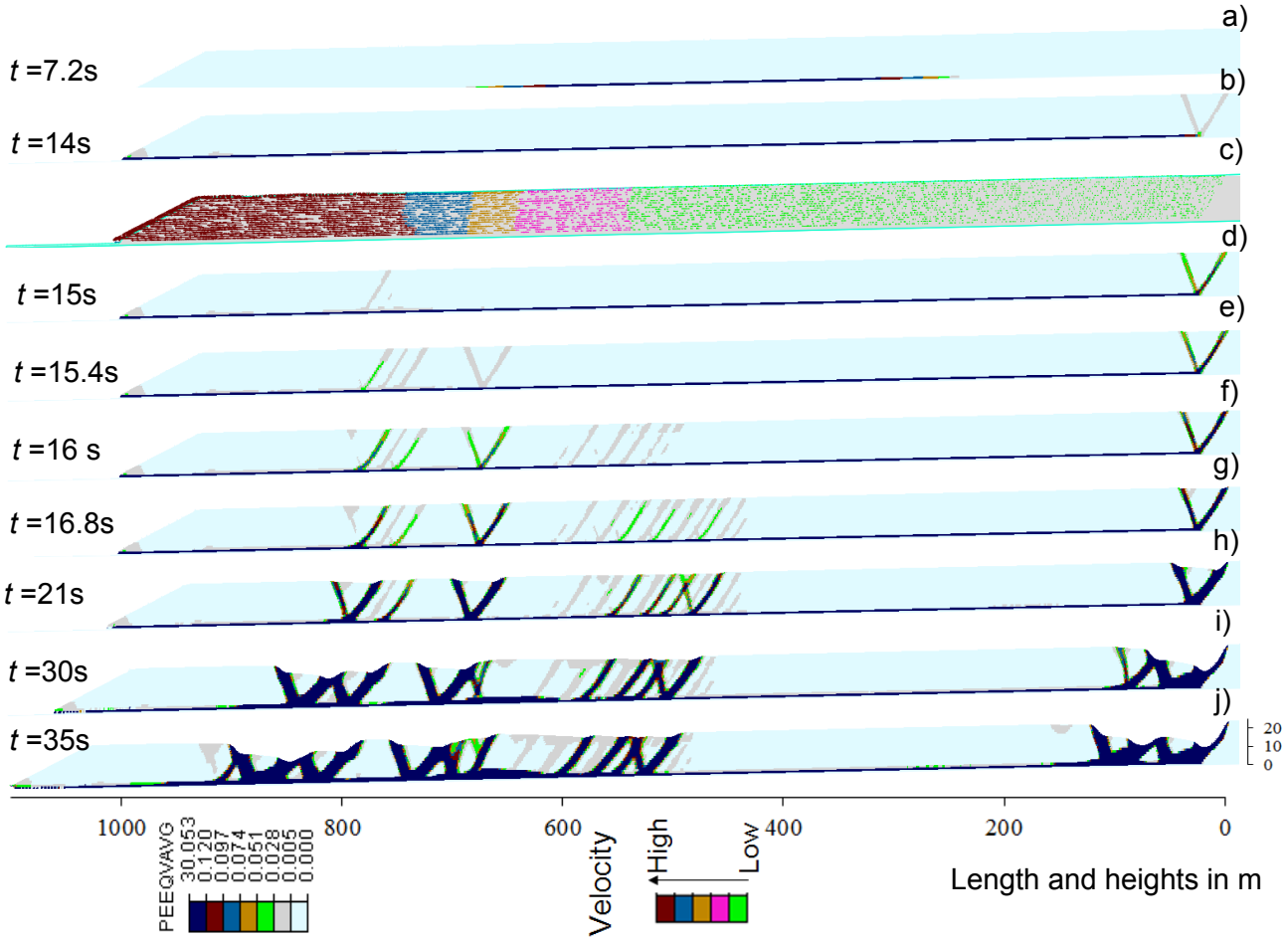

Figure 6. 8: Simulation NS-G5-M15: Development of shear surface and corresponding slope failure

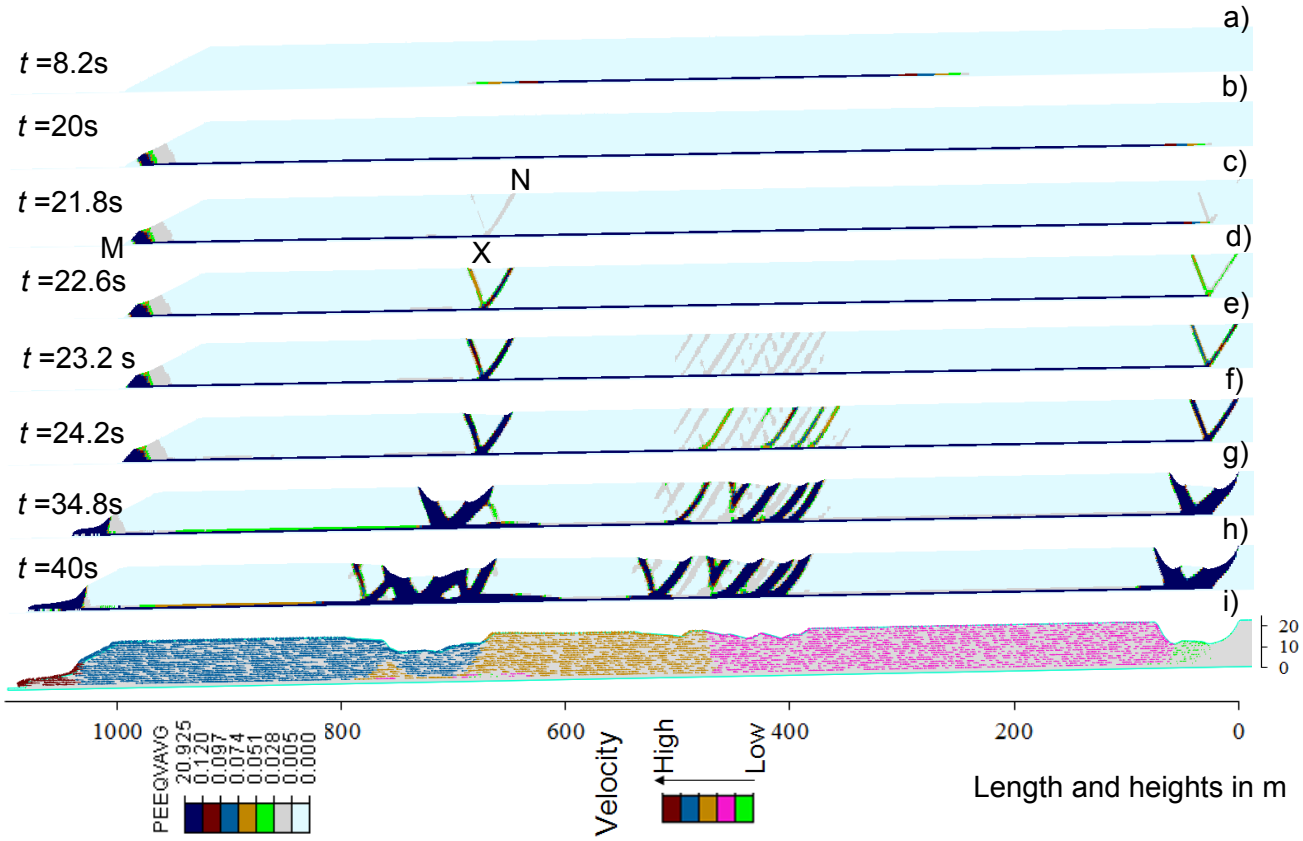

Figure 6. 9: Simulation M20: Development of shear surface and corresponding slope failure

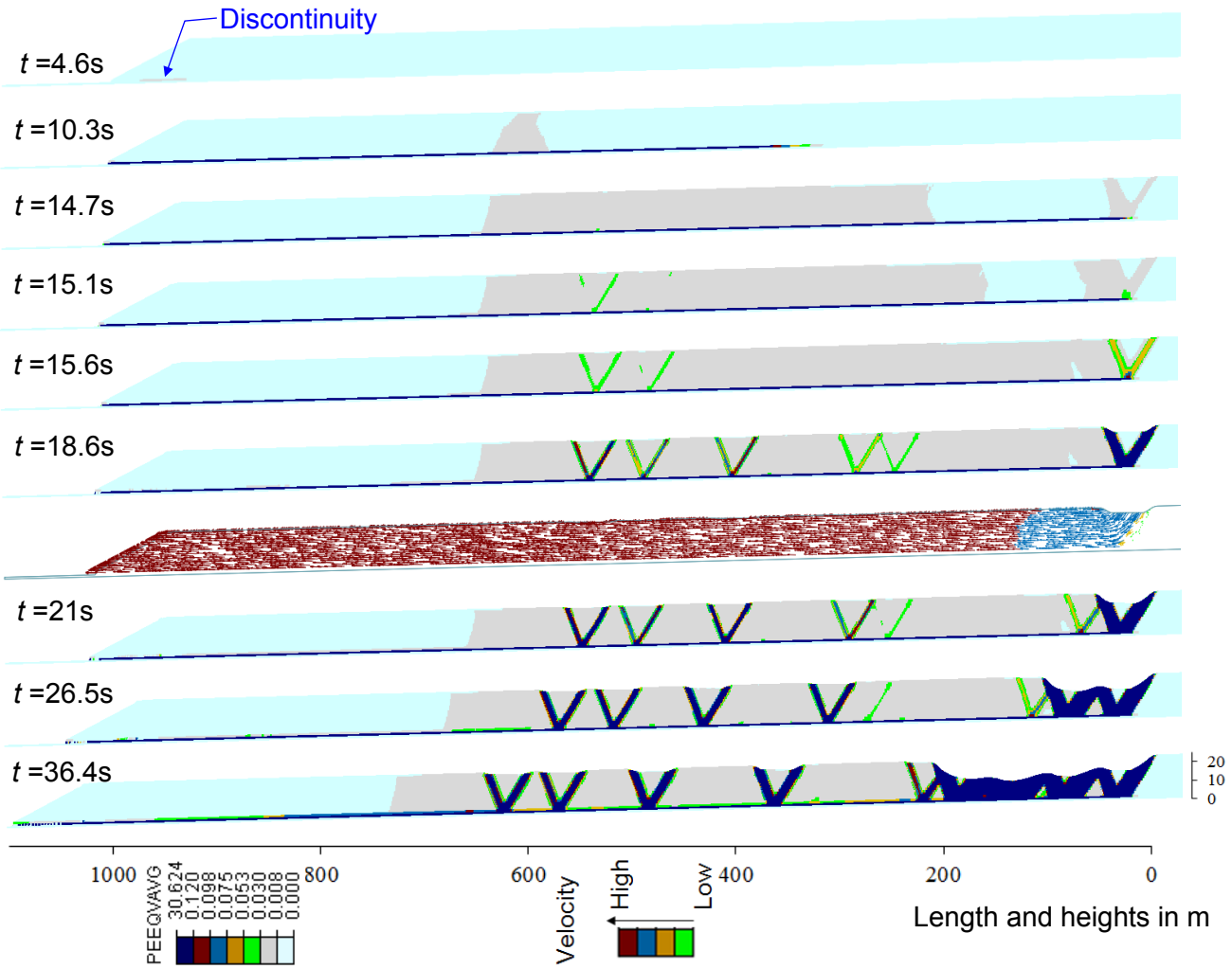

Figure 6. 10: Case-I: Development of shear surface and corresponding slope failure

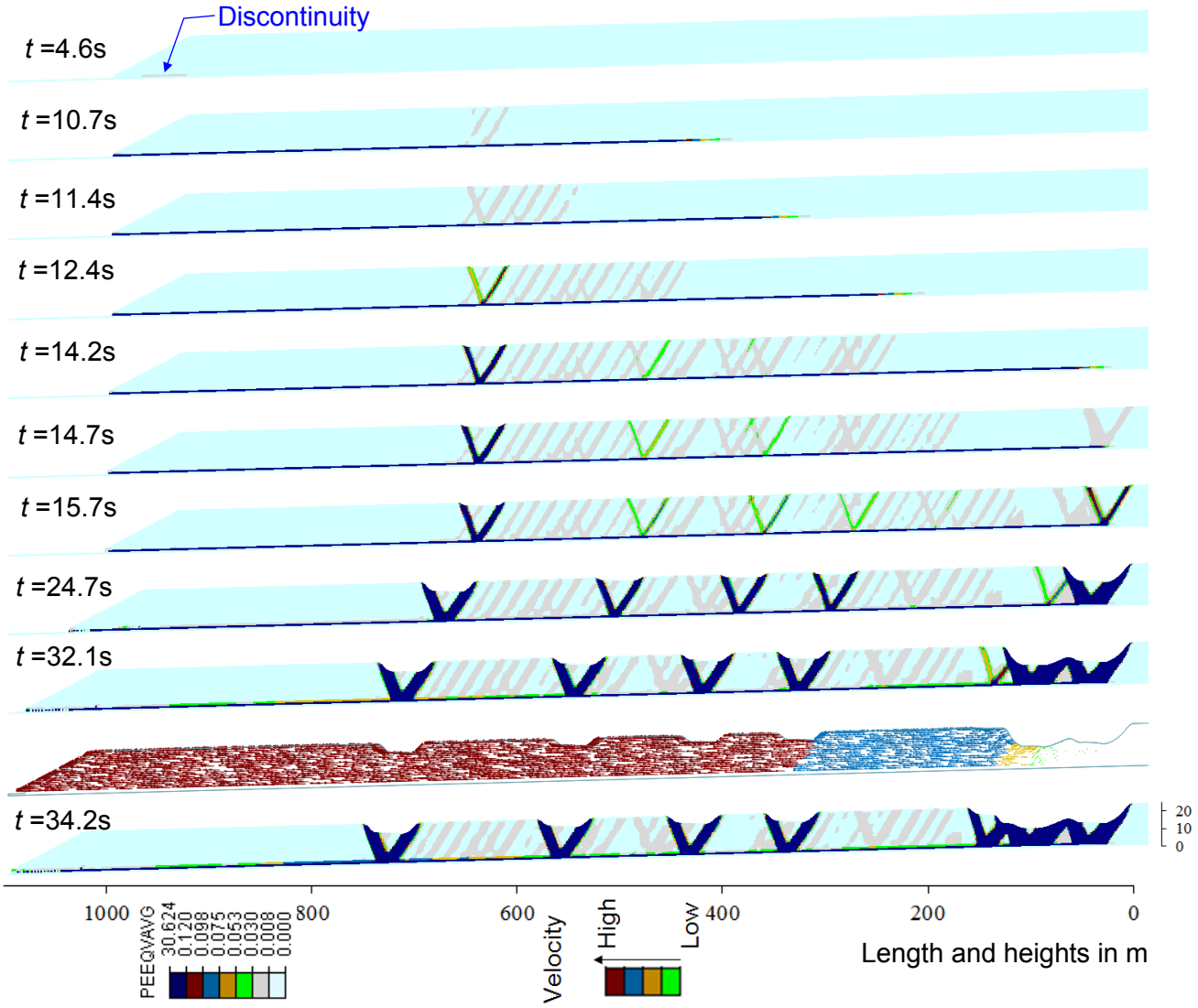

Figure 6. 11: Case-II: Development of shear surface and corresponding slope failure

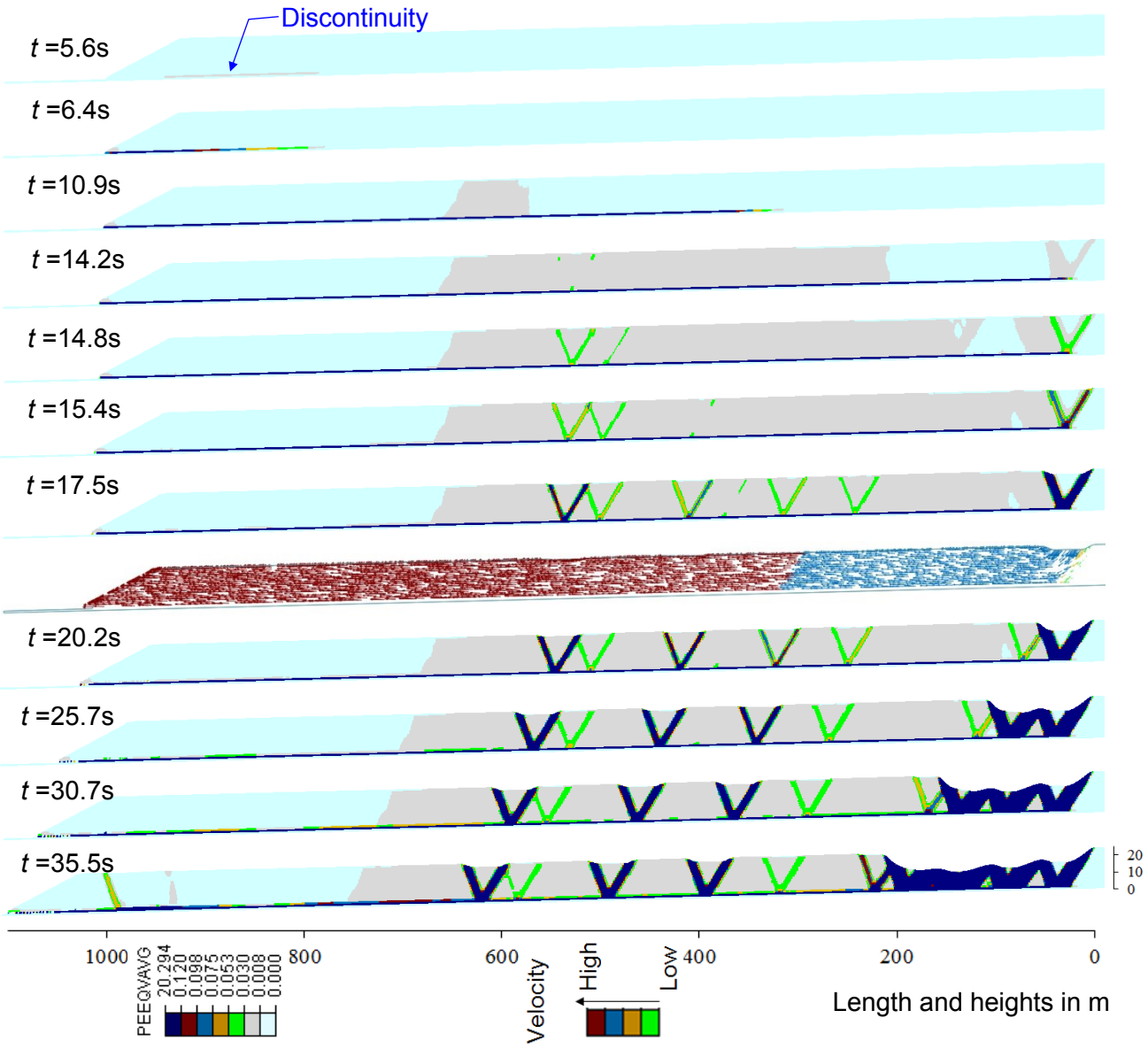

Figure 6. 12: Case-III: Development of shear surface and corresponding slope failure

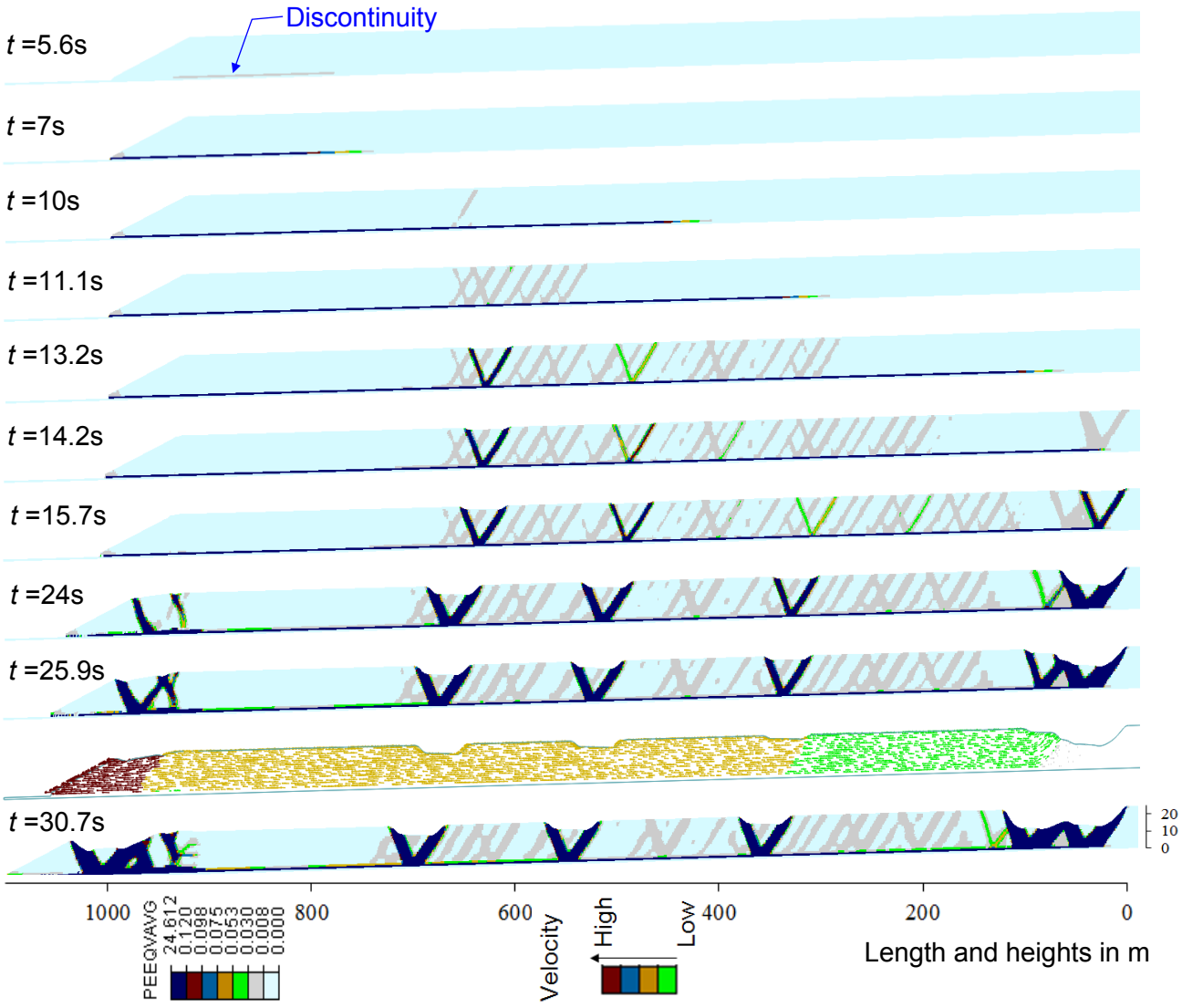

Figure 6. 13: Case-IV: Development of shear surface and corresponding slope failure

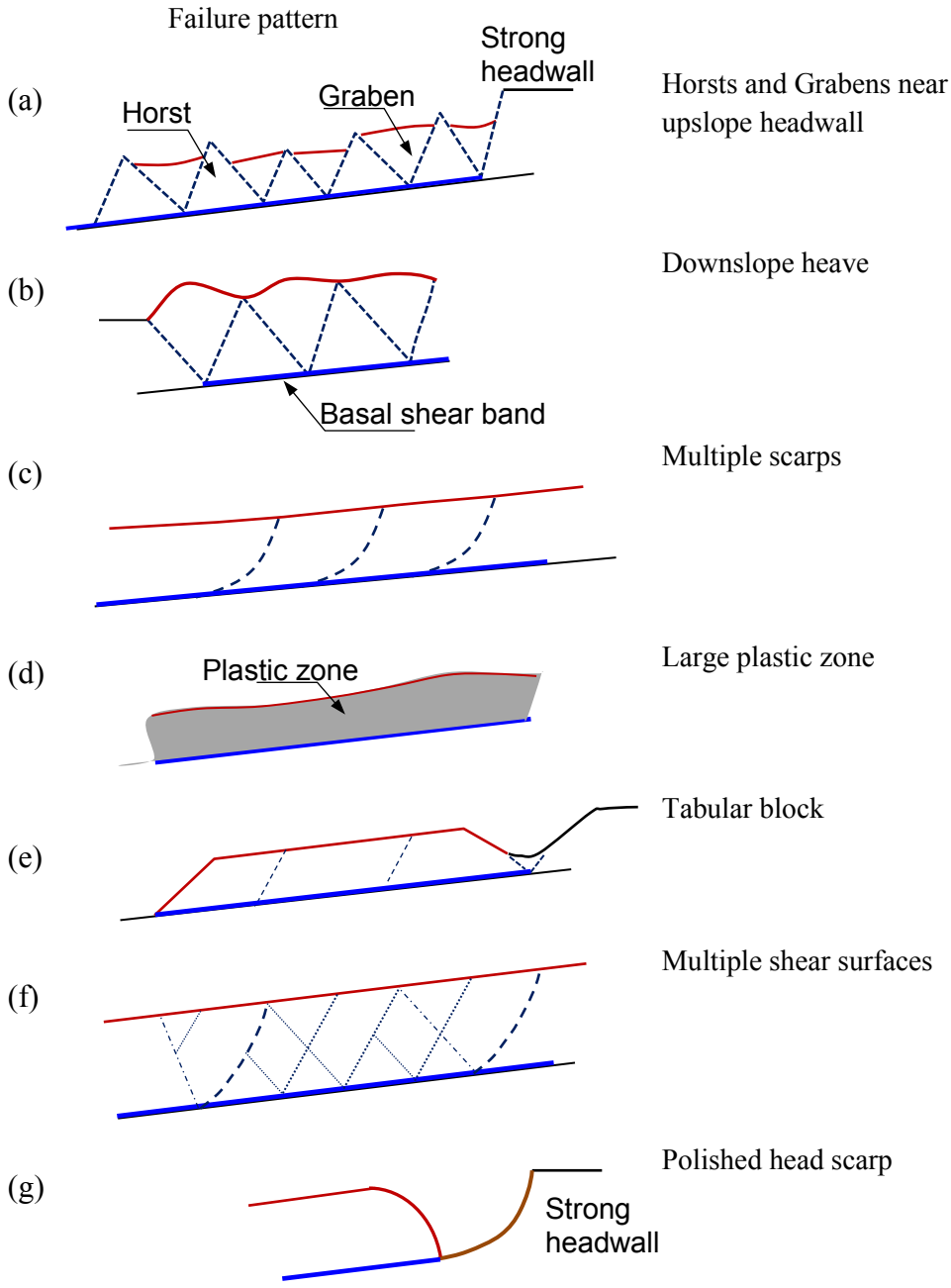

Figure 6. 14: Diagrammatic illustration of failure surface development

Table 6. 1: Parameters used for finite element modeling

Parameters	Value		
	Glacial clay	Marine clay	Base & Strong layers
Undrained Young's modulus, E_u (MPa)	30	15	200
Poisson's ratio, ν_u	0.495	0.495	0.495
Peak undrained shear strength, s_{up} (kPa)	50	40	
Sensitivity, S_t	1.5^{I}, $(1, 1.5,3)^{II}$	6	-
δ_{pc} (mm)	20^{I},$(-,20,10)^{II}$	3	-
δ_{95} (mm)	200	100	-
Submerged unit weight of soil, γ' (kN/m^3)	10	8	11

*for perfectly plastic condition δ_{pc} and δ_{95} are not applicable

[I] parameters for Model-I; [II] Parameters for Model-II

CHAPTER 7

Conclusions and Future Work

7.1 Conclusions

The stability of a slope involving a sensitive clay layer cannot be analyzed properly using the limit equilibrium methods commonly used in geotechnical engineering because the failure is progressive in nature. Finite element (FE) methods could be an alternative approach for modeling such problems. Attempts in the past for FE modeling to simulate the process of failure of slopes are mostly in the Lagrangian framework. However, in these FE modeling, significant mesh distortion occurs around the failure planes and the solutions generally suffer from mesh dependency, numerical instabilities and lack of convergence. Adopting additional measures, such as adaptive mesh refinement and inclusion of interface elements in the potential failure planes, the solution could be improved; however, predicting the location of the failure plane is required, otherwise FE modeling becomes computationally very expensive and cumbersome.

In the present study, the stability of sensitive clay slopes is analyzed using the Coupled Eulerian Lagrangian (CEL) approach in Abaqus FE software. It has numerous advantages. Firstly, the mesh is fixed and soil as Eulerian material flows through the fixed mesh; therefore, numerical issues related to mesh distortion are not expected even at very large strains in the shear band. Secondly, unlike mesh refinement techniques, a very fine mesh is not required to accommodate large strains. Finally, very large-scale landslides such as offshore landslides of more than a kilometer of length could be successfully simulated within an acceptable computational time. In

Abaqus, appropriate constitutive models for sensitive clays are not available as a built-in model. Therefore, a model has been developed for undrained stress-strain behaviour of sensitive clay.

Post-peak degradation of shear strength is the main cause of progressive failure of sensitive clay slopes. Experimental results show that the degradation of undrained shear strength (s_u) occurs over large shear strains. Based on experimental results available in the literature a nonlinear mathematical model is proposed for post-peak s_u degradation. The proposed model matches well with experimental results as compared to linear models proposed in the past. The model has been implemented in Abaqus FE software, and slope stability analyses have been performed for three classes of problems in onshore and offshore environments where progressive failure occurs through sensitive clay layers.

Toe erosion or small slides near the river bank are commonly observed in the field. Conducting large deformation FE analysis it is shown that toe erosion or small slides could be the cause of the formation of a horizontal shear band that can lead to a large landslide by formation of horsts and grabens. In the present FE model, the location of the failure plane is not predefined by the user rather they are identified by the FE program depending upon kinematic restraint. It is also shown that toe erosion will not always create horsts and grabens.

Only toe erosion may not cause global failure. In some cases toe erosion could create a horizontal shear band and subsequent loading in the upslope areas could cause a global failure of the slope. The present numerical analysis shows that for sensitive clay slopes the upslope load needs to be placed at a sufficiently large distance from the crest of the slope in order to avoid

global failure. The shear band from the upslope loaded area might propagate towards the previously developed shear band due to toe erosion.

The large deformation FE modeling of submarine slopes shows that progressive failure could create various different failure planes depending upon geometry and soil properties. A small discontinuity in the strain softening clay layer could create a long shear band parallel to the slope. While the initiation of a global failure could be calculated using the analytical model developed in Chapter 3, FE analysis is required for modeling of complete progressive failure of the slope. The failure planes and seabed deformation obtained from the present FE model are similar to seabed morphologies reported from post-failure investigations.

Finally, the above conclusions reflect the general overview of the entire thesis. Problem specific conclusions are presented at the end of each chapters (Chapter 3–6) and appendixes.

7.2 Recommendations for Future Research

While in the present study many features of failure of onshore and offshore slopes involved in sensitive clays are successfully simulated, it has some limitations. Some of the limitations are discussed at the end of Chapters 3–6. In addition, some of the following issues could be addressed in future research:

- The proposed nonlinear post-peak s_u degradation model is developed from a limited number of tests. This model could be verified further by conducting more laboratory tests on different sensitive clays.

- As mentioned in Chapter 2 (Fig. 2.2), at least three different types of progressive failure in sensitive clay were observed in the field. In the present study, mainly the spread and formation of horsts and grabens are discussed. Other types of failure and the conditions required for this type of failure need to be investigated further.
- Additional parametric study is required varying different conditions such as geometry of slope, soil properties, initial stress and size of erosion block. It is to be noted that the numerical analysis using CEL is generally computationally expensive.
- Although the element size scaling rule used in this study significantly improves the simulation further studies on mesh dependency is required.
- For submarine slopes, only one layer of strain softening clay layer is considered. However, in the field multiple layers of strain softening materials might be present.

Finally, although the analyses have been performed for selected geometry, triggering factors and undrained conditions, the present modeling technique could be extended further for other loading conditions and geometries.

References

Almagor, G. and Wiseman, G. 1991. Analysis of submarine slumping in the continental slope off the southern coast of Israel. Marine Geotechnology, **10**(3-4): 303–342.

Andresen, L. 2001. Effect of strain softening on stability analyses. Analysis of retrogressive sliding due to strain softening—Ormen Lange case study. NGI report No. 521001-10.

Andresen, L. and Jostad, H.P. 2002. A constitutive model for anisotropic and strain softening clay. *In* Proc. NUMOG VIII, Rome, Italy, 79–83.

Andresen, L. and Jostad, H.P. 2004. Analyses of progressive failure in long natural slopes. *In* Proc. 9th Symposium on Num. Models in Geomech.- NUMOG IX Ottawa, Ont., 603–608.

Andresen, L. and Jostad, H.P. 2007. Numerical modeling of failure mechanisms in sensitive soft clays- application to offshore geohazards. Offshore Tech. Conf., Texas. Paper OTC 18650.

Assier-Rzadkiewicz, S., Heinrich, P., Sabatier, P. C., Savoye, B. and Bourillet, J. F. 2000. Numerical modelling of a landslide-generated tsunami: the 1979 Nice event. Applied Geophysics, **157**:1717–1727.

Barnes, P.M. and Lewis, K.B., 1991. Sheet slides and rotational failures on a convergent margin: The Kidnappers Slide, New Zealand. Sedimentology, **38**: 205–221.

Bernander, S. 2000. Progressive failure in long natural slopes: formation, potential extension and configuration of finished slides in strain-softening soils. Licentiate Thesis, Luleå University of Technology.

Bernander S. 2008. Down-hill progressive landslides in soft clays, triggering disturbance agents, slide propagation over horizontal or gently sloping ground, sensitivity related to geometry. Luleå University of Technology, Luleå, Sweden. Research report.

Bjerrum, L. 1955. Stability of natural slopes in quick clay. Géotechnique, **5**(1): 101–119.

Bjerrum, L. 1967. Progressive failure in slopes in overconsolidated plastic clay and clay shales. Terzaghi Lecture. J. of the Soil Mech. and Found. Div., ASCE, **93**(5): 3–49.

Brink, U.S.T., Lee, H.J., Geist, E.L. and Twichell D. 2009. Assessment of tsunami hazard to the U.S. East Coast using relationships between submarine landslides and earthquakes. Marine geology, **264**(1-2): 65–73.

Bryn, P., Berg, K., and Solheim, A. 2002. Storegga Geomodel and its use in slide risk evaluation. Int. Conf. Offshore Site Investigation and Geotechnics, London, 219–232.

Bryn, P., Berg, K., Forsberg, C. F., Solheim, A. and Kvalstad, T.J. 2005. Explaining the Storegga slide. Marine Petroleum Geology, **22**: 11–19.

Burland, J.B., Longworth, T.I. and Moore, J.F.A. 1977. A study of ground movement and progressive failure caused by a deep excavation in Oxford Clay. Géotechnique, **27**(4): 557–591.

Canals, M., Lastras, G., Urgeles, R., Casamor, J. L., Mienert, J., Cattaneo, A., Batist, M. De., Haflidason, H., Imbo, Y., Laberg, J. S., Locat, J., Long, D., Longva, O., Masson, D.G., Sultan, N., Trincardi, F. and Bryn, P. 2004. Slope failure dynamics and impacts from seafloor and shallow sub-seafloor geophysical data: case studies from the COSTA project. Marine Geology, **213**(1-4): 9–72. doi:10.1016/j.margeo.2004.10.001.

Carson, M.A. 1977. On the retrogression of landslides in sensitive muddy sediments. Canadian Geotechnical Journal, **14**(4): 582–602.

Christian, J.T. and Whitman, R. V. 1969. A one dimensional model for progressive failure. In Proc. 7th Int. Conf. Soil Mechanics & Foundation Engineering, Mexico City, 541–545.

Christian, H.A., Mudler, T., Courtney, R.C., Mosher, D.C., Barrie, J.V., Currie, R.G., Olynyk, H.W., and Monahan, P.A., 1994. Slope instability on the Fraser River Delta foreslope, Vancouver, British Columbia. 47th Canadian Geotechnical Conference, Halifax, 155–165.

Chowdhury, R.N. 1978. Propagation of failure surfaces in natural slopes. Journal of Geophysical Resources, **83**(B12): 5983–5988.

Coleman J. M. and Prior, D. B. 1978. Submarine landslides in the Mississippi river delta. OTC – paper No 3170, 1067–1074.

Conte, E., Silvestri, F. and Troncon, A. 2010. Stability analysis of slopes in soils with strain-softening behaviour. Computers and Geotechnics, **37**(5): 710–722.

Conway, K. W., Barrie, J. V. and Thomson, R. E. 2012. Submarine slope failures and Tsunami Hazard in Coastal British Columbia: Douglas Channel and Kitimat Arm. Geological Survey of Canada, Current Research 2012-10, 13 p. doi: 10.4095/291732.

Cruden, D.M. and Varnes, D.J. 1996. Landslides types and processes. In Landslides investigation and mitigation. Special Report 247. Transport. Research Board, National Research Council. Ed. by A.K. Turner and R.L. Schuster. National Academy Press, Washington, 37–75.

Dan, G., Sultan, N. and Savoye, B. 2007. The 1979 Nice harbour catastrophe revisited: Trigger mechanism inferred from geotechnical measurements and numerical modelling. Marine Geology, **245**(1-4), 40–64.

Dave Peter, 2010. The mechanism of the Highway 3 landslide in Taiwan. The landslide blog, http://blogs.agu.org/landslideblog/2010/04/26/the-mechanism-of-the-highway-3-landslide-in-taiwan/.

Demers, D., Robitaille, D., Locat, P. and Potvin, J. 2013. Inventory of large landslides in sensitive clay in the province of Quebec, Canada: preliminary analysis. *In* Proc. of the 1st Int. Workshop on Landslides in Sensitive Clays, Landslides in Sensitive Clays –From Geosciences to Risk Management, Québec, Que.

DeGroot, D.J., DeJong, J.T., Yafrate, N.J., Landon, M.M. and Sheahan, T.C. 2007. Application of recent developments in terrestrial soft sediment characterization methods to offshore environments. Proc. Offshore Technology Conference, Houston, USA. OTC 18737.

DeGroot, D.J., Lunne, T. and Tjelta, T.I. 2011. Recommended best practice for geotechnical site characterisation of cohesive offshore sediments. *In* Proc. Int. Symp. on Frontiers in Offshore Geotechnics II, Gourvenec & White (eds)., 33–57.

Devin, S.C. and Sandford, T.C. 2000. Shear strength of sensitive clay slopes in maine. Proceedings of the session on Slope Stability at GeoDenver, 114–128.

Dey, R., Hawlader, B., Phillips, R. and Soga, K. 2011. Modeling of Earthquake Induced Pore Pressure and Submarine Slope Stability Analysis. 2011 Pan-Am CGS Geotechnical Conference, Toronto, Canada.

Dey, R., Hawlader, B., Phillips, R. and Soga, K. 2012. Effects of shear band propagation on Submarine Landslide. International Society of Offshore and Polar Engineering Conference-2012, Rhodes Conference, Greece.

Dey, R., Hawlader, B., Phillips, R. and Soga, K. 2013. Progressive failure of slopes with sensitive clay layers. The 18th International Conference on Soil Mechanics and Geotechnical Engineering-2013, Paris, France.

Dey, R., Hawlader, B., Phillips, R. and Soga, K. 2014. Stability analysis of a river bank slope with an existing shear band. 6th Canadian GeoHazards Conference, GeoHazards6, Ontario.

Dey, R., Hawlader, B., Phillips, R. and Soga, K. 2015(a). Modeling of large deformation behaviour of marine sensitive clays and its application to submarine slope stability analysis. Canadian Geotechnical Journal (under review).

Dey, R., Hawlader, B., Phillips, R. and Soga, K. 2015(b). Large deformation finite element modeling of progressive failure leading to spread in sensitive clay slopes. Géotechnique (accepted).

Dey, R., Hawlader, B., Phillips, R. and Soga, K. 2015(c). Numerical modeling of combined effects of upward and downward propagation of shear bands on stability of slopes with sensitive clay. Computers and Geotechnics (resubmitted addressing review comments).

Dey, R., Hawlader, B., Phillips, R. and Soga, K. 2015(d). Numerical modeling of submarine landslides in marine clays. Journal of Geotechnical and Geo-environmental Engineering, ASCE (under review).

Dey, R., Hawlader, B. and Chen, W. 2015(e). Progressive failure of offshore slopes due to construction in upslope areas. 34th International Conference on Ocean, Offshore and Arctic, St. John's, NL.

Dimakis, P., Elverhøi, A., Høeg, K., Solheim, A., Harbitz, C., Laberg, J.S., Vorren, T.O. and Marr, J. 2000: Submarine slope stability on high latitude glaciated Svalbard-Barents Sea margins. Marine Geology **162**: 303–316.

Duncan, J.M. 1996. State of the art: limit equilibrium and finite element analysis of slopes. J of Geotechnical and Geoenvironmental Engineering (ASCE), **122**(7): 577–596.

Field, M.E., Gardner, J.V., Jennings, A.E. and Edwards B.D. 1982. Earthquake-induced sediment failures on a 0.25° slope, Klamath River delta, California. Geology, **10**: 542–546.

Fine, I. V., Rabinovich, A. B., Bornhold, B. D., Thomson, R. E. and Kulikov, E. A. 2005. The Grand Banks landslide-generated tsunami of November 18, 1929: preliminary analysis and numerical modelling. Marine Geology, **215**: 45–57.

Fortin, A., Ouellet, D., P aradis, S. and Demers, D. 2008. Développement au Ministère des Transports du Québec d'un porail informatique pour l'accès à des bases de données géotechnique. *In* Proc. of the 4th Canadian Conf. on Geohazards: From Causes to Management, Québec. Edited by J. Locat, D. Perret, D. Turmel, D. Demers, and S. Leroueil. Presses de l 'Université Laval, Québec, 169–174.

Gardner, J.V., Prior, D.B. and Field, M.E. 1999. Humboldt Slide – A Large Shear-Dominated Retrogressive Slope Failure, Marine Geology, **154**: 323–338.

Gauer, P., Kvalstad, T. J., Forsberg, C. F., Bryn, P. and Berg, K. 2005. The last phase of the Storegga Slide: simulation of retrogressive slide dynamics and comparison with slide-scar morphology. Marine and Petroleum Geology, **22**(1-2): 171–178.

Gee, M. J. R., Gawthorpe, R.L. and Friedmann, J.S. 2005. Giant striations at the base of a submarine landslide. Marine Geology, **214**(1-3): 287–294.

Griffiths, D. V. and Lane, P. A. 1999. Slope stability analysis by finite elements. Géotechnique, **49**(3): 387–403.

Grondin, G. and Demers, D. 1996. The Saint-Liguori flake slide: characterization and remedial works. *In* Proc. of the 7th Int. Symposium on Landslides, Trondheim, Norway. Edited by K. Senneset. Balkema, Rotterdam, the Netherlands, **2**:743–748.

Gylland, A. S., Sayd, M. S., Jostad, H. P. and Bernander, S. 2010. Investigation of soil property sensitivity in progressive failure. *In* Proc. of the 7th European Conf. on Num. Methods in Geotech. Eng., Benz & Nordal eds., Trondheim, Norway, 515–520.

Gylland, A.S., Nordal, S., Jostad, H.P. and Mehli, M. 2011. Pragmatic approach for estimation of slope capacity in soft sensitive clay. Electronic J. of Geotechnical Engg. **16**: 575–590.

Gylland, A. S. 2012. Material and slope failure in sensitive clays. PhD thesis, Norwegian University of Science and Technology.

Hadj-Hamou, T. and Kavazanjian, E. Jr. 1985. Seismic stability of gentle infinite slopes. Journal of Geotechnical Engineering, ASCE, **111**(6): 681–697.

Haflidason, H., Lien, R., Sejrup, H. P., Forsberg, C. F. and Bryn, P. 2005. The dating and morphometry of the Storegga slide. Marine Pet. Geology **22**: 123–136.

Hampton, M.A., Lee, H.J. and Locat, J. 1996. Submarine landslides. Reviews of Geophysics, **34**: 33–59.

Harders, R., Ranero, C. R., Weinrebe, W. and Behrmann, J. H. 2011. Submarine slope failures along the convergent continental margin of the Middle America Trench. Geochemistry, Geophysics and Geosystems, **12**(6): 1–26.

Hünerbach, V., Masson, D.G. and partners of the COSTA-Project 2004. Landslides in the North Atlantic and its adjacent seas: an analysis of their morphology, setting and behaviour. Marine Geology, **213**: 343–362.

Jostad, H. P. and Andresen, L. 2002. Capacity analysis of anisotropic and strain-softening clays. *In* Proc. of NUMOG VIII, Rome, Italy, 469–474.

Jostad, H.P. and Andresen, L. 2004. Modeling of shear band propagation in clays using interface elements with finite thickness. *In* Proc. of the 9th Symposium on Num. Models in Geomech., Canada, 121–128.

Jostad, H.P., Andresen, L. and Thakur, V. 2006. Calculation of shear band thickness in sensitive clays. *In* Proc. 6th European Conf. Num. Methods in Geotech. Eng., Graz, Austria, 27–32.

Karlsrud, K. and Edgers, L. 1982. Some aspects of submarine slope stability. Marine Slides and Other Mass Movements, **6**: 61-81.

Karlsrud, K., Aas, G. and Gregersen, O. 1984. Can we predict landslide hazards in soft sensitive clays? Summary of Norwegian practice and experiences. In Proceedings of the 4th Int. Symposium on Landslides, Toronto, Ont., 16 –21 September 1984.

Kovacevic, N., Hight, D.W. and Potts, D.M. 2004. Temporary slope stability in London clay - Back analyses of two case histories. In Advances in geotechnical engineering: The Skempton Conference, London. Thomas Telford Publishing, London, **2**: 842–855.

Kovacevic, N., Hight, D.W. and Potts, D.M. 2007. Predicting the stand-up time of temporary London Clay slopes at Terminal 5, Heathrow Airport. Géotechnique, **57**(1): 63–74.

Krastel, S., Wynn, R. B., Hanebuth, T. J. J., Henrich, R., Holz, C., Meggers, H., Kuhlmann, H., Georgiopoulou, A. and Schulz, H. D. 2006. Mapping of seabed morphology and shallow sediment structure of the Mauritania continental margin, North-west Africa: some implications for geohazard potential. Norwegian Journal of Geology, **86**: 163–176.

Kvalstad, T.J., Gauer, P., Kayma, A.M., Nadim, F. and Bryn, P. 2002. Slope Stability at Ormen Lange. International Conf. Offshore Site Investigation and Geotechnics, London, 233–250.

Kvalstad, T.J., Andresen, L., Forsberg, C.F., Berg, K., Bryn, P. and Wangen, M. 2005a. The Storegga slide: evaluation of triggering sources and slide mechanics. Marine Petroleum Geology **22**: 245–256.

Kvalstad, T.J., Nadim, F., Kaynia, A.M., Mokkelbost, K.H. and Bryn, P. 2005b. Soil conditions and slope stability in the Ormen Lange area. Marine Petroleum Geology, **22**(1-2): 299–310.

Ladanyi, B., Morin, J.P. and Pelchat, C. 1994. Post-peak behavior of sensitive clays in undrained shear. Canadian Geotechnical Journal **2**: 59–68.

Laberg, J.S., Vorren, T.O., Mienert, J., Haflidason, H., Bryn, P., and Lien, R. 2003. Preconditions leading to the Holocene reconditions leading to the holocene trænadjupet slide offshore Norway. In J. Locat and J. Mienert(eds): Submarine Mass Movement and Their Consequences, 247–254.

Lastras, G., Canals, M., Urgeles, R., Hughes-Clarke, J. E. and Acosta, J. 2004. Shallow slides and pockmark swarms in the Eivissa Channel, western Mediterranean Sea. Sedimentology, **51**: 1–14.

Lee, H. J. and Edwards, B. D. 1986. Regional method to assess offshore slope stability. Journal of Geotechnical Engineering, **112**(5): 489–509.

Lee, H.J. and Baraza, J., 1999. Geotechnical characteristics and slope stability in the Gulf of Cadiz. Marine Geology, **155**: 173–190.

Lefebvre G., Ladd C., Paré J. 1988. Comparison of field vane and laboratory undrained shear strength in soft sensitive clays. ASTM special technical publication, **1014**: 233–246.

Leynaud, D., Mienert, J. and Nadim, F. 2004. Slope stability assessment of the Helland Hansen area offshore the mid-Norwegian margin. Marine Geology, **213**(1-4): 457–480.

L'Heureux, J. S., Hansen, L., Longva, O., Emdal, A. and Grande, L. 2010. A multidisciplinary study of submarine landslides at the Nidelva fjord delta, Central Norway – implications for geohazards assessments. Norwegian Journal of Geology, **90**: 1–20.

L'Heureux, J. S., Longva, O., Steiner, A., Hansen, L., Vardy, M.E., Vanneste, M., Haflidason, H., Brendryen, J., Kvalstad, T.J., Forsbeg, C.F., Chand, S. and Kopf, A. 2012. Identification of weak layers and their role for the stability of slopes at Finneidfjord, Northern Norway. Submarine mass movements and their consequences, Yamada Y et al. eds., Advances in natural and technological hazards research, **31**: 321–330.

L'Heureux, J. S., Locat, A., Leroueil, S., Demers, D. and Locat, J. 2014. Landslides in sensitive clays – From Geosciences to Risk Management. Advances in Natural and Technological Hazards Research, Springer, ISBN 978-94-007-7079-9 (eBook).

Li, W., Wu, S., Völker, D., Zhao, F., Mi, L. and Kopf A. 2014. Morphology, seismic characterization and sediment dynamics of the Baiyun Slide Complex on the northern South China Sea margin. Journal of the Geological Society, London.

Lo, K.Y. and Lee, C.F. 1973. Stress analysis and slope stability in strain softening materials. Géotechnique, **23**(1): 1–11.

Locat, J. and Lee, H. J. 2000. Submarine Landslides: Advances and Challenges. In Proceedings of the 8th International Symposium on Landslides, Cardiff, U.K., June 2000.

Locat, J. and Lee, H.J. 2002. Submarine landslides: advances and challenges. Canadian Geotechnical Journal, **39**: 193–212.

Locat, A., Leroueil, S., Bernander, S., Demers, D., Locat, J. and Ouehb, L. 2008. Study of a lateral spread failure in an eastern Canada clay deposit in relation with progressive failure: the Saint-Barnabé-Nord slide. In Proc. of the 4th Canadian Conf. on Geohazards: From Causes to Management, Québec, 89–96.

Locat, J., Lee, H., Brink, U. S., Twichell, D., Geist, E. and Sansoucy, M. 2009. Geomorphology, stability and mobility of the Currituck slide. Marine Geology, **264**(1-2): 28–40.

Locat, A., Leroueil, S., Bernander, S., Demers, D., Jostad, H.P. and Ouehb, L. 2011. Progressive failures in eastern Canadian and Scandinavian sensitive clays. Canadian Geotechnical Journal, **48**(11): 1696–1712.

Locat, A. 2012. Rupture progressive et etalements dans Les argiles sensibles. PhD thesis, Université Laval, Québec.

Locat, A., Jostad, H. P. and Leroueil, S. 2013. Numerical modeling of progressive failure and its implications for spreads in sensitive clays. Canadian Geotechnical Journal, **50**: 961–978.

Locat, J., Leroueil, S., Locat, A. and Lee, H. 2014. Weak layers: their definition and classification from a geotechnical perspective. Submarine Mass Move. and Conseq., *edited* by S. Krastel et al., Advances in Natural and Technological Hazards Research, **37**: 3–12.

Locat, A., Leroueil, S., Fortin, A., Demers, D. and Jostad, H.P. 2015. The 1994 landslide at Sainte-Monique, Quebec: geotechnical investigation and application of progressive failure analysis. Canadian Geotechnical Journal, **52**: 490–504.

Lunne, T., Berre T., Andersen, K.H., Strandvik, S., and Sjursen M., 2006. Effect of sample disturbance and consolidation procedures on measured shear strength of soft marine Norwegian clays. Can Geotech J., **43:** 726–750.

Lunne, T. and Andersen, K.H. 2007. Soft clay shear strength parameters for deep water geotechnical design. Proceedings of the 6th International Offshore Site Investigation and Geotechnics Conference, London, UK, 151–176.

Low, H.E., Lunne, T., Andersen, K. H., Sjursen, M.A., LI, X. and Randolph M. F. 2010. Estimation of intact and remoulded undrained shear strengths from penetration tests in soft clays. Géotechnique, **60**(11): 843–859.

Masson, D. G., Watts, A. B., Gee, M. R. J., Urgeles, R., Mitchell, N. C., Le Bas, T. P. and Canals, M. 2002. Slope failures on the flanks of the western Canary islands. Earth Science Rev., **57**: 1–35.

Masson, D.G., Harbitz, C.B., Wynn, R.B., Pedersen, G. and Løvholt, F. 2006. Submarine landslides: processes, triggers and hazard prediction. Phil. Trans. R. Soc. A, **364**: 2009–2039.

McAdoo, B. G. 1999. Mapping submarine slope failures. Marine and Coastal Geographical Information Systems, D. J. Wright and D. J. Barlett eds., 189–205.

McAdoo, B., Pratson, G., Orange, L.F., 2000. Submarine landslide geomorphology, US Continental Slope. Marine Geology, **169**: 103–136.

McKenna, G.T., Luternauer, J.L., and Kostaschuk, R.A. 1992. Large-scale mass-wasting events on the Fraser River delta front near Sand Heads, British Columbia. Canadian Geotechnical Journal, **29**: 151–156.

Mello, U. T. and Pratson, L. F. 1999. Regional slope stability and slope-failure mechanics from the two-dimensional state of stress in an infinite slope. Marine Geology, **154**(1-4): 339–356.

Mosher, D.C., Moran, K. and Hiscott, R.N., 1994. Late quaternary sediment, sediment mass flow processes and slope stability on the Scotian slopes. Sedimentology, **41**: 1039–1061.

Moore, J. G., Clague, D. A., Holcomp, R. T., Lipman, P. W., Normark, W. R. and Torresan, M. E.1989. Prodigious submarine landslides on the Hawaiian Ridge. Journal of Geophysical Research, **94**: 17465–17484.

Morgenstern, N.R., 1967. Submarine slumping and the initiation of turbidity currents. *In*: A.F. Richards (Editor), Marine Geotechnique, University of Illinois Press, Urbana, **Ill**., 189–210.

Mulder, T., Berry, J. A., and Piper, D. J.W. 1997. Links between the morphology and geotechnical characteristics of large debris flow deposits in the Albatross area on the Scotian Slope (SE Canada). Marine Georesources and Geotechnology, **15**: 253–281.

Murty, T.S. and Brown, R.E. 1979. The Submarine Slide of 27 April, 1975 in Kitimat Inlet and the Water Waves That Accompanied the Slide: Pacific Marine Science Report 79–11.

ICG (International Center for Geohazards) 20010. Offshore Geohazards. NGI, http://www.ngi.no/en/Geohazards/Research/Offshore-Geohazards/.

Normark, W. R., Wilde, P., Campbll, J.F., Chase, T.E. and Tsutsui, B. 1993. Submarine slope failure initiated by Hurricane Iwa, Kahe Point, Oahu, Hawaii. In: Submarine Landslide: Selected Studies in the U.S. Exclusive Economic Zone (Eds. Schwab, W.C., Lee, H.J. and Twichell, D.C.), U.S. Geological Survey Bulletin 2002, 197–204.

Odenstad, S. 1951. The landslide at Sköttorp on the Lidan River, February 2, 1946. Royal Swedish Institute Proceedings, **4:**1–38.

O'Leary, D. W. 1991. Structure and morphology of submarine slab slides: clues to origin and behaviour. Marine Geotechnology, **10**: 53–69.

Palmer, C. and Rice, J.R. 1973. The growth of slip surfaces in the progressive failure of overconsolidated clay. Proceedings of the Royal Society of London. Series A: Mathematical, Physical and Engineering Sciences, **332**: 527–548.

Piper, D. J.W., Farre, J.A. and Shor, A. 1985. Late quaternary slumps and debris flows on the Scotian Slope. Geological Society of America Bulletin, **96**: 1508–1517.

Piper, D. J.W., Cochonat, P. and Morrison, Martin L. 1999. The sequence of events around the epicenter of the 1929 Grand Banks Earthquake: initiation of a debris flow and the turbidity current inferred from side scan sonar. Sedimentology, **46**: 79–97.

Piper, D. J.W., Campbell, D.C. and MacDonald, A.W.A. 2000. Report on Properties of Nine Piston Cores near Logan Canyon. GSC (Atlantic) Internal report.

PLAXIS. (2001). *PLAXIS 2D 2001 manuals*. PLAXIS bv., Delft, the Netherlands.

PLAXIS. (2011). *PLAXIS 2D 2010 manuals*. PLAXIS bv., Delft, the Netherlands.

Potts, D.M., Dounias, G.T. and Vaughan, P.R. 1990. Finite element analysis of progressive failure of Carsington embankment. Géotechnique, **40**(1): 79–101.

Prior, D. B. and Coleman, J. M. 1982. Active slides and flows in underconsolidated marine sediments on the slope of the Mississippi delta. In Marine slides and other mass movements (*ed*. S. Saxov & J. K. Nieuwenhuis), New York, 21–49.

Prior, D. B., Bornhold, B. D., Coleman, J. M., and Bryant, W. R., 1982. Morphology of a submarine slide, Kitimat Arm, British Columbia. Geology **10**(11).

Puzrin, A.M. and Germanovich, L.N. 2003. Shear band propagation in an infinite slope. *In* Proc. of the ASCE Conference on Engineering Mechanics, Seattle, Washington.

Puzrin, A. M., Germanovich, L. N. and Kim, S. 2004. Catastrophic failure of submerged slopes in normally consolidated sediments. Géotechnique, **54**(10): 631–643.

Puzrin, A.M. and Germanovich, L.N. 2005. The growth of shear bands in the catastrophic failure of soils. Proceedings of the Royal Society of London. Series A: Mathematical, Physical and Engineering Sciences, **461**(2056): 1199–1228.

Quinn, P., Diederichs, M.S., Hutchinson, D.J. and Rowe, R.K. 2007. An exploration of the mechanics of retrogressive landslides in sensitive clay. In Proc. of the 60th Canadian Geotechnical Conf., Ottawa, Ontario, 721–727.

Quinn P. 2009. Large landslides in sensitive clay in eastern Canada and the associated hazard and risk to linear infrastructure. Doctoral thesis, Queen's University.

Quinn, P.E., Diederichs, M.S., Rowe, R.K. and Hutchinson, D.J. 2011. A new model for large landslides in sensitive clay using a fracture mechanics approach. Canadian Geotechnical Journal, **48**: 1151–1162.

Quinn, P. E., Diederichs, M. S., Rowe, R. K. and Hutchinson, D. J. 2012. Development of progressive failure in sensitive clay slopes. Canadian Geotechnical J., **49**(7): 782–795.

Schlue, B.F., Mörz, T. and Kreiter, S. 2011. Undrained shear strength properties of organic harbor mud at low consolidation stress levels. Canadian Geotechnical Journal, **48**: 388–398.

Seed, H.B. 1968. Landslides during earthquakes due to soil liquefaction. J. Soil Mech. Found. Div., **94**: 1055–1122.

Skempton, A.W. 1964. Long-term stability of clay slopes. Géotechnique, **14**(2): 77–102.

Solheim, A., Bryn, P., Sejrup, H.P., Mienert, J. and Berg, K. 2005. Ormen Lange—an integrated study for the safe development of a deep-water gas field within the Storegga Slide Complex, NE Atlantic continental margin; Executive summary. Marine and Pet. Geol., **22**(1-2): 1–9.

Sultan, N., Cochonat, P., Foucher, J. P., Mienert, J., Haflidason, H. and Sejrup, H. P. 2003. Effect of gas hydrates dissociation on seafloor slope stability. In Submarine mass movements and their consequences (*ed*. J. Locat & J. Mienert), pp. 103–111.

Sultan, N., Cochonat, P., Canals, M., Cattaneo, A., Dennielou, B., Haflidason, H., Laberg, J. S., Long, D., Mienert, J., Trincardi, F., Urgeles, R., Vorren, T. O. and Wilson, C. 2004. Triggering mechanisms of slope instability processes and sediment failures on continental margins: a geotechnical approach. Marine Geology, **213**(1-4): 291–321.

Sultan, N., Savoye, B., Jouet, G., Leynaud, D., Cochonat, P., Henry, P., Stegmann, S. and Kopf, A. 2010. Investigation of a possible submarine landslide at the Var delta front (Nice continental slope, southeast France). Canadian Geotechnical J., **47**(4): 486–496.

Stark, T., and Contreras, I.A. 1996. Constant volume ring shear apparatus. Geotechnical Testing Journal, **19**(1): 3–11.

Tavenas, F., Flon, P., Leroueil, S. and Lebuis, J. 1983. Remolding energy and risk of slide retrogression in sensitive clays. *In* Proc. of the Symposium on Slopes on Soft Clays, Linköping, Sweden, SGI Report No. 17, 423–454.

Tavenas, F. 1984. Landslides in Canadian sensitive clays — a state-of-the-art. *In* Proc. of the 4th Int. Symposium on Landslides, Toronto, Ont., 16 –21 September 1984. University of Toronto Press, Toronto, Ont. **1**:141–153.

Terzaghi, K. and Peck, R.B. 1948. Soil mechanics in engineering practice. John Wiley and Sons, Inc., New York.

Thakur, V. 2007. Strain Localization in sensitive soft clays. PhD thesis, Norwegian University of Science and Technology, Trondheim. Norway.

Tjelta, TI, Strout, J, Solheim, A, Mokkelbost, KR, Berg, K, Bryn P. 2002. Geological and geotechnical site investigations in the Storegga Slide area. International Conference Offshore Site Investigation and Geotechnics, London, 199–217.

Twichell, D.C., Chaytor, J.D., Brink, U. S. and Buczkowski, B. 2009. Morphology of the late Quaternary submarine landslides along the U.S. Atlantic continental margin. Marine Geology, **264**: 4–15.

Weaver, P. P. E. and Kuijpers, A. 1983. Climatic control of turbidite deposition on the Madeira Abyssal plain. Nature, **306**: 360–363.

Yang, SL, Solheim, A, Kvalstad, TJ, Forsberg, CF and Michael Schnellmann, M., 2006. Behaviour of the sediments in the Storegga Slide interpreted by the steady state concept, Norwegian J. of Geology, **86**(3): 243–253.

Yang, S.L., Kvalstad, T.J., Solheim, A. and Forsberg, C.F. 2007. Slope Stability at Northern Flank of Storegga slide. *In* Proc. 16th Int. Off. and Polar Eng. Conf., Lisbon, Portugal, 1524–1529. .

Appendix-I

Modeling of earthquake induced pore pressure and submarine slope stability analysis

This paper has been published and presented in 2011 Pan-Am CGS Geotechnical Conference, Toronto, Canada.

Most of the research work presented in this paper was conducted by the first author. He also prepared the draft manuscript. The other authors supervised the research and reviewed the manuscript.

Modeling of Earthquake Induced Pore Pressure and Submarine Slope Stability Analysis

Rajib Dey & Bipul Hawlader
Memorial University of Newfoundland, St. John's, NL, Canada
Ryan Phillips
C-CORE, St. John's, NL, Canada
Kenichi Soga
University of Cambridge, United Kingdom

ABSTRACT
A method to analyze submarine slope stability during an earthquake is presented in this paper. The angles of most submarine slopes are very gentle and therefore the analysis has been performed assuming them as infinite slopes. In this study, the soils involved in slope failure are contractive loose to medium dense sands. It has been shown that both earthquake induced inertia force and pore water pressure in sand layer play a critical role in slope stability. The loose sand layers may not always be continuous in an offshore slope. Considering the end forces on the sliding block a method is presented to calculate the minimum length of the loose to medium dense sand layer required to fail the slope at a given depth. An energy based model (Berrill and Davis 1985) has been used to estimate the pore water pressure generated during an earthquake. The Berrill and Davis model has been further verified using additional case histories of liquefaction.

RÉSUMÉ
Une méthode pour analyser la stabilité des talus sous-marin pendant un tremblement de terre est présenté dans le présent document. Les angles de la plupart des pentes sous-marines sont très doux et donc l'analyse a été effectuée en les considérant comme une pente infinie. Dans cette étude, les sables impliqués dans une rupture de pente sont considéré comme contractant (lâches). Il a été montré que les séismes peuvent à ;a fois induiren une force d'inertie et des pressions interstitielles dans une couche de sable lesquelles jouent un rôle crucial dans la stabilité des pentes. Les couches de sable peuvent ne pas être toujours continues dans les talus au large des côtes. Considérant les forces à la limite des blocsqui glissent,, une méthode est présentée pour calculer la longueur minimale de la couche de sable lâche requise rupture du talus à une profondeur donnée. Un modèle basé sur l'énergie (Berrill et Davis 1985) a été utilisé pour estimer la pression d'eau interstitielle produite lors d'un séisme. Le modèle de Berrill et Davis a, de plus, été vérifié à l'aide d'histoires de cas deliquéfaction

1. INTRODUCTION

The stability of sloping seafloors is an important issue that must be considered in the design of offshore facilities such as offshore pipelines, foundations and wellheads. The consequences of slope failure could have a large financial, safety and regulatory impact. Numerous failures of submarine slopes have been reported in the literature; some of them are small while some are very large such as Storegga slide in the Norwegian Sea or Grand Banks slide in offshore Newfoundland. The submarine slides may be initiated by a variety of potential triggering factors such as earthquakes, rapid sedimentation, wave action, gas hydrate dissociation, diapirism, artesian water pressure, oversteeping by erosion and minor slides, human activities, tide, sea level change, glaciations and volcanic activities (Locat and Lee 2002, Masson et al. 2006). Among them earthquakes have been considered one of the major causes of submarine landslides. Pore water pressure generated from earthquake shaking could reduce the shear strength of soil significantly and cause the failure of a submarine slope (Wright et al. 2003, Kvalstad et al. 2005).
A submarine slope might fail during and also after earthquake shaking. The response of the slope depends on the magnitude of the earthquake, soil properties and geometry of the slope. During the earthquake, seismic induced inertia force creates some additional shear stress on the potential failure plane. Seismic excitation can also generate pore water pressure in some soil, such

as loose sand, which can reduce the shear strength of the soil along the failure plane. The excess pore water pressure cannot be significantly dissipated during the earthquake as it happens in a very short period of time and therefore the analysis should be performed considering the effects of excess pore water pressure (Hadj-Hamou et al. 1985, Biondi et al. 2000).

This paper presents a method to analyze the stability of submarine slopes subjected to earthquake. The soil considered is loose to medium sand, which loses its shear strength due to the generation of excess pore water pressure. The pore water pressure has been estimated using an energy-based pore pressure model. The pore water pressure generation models have been reviewed and the model used in this study has been verified with some additional data.

A submarine slope might also fail after the earthquake shaking. One reason could be the presence of thin silt layer of low permeability above the loose sand deposit under which a water film could be developed by post-liquefaction void redistribution (Kokusho 2003) as demonstrated by Coulter and Phillips (2005). However, this type of failure is not discussed in this paper. It is also to be noted here that many submarine landslides occurred in clayey deposits (Masson et al. 2006, Brink et al. 2009). However, the present study focused mainly on failure in sand.

2. STABILITY OF AN INFINITE SLOPE UNDER EARTHQUAKE LOAD

Consider a long continuous submarine slope with an inclination of β as shown in Fig. 1. Typically submarine slopes are very gentle having a slope angle (β) less than 10° (Hadj-Hamou et al. 1985). The slope is stable under the static shear stress (τ_{static}) caused by the gravitational force. An earthquake in this area might cause the failure of this slope.

Extremely loose sand is not very common in the seabed because other environmental effects such as wave loading increase the soil density. If the slope is in the earthquake prone area, earthquakes of small intensity may not cause the failure of the slope. However, pore pressure will be generated due to these earthquakes which will be dissipated with time and densify the soil. This is known as “seismic strengthening” (Lee et al. (2004). Coulter and Phillips (2005) successfully modelled the seismic strengthening behaviour using geotechnical centrifuge. Therefore, in this study it is assumed that the soil involved in potential failure of the slope is loose sand not very loose sand.

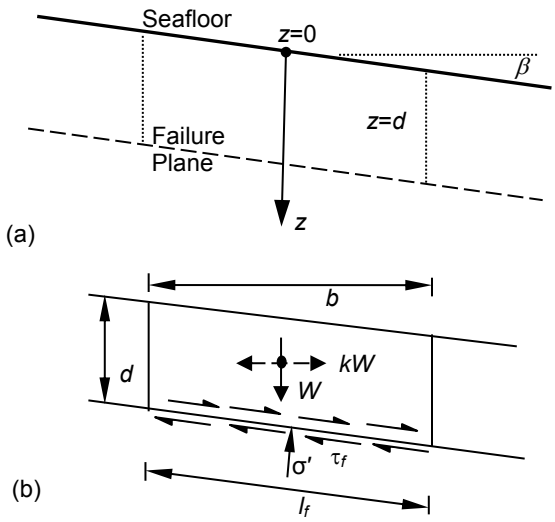

Figure 1: (a) Geometry of slope (b) Stress state

The simplest analysis of the stability of a submarine slope can be performed by assuming it as an infinite slope with a failure plane parallel to the sea floor. Let us assume a potential failure plane at depth d as shown in Fig. 1. If the length of the failure plane (l_f) is significantly greater than d, it can be considered as an infinite slope. Whether this slope will fail due to an earthquake or not depends upon the soil behaviour along the potential failure surface. The soil behaviour of loose sand is described in the following section.

3. BEHAVIOUR OF LOOSE AND COMPACT SAND AND ITS IMPLICATION TO SLOPE FAILURE

Typical behaviour of saturated contractive sand is shown schematically in Fig. 2. The point A represents the initial stress state of a soil element in the slope. The soil element is in drained equilibrium under the static shear stress (τ_{static}) and the slope in the field is stable under this stress. If this soil specimen is sheared monotonically from this initial condition in triaxial cell in undrained condition, it will follow the stress path ABC as shown in Fig. 2. Shear stress continues to increase to the peak at point B where it becomes unstable and further increase in pore water pressure strains the soil elements rapidly to the residual shear strength (τ_r) at point C. Undrained strain softening is triggered only if the static shear stress (τ_{static}) is greater than residual shear strength (τ_r). If the same specimen is loaded cyclically in undrained condition the soil

element becomes unstable at point D and then follows similar strain-softening response from D to C. It should be noted that a significant shear strain occurs during the path from B to C (in case of monotonic load) or D to C (in case of cyclic load) than that of in A to B or A to D (Fig. 2b). Although the effective stresses at point B and D are different, all these points fell in one line OB as shown in Fig. 2a (Kramer 1996; Hanzawa 1980).

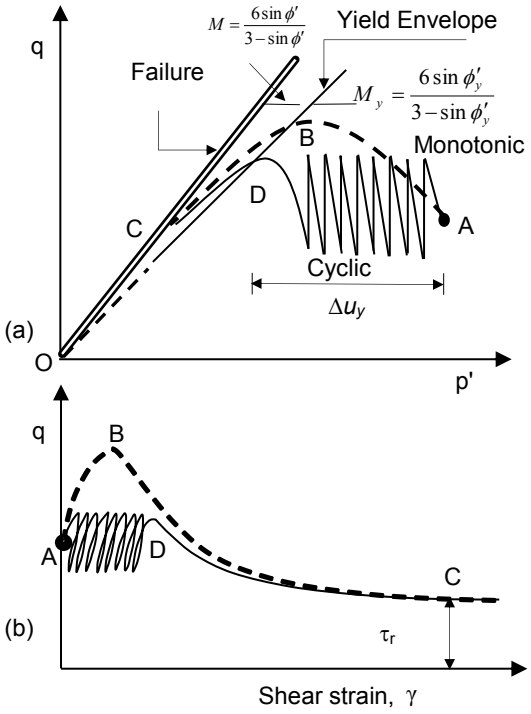

Figure 2: Behaviour of sand under monotonic and cyclic loads

Various names have been given for this line including *yield strength envelope* (Hanzawa 1980, Olson and Stark 2003), *flow liquefaction surface* (Vaid and Chern 1985,Yang 2002), *collapse surface* (Sladen et al. 1985), *instability line* (Lade and Yamamuro 2011, Chu et al. 2003), and *peak strength envelop* (Poulos 1988). In this study, the term "yield strength envelope"is used to represent this condition and the corresponding friction angle is referred as "yield friction angle, ϕ'_y."

If the pore water pressure generated from an earthquake reduces the effective stress to the yield envelope the soil sample becomes imminent to collapse. Collapse of soil structure results in strain-softening behaviour as shown in Fig. 2(b). The slope of the yield and failure envelopes could be obtained from conventional geotechnical laboratory tests. The yield strength envelope is not unique but depends upon the void ratio or relative density and confining pressure. The slope of the yield strength line (M_y) could be low for very loose sand while it could be same or very close to the slope of the critical state line (M) for higher relative densities (Sladen et al. 1985, Chu et at. 2003). In general, the slope of the yield envelope in triaxial compression is higher than that of in simple shear tests (Olson and Startk 2003, Terzaghi et al. 1996). In most of the submarine slope failures the mode of shear on the potential failure plane corresponds approximately to the simple shear condition. Lade and Yamamuro (2011) also pointed out that slope of the yield strength envelope from anisotropically (K_0) consolidated specimen is higher than that of isotropically consolidated specimen of the same void ratio. Therefore, the difference between the failure line and yield envelopes may not be very high in offshore environment since the soil is anisotropically consolidated and subsequently compacted by environmental loads. However, as the soil is still in loose state collapse after yield is possible. Therefore, the analysis should be also performed considering the residual shear strength at point C. Note that, if the static shear stress is less than the residual shear strength, the stress path can travel beneath the point C without reaching to any collapse surface (Kramer 1996). However, such a low shear stress in not considered in this study.

4. STABILITY ANALYSIS

Limit equilibrium analysis is generally performed for stability analysis of a slope. When the shear stress on the potential failure plane exceeds the shear strength of soil at that plane the slope fails. Shear stress could be generated from variety of sources, however only the gravitational and earthquake induced shear stresses are considered in this study.

Referring to Fig. 1(b) the following expression can be written for normal (σ_0') and shear (τ_0) stresses at the base of the sliding block.

$$\sigma'_0 = \gamma' d\cos^2\beta \quad \text{and} \quad \tau_0 = \gamma' d\sin\beta\cos\beta \quad [1]$$

Seismic excitation will have at least two effects on slope stability. During an earthquake excess pore water pressure (Δu) might be generated in the soil near the sliding surface. The excess pore water pressure cannot be dissipated during a very short period of earthquake duration. It will reduce the normal effective stress to σ_0'-Δu, which in turn reduce the shear strength significantly. The driving force will be also increased by earthquake shaking. Similar to pseudostatic screening analysis, the earthquake

induced horizontal force can be modelled using a horizontal earthquake coefficient (k_h). Note that, in pure pseudostatic analysis earthquake induced pore water pressure is not considered and is suitable for stability analysis of slopes when the soil involved are not expected to lose their shear strength significantly during earthquake shaking (Makdisi and Seed 1977). However, the soil considered here is loose sand; both effects need to be considered to scrutinize the shear strength reduction (Azizian and Popescu, 2001, Hadj-Hamou et al. 1985).

Therefore the factor of safety (F_s) of a given infinite slope can be written as:

$$F_s = \frac{(1-r_u)\tan\phi'_y}{\tan\beta + k_h\gamma_t/\gamma'} \quad [2]$$

where γ' and γ_t are the submerged and total unit weight of the soil above the failure plane, respectively; r_u $(=\Delta u/\sigma'_0)$ is the pore pressure ratio; and ϕ'_y is the yield friction angle.

5. EFFECTS OF SOIL LAYER ABOVE THE FAILURE PLANE

The effects of the upper soil layer above the failure plane AB in Fig. 3 have not been considered in the factor of safety calculation discussed in section 4. It has been assumed that the length of the failure plane is infinite and therefore the resistance offered by the soil above the failure plane is negligible. However, in offshore environment the soil layer involved in failure may not be homogeneous and the zone of loose contractive sand, where the failure could be initiated, may not be continuous. Several questions may arise regarding the effect of upper soil layer on slope failure such as: (i) At what depth the failure could be initiated? (ii) What is the minimum length of the weak soil layer required to initiate a failure at that depth? (iii) How does the failure propagate through the upper soil layer? (iv) How to model that propagation? A simplified modeling procedure is presented in the following sections to answer these questions.

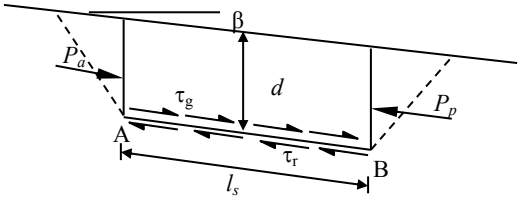

Figure 3: Slope with a finite length of weak zone

Consider a long continuous submarine slope (Fig. 3) with an inclination of β similar to Fig. 1. This time the weak contractive sand layer is not infinite but of a finite length of l_s. The sliding of the soil block is possible only if the driving force is greater than the resistance offered by the loose sand layer at the bottom and as well as two end zones. The situation at the upper and lower ends of the sliding block is very similar to the active and passive earth pressure conditions, respectively.

Based on Mazindrani and Ganjali (1997), P_p -P_a can be calculated as;

$$P_p - P_a = \frac{2d^2\gamma'\cos^2\beta(1-r_{u1})\sqrt{(\cos^2\beta-\cos^2\phi'_1)}}{\cos^2\phi'_1} \quad [3]$$

where P_a and P_p are the active and passive forces, respectively, ϕ'_1 is the angle of internal friction of the soil layer above the failure zone, and r_{u1} is the pore pressure ratio in that layer. Note that, if the stress-strain behaviour of the upper soil layer is similar to the behaviour presented in Fig. 2, $\phi'_1 = \phi'_y$ should be used. Otherwise, for example for medium to dense sand, the critical state friction angle should be used.

Using the equilibrium condition of the sliding block in Fig. 3, the factor of safety (F_s) can be calculated as

$$F_s = \frac{\tau_r l_s + P_p}{\tau_g l_s + P_a}, \quad [4]$$

where $\tau_g (=\gamma' d\cos\beta\sin\beta + k_h\gamma_t d\cos^2\beta)$ is the sum of the shear stresses resulting from gravitational and earthquake induced force and τ_r is the residual strength. If the excess pore pressure ratio is known, the residual shear strength τ_r can be also calculated as (see Fig. 2)

$$\tau_r = \gamma' d\cos^2\beta(1-r_u)\tan\phi'_{cs} \quad [5]$$

Therefore, the minimum length l_s required to cause the failure of a slope at a depth d can be obtained by putting F_s =1 in Eq. (4).

$$l_s = \frac{P_p - P_a}{\tau_g - \tau_r} \quad [6]$$

Now replacing the values of τ_g and τ_r as discussed above, the Eq. (6) can be rewritten as:

$$l_s = \frac{2d(1-r_{u1})\sqrt{(\cos^2\beta-\cos^2\phi'_1)}}{\cos^2\phi'_1\left(\tan\beta+\left(\frac{\gamma_t}{\gamma'}\right)k_h-(1-r_u)\tan\phi'_{cs}\right)} \quad [7]$$

As shown in Eq. (7), in addition to other soil parameters the pore water pressure ratios are required to determine the length l_s. The effects of various parameters in Eq. (7) are discussed in the following sections. A method for estimation of r_u is discussed in Section 7.

6. LENGTH OF WEAK LAYER

Consider a submarine slope having a loose sand layer at a depth of 20 m. The geotechnical parameters for this loose sand are: ϕ'_{cs} = 33º, yield friction angle, ϕ'_i = 28º, γ' = 7 kN/m^3, γ_t = 17 kN/m^3, r_{u1} = 0.5 and β = 5°. The solid lines in Figs. 4 to 6 show the length l_s required for failure of the slope. To explain further consider Fig. 4. If the pore pressure ratio r_u generated from an earthquake near the base of the sliding block is 0.6, the failure is possible if the length of the weak soil layer is at least 165 m. However, if the value of r_u is less than 0.5, failure of the slope is not possible for this geometry and soil conditions, because the frictional resistance along the potential failure plane is sufficient to resist the shear stress. In other words, when r_u is equal to or less than 0.5, a higher value of l_s is strongly required to initiate the slope failure for the above mentioned properties.

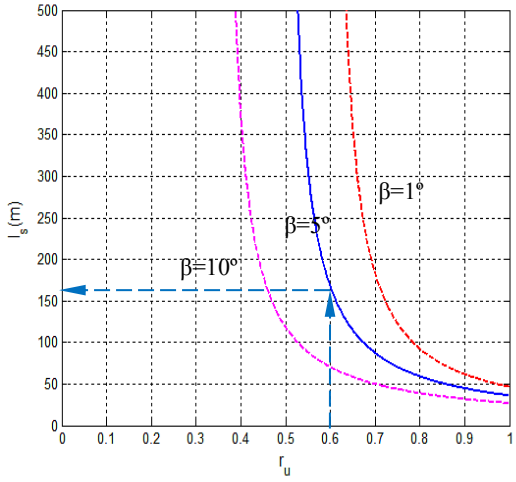

Figure 4: Effects of pore pressure parameter and slope angle, β

In addition to pore pressure ratio, three other parameters are considered to be critical for stability, which are: (i) slope angle, β; (ii) horizontal earthquake coefficient, k_h; and (iii) the depth of the potential sliding surface, d. The effects of these parameters are shown by changing one parameter at a time while keeping the other parameters same as above and shown in Figs. 4 to 6.

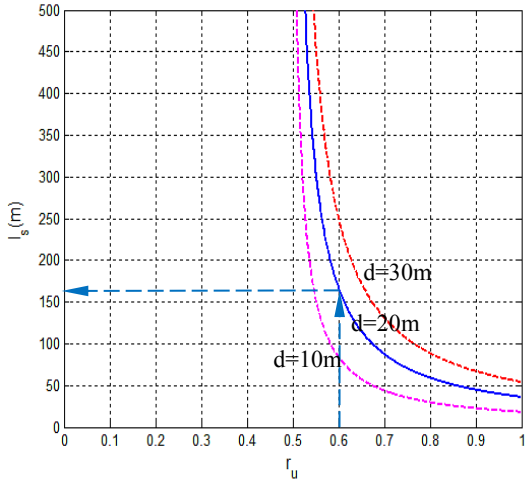

Figure 5: Effect of depth of sand layer, d

The effects of the depth of the sliding surface are shown in Fig. 5. The greater the depth of sliding surface the higher the pore pressure and l_s required to cause the failure of the slope.

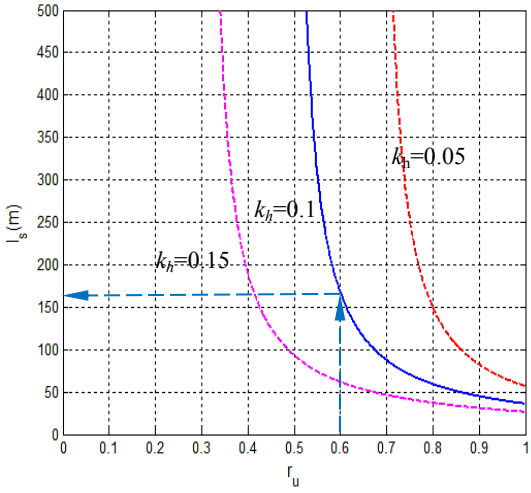

Figure 6: Influence of earthquake coefficient, k_h

Figure 6 shows the effects of k_h, which is related to seismic intensity, on the possibility of failure. As expected, the possibility of failure of a slope is higher for higher values of k_h.

7. ESTIMATION OF EARTHQUAKE INDUCED PORE PRESSURE

As shown above, the earthquake induced pore water pressure has a significant effect on submarine slope failure. Therefore, estimation of r_u is critical in analysis of submarine slope failure. A number of models have been proposed in the past to estimate the development of excess pore pressure due to earthquake. Zangeneh and Popescu (2003) undertook seismic displacement analyses of submarine slopes using the pore pressure model of Seed and Idriss (1982). In this study, a model based on energy dissipation approach has been chosen for modeling excess pore pressure. The fundamental of the energy-based model is that the increase in pore pressure (Δu) due to an earthquake is a function of dissipated energy (ΔE). The main advantages of this approach are that it is related to both cyclic stress and cyclic strain, and can be related to fundamental earthquake parameters (Kramer 1996). Law et al. (1990) mentioned that the energy dissipation approach is simpler and more reliable. In general, earthquake motions have very different amplitude, frequency content, and duration, and therefore most of the models are empirical and have been developed from statistical analysis of liquefaction case studies. There are similarities and also some differences between the proposed models. However, such comparison is not the aim of this paper and is not presented here; rather the model proposed by Berrill and Davis (1985) has been used.

Davis and Berrill (1982) proposed a model for pore water pressure increase due to earthquake based on 57 case histories. It has been shown that when $r^2\sigma_0'^{3/2}/10^{1.5M}$ is less than $450/N_1^2$ soil liquefaction occurs. Here, N_1 is the corrected SPT-N value, *M* is the earthquake magnitude, *r* is the epicentre distance in meter, σ'$_0$ is the initial vertical effective stress in kPa and $r^2\sigma_0'^{3/2}/10^{1.5M}$ is a component related to energy dissipation and pore pressure generation. Further discussion about this component is available in Davis and Berrill (1982). Note that for mild submarine slope (β<10°), σ_0' from Eq. (1) and vertical effective stress are used interchangeably. The variation of $r^2\sigma_0'^{3/2}/10^{1.5M}$ with N_1 is shown by the dashed line in Fig. 7. Based on this Davis and Berrill (1982) proposed a model to calculate the value of r_u as:

$$r_u = \frac{\Delta u}{\sigma_0'} = \frac{450}{r^2 N_1^2 \sigma_0'^{3/2}} 10^{1.5M} \qquad [8]$$

Berrill and Davis (1985) revised and extended their model based on more (90) liquefaction case histories. It has been shown that when $r^2\sigma_0'^{3/2}/\left(A10^{1.5M}\right)$ is less than $\left(120/N_1^{1.5}\right)^2$ soil liquefaction occurs. Here *A* is the attenuation factor, and other parameters are defined above. The value of *A* varies between 0.71 and 0.98. Berrill and Davis (1985) also recommended an average value of *A* equal to 0.9 for this model.

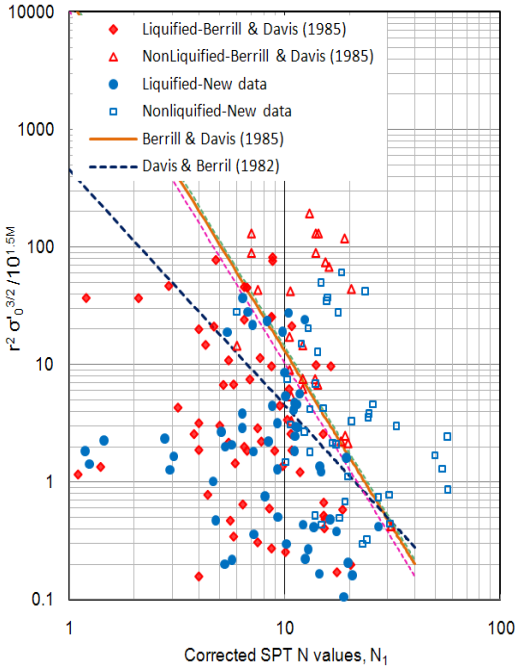

Figure 7: Comparison between liquefaction case history data and energy based models

The solid line in Fig. 7 shows the variation of $r^2\sigma_0'^{3/2}/10^{1.5M}$ with N_1 for A=0.9. The two dashed line near this solid line shows the variation for A=0.71 and 0.98. As shown, the effect of *A* within this range is not significant compared to other parameters.

Berrill and Davis (1985) also revised the pore pressure model as;

$$r_u = \frac{\Delta u}{\sigma_0'} = \frac{120}{N_1^{1.5}} \frac{\sqrt{A}\, 10^{0.75M}}{r\sigma_0'^{0.75}} \qquad [9]$$

In addition to the data used by Berrill and Davis (1985), we have compiled a large number of liquefaction case histories from the literature as plotted in Fig. 7. A total number of 188 case histories obtained from various sources (Berrill and Davis 1985; Law 1990; Seed 1975; and Xie 1984) are plotted in this figure. The additional 98 liquefaction case history data are shown by solid circles for liquefaction and open squares for non-liquefaction. The lines in Fig. 7 show the

boundary between liquefied and non-liquefied sites, where the non-liquefied cases are at the right. As shown in Fig.7, the model proposed by Berrill and Davis (1985) better covers liquefaction cases even with additional data. Therefore, Berrill and Davis (1985) model (Eq. 9) has been used in this study to calculate the value of r_u.

8. A WORKED EXAMPLE

Consider a mild submarine slope of β = 5º. Geotechnical parameters are: ϕ'_{cs} = 33º, ϕ'_y = 28º, γ' = 7 kN/m^3, γ_t = 17 kN/m^3, r_{u1} = 0.4 and N_1 = 9. The stability of this slope is required to be analyzed for an earthquake magnitude of 7.5 with an epicentre distance of 75 km. Now using Eq. (9), the pore pressure ratio (r_u) can be calculated with depth. Once the value of r_u is known, the length of the loose sand layer (l_s) can be calculated using Eq. 7. For example, at 20 m depth, r_u = 0.6 and l_s = 200m. That means, if the there is a loose sand layer that extent more than 200m at 20m depth the failure of the slope is possible.

9. CONCLUSIONS

The potential failure of the seabed due to an earthquake is one of the major concerns for the development of offshore facilities. When submarine slope failure involves loose sands, the failure can be governed by both earthquake induced inertia force and excess pore water pressure in the soil.

Both yield and residual shear strength are the critical soil parameters for stability analysis. Once the earthquake induced pore water pressure reduces the effective stress to the yield strength envelope the loose contractive soil is on the verge of collapse and a small trigger may initiate instability of the slope. However, the final failure of the slope is governed by the residual shear strength.

For offshore slope failure the weak sand layers do not have to be continuous. The minimum length required for the failure of a submarine slope can be calculated considering the effects of the forces at the end of the sliding block.

The energy-based model proposed by Berrill and Davis (1985) could be used to estimate earthquake induced pore water pressure. It has been shown that this model performs reasonably well even for additional case histories included in the present study from the literature.

NOTATIONS

The following symbols are used in this paper:

A : attenuation factor
β : slope angle
d : depth of the assumed potential sliding surface
F_s : factor of safety
k_h : horizontal earthquake coefficient
l_s : length required for failure
l_f : length of the assumed failure plane
M : earthquake magnitude
N_1 : corrected SPT-N value
ϕ'_{cs} : friction angle at critical state
ϕ'_y : friction angle at yield
P_a : active force
P_p : passive force
r : epicentre distance in m
r_u : excess pore pressure ratio
r_{u1} : excess pore pressure ratio at yield
τ_g : gravitational & earthquake induced shear stress
τ_r : residual shear strength
Δu : excess pore water pressure at failure
σ'_0 : normal effective stress
γ_t : total unit weight
γ' : submerged unit weight

ACKNOWLEDGEMENTS

The writers would like to acknowledge the financial support from Research & Development Corporation of Newfoundland and Labrador and C-CORE.

REFERENCES

Azizian, A. and Popescu, R. 2001. Back analysis of the 1929 Grand Banks submarine slope failure. *Canadian Geotechnical Society Conference*, 808–815.

Berrill, J. B. and Davis, R. O. 1985. Energy dissipation and seismic liquefaction of sands: Revised model. *Soils and Foundations*, 25(2): 106–118.

Biondi, G., Cascone, E., Maugeri, M. and Motta, E. 2000. Seismic response of saturated cohesionless slopes. *Soil dynamics and earthquake engineering*, 20: 209–215.

Brink, U.S.T., Lee, H.J., Geist, E.L. and Twichell D. 2009. Assessment of tsunami hazard to the U.S. East Coast using relationships between submarine landslides and earthquakes. *Marine geology*, 264: 65–73.

Chu, J., Leroueil, S. and Leong, W.K. 2003. Unstable behaviour of sand and its implification for slope instability. *Canadian Geotechnical Journal*, 40: 873–885.

Coulter, S.E. and Phillips, R. 2005. Seismic initiation of submarine slope failures using physical modelling in a geotechnical centrifuge. *Proc. 58th Canadian Geotechnical Conference*, Saskatoon, Paper 588.

Davis, R. O. and Berrill, J. B. 1982. Energy dissipation and seismic liquefaction of sands. *Earthquake engineering and structural dynamics*, 10: 59–68.

Hadj-Hamou, T. and Kavazanjian, E. Jr. 1985. Seismic stability of gentle infinite slopes. *Journal of Geotechnical Engineering*, ASCE, 111(6): 681–697.

Hanzawa, H. 1980. Undrained strength and stability analysis for quick sand. *Soils and Foundation*, 20 (2): 17–29.

Kokusho, T. 2003. Current state of research on flow failure considering void redistribution in liquefied deposits, *Soil Dynamics and Earthquake Engineering*, 23:585–603.

Kramer, S.L.1996. *Geotechnical Earthquake Engineering,* Upper Saddle River, N.J.: Prentice Hall.

Kvalstad, T.J., Andresen, L., Forsberg, C.F., Berg, K., Bryn, P. and Wangen, M. 2005. The Storegga slide: evaluation of triggering sources and slide mechanics. *Marine and petroleum Geology,* 22:245–256.

Law K.T., Cao Y.L. and He, G.N. 1990. An energy approach for assessing seismic liquefaction potential. *Canadian Geotechnical Journal*, 27(3): 320–329.

Lee, H.J., Orzech, K., Locat, J., Boulanger, E., and Konrad, J.M. 2004. Seismic Strengthening, A Conditioning Factor Influencing Submarine Landslide Development. *Proc. 57th Canadian Geotechnical Conference*, 7p.Quebec, Canada.

Locat, J. and Lee, H.J. 2002. Submarine landslides: advances and challenges. *Canadian Geotechnical Journal*, 39: 193–212.

Makdisi, F.I. and Seed, H.B. 1977. A simplified procedure for estimating earthquake-induced deformations in dams and embankments. In: *Rept. UCB/EERC-77/19*, Earthquake Eng. Res. Center.

Masson, D.G., Harbitz, C.B., Wynn, R.B., Pedersen, G. and Løvholt, F. 2006. Submarine landslides: processes, triggers and hazard prediction. *Phil. Trans. R. Soc. A*, 364: 2009–2039.

Mazindrani, Z.H. and Ganjali, M.H. 1997. Lateral earth pressure problem of cohesive backfill with inclined surface. *Journal of Geotechnical and Geoenvironmental Engineering,* ASCE, 123(2): 110–112.

Olson, S.M. and Stark, T.D. 2003. Yield strength ratio and liquefaction analysis of slopes and embankments. *Journal of Geotechnical and Geoenvironmental Engineering,* ASCE, 129(8): 727–737.

Poulos, S.J. 1988. Strength for static and dynamic stability analysis. *Geotechnical Special Publication*, 21: 452–474.

Seed, H.B., Arango, I. and Chan, C.K. 1975. Evaluation of soil liquefaction potential during earthquake. *Earthquake Engineering Research Center*, University of California, Berkley, Report EERC75–28.

Seed, H.B. and Idriss, I.M. 1982. On the importance of dissipation effects in evaluating pore pressure changes due to cyclic loading. *Soil Mechanics – Transient and Cyclic Loads, eds*., Pande, N., Zienkiewics, O.C.: 53–70.

Sladen, J.A., D'Hollanderr, D., and Krai-Inj. 1985. The liquefaction of sands, a collapse surface approach. *Canadian Geotechnical Journal*, 22(4): 564–578.

Terzaghi, K., Peck, R.B. and Mersi, G. 1996. *Soil Mechanics in Engineering Practice,* 3rd edition, John Wiley & Sons, New York.

Vaid, Y.P. and Chern, J.C. 1985. Cyclic and monotonic undrained response of sands. *In Proc. Advances in the Art of Testing Soils under Cyclic Loading*, Detroit, pp. 120–147.

Wright, S.G. and Rathje, E.M. 2003. Triggering mechanisms of slope instability and their relationship to earthquakes and tsunami. *Pure and applied geophysics*, 160: 1865–1877.

Xie, J.F. 1984. Some comments on the formula for estimating the liquefaction of sand in revised a seismic design code. *China Earthquake Engineering and Engineering Vibration,* 2: 95–126.

Yamamuro, J.A. and Lade, P.V. 2011. Evaluation of static liquefaction potential of silty sand slopes. *Canadian Geotechnical Journal*, 48: 247–264.

Yang, J. 2002. Non-uniqueness of flow liquefaction line for loose sand. *Géotechnique,* 52(10): 757–760.

Zangeneh, N. and Popescu, R. 2003. Displacement Analysis of Submarine Slopes using Enhanced Newmark Method. *Proc. 1st Int. Symp. Submarine Mass Movements and their Consequences*, Nice, France, pp.193–204.

Appendix-II

Effects of shear band propagation on submarine landslide

This paper has been published in 2012 International Offshore and Polar Engineering Conference, Rhodes, Greece.

Most of the research work presented in this paper was conducted by the first author. He also prepared the draft manuscript. The other authors supervised the research and reviewed the manuscript.

Effects of Shear Band Propagation on Submarine Landslide

Rajib Dey
Graduate Student, Memorial University of Newfoundland,
St. John's, NL, Canada
Dr. Bipul Hawlader
Associate Professor, Memorial University of Newfoundland,
St. John's, NL, Canada
Dr. Ryan Phillips
Principal Consultant, C-CORE,
St. John's, NL, Canada
Dr. Kenichi Soga
Professor, Department of Engineering, University of Cambridge,
Cambridge, United

ABSTRACT

Interbedded layers of glacial deposits and marine or glacimarine clay layers are a common feature of offshore sediment. Typically, offshore marine clays are lightly overconsolidated sensitive clay. Some case histories on submarine landslides show that the slip surface passes through these marine clay layers. In this paper a model is proposed for post-peak strain softening behavior of marine sensitive clay. The slope failure mechanism is examined using the concept of shear band propagation. It is shown that shear band propagation and post-peak stress-strain behavior of clay layers are two major factors in submarine slope stability analysis.

KEY WORDS: Submarine slope failure; shear band propagation; sensitive clay; limit equilibrium method.

INTRODUCTION

Over the last few decades, offshore oil and gas development activities have rapidly increased with significant increase in demand of energy. For planning and design of offshore facilities, the stability of the seabed is an important issue that must be taken into consideration. The consequences of catastrophic submarine slope failure might be very devastating and could have a significant financial loss, safety and regulatory implications. Numerous failures of submarine slopes have been reported in the literature some of which are small while others are very large, such as Storegga slide in the Norwegian Sea or Grand Banks slide in offshore Newfoundland. Various potential triggering mechanisms have been identified in the past (e.g. sedimentation, earthquake induced pore pressure increase, gas hydrate dissociation) that could weaken a section of a soil layer from where failure might be initiated. Failure might occur from a single triggering factor or could be the combined effect of a number of factors. For example, in case of Storegga slide and Trænadjupet slide, it is believed that initial triggering was developed by excess pore pressure caused by rapid deposition of overlying sediments possibly combined with effects from earthquake loading and/or accumulation of gas (Bryn et al. 2005; Kvalstad et al. 2005; Laberg et al. 2003).

The offshore continental slope has been affected by numerous large scale submarine slides all over the world. The Storegga slide is one of them which have been investigated intensively during the development of the Ormen Lange gas field. Evaluation of possible triggering mechanisms of the Storegga slide, geological and geotechnical site investigations in the slide area and current state of slope stability analysis at Ormen Lange area have been described by Tjelta et al. 2002; Kvalstad et al. 2005; Bryn et al. 2002 and 2005; Solheim et al. 2005 and Yang et al. 2006. Typical seismic profiles of two well-known slide sites are shown in Figs. 1 and 2. It is noted that extensive site investigation has been carried out in these areas through high resolution mapping, field investigation, geoborings up to several hundred meters below the seabed and laboratory testing. By interpreting the field and laboratory investigation results and seismic stratigraphy, it was concluded by previous researchers that such offshore sediments primarily consist of slightly inclined interbedded layers of glacial deposits and marine or glacimarine clay layer. The dashed line BC in Figs. 1 and 2 show two locations of the marine clay layer.

In general marine and/or glacimarine clays have higher water contents, plasticity indices, liquidity indices and clay content as compared to glacial clays. The sensitivity of these clays is in the range of 3 to 6 or more (Kvalsted et al. 2005; Yang et al. 2006). In undrained loading they show contractive and strain softening behavior at large strain. Therefore, the slip surface primarily passes through the marine clay layer, for example as in the case of the Storegga slide.

This paper presents a new method of slope stability analysis considering the strain-softening behavior of marine clay. It is shown that the propagation of shear band through this clay layer could cause the failure of a submarine slope. The limitations of the limit equilibrium method in offshore slope stability analysis are also presented as compared to the results obtained from the present model.

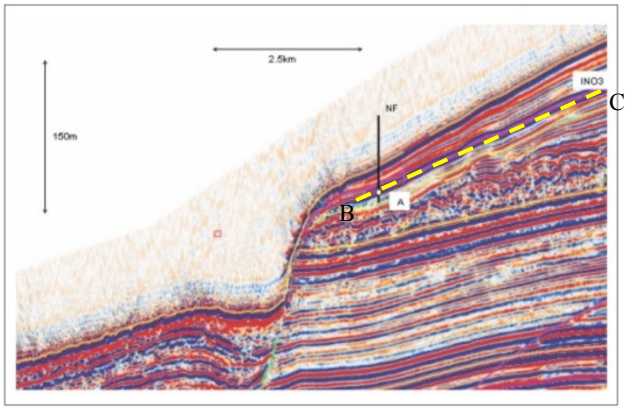

Figure 4.14: Seismic profile across North Flank in Storegga Slide (Yang et al. 2006)

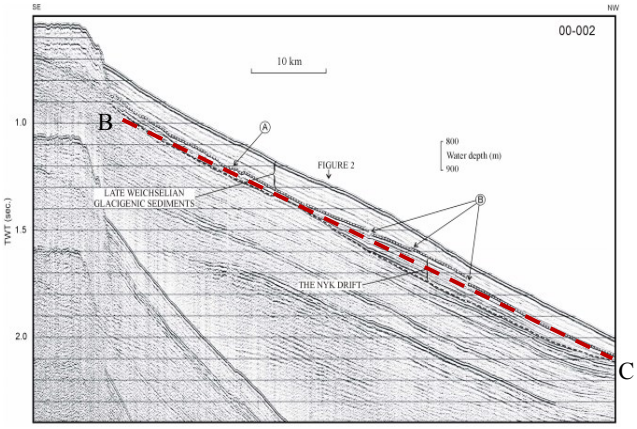

Figure 4.15: Seismic profile near the Trænadjupet slide (Laberg et al. 2003)

BEHAVIOR OF MARINE CLAY

Several researchers (e.g. Laberg et al. 2003; Tjelta et al. 2002; Kvalsted et al. 2005; Yang et al. 2006) conducted triaxial, direct simple shear and/or ring shear tests to understand the behavior of marine clays. The collection of undisturbed marine clay is relatively difficult and disturbance could affect geotechnical parameters such as undrained shear strength, over-consolidation ratio, sensitivity and stress-strain behavior. However, it has been observed that typical marine clays are lightly overconsolidated sensitive clay.

Fig. 3a shows the stress-strain behavior of marine clay. The soil specimens were consolidated anisotropically and then sheared in undrained condition. As shown, shear stress increases to the peak at about 1% axial strain and then reduces with increase in axial strain. This strain softening behavior is commonly observed in sensitive clays. The tests were stopped at an axial strain of 10%; however it is clear from this figure that the shear strength would be reduced further to the remoulded value if the tests were continued to a higher strain level. Fig. 3b shows the stress path of this soil. As shown, there is a significant increase in pore water pressure after the peak and the undrained shear strength is reduced. It is noted that similar behavior of marine clay from other offshore sites been reported by many researchers (Yang et al. 2006; Tjelta et al. 2002; Lunne et al. 2006; Jostad et al. 2006).

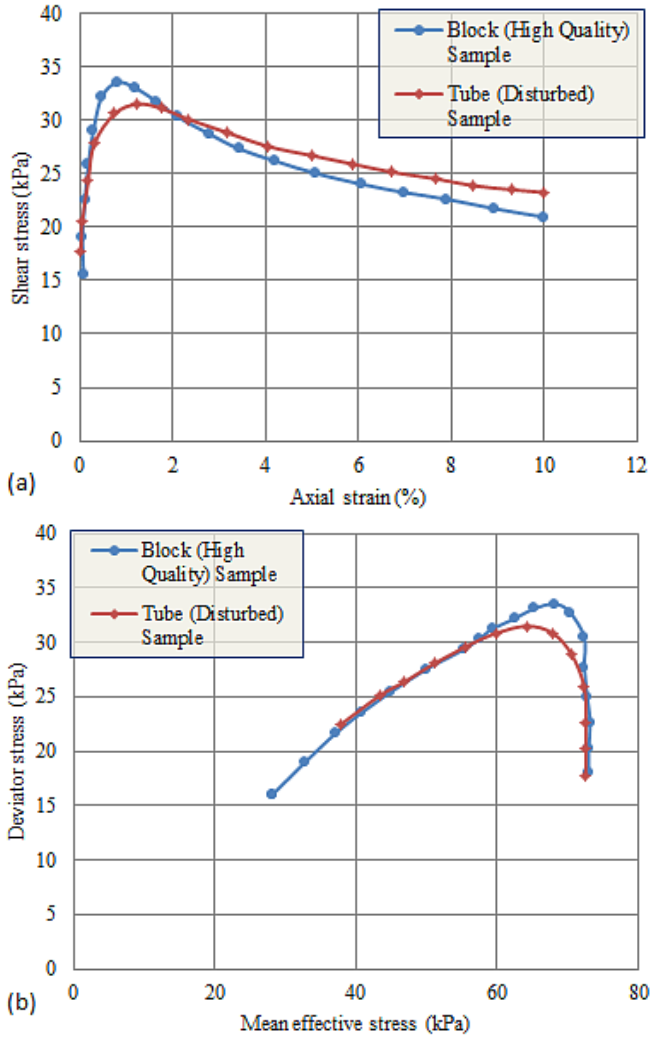

Fig. 3: Typical behavior of marine clay: (a) Stress-strain curves (b) stress-path (Landon, 2007)

PROBLEM STATEMENT

Typically submarine slopes are very gentle having a slope angle (β) less than 10° (Hadj-Hamou et al. 1985). The slope might contain a strain softening soil layer such as a marine clay layer. The typical stress-strain behavior of this type of clay layer is shown in Fig. 3. An initial discontinuity in the form a shear band might be formed in this clay layer because of many reasons including: (i) increase in external load such as earthquake loading or rapid sedimentation and/or (ii) decrease in soil strength such as gas (methane) hydrate dissociation or increase in water content as a result of pore water migration. The formation of this initial

discontinuity could be the effect of one or combined effects. Here the term "initial discontinuity" means the discontinuity initially formed by such causes. The length of the discontinuity might be increased further as discussed in the following sections.

Once the initial discontinuity is formed and the slope moves downward along this localized slip surface, significant strain softening occurs with shear displacement and the shear strength drops towards its remoulded value at large shear displacement (Fig. 3a). The thick dotted lines in Figs. 4a and 4b show the zone where the initial discontinuity formed. As the shear strength along the initial discontinuity decreases, the downward driving force will be transferred to the adjacent soil elements near the end of discontinuity. If the initial discontinuity is at shallow depth and the soil above this discontinuity is weak then the shear band might simply propagate upward approximately at active and passive failure mode to the seabed. However, most of the large scale offshore landslides occur at moderate depth and the soil above the initial discontinuity is relatively stronger such as glacial deposits as discussed in previous sections. Therefore, the shear band might propagate further along the initial discontinuity as shown by thin dotted lines in Figs. 4a and 4b. This transition zone is referred to as the "end zone."

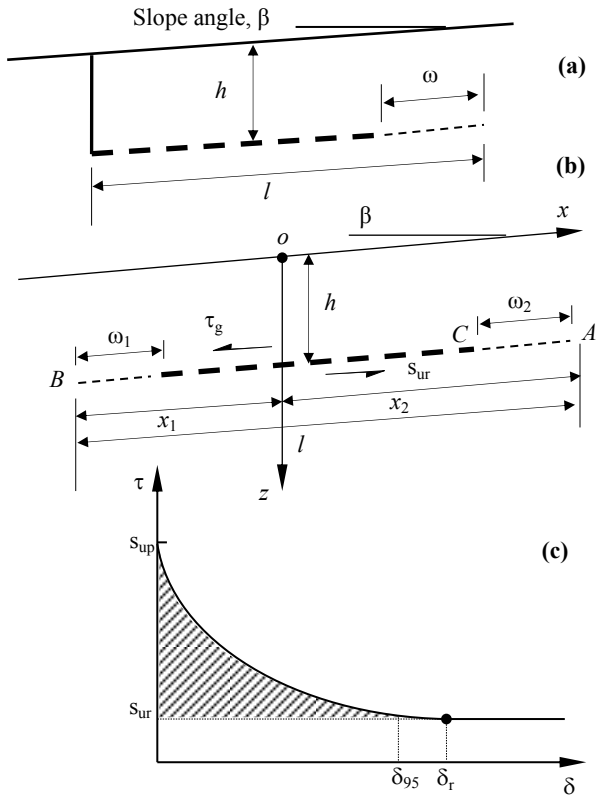

Fig. 4: (a) Shear band propagation behind a vertical cut slope; (b) Shear band propagation in a slope; (c) Post-peak stress-strain behavior of soil in discontinuous zone along the shear band

Total shear displacement (δ_{total}) in the zone of initial discontinuity is greater than or equal to the residual shear displacement (δ_r). However, in the end zone $\delta_p \leq \delta_{total} \leq \delta_r$, where δ_p is the shear displacement required to attain peak strength (s_{up}). In other words, shear strength in the end zone could vary between peak (s_{up}) and remoulded (s_{ur}) shear strength. In Fig. 4b at point *A* it is s_{up} and at point *C* it is s_{ur}

MODELING OF SHEAR BAND PROPAGATION

After Skempton (1964) and Bjerrum (1967), several researchers (e.g. Palmer and Rice, 1973; Rice, 1973; Chowdhury, 1978; Quinn et al. 2011) used the concept of fracture mechanics for analysis of localized shear band propagation and progressive failure of slopes in overconsolidated clays. In their analyses, a long inclined slope having a vertical cut *h* have been considered (Fig. 4a) assuming that the length of discontinuity (*l*) is large enough comparing to layer thickness (*h*) and end zone (ω). Note that, length of discontinuity is the sum of the length of initial discontinuity and end zone(s).

In this study shear band propagation in an offshore slope, as shown in Fig. 4b, has been modeled. Unlike the vertical cut in Fig. 4a, there are two end zones (ω_1 & ω_2) in the length of discontinuity l ($=x_1+x_2$). The normal stress acting parallel to the slope (σ_x) increases with depth, however for simplicity in mathematical formulation the average normal stress ($\overline{\sigma}_x$) over depth *h* is used. Assume that $\overline{\sigma}_x = p_0$ far from the discontinuous zone *AB*. There is also a point *O* (Fig. 4b) above the discontinuous zone where $\overline{\sigma}_x = p_0$. The point *O* has been considered as the origin of *x*-*z* axes system used for modeling.

Similar to previous work (e.g. Palmer and Rice, 1973; Puzrin and Germanovich, 2005) the stress-strain behavior of soil above the discontinuous layer is considered to be elastic as the strain in this soil layer is not very significant. Similarly, the strain in soil below the layer of discontinuity is neglected. During slope movement/failure, shear deformation occurs along the thin layer of discontinuity that results in large shear strain. Typical post-peak stress-deformation behavior of marine clay is schematically shown in Fig. 4c. The horizontal axis in this figure represents the displacement from the peak, which means $\delta=\delta_{total}-\delta_p$, where δ_p is the displacement required to attain peak undrained shear strength (s_{up}). As shown in Fig. 4c, the shear strength was reduced to the residual value s_{ur} at large displacement δ_r. In this figure, δ_{95} represents the displacement required for 95% reduction of strength from the peak to remoulded.

MODELING OF POST-PEAK STRESS STRAIN OR DISPLACEMENT BEHAVIOR

Post-peak stress-strain behavior has significant effects on modeling of progressive failure of slopes. Several researchers conducted laboratory tests to understand post-peak behavior of clay both in drained (Lo, 1972; Burland et al. 1977; Burland et al. 1996) and undrained conditions

(Randolph, 2004; Zhou and Randolph, 2007; Burland, 1990; Burland et al. 1996; Tjelta et al. 2002). Based on triaxial drained test results on sensitive overconsolidated clays from various locations, Lo (1972) proposed a hyperbolic relationship between post-peak strength with accumulated strain. Others (e.g. Palmer and Rice, 1973; Puzrin and Germanovich, 2005) used simple linear relationship for modeling shear band formation and progressive failure under drained and undrained conditions. Chowdhury (1978) assumed an arbitrary distribution of shear resistance along the shear band for developing shear band propagation criteria. The main interest of this study is to model progressive slope failure where slip surface passes through marine sensitive clay which is typically found in offshore environments. Compared to drained behavior, relatively less information is available for undrained post-peak behavior of offshore marine sensitive clays. Tavenas et al. (1983) conducted undrained shear strength tests on typical Eastern Canadian marine clays of various level of sensitivity and overconsolidation ratio (OCR), which provide some basis of modeling post-peak behavior. In this study, the degradation of undrained shear strength with post-peak shear displacement has been modeled using the following relationship.

$$s_u = (1+(S_t-1)e^{-3\delta/\delta_{95}})s_{ur} \quad (1)$$

where s_u is the strain-softened undrained shear strength at δ and S_t is the sensitivity of the soil. Equation 1 is a modified form of strength degradation equation proposed by Einav and Randolph (2005). As the displacement and shear band propagation mainly occurs in the thin layer of discontinuity, shear strength degradation equation has been modified in terms of displacement after the peak.

MATHEMATICAL FORMULATION

Using stress equilibrium in the x-direction, the variation of average normal stress in the layer of soil above the discontinuity can be written as

$$h\frac{\partial \bar{\sigma}_x}{\partial x} = -\left(\tau_g - s_u(x)\right) \quad (2)$$

where the value of $\tau_g = \gamma' h \sin\beta$ and $s_u(x)$ in the end zones can be found using Eq. (1), and in the layer of initial discontinuity $s_u(x)= s_{ur}$.

Now, consider the upper end zone ω_2 of the shear band. As the soil block tends to move downward because of gravitational force, unloading occurs in the soil above the layer of discontinuity. Deformation of this soil is assumed to be elastic. The change in average normal stress in this soil layer can be expressed as:

$$\frac{\partial \bar{\sigma}_x}{\partial x} = E_u\frac{\partial \bar{\varepsilon}_x}{\partial x} = E_u\frac{\partial^2 \delta}{\partial x^2}, \text{where: } \delta(x) = \int \bar{\varepsilon}_x dx \quad (3)$$

where E_u is the undrained plain strain elastic modulus for unloading, $\bar{\varepsilon}_x$ is the average normal strain in *x*-direction

Now substituting Eqs. (1) and (3) in Eq. 2 gives:

$$hE_u\frac{\partial^2 \delta}{\partial x^2} = (s_{up}-s_{ur})e^{-3\delta/\delta_{95}} - (\tau_g - s_{ur}) \quad (4)$$

Equation (4) can be written in terms of normalized displacement and coordinate in a form of second order partial differential equation as:

$$\frac{\partial^2 \hat{\delta}}{\partial \hat{x}^2} = e^{-3\hat{\delta}} - r \quad (5)$$

where $\hat{\delta} = \delta/\delta_{95}$ and $\hat{x} = x/l_u'$. Here, l_u' $(=\sqrt{hE_u\delta_{95}/(s_{up}-s_{ur})}$) represents a characteristics length and *r* denotes a stress ratio, $(\tau_g - s_{ur})/(s_{up}-s_{ur})$.

As shown in Fig. 4c, the slope of the shear strength degradation curve is very small near the remolded shear strength and therefore it is very difficult to find the exact value of δ_r from laboratory tests. For practical purpose it could be assumed that the undrained shear strength reduced to s_{ur} at shear displacement δ_{95}.

The boundary conditions at the tips of the upper end zone are (see Fig. 4b):

$\hat{\delta}(\hat{x}_2) = 0$ at point A

$\hat{\delta}(\hat{x}_2 - \hat{\omega}_2) = 1$ at point C (6)

where $\hat{x}_2 = x_2/l_u'$ and $\hat{\omega}_2 = \omega_2/l_u'$.

Consider a point on initial discontinuity just left of point *C*. The average normal stress in the soil layer above this point is

$$\bar{\sigma}_x(x_2-\omega_2) = p_0 - (\tau_g - s_{ur})(x_2-\omega_2)/h \quad (7)$$

On the other hand, just right side of point *C*, the average normal stress is

$$\bar{\sigma}_x(x_2-\omega_2) = p_0 + E_u\bar{\varepsilon}_x = p_0 + E_u\frac{\partial \delta}{\partial x} \quad (8)$$

Equating Eqs. (7) and (8), we obtain the following equation (9) in normalized form.

$$\frac{\partial \hat{\delta}}{\partial \hat{x}} = -r(\hat{x}_2 - \hat{\omega}_2) \quad (9)$$

This actually denotes the slope of the displacement curve at point C where $x=x_2-\omega_2$. The negative sign indicates the reduction of displacement with distance.

Assuming $\partial\hat{\delta}/\partial\hat{x} = \hat{Y}$, Eq. 5 can be written as a first order differential equation as:

$$\frac{\partial \hat{Y}}{\partial \hat{x}} = e^{-3\hat{\delta}} - r \quad (10)$$

which can be rearranged further as

$$\hat{Y}\cdot\partial\hat{Y} = \left(e^{-3\hat{\delta}} - r\right)\partial\hat{\delta} \quad (11)$$

Now, integrating equation (11) with boundary conditions at point C and then equating it with the slope of displacement curve shown in Eq. 9 the following expression is found after some algebraic calculation.

$$\frac{\partial \hat{\delta}}{\partial \hat{x}} = \sqrt{-(2/3)\cdot e^{-3\hat{\delta}} - 2\cdot r\cdot\hat{\delta} + r^2(\hat{x}_2-\hat{\omega}_2)^2 + (2/3)\cdot e^{-3} + 2\cdot r} \quad (12)$$

The integration of the above equation gives the variation of normalized displacement ($\hat{\delta}$) with normalized distance ($\hat{x}$). However, this integration cannot be done analytically.

Therefore, Eq. 12 has been integrated numerically within the interval between $(\hat{x}_2 - \hat{\omega}_2)$ and $\hat{x}_2$, which has been used to calculate the length of initial discontinuity required for shear band propagation to failure.

So far calculation has been shown only for the upper part (x_2 and ω_2), which means the right side of origin O in Fig. 4b. The soil above the layer of discontinuity in the lower part (i.e. the left side of the origin) is under loading (i.e. compressed along x-direction) because of relative movement of the soil block along the layer of discontinuity. Therefore, the undrained elastic modulus (E_l) for loading in plane strain condition should be used to calculate the strain. Note that the soil in the right side of the origin is under unloading conditions. The normal strain in the soil block at x=0 is zero ($\varepsilon_x = 0$). Moreover, the relative displacement (δ) at x=-x_1 and x=x_2 is also zero. Using these boundary conditions, elastic stress-strain relationships of the soil block and equilibrium condition, it can be shown that:

$$\frac{x_1}{x_2} = \sqrt{\frac{E_l}{E_2}} \tag{13}$$

Once the value of $\hat{x}_2$ is known, the total length of the shear band (l=x_1+ x_2) can be calculated as

$$l = \hat{x}_2\left(1 + \sqrt{E_l / E_u}\right)l'_u \tag{14}$$

RESULTS

Soil Parameters and Slope Geometry

As mentioned before, the failure of the slope mainly occurs through the weak marine clay layer which is typically lightly overconsolidated and sensitive. Peak undrained shear strength of this marine clay layer can be determined using the following equation (Koutsoftas and Ladd, 1985; Kvalsted et al. 2005).

$$\frac{s_{up}}{\sigma'_v} = S(OCR)^m \tag{15}$$

where S is the value of s_{up}/σ'_v for normally consolidated marine clay, OCR is the overconsolidation ratio, and m is the exponent for undrained shear strength increase. Based on geotechnical properties of marine clays available in the literature (Tjelta et al. 2002; Kvalsted et al. 2005) the following soil properties have been used in this study: S = 0.2, m = 0.7 and S_t = 6.

The soil layer above the weak clay layer is assumed to be an overconsolidated glacial deposit. The average undrained shear strength ($\bar{s}_u$) of the upper 20 m of glacial deposit is assigned as 50 kN/m^2. Moreover, $E_u / \bar{s}_u$ = 600 and γ'=10 kN/m^3 have been used.

It is also assumed that the depth of the weak marine clay layer (h) is 20 m along which there is potential of shear band propagation and possible failure. The performance of the model has been shown for three slope angles of 3°, 4° and 5°.

Propagation of Shear Band to Failure

Due to some triggering activities such as dissociation of gas hydrate or effect of earthquake, a layer of initial discontinuity might be formed as shown by the thick dashed line in Fig. 4(b). If a limit equilibrium analysis considers the reduced shear strength in this initial layer of discontinuity it may not predict any failure of the slope. However, several large scale submarine slope failure shows that the failure occurs not only over this small finite length of initial discontinuity but over a large distance. Now the question is how this layer of discontinuity (or shear band) propagated such that a failure might occur and lead to a progressive failure.

Using the model presented above the propagation of shear band has been examined. Fig. 5 shows the variation of normalized length of end zone ($\hat{\omega}_i$) with normalized length of shear band ($\hat{x}_i$) from the origin O, where the subscript i could be 1 or 2 (see Fig. 4b). Note that both lengths ($\hat{\omega}_i$ and $\hat{x}_i$) have been normalized by the same characteristic length, l'_u or l'_l. The left side of the curve is asymptotic to vertical. Once the value of $\hat{x}_i$ (i.e. $\hat{x}_2$) is known at this point, the value of l is calculated using Eq. 14. The value of l at this point is referred as "critical length (l_{cr})". For a given condition if the length of the discontinuity is greater than the critical length, the shear band will propagate further along the weak marine clay layer and the failure of the slope is possible even if there are no other additional external loads. This scale failure is referred as "global failure." If the length of discontinuity is less than the critical length no global failure is expected.

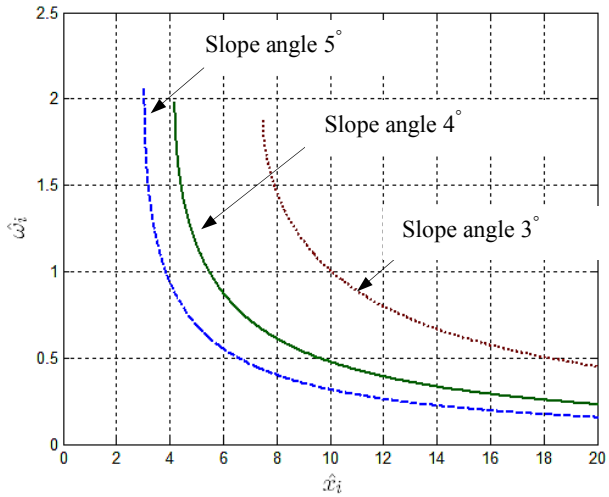

Fig. 5: Relation between normalized length of shear band and its end zone length

These curves also show that $\hat{\omega}_i$ decreases with increase in $\hat{x}_i$. That means the length of end zone decreases with increase in total length of discontinuity. For a large value of

$\hat{x}_i$ the length of the end zone is negligible. In that case, almost along the whole length of discontinuity the shear strength reduced to the remolded value (s_{ur}). Fig. 5 also shows that with increase in slope angle $\hat{\omega}_i$ vs. $\hat{x}_i$ curves shift towards the left, means the lower value of critical length for higher slope angle. In other words, for a higher slope angle even a lower value of initial discontinuity could cause the failure of the slope. For example, for β=3°, r=0.11, $\hat{x}_i$ =7.5 and $\hat{\omega}_i$ =1.9 while for β=5°, r=0.33, $\hat{x}_i$ =3.1 and $\hat{\omega}_i$ =2.1. That means at critical length for β=5°, 68% (=$\hat{\omega}_i / \hat{x}_i$) of the length of discontinuity is the end zone where the shear strength varies between peak and remoulded shear strength. Only in the remaining part 32% (=100-68%) the shear strength reduced to the remoulded value. Therefore, single value of shear strength as typically used in limit equilibrium analysis does not give realistic results. Similarly, for β=5° it can be shown that for a large value of $\hat{x}_i$, for example $\hat{x}_i$ =50, almost in 100% length of discontinuity the shear strength reduced to remolded value. That means, if the initial length of discontinuity is very large then use of unique value of shear strength along the layer of discontinuity is acceptable.

So far the results have been presented in normalized form. To calculate the actual value of critical length, δ_{95}=100 mm and E_l=E_u /4 have been used. Using these parameters the value of characteristic length, l'_u = 42.5 m can be calculated. That gives critical lengths of 478 m and 197 m for slope angle 3° and 5°, respectively. The total length of end zone (ω_1+ω_2) is 121 m and 133m for slope angle 3° and 5°, respectively. Note that the length of end zone is significantly greater than the depth of slide of 20 m.

Length of Submarine Landslide

In offshore, submarine slides of several kilometer lengths have been reported in the past. In this section, we will examine how a relatively small length of initial discontinuity could lead to a large scale submarine slide.

Using limit equilibrium concept the factor of safety (F_s) of the soil block above the layer of discontinuity can be calculated as:

$$F_s = \frac{\bar{p}_p h + s_{ur} l}{\bar{p}_a h + \tau_g l} \tag{16}$$

where $\bar{p}_a$ and $\bar{p}_p$ are the average active and passive earth pressure in the upper and lower end, respectively.

The minimum length (l_f) required to cause the failure of a slope in undrained condition can be obtained by using F_s=1 and l= l_f in Eq. 16.

$$l_f = \frac{4\bar{s}_u h}{\tau_g - s_{ur}} \tag{17}$$

where $\bar{s}_u$ is the average undrained shear strength of the soil layer above the layer of discontinuity.

Now for a given length of discontinuity (l) the factor of safety equation for shallow depth of discontinuity (h<<l) in limit equilibrium analysis can be expressed in terms of l_f as:

$$F_s = \frac{s_{ur}}{\tau_g} + \frac{l_f}{l}\left(1 - \frac{s_{ur}}{\tau_g}\right) \tag{18}$$

The failure is possible only if $l \geq l_f$.

On the other hand in the method presented in this study if $l \geq l_{cr}$ the shear band propagates further until it reaches to l_f and global failure occur. Therefore, the factor of safety in this study can be defined by replacing l_f by l_{cr} in Eq. 18.

$$F_s = \frac{s_{ur}}{\tau_g} + \frac{l_{cr}}{l}\left(1 - \frac{s_{ur}}{\tau_g}\right) \tag{19}$$

Fig. 6 shows the calculated F_s using Eqs. 18 and 19 for slope angle of 3°. Other parameters used in this calculation are listed above. As shown, limit equilibrium analysis (Eq. 18) gives a higher value of F_s. For example, if the length of discontinuity is 500 m, limit equilibrium method gives F_s=1.4, implying that the slope is stable. However, using the proposed method F_s is less than 1.0, which means the slope is unstable. The minimum length of discontinuity required to cause the failure of the slope can be found from this graph when F_s=1. The proposed method predicts that the slope will fail only if $l \geq$ 478 m (l_{cr}) while in limit equilibrium method it will fail only if $l \geq$ 1050 m (l_f). Note that, in the proposed method shear band propagation starts from l=478 m and will reach to l=1050 m and fail. That means the final length of failure using both methods is same.

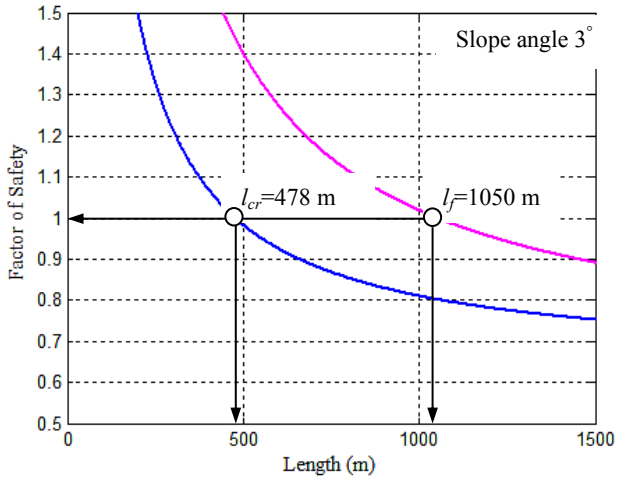

Fig. 6: Variation of factor of safety with length of discontinuity

Once such a block of soil fails the support in the remaining slope might be lost or reduced. This in turn might cause retrogressive failure of the upper slope which could be one of the causes of large scale landslides.

CONCLUSIONS

This paper presents an application of fracture mechanics technique to shear band propagation in marine sensitive clays as implied in several submarine landslides locations. The degradation of undrained shear strength of clay with shear displacement is modeled using a simple relationship. It is shown that the limit equilibrium method over predicts the factor of safety. The calculated length of weak zone or shear discontinuity required to cause the failure of a submarine slope using the proposed method is significantly less than that from the limit equilibrium method.

ACKNOWLEDGEMENTS

The writers would like to acknowledge the financial support from Research & Development Corporation of Newfoundland and Labrador and C-CORE.

REFERENCES

Bjerrum, L (1967)."Progressive failure in slopes of overconsolidated plastic clay and clay shales," *J Soil Mech Found Engng Div*, ASCE, Vol 93, No SM5, pp 1–4.

Bryn, P, Berg, K, Forsberg, CF, Solheim, A and Kvalstad, T (2005). "Explaining the Storegga slide," *Marine and Petroleum Geology*, Vol 22, No 1-2, pp 11–19.

Bryn, P. Berg, K. and Solheim, A (2002). "Storegga Geomodel and its use in slide risk evaluation," *Int Conf Offshore Site Investigation and Geotechnics*, London, pp 219–232.

Burland, JB, Longworth, TI and Moore, JFA (1977). "A study of ground movement and progressive failure caused by a deep excavation in Oxford Clay," *Géotechnique*, Vol 27, No 4, pp 557–591.

Burland, JB (1990). "On the compressibility and shear strength of natural clays," *Géotechnique*, Vol 40, No 3, pp 329–378.

Burland, JB, Rampello, S, Georgiannou, VN and Calabresi, G (1996). "A laboratory study of the strength of four stiff clays," *Géotechnique*, Vol 46, No 3, pp 491–514.

Chowdhury, RN (1978). "Propagation of failure surfaces in natural slopes," *J Geophysical Res*, Vol 83, No B12, pp 5983–5988.

Einav, I and Randolph, MF (2005). "Combining upper bound and strain path methods for evaluating penetration resistance," *Int J Num Methods Eng*, Vol 63, No 14, pp 1991–2016.

Hadj-Hamou, T. and Kavazanjian, E. Jr (1985). "Seismic stability of gentle infinite slopes," *J Geotechnical Eng*, ASCE, Vol 111, No 6, pp 681–697.

Joasted, HP, Andersen, L and Thakur, V (2006). "Calculation of shear band thickness in sensitive clays," *Proc 6th European Conf on Num Methods in Geotechnical Eng*, Graz, Austria, pp 27–32.

Koutsoftas, DC and Ladd, CC (1985). "Design strengths for an offshore clay," *J Geotechnical Eng*, ASCE, Vol 111, No 3, pp 337–355.

Kvalstad, TJ, Andresen, L, Forsberg, CF, Berg, K and Bryn, P (2005). "The Storegga Slide: evaluation of triggering sources and slide mechanisms," *Marine and Petroleum Geology*, Vol 22, No 1-2, pp 245–256.

Kvalstad, TJ, Nadim, F, Kaynia, AM, Mokkelbost, KH and Bryn, P (2005). "Soil conditions and slope stability in the Ormen Lange area, " *Marine and Petroleum Geology*, Vol 22, No 1-2, pp 299–310.

Laberg, JS, Vorren, TO, Mienert, J, Haflidason, H, Bryn, P and Lien, R (2003). "Preconditions leading to the Holocene reconditions leading to the holocene trænadjupet slide offshore norway," *In* J Locat and J Mienert(eds): *Submar Mass Movem and Their Conseq*, pp 247–254.

Landon, MM (2007). "Development of a Non-Destructive Sample Quality Assessment Method for Soft Clays," *Ph.D. Thesis*, Univ. of Massachusetts Amherst, Amherst.

Lo, KY (1972). "An approach to the problem of progressive failure," *Can Geotech J*, Vol 9, No 4, pp 407–429.

Lunne, T, Berre T, Andersen, KH, Strandvik, S and Sjursen M (2006). "Effect of sample disturbance and consolidation procedures on measured shear strength of soft marine Norwegian clays," *Can Geotech J*, Vol 43, pp 726–750.

Palmer, C. and Rice, JR (1973). "The growth of slip surfaces in the progressive failure of overconsolidated clay," *Proc R Soc A*, 332, pp 527–548.

Puzrin, AM. and Germanovich, LN (2005). "The Growth of Shear Bands in the Catastrophic Failure of Soils," *Proc R Soc A*, Vol 461, No 2056, pp 1199–1228.

Quinn, PE, Diederichs, MS, Rowe, RK and Hutchinson, DJ (2011). "A new model for large landslides in sensitive clay using a fracture mechanics approach," *Can Geotech J*, Vol 48, pp 1151–1162.

Randolph MF (2004). "Characterization of soft sediments for offshore applications," Keynote Lecture, *Proc Second Int Conf on Site Characterisation*, Porto, Vol 1, pp 209 –231.

Rice, JR (1973). "The initiation and growth of shear bands," *In Plasticity and soil mechanics* (ed. A. C. Palmer), Cambridge, pp 263–274.

Skempton, AW (1964). "Long-term stability of clay slopes," *Géotechnique*, Vol 14, No 2, pp 77–102.

Solheim, A, Bryn, P, Sejrup, HP, Mienert, J, Berg, K (2005). "Ormen Lange—an integrated study for the safe development of a deep-water gas field within the Storegga Slide Complex, NE Atlantic continental margin; Executive summary," *Marine and Petroleum Geology*, Vol 22, No 1-2, pp 1–9.

Tjelta, TI, Strout, J, Solheim, A, Mokkelbost, KR, Berg, K, Bryn P. (2002). "Geological and geotechnical site investigations in the Storegga Slide area," *International Conference Offsh Site Investigation and Geotechnics*, London, pp 199–217.

Tavenas, F., Flon, P., Leroueil, S., and Lebuis, J (1983). "Remolding energy and risk of slide retrogression in sensitive clays," *Proc of the Symp on Slopes on Soft Clays*, Linköping, Sweden, Swedish Geotechnical Institute (SGI) Report No. 17, pp. 423–454.

Yang, SL, Solheim, A, Kvalstad, TJ, Forsberg, CF and Michael Schnellmann, M (2006). "Behaviour of the sediments in the Storegga Slide interpreted by the steady state concept," *Norwegian J of Geology,* Vol 86, No 3, pp 243–253.

Zhou, H and Randolph, MF (2007). Computational techniques and shear band development for cylindrical and spherical penetrometers in strain-softening clay. *Int J Geomech*, ASCE, Vol 7, No 4, pp 287–295.

Appendix-III

Progressive failure of slopes with sensitive clay layers

This paper has been published and presented in the 18th International Conference on Soil Mechanics and Geotechnical Engineering, Paris, 2013.

Most of the research work presented in this paper was conducted by the first author. He also prepared the draft manuscript. The other authors supervised the research and reviewed the manuscript.

Progressive failure of slopes with sensitive clay layers

Le non progressive des pentes avec des couches d'argile sensible

R. Dey & B. Hawlader
Memorial University of Newfoundland, St. John's, Canada.
R. Phillips
C-CORE, St. John's, Canada.
K. Soga
University of Cambridge, Cambridge, UK.

ABSTRACT: Progressive failure of slopes can trigger large scale landslides. The presence of sensitive clay layers is one of the main reasons for progressive failure of a slope. The whole soil mass involved in a potential landslide might be of sensitive clay, while in some cases there exist only thin layers of sensitive clay interbedded with relatively strong soils. The movement of a slope might be initiated due to the presence of a weak soil layer, where the shear stress is increased or soil strength is reduced by various triggering factors. Once the failure/movement is initiated in a small zone, the imbalanced force is transferred to the surrounding soil in which slip surface might propagate in the form of a shear band through the sensitive clay layer even though the sensitive clay layer is relatively thin. The propagation of shear band in sensitive clay is also associated with post-peak strain softening behaviour of soil. In this study, upward progressive failure due to river bank erosion has been modelled using nonlinear post-peak strain softening behaviour. It is shown that the pattern of propagation of shear band varies with soil type and slope geometry.

RÉSUMÉ :Défaillance progressive des pentes peuvent déclencher des glissements de terrain de grande envergure. La présence de couches d'argile sensible est l'une des principales raisons de la rupture progressive d'une pente. La masse du sol tout impliqué dans un glissement de terrain potentiel pourrait être d'argile sensible, alors que dans certains cas, il existe des couches minces de seulement argile sensible interstratifiées avec des sols relativement fortes. Le mouvement d'une pente peut être initié en raison de la présence d'une couche de sol faible, où le rapport contrainte de cisaillement augmente ou diminue la résistance du sol par divers facteurs de déclenchement. Une fois la panne / mouvement est initié dans une petite zone, la force de déséquilibre est transféré vers le sol environnant, dans lequel la surface de glissement peut se propager sous la forme d'une bande de cisaillement à travers la couche d'argile sensible, même si la couche d'argile sensible est relativement mince. La propagation des bandes de cisaillement dans l'argile sensible est également associée à post-pic souche ramollissement comportement du sol. Dans cette étude, l'échec à la hausse progressive due à l'érosion des berges a été modélisée à l'aide non-linéaire post-pic souche ramollissement comportement.Il est montré que le modèle de propagation des bandes de cisaillement varie en fonction du type de sol et de géométrie de la pente.

KEYWORDS: Sensitive clay, progressive failure, spread, shear band propagation, strain softening.

INTRODUCTION

Large landslides in soft sensitive clays are common in Eastern Canada and Scandinavia. Most of the onshore slides which occurred in soft sensitive clay have been reported as progressive in nature (Bernander 2000, Locat et al. 2008, Quinn 2009, Locat et al. 2011). The presence of strain-softening clay layers is one of the main reasons for progressive failure of a slope.These slides could be in the form of multiple retrogressive, translational progressive or spreads (Tavenas 1984, Karlsrud et al. 1984). Failure might be initiated in a fully stable and/or marginally stable slope depending on the nature of triggering factors. Failure could propagate either in upward or downward direction and the movement of the slope might be initiated due to the presence of a weak soil layer, where the shear stress is increased or soil strength is reduced by various triggering factors. Large landslides in sensitive clays classified as spread (Cruden and Varnes 1996) might be triggered by erosion near the toe of the river bank slope (Quinn et al. 2007, Locat et al. 2008). Numerous spread failures such as Sköttorp landslide in Sweden (Odenstad 1951) and the landslides occurred in Quebec including 1989 Saint-Liguori landslide (Grondin and Demers 1996), Saint-Ambroise-de-Kildare landslide (Carson 1979), Saint-Barnabé-Nord slide (Locat et al. 2008) have been reported to be triggered by erosion at the toe of the slope (Bernander 2000, Locat et al. 2008, Quinn et al. 2007, Locat et al. 2011), although it is very difficult to identify the true disturbing agents which caused these spread failures.

Progressive failure might occur in drained as well as undrained conditions. Bjerrum (1967) explained upward progressive failure initiation in an intact slope containing overconsolidated plastic clays and clay shales and considered the failure as drained. Sensitive clays from Eastern Canada and Scandinavia show strain softening behavior under undrained loading which has been considered as one of the main reasons for developing progressive failure (Bernander 2000, Locat et al 2008, Quinn 2009, Locat et al 2011). Hence undrained condition is considered in this study for analyzing spread failure.

During Ormen Lange field development, numerical simulations have been carried out by Norwegian Geotechnical Institute (NGI) using PLAXIS software to analyze the potential of retrogressive sliding due to strain softening effect in mild clay slopes (NGI 2001). Anderson and Jostad (2007) conducted numerical analyses of progressive failure of slope by modeling the shear band as an interface element using the NGI finite element (FE) code BIFURC. Quinn (2009) also demonstrates the use of linear elastic fracture mechanics concept in progressive failure of slopes.

This paper describes a numerical technique which can be used to analyze the spread or upward progressive failure of a slope typically occurs in river banks due to toe erosion.

PROBLEM DEFINITION

The geometry of the slope modeled in this study is shown in Fig. 1. The river bank has a slope of 30° to the horizontal. A thick crust of overconsolidated clay near the face of the slope and below the ground surface is assumed. For simplicity the groundwater table is assumed at the crest of the slope and the river is full. A block of soil near the toe of the slope shown by the hatched zone is removed, which could be caused by erosion or by excavation in the field. This block will be referred as "excavated/eroded soil block." It is also assumed that the erosion or excavation is occurred relatively fast such that the deformation/failure of remaining soil is in undrained condition.

Three cases are simulated in this study. In Case-I, the ground surface is horizontal and there is a 15 m thick layer of sensitive clay below the 5 m crust. The Case-II is same as Case-I but the ground surface is inclined upward at 4°. Sometimes in the field there may not be a thick sensitive clay layer. To investigate the effect of thickness of the sensitive clay layer, in Case-III only 1.0 m thick sensitive clay layer parallel to the horizontal ground surface from the toe of the slope is assumed. The soil above this layer has the same geotechnical properties of the crust used in Cases I & II. In all three cases, the base layer below the toe of the slope is very stiff and therefore the failure is occurred in the soil above the base layer. The length of the soil domain in the present FE model is 500 m and therefore no significant effects on the results are expected from the right boundary.

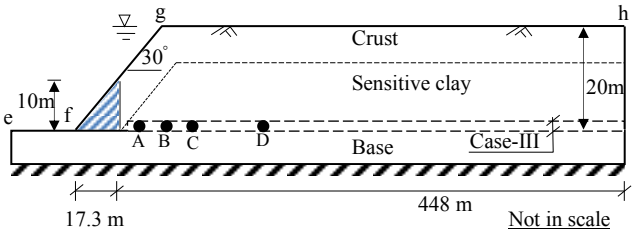

Figure 1. Geometry of the slope used in numerical analysis

FINITE ELEMENT MODELING

Numerical technique

ABAQUS 6.10 EF-1 is used in this study. The progressive slope failure is fundamentally a large deformation problem as very large plastic shear strain is developed in a thin layer of soil through which the failure of the slope is occurred. Conventional finite element techniques developed in Lagrangian framework cannot model such large strain problems because significant mesh distortion occurs. In order to overcome these issues, Coupled Eulerian-Lagrangian (CEL) technique currently available in ABAQUS FE software is used. The finite element model consists of three parts: (i) soil, (ii) excavated/eroded soil block, and (iii) void space to accommodate displaced soil mass. The soil is modeled as Eulerian material using EC3D8R elements, which are 8-noded linear brick, multi-material, reduced integration with hourglass control elements. In ABAQUS CEL, the Eulerian material (soil) can flow through the fixed mesh. Therefore, there is no numerical issue of mesh distortion or mesh tangling even at large strain in the zone around the failure plane.

The excavated/eroded soil block is modeled in Lagrangian framework as a rigid body, which makes the model computationally efficient. A void space is created above the model shown in Fig. 1 using the "volume fraction" tool. Soil and void spaces are created in Eulerian domain using Eulerian Volume Fraction (EVF). For void space EVF is zero (i.e. no soil). On the other hand, EVF is unity in clay layers shown in Fig. 1, which means these elements are filled with Eulerian material (soil).

Zero velocity boundary conditions are applied at all faces of the Eulerian domain (Fig.1) to make sure that Eulerian materials are within the domain and cannot move outside. That means, the bottom of the model shown in Fig. 1 is restrained from any movement, while all the vertical faces are restrained from any lateral movement. No boundary condition is applied at the soil-void interface (*efgh* in Fig. 1) so that the soil can move into the void space when displaced.

Only a three-dimensional model can be generated in ABAQUS CEL. In the present study the model is only one element thick, which represents the plane strain condition.

The numerical analysis consists of two steps of loading. In the first step geostatic load is applied to bring the soil in in-situ condition. Note that under geostatic step the slope is stable with some shear stress especially near the river bank. In the second step, the rigid block of excavated/eroded soil is moved horizontally 2 m to the left using displacement boundary condition.

Soil parameters

Table 1 shows the geotechnical parameters used in this study. The crust has an average undrained shear strength of 60 kPa, and a modulus of elasticity of 10 MPa (=167s_u). The soil in the base layer is assumed to be very strong and s_u=250 kPa and E_u=100 MPa is used.

Table 1. Parameters for finite element modelling.

Crust	
Undrained modulus of elasticity, E_u (kPa)	10,000
Undrained shear strength, s_u (kPa)	60
Submerged unit weight of soil, γ' (kN/m^3)	9.0
Poisson's ratio, ν_u	0.495
Sensitive clay	
Undrained modulus of elasticity, E_u (kPa)	7,500
Poisson's ratio, ν_u	0.495
Peak undrained shear strength, s_{up} (kPa)	50
Residual undrained shear strength, s_{ur} (kPa)	10
Submerged unit weight of soil, γ' (kN/m^3)	8.0
Plastic shear strain for 95% degradation of soil strength, γ^p_{95} (%)	33

Proper modeling of stress-strain behavior of sensitive clay layer is the key component of progressive failure analyses in sensitive clays. When sensitive clay is subjected to undrained loading it shows post-peak softening behavior. Various authors (e.g. Tavenas et al. 1983, Quinn 2009) showed that the post-peak softening behavior is related to post-peak displacement or plastic shear strain. The following exponential relationship of shear strength degradation as a function of plastic shear strain is used in the present study.

$$s_u=[1+(S_t-1)\exp(-3\delta/\delta_{95})]s_{ur} \quad (1)$$

where s_u is the strain-softened undrained shear strength at δ; S_t is sensitivity of the soil; $\delta=\delta_{total}-\delta_p$ where δ_p is the displacement required to attain the peak undrained shear strength (s_{up}); and δ_{95} is the value of δ at which the undrained shear strength of the soil is reduced by 95% of (s_{up}-s_{ur}). Equation 1 is a modified form of strength degradation equation proposed by Einav and Randolph (2005) and was used by the authors (Dey et al. 2012) to model submarine landslides. If the thickness of shear band (t) is known, the corresponding plastic shear strain (γ^p) can be calculated as, $\gamma^p=\delta/t$ assuming simple shear condition. Therefore, Eq.1 in terms of γ^p can be written as

$$s_u = [1+(S_t-1)\exp(-3\gamma^p/\gamma^p_{95})]s_{ur} \quad (2)$$

where γ^p_{95} is the value of γ^p at 95% strength reduction (i.e. $\gamma^p_{95}=\delta_{95}/t$). Note that, it is very difficult to determine the thickness of the shear band in the field. Similar to some previous studies (e.g. Quinn 2009) t=0.375 m is used which is same as the mesh height used in the present FE analysis. In ABAQUS the degradation of shear strength of sensitive clay is varied as a function of plastic strain. The parameters used to model the sensitive clay using Eq. 2 are also shown in Table 1. These parameters are estimated based on the laboratory tests conducted on sensitive clays (e.g. Tavenas et al., 1983) and the interpretation of test data and constitutive model development by other researchers (e.g. Bernander 2000, Leroueil 2001, Locat et al. 2008, Quinn 2009, Locat et al. 2011).

FINITE ELEMENT RESULTS

Propagation of shear band

Figure 2 shows the variation of equivalent plastic shear strain for three cases. In Cases-I & II the shear band initially propagates horizontally and then curved upward resulting in global failure. The failed soil mass follows the excavated/eroded soil block. Figures 2(a) & 2(b) show the equivalent plastic shear strain when the plastic shear strain in the entire failure plane is greater than γ^p_{95}. Global failure does not occur in Case-III (Fig. 2c). There is an approximately 1.4 m gap between the vertical face of the block and soil mass at the right. The shear band propagates horizontally and finally ended at certain length. Figure 2(c) also shows the plastic shear strain when the shear band propagation is ended. Whether the shear

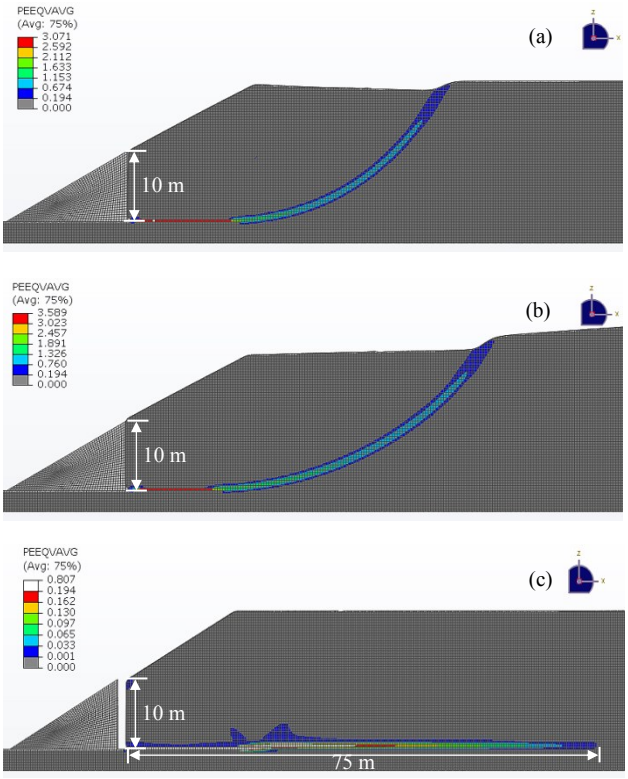

Figure 2. Developed equivalent plastic strain in the softening layer in case I, II and III respectively

band will propagate upward and cause the global failure or not, depends on the shear strength of the upper soil layer and mobilized shear strength along the shear band. For the soil properties and geometry used in the present study the failure pattern is almost same for Cases-I and II. However, the released energy from the excavated/eroded soil block is not sufficient to move the shear band upward in Case-III to cause the failure of the slope.

The equivalent plastic shear strain, denoted by the symbol PEEQVAVG in Fig. 2, is related to γ^p as PEEQVAVG= $\gamma^p/\sqrt{3}$. According to Eq. (2), when $\gamma^p \geq \gamma^p_{95}$ (=33%), that means PEEQVAVG=0.194, the undrained shear strength is less than 12 kPa (=50-0.95(50-10)). Figure 2(c) shows that the equivalent plastic shear strain greater than 0.194 is developed in the shear band only near the vertical face of excavated/eroded block in Case-III. However, the equivalent plastic shear strain greater than 0.194 is developed in the entire length of the failure plane in Case-I & Case-II. Therefore, the failure of the slope is occurred in both cases at residual shear strength on the failure plane as large strain is developed.

Shear stress and mobilized shear strength

The Case-III is considered for further examination of the development of shear stress and mobilized shear strength along the potential failure plane. Figure 3 shows the variation of shear stress along the failure plane with movement of excavated/eroded block. Shear stress for four displacements (115 mm, 245 mm, 380 mm and 500 mm) are shown. In order to explain the process, consider the shear stress on the potential failure plane for the block displacement of 115 mm. The maximum shear stress (50 kPa) is developed at 12.5 m from the vertical face of the cut. The shear stress between 0 to 12.5 m is less than 50 kPa (i.e. s_{up}) and greater than 10 kPa (i.e. s_{ur}). That means, 0-12.5 m of the shear band represents the post-peak softening zone where the reduction of shear strength is occurred because of plastic strain as Eq. 2, and the mobilized shear strength is in between the peak and residual shear strength of the soil. In the right side of the peak (i.e. distance greater than 12.5 m) the shear stress is again reduced with distance. For this displacement of the block (115 mm), the shear stress in the

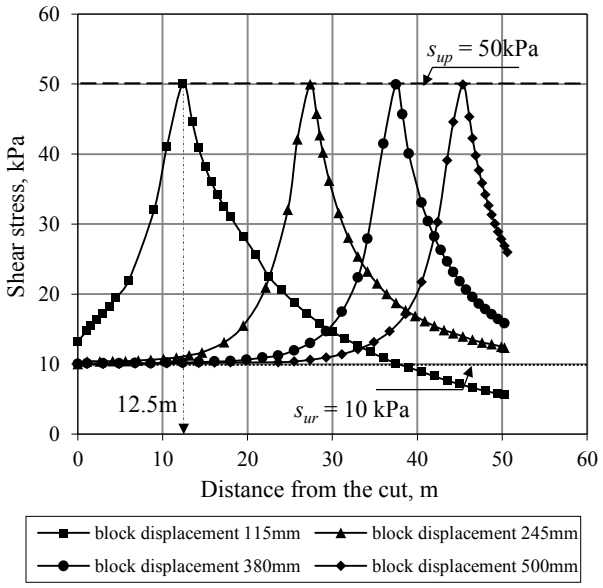

Figure 3. Shear stress along the potential failure plane

potential failure plane at a distance greater than 12.5 m is not increased to the peak, and therefore it represents the pre-peak behavior. At a very large distance, the shear stress is reduced to zero in Case-III as the ground surface is horizontal. The pattern of shear stress development for any other displacement of the

block is similar as shown in Fig. 3. The location of the peak shear stress shifts to the right with increase in block displacement; that means a greater length of the potential failure plane is in post-peak stress-strain condition. For example, for 500 mm block movement the peak is occurred at 45.5 m and therefore 0-45.5 m is in post-peak condition with approximately 30 m in residual shear strength level. This process will be continued until the shear band propagation is ended for stable slopes as in Case-III. However, if the failure is occurred, as in Case-I and II, the large plastic shear strain will reduce the shear strength of soil in the entire failure plane to the residual shear strength and global failure will occur.

Figure 4 shows the variation of shear stress at 4 different locations A, B, C and D (Fig. 1) which are located from the vertical face of the excavated/eroded block at horizontal distance of 3 m, 12.5 m, 25 m and 35 m, respectively. Consider the soil element B at 12.5 m distance. The shear stress in this element is increasing with movement of the excavated/eroded soil block. When the block is displaced by an amount of 115 mm, the shear stress in this element is reached to the peak shear strength of the soil (50 kPa). However, at this displacement of the block, the element A is almost at the residual shear strength. On the other hand, the elements C and D are still in the pre-peak state. That means the shear stress is gradually transferred to the soil elements in the right with displacement of the excavated/eroded soil block. For the soil element under the slope of the river bank there is an initial shear stress. With movement of the block the shear stress is increased from that initial value. However, the initial shear stress is less in the elements far from the river bank. Similar variation in shear stress and mobilized shear strength are obtained for Case-I and II.

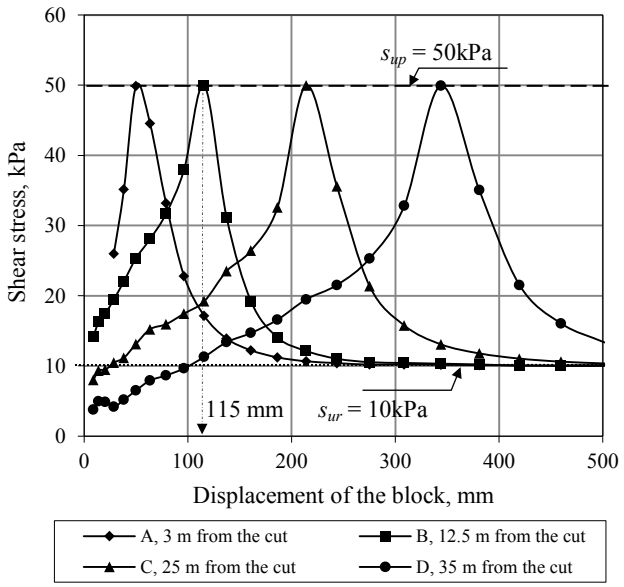

Figure 4. Variation of shear stress at four different locations from the cut

CONCLUSION

This paper presents a new numerical approach to model the initiation and propagation of shear band in upward progressive failure as encountered near the river banks. Toe erosion is considered as the triggering factor. Coupled Eulerian-Lagrangian (CEL) approach currently available in ABAQUS FE software is used for numerical analysis. Nonlinear strain softening behavior of sensitive clay is incorporated in this large deformation finite element analysis. Three cases are analyzed in this study. In Cases I and II global failure is occurred. However, in Case-III, although global failure is not occurred, the shear band propagation reduced the shear strength in the potential failure plane significantly over a large distance and the slope might be marginally stable for further loading.

ACKNOWLEDGEMENTS

The writers would like to acknowledge the financial support from Research & Development Corporation of Newfoundland and Labrador and C-CORE.

REFERENCES

Anderson L. and Jostad H.P. 2007. Numerical modeling of failure mechanisms in sensitive soft clays — application to offshore geohazards. *Offshore Tech. Conf.*, Texas. Paper OTC 18650.

Bernander S. 2000. Progressive failure in long natural slopes: formation, potential extension and configuration of finished slides in strain-softening soils. Licentiate Thesis, Luleå University of Technology.

Bjerrum L. 1967. Progressive failure in slopes in overconsolidated plastic clay and clay shales. Terzaghi Lecture. *J. of the Soil Mech. and Found. Div.*, ASCE 93(5), 3-49.

Carson M.A. 1979. On the retrogression of landslides in sensitive muddy sediments: Reply. *Can. Geotech. J.* 16(2), 431-444.

Cruden D.M. and Varnes D.J. 1996. Landslides types and processes. In Landslides investigation and mitigation. *Special Report 247.* Transportation Research Board, NRC. Edited by A.K. Turner and R.L. Schuster. National Academy Press, Washington, D.C., 37-75.

Dey R., Hawlader B., Phillips R. and Soga K. 2012. Effects of shear band propagation on submarine landslide. *Proc. of the 22nd Int. Offshore and Polar Engineering Conf.,* Rhodes, Greece,766- 773.

Einav I. and Randolph M.F. 2005. Combining upper bound and strain path methods for evaluating penetration resistance. *Int. J. Num. Methods Engineering*63(14), 1991-2016.

Grondin G. and Demers D. 1996. The Saint-Liguori flakeslide: Characterization and remedial works. *In Proc. of the 7th Int. Symposium on Landslides*, Trondheim, Norway, 2, 743-748.

Gregersen O. 1981. The quick clay landslide in Rissa, Norway. *In Proc. of the 10th Int. Conf. on Soil Mech. and Foundation Engineering,* Stockholm, Sweden. NGI, Publication No. 135, 421-426.

Karlsrud K., Aas G. and Gregersen O. 1984. Can we predict landslide hazards in soft sensitive clays? Summary of Norwegian practice and experiences. *In Proc. of the 4th Int. Symposium on Landslides,* Toronto, Ont., 1, 107-130.

Leroueil S. 2001. Natural slopes and cuts: movement and failure mechanisms. *Géotechnique* 51 (3), 197-243.

Locat A., Leroueil S., Bernander S., Demers D., Locat J. and Ouehb L. 2008. Study of a lateral spread failure in an eastern Canada clay deposit in relation with progressive failure: the Saint-Barnabé-Nord slide. *In Proc. of the 4th Canadian Conf. on Geohazards: From Causes to Management,* Québec, Que., 89-96.

Locat A., Leroueil S., Bernander S., Demers D., Jostad H.P. and Ouehb L. 2011. Progressive failures in eastern Canadian and Scandinavian sensitive clays. *Can. Geotech. J.* 48 (11), 1696-1712.

NGI Report 2001. Effect of strain softening on stability analysis. Analysis of retrogressive sliding due to strain softening-Ormen Lange case study, Report No 521001 (10).

Odenstad S. 1951. The landslide at Sköttorp on the Lidan River, February 2, 1946. *Royal Swedish Institute Proceedings* 4, 1-38.

Quinn P., Diederichs M.S., Hutchinson D.J. and Rowe R.K. 2007. An exploration of the mechanics of retrogressive landslides in sensitive clay. *In Proc. of the 60th Canadian Geotechnical Conf.*, Ottawa, Ontario, 721-727.

Quinn P. 2009. Large Landslides in Sensitive Clay in Eastern Canada and the Associated Hazard and Risk to Linear Infrastructure. Doctoral thesis, Queen's University.

Tavenas F., Flon P., Leroueil S. and Lebuis J. 1983. Remolding energy and risk of slide retrogression in sensitive clays. *Proc. of the Symposium on Slopes on Soft Clays,* Linköping, Sweden, SGI Report No. 17, 423-454.

Tavenas F. 1984. Landslides in Canadian sensitive clays — a state-of the-art. *In Proc. of the 4th Int. Symposium on Landslides*, Toronto, Ont., 1, 141-153.

Appendix-IV

Stability analysis of a river bank slope with an existing shear band

This paper has been published and presented in 6th Canadian Geohazard Conference, Kingston, Ontario, 2014.

Most of the research work presented in this paper was conducted by the first author. He also prepared the draft manuscript. The other authors supervised the research and reviewed the manuscript.

Stability analysis of a river bank slope with an existing shear band

Rajib Dey & Bipul Hawlader
Faculty of Engineering – Memorial University of Newfoundland, St. John's, Canada
Ryan Phillips
C-CORE, St. John's, Canada
Kenichi Soga
Faculty of Engineering – University of Cambridge, Cambridge, UK

ABSTRACT
Progressive failure of slopes near a river bank can cause large scale landslides. The presence of sensitive clay layers which show strain softening behaviour is considered as one of the main factors facilitating the progressive failure of such slopes. Various triggering factors such as river bank erosion, construction and other activities near the bank might initiate the failure of slopes. Once the movement is initiated in a small zone where sensitive clay layers exist, the imbalanced force is transferred to the surrounding soil in which slip surfaces might propagate in the form of a shear band through the sensitive clay layer. In this study, upward progressive failure due to river bank erosion has been modelled numerically incorporating nonlinear post-peak strain softening behaviour. Then the stability of this so-called stable slope, with an existing shear band in the sensitive clay layer, is further analysed for additional triggering loads. It is shown that additional loads from human activities near river banks such as embankment/road construction could cause a global failure of slopes with pre-existing shear bands. It is also shown that the brittleness of sensitive clay could accelerate the progressive failure of slopes.

RÉSUMÉ
Défaillance progressive des pentes près d'une rivière peut provoquer des glissements de terrain à grande échelle. La présence de couches d'argile sensible qui présentent un comportement souche de ramollissement est considéré comme l'un des principaux facteurs favorisant la rupture progressive de ces pistes. Divers facteurs déclenchants tels que l'érosion des berges, la construction et d'autres activités à proximité de la banque pourraient engager l'échec des pistes. Une fois que le mouvement est initié dans une petite zone où les couches d'argile sensible existe, la force de déséquilibre est transférée vers le sol environnant dans lequel les surfaces de glissement peuvent se propager sous la forme d' une bande de cisaillement à travers la couche d'argile sensible. Dans cette étude , la rupture progressive à la hausse en raison de l'érosion des berges de la rivière a été modélisé numériquement intégrant le comportement post-pic souche de ramollissement non linéaire. Ensuite, la stabilité de cette pente dite stable, avec une bande de cisaillement existant dans la couche d'argile sensible, est en outre analysé pour déterminer les charges de déclenchement supplémentaires. Il est montré que les charges supplémentaires résultant des activités humaines à proximité des berges tels que la construction du remblai / route pourraient provoquer une panne mondiale de pistes avec des bandes de cisaillement préexistantes. Il est également montré que la fragilité de l'argile sensible pourrait accélérer la défaillance progressive des pentes.

INTRODUCTION

Large landslides in soft sensitive clays are common in Eastern Canada and Scandinavia and considered a major hazard in these countries because of their retrogressive potential and high mobility. Most onshore landslides which occurred in soft sensitive clay have been reported as progressive in nature (Bernander 2000, 2008, Locat et al. 2008, Quinn 2009, Locat et al. 2011, 2013). Progressive failure might be initiated in a fully stable and/or marginally stable slope depending on the nature of the triggering factors. Failure could propagate either in an upward or downward direction, towards the river bank, and the movement of the slope might be initiated because of the presence of a weak soil layer, where the shear stress is increased or soil strength is reduced by the triggering factors. The presence of strain-softening clay layers is one of the main reasons for progressive failure of a slope. These landslides could be in the form of multiple retrogressive, translational progressive or spreads (Tavenas 1984, Karlsrud et al. 1984). Upward progressive failure might be initiated near river banks due to the presence of weak soil layers, where shear stress ratio is increased or soil strength is reduced by various triggering factors such as toe erosion. Large landslides in sensitive clays classified as spreads (Cruden and Varnes 1996) might be triggered by erosion near the toe of the river bank slope (Quinn et al. 2007, Locat et al. 2008). Numerous spread failures have been reported to be triggered by erosion at the toe of the slope (Bernander 2000, Locat et al. 2008, Quinn et al. 2007, Locat et al. 2011), although it is very difficult to identify the true disturbing agents which caused these spread failures. On the other hand, it has also been reported that additional applied loads or disturbance near the river bank due to human activities such as embankment construction, could cause disastrous landslides (for examples, the Svärta river slide, the Surte landslide in Sweden, the Tre-stycke

vattnet slide, and the Småröd slide) in a marginally stable or globally stable river bank slope if there is the presence of a sensitive clay deposit (Bernander 2000). Once this type of slide is initiated, the movement of the slide mass could constrict or completely block the river path, for example, as happened during the Surte landslide in Sweden. Triggering of these landslides in sensitive clay layers might be caused by a combination of both natural factors (e.g. toe erosion) and human activity (e.g. placement of fill) (L'Heureux et al. 2014). Therefore the failure might be a combination of both upward and downward progression in nature. The mechanisms of upward and downward progressive failure have been well documented in the literature (Bernander 2000, 2008, Locat et al. 2008, 2011).

Progressive failure might occur in drained as well as undrained conditions. Bjerrum (1967) explained drained upward progressive failure initiation in an intact slope containing overconsolidated plastic clays and clay shales. Sensitive clays from Eastern Canada and Scandinavia show strain softening behavior under undrained loading which has been considered as one of the main reasons for developing progressive failure (Bernander 2000, Locat et al. 2008, Quinn 2009, Locat et al. 2011). An undrained condition is considered in this study for analyzing progressive failure.

During the Ormen Lange field development, numerical simulations have been carried out by Norwegian Geotechnical Institute (NGI) using PLAXIS software to analyze the potential of retrogressive sliding due to strain softening effect in shallow clay slopes (NGI 2001). Anderson and Jostad (2007) conducted numerical analyses of progressive failure by modeling the shear band as an interface element using the NGI finite element (FE) code BIFURC. Quinn (2009) also demonstrated the use of linear elastic fracture mechanics concept in progressive failure of slopes. Recently, new numerical methods have been presented by Dey et al. (2013) to model the progressive failure of slopes with sensitive clay layers.

This paper uses the same numerical technique first published in Dey et al. (2013). This study initially describes how a small unloading event near the toe of the slope could cause local upward progressive failure in a sensitive clay deposit. Then it shows how a small triggering load due to human activities could trigger a downward progressive failure in this so-called stable slope and finally cause global failure of the slope due to combined triggering factors.

PROBLEM DEFINITION

The geometry of the slope used in the present FE modelling is shown in Figure 1. A 19 m high river bank slope is chosen for this study which has an angle of 30° with the horizontal. The ground surface is considered flat. The slope has two layers of soil above the strong base layer. A thick crust of strong clay is assumed near the face which overlies the 9 m high sensitive clay layer. For simplicity it is assumed that the groundwater table is at the crest of the slope and the river level is at the ground surface. The failure of this slope could also occur in drained condition with no additional load; however, the focus of this study is to model the failure in undrained conditions under additional load. A triangular shape soil block near the toe of the slope shown by the hatched zone in Figure 1 is removed, which could be caused by erosion or by excavation during construction activities. This block will be referred as "excavated/eroded soil block." The erosion of this block might cause upward progressive failure. In addition, downward progressive failure is modeled by later applying a vertical load on a rigid block located at 160 m from the crest of the slope. The width of the load block is 20 m. This load might come from various human activities such as construction of an embankment, stockpile of materials or other reasons. It is also assumed that the erosion and vertical loading from the load block occur relatively fast such that the deformation/failure of remaining soil occurs in undrained condition.

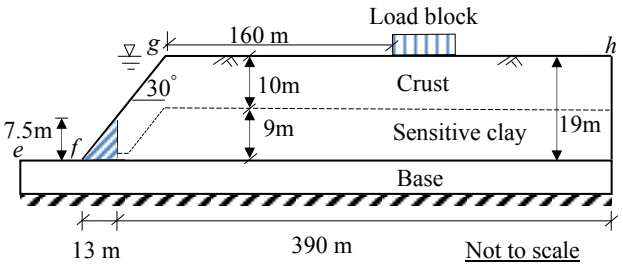

Figure 1. Geometry of the slope used in finite element modeling

Five different cases are analyzed in this study.

Case-1: Modeling of upward progressive failure is performed where toe erosion is assumed to be the triggering factor. The 9 m thick sensitive clay layer might exist in the field as a thin or thick layer. The thickness of the sensitive clay layer could affect the pattern of progressive failure as shown in Dey et al. (2013).

Case-2: Modeling of downward progressive failure is performed. A displacement-controlled load is applied at a distance of 160 m from the crest of the slope using the load block. No erosion of the toe of the slope is considered in this case.

Case-3: The combined effects of toe erosion and loading from the load block are investigated. The toe erosion is generated first. Then the vertical load is applied. The toe erosion causes upward progress of a shear band. The subsequent loading from the load block creates downward progress of other shear bands. The combined effects might result in global failure of the slope.

Case-4: The term "brittleness parameter" is used to model the rate of decrease of undrained shear strength with displacement, which is similar to Quinn et al. (2011). The effects of the brittleness parameter are examined in this case.

Case-5: The ground deformation or possible failure of the slope is analyzed when the clay layers are not sensitive. By comparing the results of this case with previous cases (1-4), it is shown how the sensitivity changes the soil deformation pattern, formation of shear failure planes and the stability of the slope.

FINITE ELEMENT MODELING

Numerical Technique

Abaqus 6.10 EF-1 is used in this study. The cases described above fundamentally involve large deformation

as very significant plastic shear strain is developed in a thin layer of soil (also known as shear band) through which failure of the slope occurs. Conventional finite element techniques developed in a Lagrangian framework cannot model such large strain problems accurately because of significant mesh distortion. In order to overcome these issues, Coupled Eulerian-Lagrangian (CEL) technique currently available in Abaqus FE software is used. The finite element model consists of four parts: (i) soil, (ii) excavated/eroded soil block, (iii) rectangular load block to apply vertical load, and (iv) void space to accommodate the displaced soil mass. The soil is modeled as Eulerian material using EC3D8R elements, which are 8-noded linear brick, multi-material, reduced integration elements with hourglass control. In Abaqus CEL, the Eulerian material (soil) can flow through the fixed mesh. Therefore, there is no numerical issue of mesh distortion or mesh tangling even at very large strain in the zone around the failure plane.

The excavated/eroded soil block and load block are modeled in a Lagrangian framework as a rigid body, which makes the model computationally efficient. A void space is created above the model shown in Figure 1. Soil and void spaces are created in Eulerian domain using the Eulerian Volume Fraction (EVF) tool. For void space EVF is zero (i.e. no soil). On the other hand, EVF is unity in clay layers shown in Figure 1, which means these elements are filled with Eulerian material (soil).

Zero velocity boundary conditions are applied normal to the bottom and all the vertical faces (Figure 1) to make sure that Eulerian materials remain within the domain. That means, the bottom of the model shown in Figure 1 is restrained from movement in the vertical direction, while the vertical sides are restrained from any lateral movement. No boundary condition is applied at the soil-void interface (*efgh* in Figure 1).

Only three-dimensional models can be generated in the Abaqus CEL. In the present study, the model is only one element thick, which represents a plane strain condition.

.Table 1. Parameters used in numerical modelling.

Crust	
Undrained modulus of elasticity, E_u (kPa)	10,000
Undrained shear strength, s_u (kPa)	60
Submerged unit weight of soil, γ' (kN/m^3)	9.0
Poisson's ratio, ν_u	0.499
Sensitive clay	
Undrained modulus of elasticity, E_u (kPa)	7,500
Poisson's ratio, ν_u	0.499
Peak undrained shear strength, s_{up} (kPa)	50
Sensitivity, S_t	6
Submerged unit weight of soil, γ' (kN/m^3)	8.0
Plastic shear strain for 95% degradation of soil strength, γ^p_{95} (%)	25

The numerical analysis involved a number of steps. In the first step, geostatic load is applied to bring the soil to an in-situ condition. The slope is stable at the end of geostatic step with some shear stress, especially near the river bank. In the second step, the rigid excavated/eroded soil block is moved horizontally 750 mm to the left using displacement boundary condition except in Case-2. Finally, in third step the load block is moved vertically except in Case-1

Modeling of soil

Table 1 shows the geotechnical parameters used in this study. The crust has an undrained shear strength of 60 kPa, and a modulus of elasticity of 10 MPa (=167s_u). The soil in the base layer is assumed to be very strong and hence only an elastic property, E_u=200 MPa is considered.

Modeling of stress softening behavior

Proper modeling of stress-strain behavior of sensitive clay layer is the key component of progressive failure analyses in sensitive clays. Sensitive clay shows post-peak softening behavior when it is subjected to undrained loading. Several authors (e.g. Tavenas et al. 1983, Quinn 2009) showed that the post-peak softening behavior is related to post-peak displacement or plastic shear strain. During any slope movement/failure in sensitive clays, shear deformation occurs along the thin layer of discontinuity (also known as shear band) that results in significant plastic shear strain. Brittleness of sensitive soils is one of the most important factors that controls the mobilized post-peak shear strength, especially in the zone of strain localization. Therefore, it is important to define the post-peak softening behavior properly. The following exponential relationship of shear strength degradation as a function of displacement is used in the present study.

$$s_u=[1+(S_t-1)\exp(-3\delta/\delta_{95})]s_{ur} \quad [1]$$

where s_u is the strain-softened undrained shear strength at δ; S_t is sensitivity of the soil; $\delta=\delta_{total}-\delta_p$ where δ_p is the displacement required to attain the peak undrained shear strength (s_{up}); and δ_{95} is the value of δ at which the undrained shear strength of the soil is reduced by 95% of (s_{up}-s_{ur}). Equation 1 is a modified form of strength degradation equation proposed by Einav and Randolph (2005) and was used by the authors (Dey et al. 2012, 2013) for modeling onshore and offshore slopes. If the thickness of shear band (t) is known, the corresponding plastic shear strain (γ^p) can be calculated as, $\gamma^p=\delta/t$ assuming simple shear condition. Therefore, Equation 1 in terms of γ^p can be written as

$$s_u = [1+(S_t-1)\exp(-3\gamma^p/\gamma^p_{95})]s_{ur} \quad [2]$$

where γ^p_{95} is the value of γ^p at 95% strength reduction (i.e. $\gamma^p_{95}=\delta_{95}/t$). Note that, it is very difficult to determine the thickness of the shear band in the field. Similar to previous studies (e.g. Quinn 2009) t=0.5 m is used which is same as the element height used in the present FE analysis. In the Abaqus FE software, the degradation of shear strength of sensitive clay is varied as a function of plastic strain. The parameters used to model the sensitive clay using Eq. 2 are also shown in Table 1. These parameters are estimated based on the laboratory tests conducted on sensitive clays (e.g. Tavenas et al. 1983) and the interpretation of test data and constitutive model

development by other researchers (e.g. Bernander 2000, Leroueil 2001, Locat et al. 2008, Quinn 2009, Locat et al. 2011, and Locat et al. 2013).

FINITE ELEMENT RESULTS

Propagation of Shear Band

Figure 2 shows the generated equivalent plastic shear strain in Case-1 after the eroded soil block is moved to the left. In this case, the formation of the horizontal shear band is initiated along the sensitive clay layer just above the strong base when the movement of the excavated/eroded soil block is started. As the top soil mass is displaced due to the movement of eroded soil block, large plastic shear strain is generated in a thin layer of soil. The shear band propagates horizontally and finally ended with a length of 51.5 m when a gap is formed between the vertical face of eroded soil block and the soil mass at the right. Note that the shear band might go upward and cause slope failure depending on factors such as geometry of the slope, geotechnical properties of sensitive clay and amount of toe erosion as shown in Dey et al. (2013). However, no global failure occurred in this case as the released energy from the excavated/eroded soil block is insufficient. Also there is no sign of significant deformation at the ground surface.

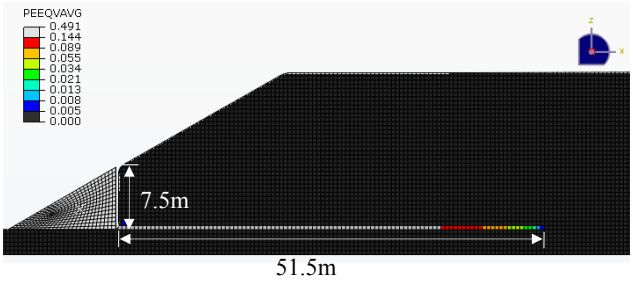

Figure 2. Equivalent plastic shear strain

The equivalent plastic shear strain, denoted by the symbol PEEQVAVG in Figure 2, is related to γ^p as PEEQVAVG= $\gamma^p/\sqrt{3}$. According to Eq. 2, when $\gamma^p \geq \gamma^p_{95}$ (=0.25), that means PEEQVAVG≥0.25/$\sqrt{3}$ =0.144, the undrained shear strength is less than 10.4 kPa. The PEEQVAVG contour in Figure 2 shows that the generated shear band can be divided into two segments. The first segment, shown by the white color elements, covers almost 75% of the generated shear band in this case where the developed equivalent plastic shear strain is greater than 0.144. That means the soil elements in this section have shear strength less than 10.4 kPa (=s_{u95}). The remaining 25% length of the generated shear band is known as “end zone” (colored section) where the shear strength gradually increases from s_{u95} to s_{up}.

Mobilized Shear Strength

Once the local failure is initiated in a small zone where sensitive clay layers exist, the imbalanced force is transferred to the surrounding soil in which the slip surface might propagate in the form of a shear band through the sensitive clay layer as shown in Figure 2. The progressive mobilization of shear strength along this shear band is explained in this section. Figure 3 shows the variation of shear stress along the failure plane with movement of excavated/eroded block for Case-1. The variation of shear stresses along the developed shear band is shown for three different block displacements (103 mm, 165 mm, and 305 mm). In order to explain the process, consider the shear stress on the potential failure plane for the block displacement of 103 mm. The maximum shear stress (50 kPa) is developed at 16 m from the vertical face of the cut. The shear stress between 0 to 16 m is less than 50 kPa (i.e. s_{up}) and greater than 8.33 kPa (i.e. s_{ur}). That means, 0-16 m of the shear band represents the post-peak softening zone where the reduction of shear strength occurred because of plastic strain as per Eq. 2, and the mobilized shear strength is in between the peak and residual shear strength of the soil. To the right side of the peak (i.e. distance greater than 16 m) the shear stress is again reduced with distance. For this displacement of the block (103 mm), the shear stress in this potential failure plane at a distance greater than 16 m has reached the peak, and therefore it represents the pre-peak behavior. At a very large distance, the shear stress is almost zero as the ground surface is horizontal. The pattern of shear stress development for other displacements of the block is similar as shown in Figure 3. The location of the peak shear stress shifts to the right with increase in block displacement; that means a greater length of the potential failure plane is in a post-peak stress-strain condition. For example, for 305 mm block movement the peak is at 39 m and therefore 0-39 m is in post-peak condition with approximately 20 m in residual shear strength level. This process will continue until the shear band propagation is ended for globally stable slopes as in Case-1.

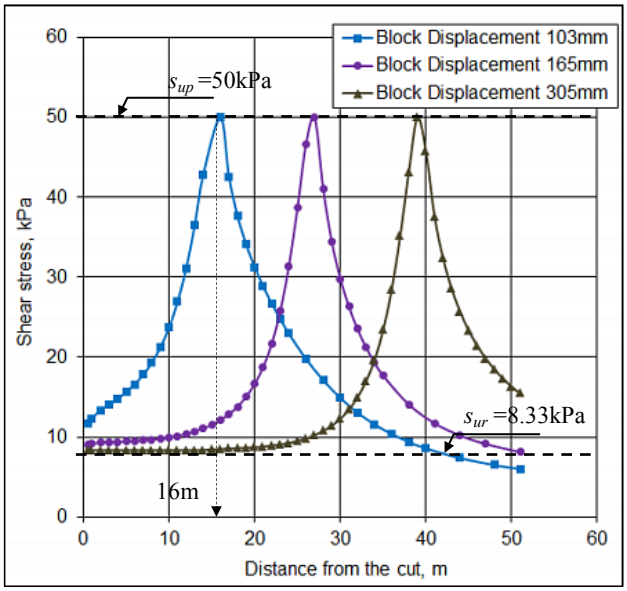

Figure 3. Variation of shear stress for different displacement of eroded block

COMPARISON WITH DIFFERENT CASES

In Case-1, it is shown that an upward progressive failure is initiated due to movement of the eroded soil block

(Figure 2). A shear band propagates horizontally in to the soil and finally ends at a certain length. Therefore, the slope remains globally stable although it contains a 51.5 m long shear band. Toe erosion is the only triggering factor in this case. The generated shear band might propagate further and might result in global slope failure if; (i) additional triggering load is applied, (ii) quick degradation of soil shear strength occurs, or (iii) combination of both. The effects of these factors are discussed in the following sections.

Additional Triggering Load

To understand the effects of additional triggering load on slope stability, a displacement controlled load is applied vertically at a distance of 160 m from the point *g* in Figure 1. The rectangular load block is displaced vertically at a constant rate. Two cases are considered in this section. Figure 4 shows the FE results of Case-2 where only the displacement controlled load is applied. The following figures of this type are not to scale with the horizontal dimension reduced by a factor of 3. The slope is stable under gravity load and no shear band propagation occurs as no toe erosion is considered in this case. A triangular failure wedge is formed underneath the load block as expected as the load block is penetrated into the soil by an amount of approximately 200 mm (Figure 4a). At this stage, the vertical pressure on the soil from the load block is approximately 230 kPa. If the load block is pushed further, two shear bands are formed at both sides below the load block (Fig. 4b). Figure 4(b) shows the shear band formation at 790 mm movement of the block. It is shown later that soil pressure does not increase due to movement of the load block from 200 to 790 mm. In other words, the ultimate capacity is reached at 200 mm displacement at a vertical pressure of 230 kPa. One interesting observation is that, shear band propagates horizontally through the sensitive clay layer due to the strain softening behavior of sensitive clay. In conclusion, although significant settlement of the load block occurred because of reduction of shear strength along the shear band, no global failure of the slope is calculated in this case.

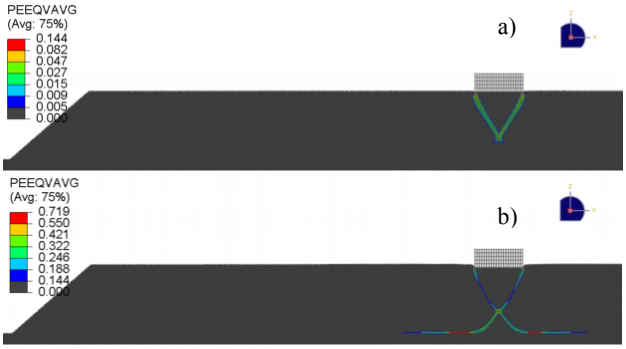

Figure 4. Equivalent plastic shear strain in Case-2 for two vertical displacement of load block: a) 195 mm b) 790 mm

The combined effects of toe erosion and vertical loading (Case 3) are shown in Figure 5. As mentioned before in Case-3 the toe erosion is applied first, which creates a shear band of 51.5 m length as shown in Fig. 5(a). Therefore, the FE analysis in the third step for loading from the load block represents a downward progressive failure of a slope with a pre-existing shear band. Figures 5b to 5e show the shear band for four different vertical displacements of the load block. The propagation of shear bands started after a certain vertical displacement of the load block. There is a separation between the pre-existing shear band from toe erosion and the shear band formed by load block. For example, Figure 5b shows that there is a separation of 130.5 m when the load block is displaced vertically by an amount of 200 mm. As mentioned before, the ultimate capacity is reached at this stage. Further increase in load (pressure) will cause significant settlement. In the numerical analysis, vertical displacement is applied to the load block. The separation between the shear bands is reduced to 60.5 m as shown in Figure 5d when the load block is additionally displaced by 360 mm. Figure 5e shows that a complete failure surface is formed where shear strength drops almost to its residual value under a further 175 mm displacement. PEEQVAVG greater than 0.144 is generated along the whole shear band and finally causes global failure of the slope. The comparison of Figures 4(a) and 5(b) shows that the formation of a triangular wedge under the load block is similar in Case 2 and Case-3. For additional vertical displacement of the load block, the shear band in Case-3 is different from that in Case-2 (compare Figures 4(b) and 5c to 5e). In Case-3 there is a pre-existing shear band from toe erosion where the shear strength is reduced almost to the residual value. As the resistance is reduced, the soil block in the left side of the load block has more freedom to move leftward. This creates another triangular wedge and the soil mainly moves to the left. When sufficient leftward movement occurred, the shear band in the right side of the load block starts to grow as shown in 5(d). This is very different from Case-2 where the shear bands are almost symmetric under the load block. The FE analysis of this case shows that the existence of a shear band in the strain softening clay layer in a so-called globally stable slope could cause a massive slope failure if there are some human activities that create sufficient vertical load at a certain distance from the slope. This might even come from temporary works such as stockpile of materials. Moreover, the combined effects of two triggering factors cause the global failure in Case-3, while global failure is not caused either in Case-1 or Case-2 with single triggering factor for the assumed conditions.

Effect of Strain Softening Curve

Strain softening behavior is considered one of the most important properties of sensitive clay. Besides sensitivity, the value of δ_{95} or γ^{p}_{95} controls the strain softening behavior of sensitive clay as shown in Eq. 1 or Eq. 2. In this study, the clay sensitivity is kept constant, however two different values of δ_{95} are considered as shown in Figure 6. The upper line in Fig. 6 is less brittle than the lower one. The analyses presented in the previous sections are based on the upper line. To show the effects on brittleness, Case-3 is analysed again using the lower curve in Figure 6, where the δ_{95}=90 mm is used. The shear band formation for this soil parameter is shown in Figure 7. The length of the shear band due to toe erosion is increased to 63.5 m (Fig. 7a) which was 51.5 m with the lower brittleness value (Fig. 5a). Similar to Fig. 5(b), a triangular wedge is formed due to the vertical displacement of the load block (Fig. 7b). However, the

global failure occurred at 450 mm of vertical displacement of the load block (Fig. 7d), which is lower that the value presented in Fig. 5. In other words, the brittleness of shear strength curve (Fig. 6) has significant effects on shear band formation and failure of the slope.

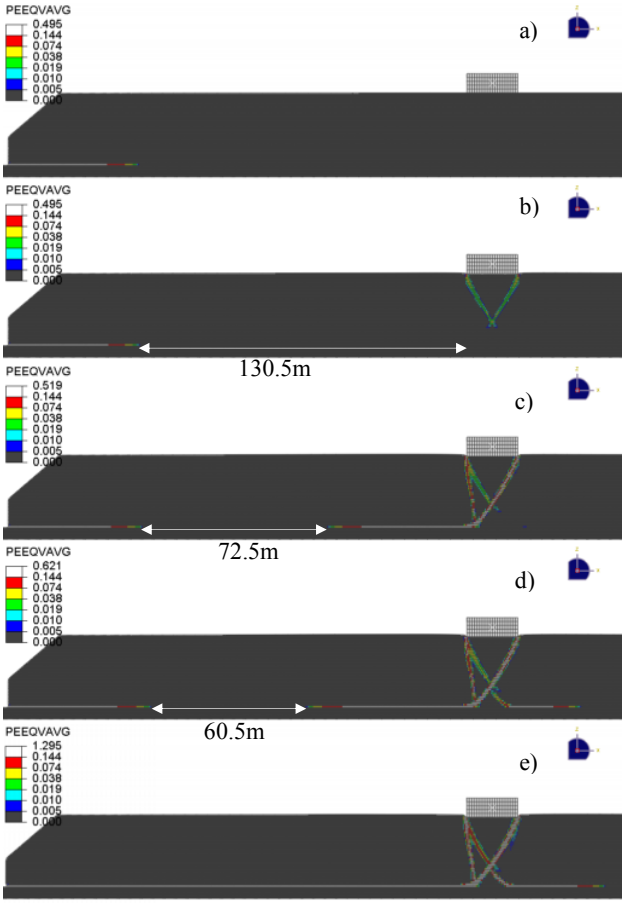

Figure 5. Position of shear band in Case-3 for different vertical displacement of load block; a) zero mm, b) 200 mm, c) 460 mm, d) 560 mm, e) 735 mm

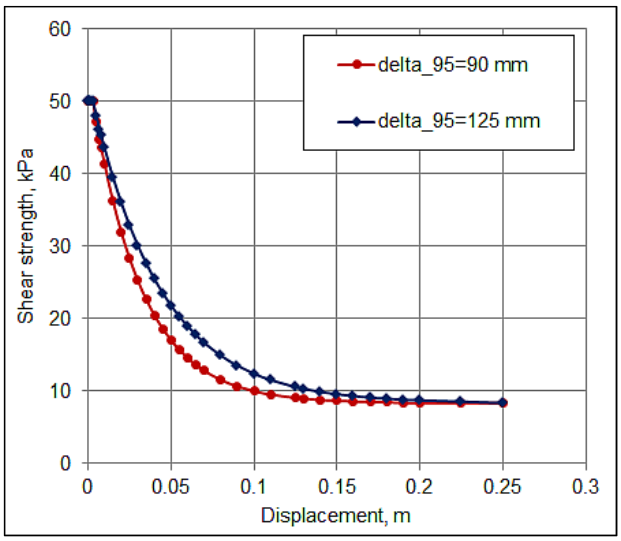

Figure 6. Variation of strain softening curve

To understand softening effects on deformation/failure mechanism, Case-4 is reanalyzed without any softening. That means, the soil is simply modeled as elasto-plastic material of undrained shear strength s_u=50 kPa. Figure 8(a) shows that plastic shear strain is developed in a small zone of soil due to toe erosion. During vertical movement of the load block, a triangular wedge is formed at a vertical displacement of 235 mm. If the displacement is continued, local shear failure type slip surfaces are generated at a vertical displacement of 900 mm (Figure 8c).

Pressure under load block

Vertical displacement is applied to the load block to simulate the loading. Average pressures developed below the load block due to applied vertical displacement for the different cases are shown in Figure 9. A triangular failure wedge is initially developed in all cases at an approximate displacement of 200 mm.

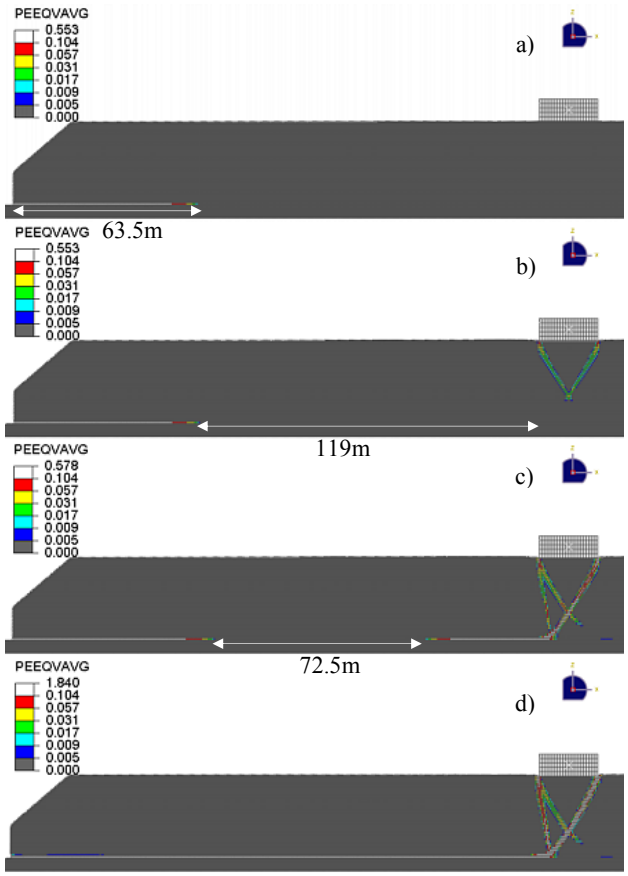

Figure 7. Shear band in Case-4 for four vertical displacement of load block: a) zero mm, b) 185 mm, c) 310 mm, d) 450 mm

The load displacement curve in Figure 9 is almost the same up to 200 mm displacement for all cases. However, the pressure starts to drop with further displacement in Cases 2-4 where strain depended softening is used. On the contrary, in Case-5 the average pressure continuously increases with displacement as no softening is considered

in this case. The rate of decrease of vertical pressure in Case 4 is higher than that of in Cases 2 and 3, because of faster degradation of shear strength. The pressure decreases significantly in Cases 3 and 4 at vertical displacement of load block of 715 mm and 435 mm, respectively. Both of these cases contain a pre-existing shear band due to toe erosion. When the shear band generated due to downward movement of the load block merges with the pre-existing shear band, a complete failure surface is developed and the slope starts to move towards the river and global failure of the slope occurs. Approximately 280 mm less vertical displacement of the load block is required to cause global failure of the slope when the value of δ_{95} is reduced to 90 mm (Case-4) from 125 mm (Case-3). On contrary, no such drop is calculated in Case-2 because the global failure of the slope does not occur. However, if the applied pressure is more than 230 kPa, a very large settlement will occur and result in punching failure.

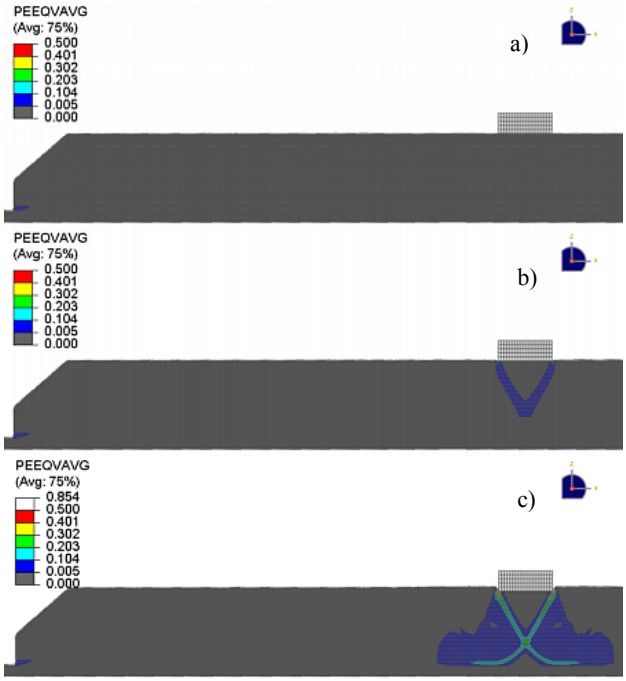

Figure 8. Plastic shear strain in Case-5; a) after toe erosion, b) at 235 mm, & c) at 900 mm vertical displacement of the rectangular block

CONCLUSIONS

A new numerical approach to model the initiation and propagation of shear bands in both upward and downward progressive failure, as might be encountered near river banks comprising sensitive clays, is presented in this paper. The numerical technique of modeling progressive failure using Coupled Eulerian-Lagrangian (CEL) approach currently available in Abaqus FE software is first introduced by the authors in Dey et al. (2013). Nonlinear strain softening behavior of sensitive clay is incorporated in this large deformation finite element analysis. Five cases are analyzed in this study. Toe erosion is considered as an initial triggering factor and a displacement controlled load is applied as additional triggering factor. Additional triggering load from human activities such as embankment construction could cause a disastrous slope failure in Cases-3 and 4 due to presence of an existing shear band generated from toe erosion. Failure could be accelerated (fails at lower additional triggering load) if the brittleness of the sensitive clay is comparatively higher.

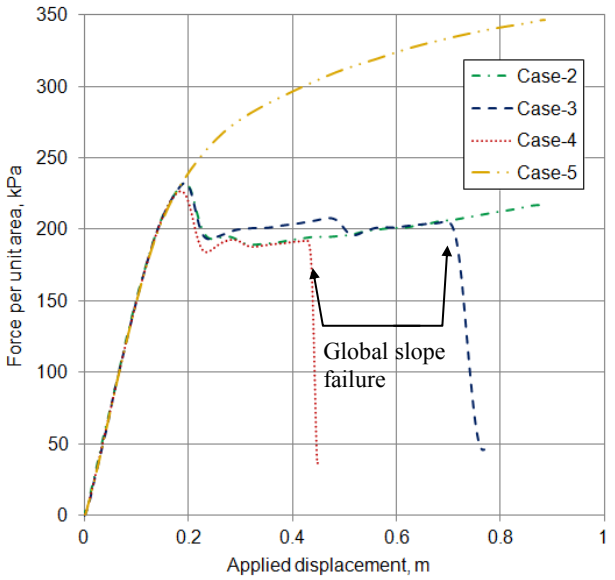

Figure 9. Comparison on force-displacement plot among Case-2 to Case-5

ACKNOWLEDGEMENTS

The writers would like to acknowledge the financial support from Research & Development Corporation of Newfoundland and Labrador, NSERC and C-CORE.

REFERENCES

Anderson, L. and Jostad, H.P. 2007. Numerical modeling of failure mechanisms in sensitive soft clays — application to offshore geohazards. *Offshore Technology Conference*, Texas. Paper OTC 18650.

Bernander, S. 2000. Progressive failure in long natural slopes: formation, potential extension and configuration of finished slides in strain-softening soils. Licentiate Thesis, Luleå University of Technology.

Bernander, S. 2008. Down-hill progressive landslides in soft clays, triggering disturbance agents, slide propagation over horizontal or gently sloping ground, sensitivity related to geometry. Luleå University of Technology, Luleå, Sweden. Research report.

Bjerrum, L. 1967. Progressive failure in slopes in overconsolidated plastic clay and clay shales. Terzaghi Lecture. *Journal of the Soil Mechanics and Foundation Division*, ASCE, 93(5): 3-49.

Cruden, D.M. and Varnes, D.J. 1996. Landslides types and processes. In Landslides investigation and mitigation. *Special Report 247.* Transportation Research Board, NRC. Edited by A.K. Turner and R.L. Schuster. National Academy Press, Washington, D.C., 37-75.

Dey, R., Hawlader, B., Phillips, R. and Soga, K. 2012. Effects of shear band propagation on submarine landslide. *Proc. of the 22nd Int. Offshore and Polar Engineering Conf.,* Rhodes, Greece, 766- 773.

Dey, R., Hawlader, B., Phillips, R. and Soga, K. 2013. Progressive failure of slopes with sensitive clay layers. *Proc. of the 18th Int. Conference on Soil Mechanics and Geotechnical Engineering,* Paris.

Einav, I. and Randolph, M.F. 2005. Combining upper bound and strain path methods for evaluating penetration resistance. *Int. Journal Numerical Methods Engineering,* 63(14): 1991-2016.

Karlsrud, K., Aas, G. and Gregersen, O. 1984. Can we predict landslide hazards in soft sensitive clays? Summary of Norwegian practice and experiences. *In Proc. of the 4th Int. Symposium on Landslides,* Toronto, Ont., 1:107-130.

L'Heureux, J.S., Locat, A., Leroueil, S., Demers, D. and Locat, J. 2014. *Landslides in sensitive clays: From geosciences to risk management,* 2nd ed., Springer, Dordrecht, Netherlands.

Leroueil, S. 2001. Natural slopes and cuts: movement and failure mechanisms. *Géotechnique,* 51(3): 197-243.

Locat, A., Leroueil, S., Bernander, S., Demers, D., Locat, J. and Ouehb, L. 2008. Study of a lateral spread failure in an eastern Canada clay deposit in relation with progressive failure: the Saint-Barnabé-Nord slide. *In Proc. of the 4th Canadian Conf. on Geohazards: From Causes to Management,* Québec, Que., 89-96.

Locat, A., Leroueil, S., Bernander, S., Demers, D., Jostad, H.P. and Ouehb, L. 2011. Progressive failures in eastern Canadian and Scandinavian sensitive clays. *Canadian Geotechnical Journal,* 48(11): 1696-1712.

Locat, A., Jostad, H.P. and Leroueil, S. 2013. Numerical modeling of progressive failure and its implications for spreads in sensitive clays. *Canadian Geotechnical Journal*, 50: 961-978.

NGI Report 2001. Effect of strain softening on stability analysis. Analysis of retrogressive sliding due to strain softening-Ormen Lange case study, Report No 521001 (10).

Quinn, P., Diederichs, M.S., Hutchinson, D.J. and Rowe, R.K. 2007. An exploration of the mechanics of retrogressive landslides in sensitive clay. *In Proc. of the 60th Canadian Geotechnical Conf*., Ottawa, Ontario, 721-727.

Quinn, P. 2009. Large Landslides in Sensitive Clay in Eastern Canada and the Associated Hazard and Risk to Linear Infrastructure. Doctoral thesis, Queen's University.

Tavenas, F., Flon, P., Leroueil, S. and Lebuis, J. 1983. Remolding energy and risk of slide retrogression in sensitive clays. *Proc. of the Symposium on Slopes on Soft Clays,* Linköping, Sweden, SGI Report No. 17: 423-454.

Tavenas, F. 1984. Landslides in Canadian sensitive clays — a state-of the-art. *In Proc. of the 4th Int. Symposium on Landslides*, Toronto, Ont., 1:141-153.

Appendix-V

Progressive failure of offshore slopes due to construction in upslope areas

This paper has been published in the 34th International Conference on Ocean, Offshore and Arctic Engineering, OMAE, 2015.

Most of the research work presented in this paper was conducted by the first author. He also prepared the draft manuscript. The other authors supervised the research and reviewed the manuscript.

PROGRESSIVE FAILURE OF OFFSHORE SLOPES DUE TO CONSTRUCTION IN UPSLOPE AREAS

Rajib Dey
PhD Candidate,
Memorial University
St John's, NL, Canada

Bipul Hawlader
Associate Professor,
Memorial University
St John's, NL, Canada

Chen Wang
PhD Student,
Memorial University
St. John's, NL, Canada

ABSTRACT

Human activities such as construction loading in upslope areas could be a potential triggering factor for many offshore landslides such as the 1979 Nice landslide. Post-slide investigations show that the existence of marine sensitive clay layers might be one of the potential causes of many large-scale submarine landslides. In this paper, a finite element (FE) modeling technique is developed to analyze the failure of a slope in undrained condition. Nonlinear strain softening behaviour of undrained shear strength of marine sensitive clays is incorporated in the FE analysis. Strain localization in narrow zones (i.e. shear bands) could be successfully simulated. The formation of shear bands and their propagation could explain some potential failure mechanisms. The FE results show that large-scale catastrophic failure of submarine slopes might have occurred due to shear band propagation through strain softening clay layers, which cannot be explained using the traditional limit equilibrium methods for slope stability analysis. Effects of different factors, such as thickness of the marine clay layer and its sensitivity, on stability of submarine slope are also examined.

INTRODUCTION

Stability of the seabed is an important issue that must be taken into consideration during planning and design of offshore and nearshore facilities. Various triggering factors (e.g. earthquake, gas hydrate dissociation, rapid sedimentation) have been identified in the past that could contribute to the initiation of large scale offshore landslides. Most of the previous case studies on submarine landslides identified the involvement of multiple triggering factors [1-3]. Human activities, such as placement of fills in the upslope areas, are also a potential triggering factor. For example, loading in the upslope areas during airport extension has been considered as a potential cause of the catastrophic 1979 Nice landslide accompanied by small tsunami and loss of human lives [4,5]. Post-slide field investigations show that the presence of marine sensitive clay layers, which are generally encountered in many seabed sediments, could be one of the main causes of many offshore landslides [4,6,7].

In the case of Nice landslide, recent studies [4] identified the existence of a thick sensitive clay layer. It has been also mentioned that the 1979 slope failure occurred shortly after the land filling which were carried out as a part of airport extension. The FE analyses in undrained condition also show that failure occurred at the sensitive clay layer [4].

Strain softening behaviour of marine sensitive clays during undrained loading is a well-known phenomenon. The large landslides often associated with strain localization and formation of shear bands lead to progressive failure. However, limited analytical and numerical models are available in the literature for

modeling progressive development of failure planes in sensitive clays [8–13]. During the Ormen Lange field development, researchers [e.g. 14] at the Norwegian Geotechnical Institute (NGI) conducted numerical modeling for undrained progressive failure using PLAXIS 2D software [15]. Bernander [8,9] presented a finite difference method to simulate the downward progressive failure of long infinite slopes. This modeling technique of downward progressive failure has been further used by Andresen and Jostad [16] to analyze the undrained stability of submarine slopes involved with marine clays using the FE program BIFURC [17,18] where the strain softening behaviour of the predefined failure zone is modeled using a finite thickness interface element.

In this study, large deformation finite element (FE) analyses are performed using the Coupled Eulerian Lagrangian (CEL) approach available in Abaqus FE software. A nonlinear model for post-peak degradation of mobilized undrained shear strength (s_u) is incorporated in the FE model. The advantage of present FE model is that it can successfully simulate extremely large deformation without numerical issues, and a priori definition of shearing zones is not required to tackle severe strains in the shear bands. The FE program automatically identifies the location of critical shear band formation and direction of propagation. The simulation results are used to explain the mechanics involved in large-scale offshore slope failure.

PROBLEM DEFINITION

Fig. 1 shows the geometry of the offshore slope considered in this study for FE modeling. The slope is gentle having a 4° angle with the horizontal. The slope contains a 1 m thick marine clay layer at 19 m depth. The upper soil layer above the marine clay layer is not sensitive as typically observed in offshore environments [19]. Below the marine clay layer there exists a strong base layer which is parallel to the ground surface of the slope. In the downslope, a steep slope of 15° is assumed as typically observed just beyond the shelf. As happened in the 1979 Nice landslide, construction load or fill might be placed in the upslope areas that could cause the failure of the slope. This loading is simulated by placing a 40 m wide rigid block (Fig. 1), which is displaced vertically downwards. This block is referred as the "load block" and its vertical displacement is denoted by Δ. It is to be noted that although the geometry of the slope considered in this study is not exactly same as the Nice landslide, the current study could explain potential failure mechanisms involved in similar type of landslides due to construction loading in the upslope. It is also to be noted here that multiple marine clay layers might exist at different depths as observed from the seismic and geoborings data of the Storegga slide region [7]; however, for simplicity, only one marine clay layer is considered in this study.

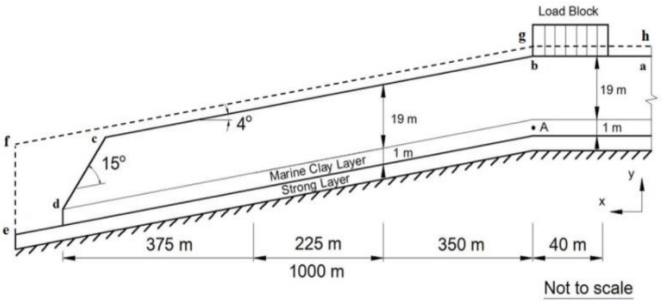

Figure 1. Geometry of the slope used in FE modeling

FE analyses are conducted for the following four cases.

Case-1: Downslope progressive failure is modeled in this case by placing a fill in the upslope area as the triggering factor for slope failure. 19 m thick non sensitive clay (e.g. glacial clay) layer is considered above 1 m thin marine sensitive clay layer. The sensitivity of the marine clay (S_t) is assumed to be 6. It is shown that load from the upslope area could cause the failure of the slope.

Case-2: It is assumed that the slope contains a 20 m thick marine sensitive clay layer in this case instead of 1 m. Also no glacial clay is present above the marine layer. The effect of thickness of marine sensitive clay layer on progressive failure and corresponding movement of failed soil mass is investigated in this case. The sensitivity of the marine clay is same as in Case-1 (i.e. S_t=6).

Case-3: Effects of sensitivity on initiation of shear band, its propagation towards downslope areas, and associated global slope stability is examined in this case. Similar to Case-2, a 20 m thick marine clay layer is considered. However, the sensitivity is varied as S_t=5 and 4.

Case-4: In order to check the effect of strain softening behavior of the marine clay layer on slope failure, analysis is performed in this case without allowing strain softening in the marine clay layer (i.e. S_t=1). The soil is modeled as elastic-perfectly-plastic material.

FINITE ELEMENT MODELING

ABAQUS 6.10 EF-1 is used in this study. The cases described above are associated with modeling of progressive failure of an offshore slope. This is fundamentally a large deformation problem, and large plastic shear strain concentration occurs in narrow zones in marine clay layer through which the failure of the slope occurs. Conventional FE modeling techniques developed in Lagrangian framework cannot model such large strain problems accurately because significant mesh distortion occurs. In order to overcome these issues, the Coupled Eulerian-Lagrangian (CEL) technique currently available in Abaqus FE software [20] is used. In Abaqus CEL, the Eulerian material (soil) can flow through the fixed mesh. Therefore, there is no numerical issue of mesh distortion or mesh tangling even at large strains in the zone around the failure plane.

The FE model consists of three parts: (i) soil, (ii) the load block which represents the construction loading in the upslope area, and (iii) void space (i.e. space abcdefgh)

to accommodate the displaced soil mass. The soil is modeled as Eulerian material using EC3D8R elements, which are 8-noded linear brick, multi-material, reduced integration with hourglass control elements. The load block is modeled in Lagrangian framework as a rigid body, which makes the model computationally efficient. Soil and void spaces are created in Eulerian domain using Eulerian Volume Fraction (EVF) tool. For void space EVF is zero (i.e. no soil). On the other hand, EVF is unity in the soil domain, which means these elements are filled with Eulerian materials (soil).

Zero velocity boundary condition perpendicular to the plane is applied to all faces of the Eulerian domain to make sure that Eulerian materials remain within the domain and cannot move outside. This implies that the bottom of the model shown in Fig. 1 is restrained from any vertical movement, while all the vertical faces are restrained from any lateral movements. No boundary condition is applied at the soil-void interface (abcde in Fig. 1) so that the soil can move into the void space when displaced.

Only three-dimensional model can be generated in Abaqus CEL. In the present study, the model is only one element thick, and the movements of soil perpendicular to the *x-y* plane is restricted by applying zero velocity boundary condition in order to mimic plane strain condition.

The numerical analysis mainly consists of two steps of loading. In the first step gravity load is applied to bring the soil in in-situ condition. The slope is stable at the end of gravity (geostatic) step and no plastic strain develops in the model. In the second step, load block is displaced vertically downwards at a constant velocity 6.67 mm/s (i.e. displacement-controlled loading).

MODELING OF SOIL

Since marine clay layers have been reported as the glide planes for many historical submarine landslides [7,19], behaviour of marine clay is carefully considered in this study. Marine clays are typically moderate sensitive in undrained loading because it shows reduction of undrained shear strength (softening) with plastic shear strain/displacement [19]. The strain softening behaviour has been considered as one of the main reasons for progressive failure of submarine slopes [21,22].

Previous studies [e.g. 23,24] show that the post-peak softening behaviour is related to post-peak displacements or plastic shear strains. Linear variation of s_u with plastic shear displacement has been used by some previous authors for modeling strain-softening behaviour of sensitive clays [11,13]. It is also to be noted here that the strength softening behavior of sand and clay in drained condition has been also considered in some other applications [25,26]. Figure 2 shows the variation of s_u used in the present study to model the stress-strain behavior of marine sensitive clays. The linear elastic pre-peak (line oa in Fig. 2) behavior is defined by the elastic properties (E_u and ν_u). The peak undrained shear strength (s_{up}) is mobilized at point a and remains constant up to point b for a displacement of δ_{pc} from point a. Following nonlinear relationship is used for modeling post-peak softening behaviour.

$$s_u = [1 + (S_t - 1)\exp(-3\delta/\delta_{95})]s_{uR} \qquad (1)$$

where s_u is the mobilized undrained shear strength; S_t is the sensitivity of the soil; $\delta = \delta_t - (\delta_e + \delta_{pc})$ where δ_e and δ_t are the elastic and total shear displacements, respectively; and δ_{95} is the value of δ at which the undrained shear strength of the soil is reduced by 95% of (s_{up}-s_{uR}). In FE implementation, s_u up to $2\delta_{95}$ is defined by Eq. (1) and after that s_u remains constant (line *de*) which is denoted as $s_{u\infty}$. Equation (1) is a modified form of strength degradation equation proposed by Einav and Randolph [27] but in terms of displacement. This model has been used previously by the authors [28,29] to model submarine landslides, and progressive failure of slopes.

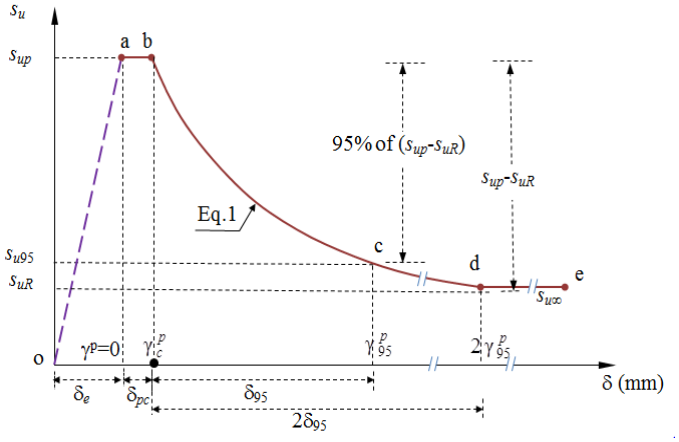

Figure 2: Stress-strain behavior used in finite element modeling

In Abaqus, the degradation of shear strength of marine clay is given as an input by varying yield strength (=$2s_u$) as a function of plastic shear strain (γ^p), which is calculated as $(\delta_t - \delta_e)/t$ assuming simple shear condition. Here t represents the thickness of the soil element. Authors understand that change of mesh size could affect the results and the corresponding failure mechanisms. However, this is beyond the scope of current study. In this study, t=1 m is used which is same as the element height. The parameters used in FE modeling are also shown in Table 1. The undrained shear strength of the upper glacial clay layer is assumed as s_u=50 kPa and undrained Young's modulus E_u=30 MPa (=$600s_u$). In this study, the soil below the marine clay layer is assumed to be very strong having undrained Young's modulus E_u=200 MPa. These parameters are estimated based on the laboratory tests conducted on various sensitive and marine clays [e.g. 23,30-32], interpretation of the test data, and constitutive model development by other researchers [e.g. 8,11,21,24,33,34].

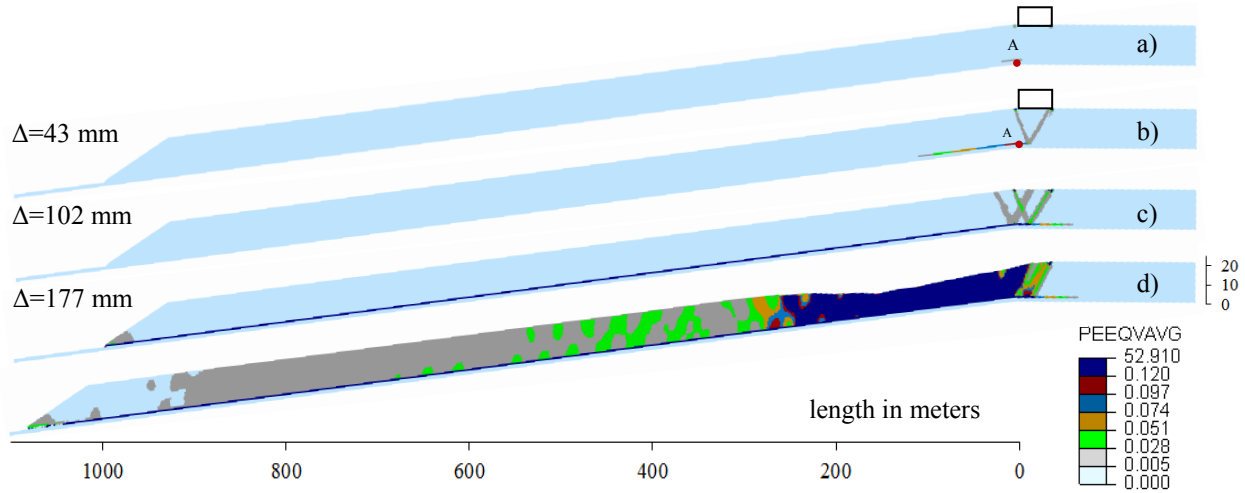

Figure 3. Failure process in Case-1

Table 1. Parameters used in FE modelling

Glacial clay (upper clay layer)	
Undrained Young's modulus, E_u (MPa)	30
Poisson's ratio, ν_u	0.499
Undrained shear strength, s_u (kPa)	50.0
Submerged unit weight of soil, γ' (kN/m^3)	10.0
Marine sensitive clay	
Undrained Young's modulus, E_u (MPa)	15
Poisson's ratio, ν_u	0.499
Peak undrained shear strength, s_{up} (kPa)	40.0
Sensitivity of marine clay, $S_t=s_{up}/s_{uR}$	6.0
Submerged unit weight of soil, γ' (kN/m^3)	8.0
Plastic shear displacement at point b, δ_{pc}	3
Plastic displacement for 95% degradation of soil strength, δ_{95} (mm)	100

FE RESULTS

Propagation of Shear Band

Figure 3 shows the generated equivalent plastic shear strains (PEEQVAVG) in Case-1 during the failure process. Note that, PEEQVAVG is related to plastic shear strain (γ^p) as $\gamma^p = \sqrt{3}$PEEQVAVG.

Fig. 3a shows that the plastic shear strain starts generating around point A (the junction of the slope and flat upslope area) in the marine clay layer when the vertical displacement of the load block Δ=43 mm. With further displacement (e.g. Δ=102 mm), a triangular wedge is formed below the load block, and the shear band in the marine clay layer propagates further downward (Fig. 3b). Note that the triangular wedge is not symmetric because the left side of the load block is a slope and thereby kinematically less restrained. The two failure surfaces under the load block meet the sensitive clay layer at a point 16 m right of A. With further increment of Δ, the shear band through the sensitive clay layer propagates to the left and reaches the toe of the slope when Δ=177 mm (Fig. 3c). After that, a soil mass above the basal failure plane of marine clay slides as a block (Fig. 3d). Although the slope was stable at the end of the gravity step, the slope is not stable at this stage because the shear strength of the sensitive clay layer along the basal failure plane is significantly reduced by softening. In other words, the driving force is greater than the resisting force, and the soil mass above the failure plane can slide even without any load from the load block in the upslope area.

Mobilized Shear Strength

As shown above (Fig. 3), shear band propagation mainly occurs through the marine clay layer in the left side of point A. The progressive mobilization of shear strength along the generated shear band is explained in this section.

Figure 4a shows the variation of shear stress in the sensitive clay layer while Fig. 4b shows the plastic shear displacement of the top of the sensitive clay layer for different values of Δ. The horizontal axis of these figures represents the inclined distance along the sensitive clay layer from point A in Fig. 1. Due to strain softening behaviour of sensitive clay, strain localization occurs in a small zone in the sensitive clay when the load block is displaced vertically to certain distance (e.g. Δ=50 mm). As the mobilized shear strength is less than the shear stress, the imbalanced force is transferred to the next soil elements at the tip of the existing shear band, which causes propagation of the shear band through the sensitive clay layer as shown in Fig. 3. For example, degradation of shear strength of sensitive clay occurs in a length of 25 m when Δ=50 mm (Fig. 4a). As shown in Fig. 4(b), the maximum plastic shear displacement occurs near point A. Here, the plastic shear displacement is calculated from FE result as $\delta=\gamma^p \times t$. To explain the process, consider the shear stress at marine clay layer for Δ=60 mm. The maximum shear stress (40 kPa) is mobilized at 43 m from point A. The corresponding displacement profile in Fig. 4(b) also shows that the plastic shear displacement is zero at 43 m for Δ=60 mm. As the plastic shear displacement occurs, the shear stress between 0 to 43 m is less than 40 kPa ($<s_{up}$) and greater than 8.33 kPa ($>s_{u95}$).

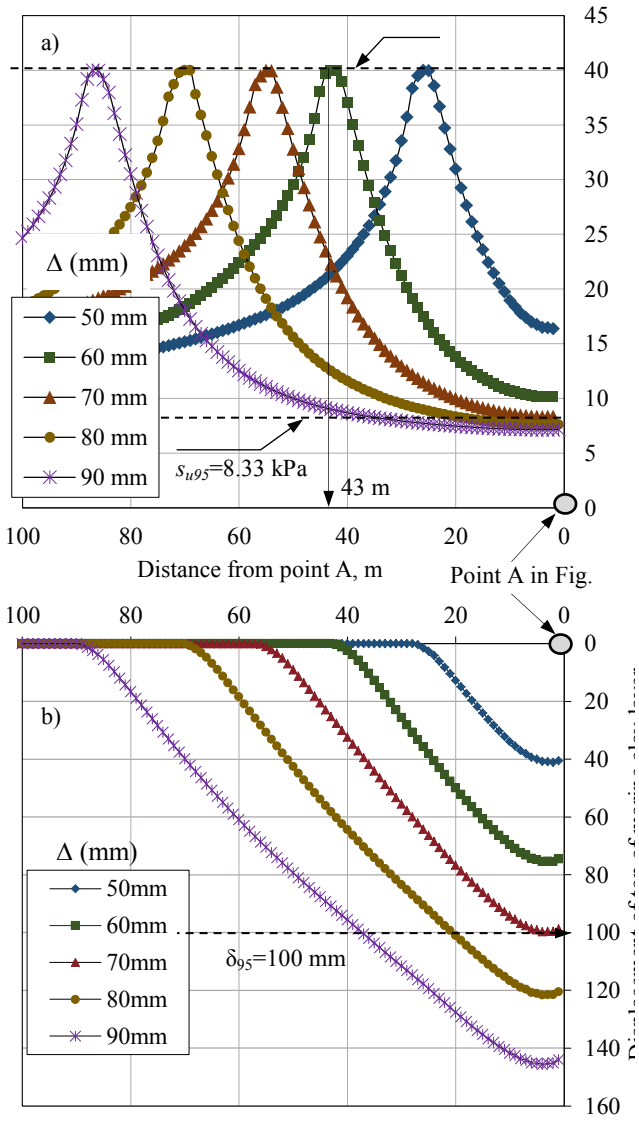

Figure 4. Variation of shear stress and plastic shear displacement in sensitive clay layer

That means, 0-43 m of the shear band represents the post-peak softening zone where the reduction of shear strength occurs because of plastic strain (see Eq. 1 and Fig. 2). In the left side of the peak (i.e. distance greater than 43 m) the shear stress is again less than 40 kPa, which represents that, the shear stress in this area is in pre-peak condition for this displacement. For higher values of Δ (e.g. 70 mm, 80 mm, and 90 mm), the point of peak shear stress shifts towards the left because the length of the shear band increases (also see Fig. 3). This process continues until the shear band propagates to the toe of the steep slope.

COMPARISON BETWEEN FE SIMULATIONS OF DIFFERENT CASES

In Case-1, it is shown that a shear band generates and propagates downward due to vertical displacement of the load block (Fig. 3). With increase in Δ, the shear band propagates downward along the marine clay layer, and finally reaches the toe of the slope and causes global failure. However, failure mechanisms and slope capacity (the maximum vertical pressure that can be applied in the upslope area) might be different in other cases as they depend on geometry and soil properties. This section discusses the effects of these factors based on the cases analyzed in this study.

Thickness of the marine clay layer

Figure 5 shows the propagation of shear band and corresponding failure processes for Case-2. The initation of shear band formation under the load block is similar to Case-1. However, the failure pattern and slope capacity is different which is discussed later. Figure 5a shows that a shear band starts to develop when Δ=65 mm and a 100 m long band is generated when Δ=184 mm (Fig. 5b). If we compare the Figs. 3(a-b) (Case-1) and Figs. 5(a-b), higher value of Δ is required for Case-2. This is because of the lower stiffness of the marine clay layer as compared to the glacial clay layers used in Case-1.

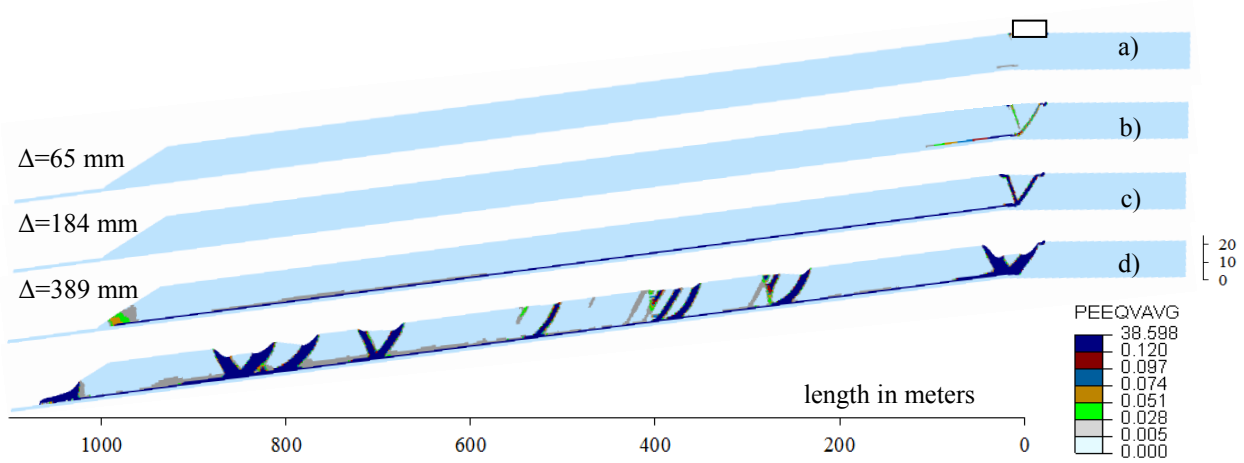

Figure 5. Failure process in Case-2

Therefore, slightly larger value of Δ is required to initiate the progressive failure in Case-2. Figures 5(c) and 5(d) show that failure pattern is completely different from Case-1. In Case-2 when the failed soil mass starts to move downward, multiple shear surfaces develop in the upper soil mass. The reason is that there is no glacial clay and strain softening is allowed in the upper clay layer (Fig. 5). That means the upper clay layer is also sensitive. On the other hand, in Case-1, the failed soil mass move as a block (Fig. 3d), and plastic shear deformation mainly concentrates in the upslope areas with fomation of a number of triangular wedges. In summary, the thickness of the marine clay layer could change the failure patterns through initiation and propagation of the shear bands.

Sensitivity of the marine clay layer

Using the same model discussed in Case-2, two more analyses are performed to investigate the effects of sensitivity of the marine clay layer on shear band propagation and failure of the slope. In these analyses, S_t=4 and S_t=5 are used. The other parameters are same as Table 1. Analyses are carried out displacing the load block by an amount of 400 mm. Figures 6(a) and 6(b) show that the shear band propagates only 334 m and 205 m for S_t of 5 and 4, respectively, and no global failure occurs. However, such displacements are sufficient to cause global failure of the slope in Case-2. The reason is that overall undrained shear strength increases with decrease in S_t. Hence for these sensitivities, continuous shear band propagation due to gravitational load is not possible at such displacements.

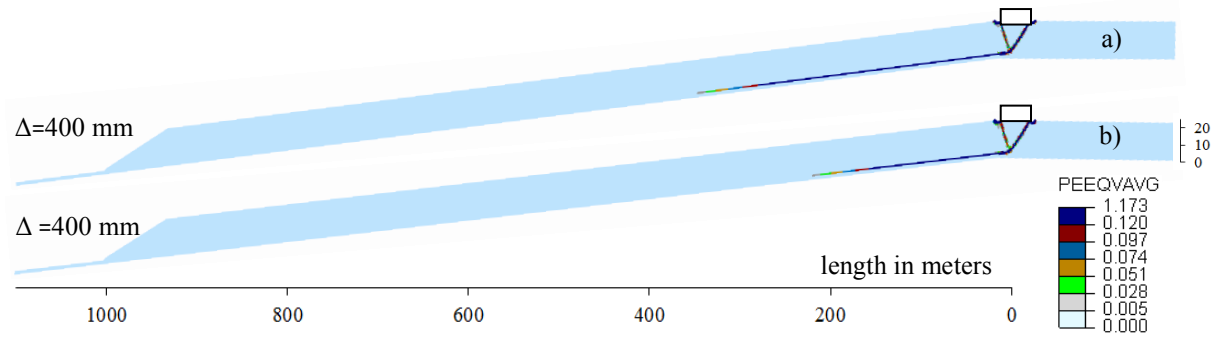

Figure 6. Failure process in Case-3: a) S_t=5, b) S_t=4

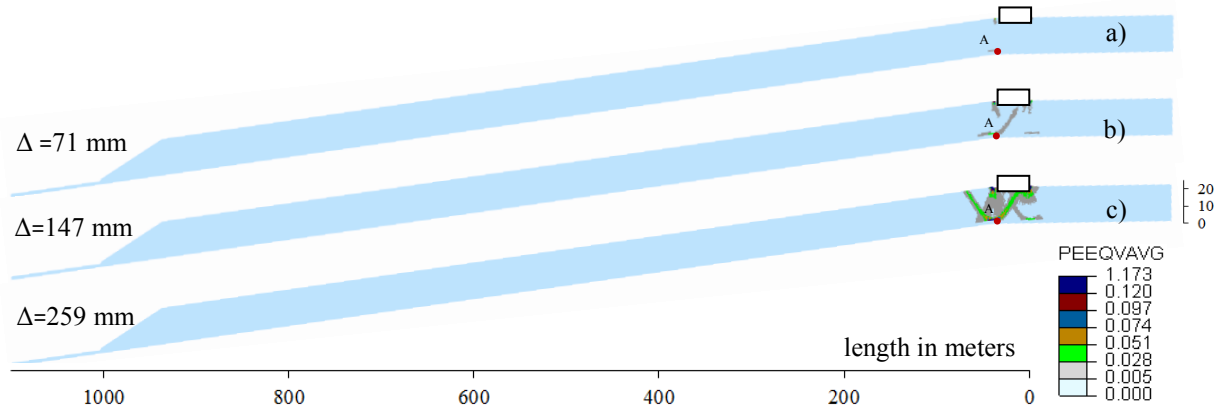

Figure 7. Failure process in Case-4

Finally, in Case-4, analysis is performed for a case where strain softening is not allowed in the whole clay layer. As shown in Fig. 7, no slope failure occurs in this case as the shear band does not propagate in downslope. The failure planes are similar to the typical failure surfaces under a shallow foundation.

Slope Capacity

The average pressure developed under the load block is shown in Fig. 8 for the different cases analyzed in this study. The pressure is calculated by dividing the vertical force at the reference point of the load block by area (40 m × 1 m). As shown in this figure, the pressure increases with vertical displacement of the load block and then decreases reaching after the peak.

For Case-1, a considerable length of shear band develops in the marine clay layer at Δ≈100 mm (Fig. 3). As the shear strength is reduced in the failure plane, the pressure under the load block decreases. At large displacements (e.g. Δ≈200 mm), the pressure under the load block is very small, which implies that the soil mass above the failure plane becomes almost unstable under its gravity load because of significant reduction in shear strength along the basal failure plane.

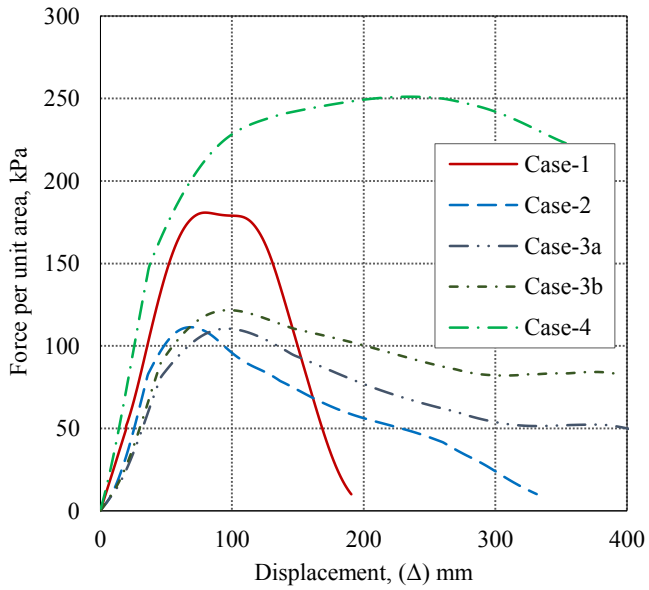

Figure 8. Force-displacement plot for all cases

Figure 8 also shows that the maximum pressures for Case-2 and 3 are smaller than that of Case-1, because in these two cases the upper soil layer is also assumed to be sensitive. Because of the same reason the reduction of forces starts at low values of Δ. This reduction is because of reduction of s_u in the thick sensitive clay layer. Figure 8 also shows less post-peak reduction of pressure in Case-3 than Case-2 because of lower S_t in Case 3.

Finally, in Case-4, the calculated maximum pressure is higher than other cases. Very small post-peak reduction of pressure is calculated, because no post-peak softening of s_u is allowed.

In summary, the comparison of above simulation shows that the magnitude of pressure that could be applied in the upslope area depends on soil properties and geometry of the slope. Although the load is placed on a gentle slope, the failure is governed by the sensitive clay layer even though it is thin in some cases. Failure pattern is similar to the failure under a shallow foundation only if the soil is not sensitive. Therefore, it is recommended that when there exists sensitive clay layers in offshore environments, as reported by many researchers, the shear band propagation should be considered in stability analysis of the slope as presented in this study.

CONCLUSIONS

Different approaches have been taken in the past to model the failure of a submarine slopes. Among them limit equilibrium method has been widely used to check the stability of submarine slopes assuming infinite slope configuration. However, this method is not applicable when shear band propagation occurs through sensitive clay layers.

The main aim of this paper is to study the stability of a submarine slope subjected to construction loading in the upslope area. It is shown that the new numerical approach developed in Abaqus CEL can successfully model this behaviour. Nonlinear strain softening behaviour of sensitive clay is incorporated in this large deformation FE analysis. Failure mechanisms involved in large-scale submarine landslides due to loading at upslope area, such as the 1979 Nice landslide, can be better explained using the modeling technique used in this study. It is also shown that a number of factors such as thickness of the marine sensitive clay layer and its sensitivity significantly influence the capacity of a submarine slope and the failure processes.

While the present numerical modeling techniques shows some promising results, analyses based on case-specific soil properties (e.g. the Nice landslide area) might further validate the proposed FE modeling tool.

ACKNOWLEDGMENTS

The writers would like to acknowledge the financial support from Research & Development Corporation of Newfoundland and Labrador, NSERC and C-CORE.

REFERENCES

[1] Hampton, M.A., Lee, H.J., and Locat, J., 1996, "Submarine landslides," Review of Geophysics, 34(1), pp. 33–59.

[2] Locat, J., and Lee, H.J., 2002, "Submarine landslides: advances and challenges," Canadian Geotechnical Journal, 39(1), pp. 193–212.

[3] Masson, D.G., Harbitz, C.B., Wynn, R.B., Pedersen, G., and Løvholt, F. A., 2006, "Submarine landslides: processes, triggers and hazard prediction," Phil. Trans. R. Soc. A., Vol. 364, pp. 2009–2039.

[4] Dan, G., Sultan, N., and Savoye, B., 2007, "The 1979 Nice harbour catastrophe revisited: Trigger mechanism inferred from geotechnical measurements and numerical modelling," Marine Geology, 245(1–4), pp. 40–64.

[5] Sultan, N., Savoye, B., Jouet, G., Leynaud, D., Cochonat, P., Henry, P., Stegmann, S., and Kopf, A., 2010, "Investigation of a possible submarine landslide at the Var delta front (Nice continental slope, southeast France)," Canadian Geotechnical Journal, 47(4), pp. 486–496.

[6] Bryn, P., Berg, K., Forsberg, C.F., Solheim, A., and Kvalstad, T., 2005, "Explaining the Storegga slide," Marine and Petroleum Geology, 22(1-2), pp. 11–19.

[7] Solheim, A., Berg, K., Forsberg, C. F. and Bryn, P., 2005, "The Storegga slide complex: repetitive large scale sliding with similar cause and development," Marine and Petroleum Geology, 22(1-2), pp. 97–107.

[8] Bernander, S., 2000, "Progressive failure in long natural slopes: formation, potential extension and configuration of finished slides in strain-softening soils," Licentiate Thesis, Luleå Univ. Tech., Luleå, Sweden.

[9] Bernander, S., 2008, "Down-hill progressive landslides in soft clays, triggering disturbance agents, slide propagation over horizontal or gently sloping ground, sensitivity related to geometry," Research report, Luleå Univ. of Tech., Luleå, Sweden.

[10] Locat, A., Leroueil, S., Bernander, S., Demers, D., Jostad, H.P. and Ouehb, L., 2011, "Progressive failures in eastern Canadian and Scandinavian sensitive clays," Canadian Geotechnical Journal, 48(11), pp. 1696–1712.

[11] Locat, A., Jostad, H.P. and Leroueil, S., 2013, "Numerical modeling of progressive failure and its implications for spreads in sensitive clays," Canadian Geotechnical Journal, 50(9), pp. 961–978.
[12] Quinn, P. E., Diederichs, M. S., Rowe, R. K., and Hutchinson, D. J., 2011, "A new model for large landslides in sensitive clay using a fracture mechanics approach," Canadian Geotechnical Journal, 48(8), pp. 1151–1162.
[13] Quinn, P.E., Diederichs, M.S., Rowe, R.K., and Hutchinson, D.J., 2012, "Development of progressive failure in sensitive clay slopes," Canadian Geotechnical Journal, 49(7), pp. 782–795.
[14] Andresen, L., 2001, "Effect of strain softening on stability analysis. Analysis of retrogressive sliding due to strain softening-Ormen Lange case study," Report No 521001 (10), NGI, Norway.
[15] PLAXIS., 2011, PLAXIS 2D 2010 manuals, PLAXIS bv., Delft, the Netherlands.
[16] Andresen, L. and Jostad, H.P., 2007, "Numerical modeling of failure mechanisms in sensitive soft clays - application to offshore geohazards," Offshore Technology Conference, Texas. Paper OTC 18650.
[17] Jostad, H.P., 1995, "Bifurcation analysis of frictional materials," Proc. NUMOG V., Davos, Switzerland, pp. 173–179.
[18] Jostad, H.P., and Andresen, L., 2002, "Bearing capacity analysis of anisotropic and strain-softening clays," In Proc. of NUMOG VIII, Rome, Italy, pp. 469–474.
[19] Kvalstad, T.J., Andresen, L., Forsberg, C.F., Berg, K., and Bryn, P., 2005a, "The Storegga Slide: evaluation of triggering sources and slide mechanisms," Marine and Petroleum Geology, 22(1-2), pp. 245–256.
[20] Abaqus 6.10, 2010, Abaqus Analysis Users' Manual, Dassault Systems Simulia Corp.
[21] Kvalstad, T.J., Nadim, F., Kaynia, A.M., Mokkelbost, K.H., and Bryn, P., 2005b, "Soil conditions and slope stability in the Ormen Lange area," Marine and Petroleum Geology, 2(1-2), pp. 299–310.
[22] DeGroot, D. J., DeJong, J. T., Yafrate, N. J., Landon, M. M., and Sheahan, T. C., 2007, "Application of recent developments in terrestrial soft sediment characterization methods to offshore environments," Offshore Technology Conference, Texas. Paper OTC 18737.
[23] Tavenas, F., Flon, P., Leroueil, S. and Lebuis, J., 1983, "Remolding energy and risk of slide retrogression in sensitive clays," Proc. of the Symposium on Slopes on Soft Clays, Linköping, Sweden, SGI Report No. 17: 423–454.
[24] Quinn, P., 2009, "Large Landslides in Sensitive Clay in Eastern Canada and the Associated Hazard and Risk to Linear Infrastructure," Ph.D. Thesis, Queen's Univ., Kingston, ON.
[25] Anastasopoulos, I., Callerio, A., Bransby, M.F., Davies M.C.R., Nahas, A.El., Faccioli, E., Gazetas, G., Masella, A., Paolucci, R., Pecker, A., and Rossignol, E., 2008, "Numerical analyses of fault–foundation interaction", Bulletin of Earthquake Engineering, 6(4), pp. 645–675.
[26] Gerolymos, N., Vardoulakis, I., and Gazetas, G., 2007, "A thermos-poro-visco-plastic shear band model for seismic triggering and evolution of catastrophic landslides", Soils and Foundations, 47(1), pp. 11–25, Japanese Geotechnical Society.
[27] Einav, I., and Randolph, M.F., 2005, "Combining upper bound and strain path methods for evaluating penetration resistance," International Journal for Numerical Methods in Engineering, 63(14), pp. 1991–2016.
[28] Dey, R., Hawlader, B., Phillips, R., and Soga, K., 2012, "Effects of shear band propagation on submarine landslide," Proc. of the 22nd Int. Offshore and Polar Engineering Conf., Rhodes, Greece, 766–773.
[29] Dey, R., Hawlader, B., Phillips, R., and Soga, K., 2013, "Progressive failure of slopes with sensitive clay layers," Proc. of the 18th Int. Conference on Soil Mechanics and Geotechnical Engineering, Paris.
[30] Bjerrum, L., and Landva, A., 1966, "Direct simple-shear tests on a Norwegian quick clay," Géotechnique, 16(1), pp. 1–20.
[31] Stark, T., and Contreras, I.A., 1996, "Constant volume ring shear apparatus," Geotechnical Testing Journal, 19(1), pp. 3–11.
[32] Yang, S.L., Solheim, A., Kvalstad, T.J., Forsberg, C.F., and Michael Schnellmann, M., 2006, "Behaviour of the sediments in the Storegga Slide interpreted by the steady state concept," Norwegian Journal of Geology, 86(3), pp. 243–253.
[33] Leroueil, S., 2001, "Natural slopes and cuts: movement and failure mechanisms," Géotechnique, 51(3), pp. 197–243.
[34] Lunne, T., and Andersen, K. H., 2007, "Soft clay shear strength parameters for deepwater geotechnical design," In Proc. of the 6th Int. Off. Site Investigations and Geotechnics Conf., London, UK. pp. 151–176.